Wenliang Li

# Advancing Biosensing Techniques for Detection of Antimicrobial Resistance Genes and Antibiotics in Water

School of Water, Energy and Environment

PhD in Water

PhD

Academic Year: 2020 - 2024

Supervisor: Prof. Zhugen Yang

Associate Supervisor: Prof. Frederic Coulon

09/2024

School of Water, Energy, and Environment
PhD in Water

PhD

Academic Year 2020 - 2024

Wenliang Li

# Advancing Biosensing Techniques for Detection of Antimicrobial Resistance Genes and Antibiotics in Water

Supervisor: Prof. Zhugen Yang
Associate Supervisor: Prof. Frederic Coulon

09/2024

© Cranfield University 2024. All rights reserved. No part of this publication may be reproduced without the written permission of the copyright owner.

## Academic integrity declaration

I declare that:

- the thesis submitted has been written by me alone.
- the thesis submitted has not been previously submitted to this university or any other.
- that all content, including primary and/or secondary data, is true to the best of my knowledge.
- that all quotations and references have been duly acknowledged according to the requirements of academic research.

I understand that to knowingly submit work in violation of the above statement will be considered by examiners as academic misconduct.

# Abstract

Antimicrobial resistance (AMR) poses a significant global public health threat requiring urgent attention for surveillance of antibiotic resistance genes (ARGs) and antibiotics in the environment. In this PhD study, a real-time fluorescent detection assay of antimicrobial resistance genes (ARGs) was developed to specifically target two key ARGs, tet(M) and tet(x3) to detect tetracycline and tigecycline resistance respectively in water samples. Additionally, crassphage gene was investigated for anthropogenic activities since they also play a vital role in the AMR transmission. The advanced ARG detection assay was based on multiplexing recombinase polymerase amplification (RPA) and subsequent sequence-specific recognition by the trans-cleavage activity of Clustered Regularly Interspaced Short Palindromic Repeats (CRISPR)/Cas12a. The assay achieved limits of detection (LODs) of 1 copy $\mu L^{-1}$ for all three gene targets with an accuracy of 100% in spiked tap and surface water samples.

Expanding the assay by including two additional end-point detection modalities, lateral flow assay (LFA) and voltametric detection, further demonstrate its versatility. LODs of 1 copy $\mu L^{-1}$ for tet(x3) and crassphage, and 10 copies $\mu L^{-1}$ for tet(M) (LFA) and 10 copies $\mu L^{-1}$ for all three targets (electrochemical) were reached. Validation against gold standard quantitative polymerase chain reaction (qPCR) using real water samples, including wastewater and drinking water samples, revealed a remarkable 100% accuracy rate.

Antibiotics detection assay was conceptualised based on the amplification of hybridisation chain reaction (HCR) followed by CRISPR/Cas mediated cleavage within a DNA hydrogel matrix. This approach aimed to release electroactive methylene blue (MB) particles, detectable and quantifiable by square wave voltammetry (SWV). While unforeseen circumstances impeded full assay development, the preliminary data illustrated the viability of the proposed method, suggesting avenues for further research to develop rapid and onsite antibiotics detection methods.



**Keywords:** AMR, RPA, CRISPR/Cas, lateral flow assay, fluorescence, electrochemistry, hydrogel, aptamer

# Acknowledgements

First and foremost, I would like to express my sincere appreciation to my supervisors, Professor Zhugen Yang and Professor Frederic Coulon, for giving me the opportunity to pursue my PhD and for their supervision in my experimental designs and thesis write up. Their expertise and insightful advice have supported and guided me throughout my PhD study.

I would also like to thank Royal Academy of Engineering for their funding support both on my research and my life at Cranfield.

I am also grateful to all technicians and administrative staff at Cranfield for supporting me on instrument operations, lab maintenance, and consumable purchases.

Many thanks to my friends in UK and worldwide for encouraging and accompanying me.

Finally, I would like to thank my parents for their spiritual and financial support, without whom I wouldn't be able to complete this work.

# Table of Contents

Academic integrity declaration ..... i

Abstract ..... ii

Acknowledgements ..... iii

List of Figures ..... viii

List of Tables ..... xvi

List of Equations ..... xvii

List of Abbreviations ..... xviii

Publications list ..... xxii

1 Introduction ..... 23

1.1 Aims and Objectives ..... 24
1.2 Thesis structure ..... 25

2 Addressing Antimicrobial Resistance: Strategies, Technologies, and Future Prospects ..... 28

2.1 Introduction ..... 28
2.2 AMR transmission routes in water ..... 30
2.2.1 Fundamental SPR paradigms in the environment ..... 32
2.2.2 External factors influencing AMR transmission in the environment. ..... 34
2.3 Rapid detection methods of AMR in the environment ..... 36
2.3.1 Antimicrobial resistant gene detection ..... 43
2.3.2 Antimicrobial reagent detection ..... 61
2.4 Conclusion and perspectives ..... 68

3 Enhanced Detection of Antibiotic Resistance Genes and Microbial Source Tracking Using Real-Time Fluorescent mRPA-CRISPR/Cas Assay: A Versatile Tool for Resource-Limited Settings ..... 72

3.1 Introduction ..... 72
3.2 Materials and Methods ..... 75
3.2.1 Chemicals and apparatus ..... 75
3.2.2 DNA template concentration and extraction from wastewater ..... 76
3.2.3 Quantification of nucleic acid concentration ..... 77
3.2.4 RPA assay ..... 78
3.2.5 CRISPR/Cas assay ..... 79
3.2.6 Multiplexed RPA (mRPA) integrated CRISPR/Cas assay ..... 79
3.2.7 Analytical performance evaluation in spiked water samples ..... 81
3.2.8 Data analysis and evaluation ..... 82
3.3 Results and discussion ..... 83
3.3.1 Optimisation of RPA assay ..... 83
3.3.2 Optimisation of CRISPR/Cas assay ..... 90
3.3.3 Real-time fluorescent mRPA-CRISPR/Cas assay for ARG detections ..... 95
3.4 Conclusions ..... 102

4 Enhancing Environmental Monitoring with Integrated Detection Approaches: Lateral Flow and Electrochemical Assays with mRPA-CRISPR/Cas ..... 104

4.1 Introduction ..... 104
4.2 Materials and Methods ..... 107
4.2.1 Chemicals and apparatus ..... 107
4.2.2 DNA template extraction from wastewater samples and quantification ..... 108
4.2.3 mRPA-CRISPR/Cas assay ..... 108
4.2.4 Electrochemical detection ..... 108
4.2.5 Lateral flow strips detection ..... 111
4.2.6 Real sample validation ..... 114
4.2.7 Data analysis and evaluation ..... 114

4.3 Results and discussion ..... 115
4.3.1 Optimisation of lateral flow assay (LFA) ..... 115
4.3.2 Optimisation of electrochemical assay ..... 120
4.3.3 mRPA-CRISPR/Cas lateral flow for ARG detection in real samples ..... 128
4.3.4 mRPA-CRISPR/Cas electrochemical ARG detection in real samples ..... 131
4.4 Conclusions ..... 134

5 Feasibility and Challenges in Hydrogel-based HCR-CRISPR/Cas Assay for Antibiotic Detection: A Path Forward ..... 136

5.1 Introduction ..... 136
5.2 Materials and Methods ..... 140
5.2.1 Chemicals and apparatus ..... 140
5.2.2 Initiator release from target binding ..... 141
5.2.3 HCR assay ..... 143
5.2.4 CRISPR/Cas assay ..... 143
5.2.5 Hydrogel formation ..... 144
5.2.6 Electrochemical detection ..... 144
5.2.7 Molecular dynamics simulation ..... 145
5.3 Results and discussion ..... 147
5.3.1 Initiator release ..... 147
5.3.2 Optimisation of HCR assay ..... 149
5.3.3 Optimisation of CRISPR/Cas assay ..... 152
5.3.4 Hydrogel formation ..... 153
5.3.5 Molecular dynamics simulation for evaluation ..... 155
5.4 Conclusions ..... 158

6 Conclusions and Future Work ..... 161

6.1 Conclusions ..... 161
6.2 Future Work ..... 162

References ..... 168

Appendices ..... 210

# List of Figures

Figure 1.1 Flow chart of thesis structure with corresponding research objectives and expected outcomes..... 27

Figure 2.1 Illustration of loop shaped SPR paradigm. ..... 31

Figure 2.2 Schematics of AMR (including ARG and antibiotics) detection using different type of microfluidic devices. a) Biological small-molecule assays using gradient-based microfluidics b) Microfluidics for antibiotic susceptibility testing c) Silica bead-based microfluidic device with integrated photodiodes for the rapid capture and detection of rolling circle amplification (RCA) products in the femtomolar range. Reprinted from [86–88]..... 43

Figure 2.3 Schematic illustration of one PCR cycle..... 45

Figure 2.4 Schematics of LAMP amplification mechanisms. a) Initial phase where dumbbell structured intermediates are generated. b) Cyclic amplification phases where DNA template is exponentially amplified. F1c, F2c, B1c, B2c is complementary to F1, F2, B1, B2, respectively..... 47

Figure 2.5 Schematic illustration of RPA working principle. ..... 50

Figure 2.6 Schematic illustration of RCA working mechanism. a) Formation of circular DNA product via ligation between circular DNA template and primer. b) Linear DNA product formation from the circular DNA product and the primer with the aid of DNA polymerase. c) multiprimed RCA where more than one primer can bind to the circular template. d) hyperbranched RCA where circular DNA product was employed as template for further amplification with different primer sets. ..... 52

Figure 2.7 Schematic illustration of CRISPR/Cas working mechanism. ..... 56

Figure 2.8. Schematics of antimicrobial detection using µPADs. a), b) and c) as mentioned in the main text. d) schematic lateral flow test design for ampicillin (AMP) detection. a) b) c) d) Reprinted from [149–151,153] ..... 63

Figure 2.9 Illustration of HCR mechanisms. a) the process of exponential amplification of hairpins with the presence of the initiator b) structure of a hairpin, composed of a loop, a stem, and a toehold. ..... 64

Figure 3.1 Chemical structures of a) tetracycline core structure b) tetracycline c) tigecycline. ..... 74

Figure 3.2 Schematic illustration of mRPA-CRISPR/Cas assay. X, tet(x3), M, tet(M), and C, crassphage. S1 represents sample one, and the first row of the 96-well plate indicates detection of X, M and C in sample 1 in triplicates. ..... 81

Figure 3.3 Workflow of ARG detection with fluorescent mRPA/CRISPR-Cas assay. ..... 82

Figure 3.4 Preparation of templates of crassphage and tet(M). a) Mean amplification curves of crassphage and tet(M) from DNAs of extracted wastewater via PCR. Experiments were conducted in triplicates. PC: positive control. NC: negative control. b) schematic illustration of the workflow of preparation of templates from PCR amplicons isolated from wastewater DNA extracts. ..... 84

Figure 3.5 Optimisation of real-time fluorescent RPA assay. a) primer concentration with a broad range from 150 nM to 650 nM, and b) a narrower concentration range was then evaluated from 550 nM to 640 nM. (constant temperature at 39 °C and constant $Mg^{2+}$ concentration of 14 mM) c) $Mg^{2+}$ ion concentration ranging from 12 mM to 24 mM. (constant primer concentration at 570 nM and constant temperature at 39 °C) d) reaction temperature of 37 °C, 39 °C, 42 °C. (constant primer concentration at 570 nM and con constant $Mg^{2+}$ concentration of 14 mM) NC: negative control ($ddH_2O$ substituted template). All assays were repeated three times. The presented curve is a mean of triplicates. ..... 86

Figure 3.6 Sensitivity of RPA assay of a) and b) tet(M), c) and d) crassphage, and e) and f) tet(x3). a), b), c) represent the real-time fluorescent curves against time under different concentration, ranging from $10^4$ copies $\mu L^{-1}$ to $10^{-1}$ copies $\mu L^{-1}$, while b), d) and f) represent the gel electrophoresis results of RPA assay. L represents 100 bp DNA ladder, Lane 1: $10^4$ copies $\mu L^{-1}$, Lane 2: $10^3$ copies $\mu L^{-1}$, Lane 3: $10^2$ copies $\mu L^{-1}$, Lane 4: $10^1$ copies $\mu L^{-1}$, Lane 5: $10^0$ copies $\mu L^{-1}$. NC: negative control. The presented curve is a mean of triplicates. The RPA assay conditions were the chosen ones as described above. ..... 89

Figure 3.7 Optimisation of CRISPR/Cas assay using tet(x3) as a model target. a) cas12a: crRNA ratio optimisation b) reaction temperature optimisation c) cas12a: ssDNA probe ratio optimisation d) Real-time fluorescent RPA-CRISPR/Cas on all three targets, including tet(x3) (X). PC: positive control. NC: negative control. The presented curve is a mean of triplicates. ..... 93

Figure 3.8 Sensitivity of real-time fluorescent RPA-CRISPR/Cas assay. a) RPA-CRISPR/Cas for tet(M). b) RPA-CRISPR/Cas for crassphage. c) RPA-CRISPR/Cas for tet(x3). Target concentrations are from $10^{4}$-$10^{-1}$ copies $\mu L^{-1}$. NC: negative control. The plotted curve is a mean of triplicates. ..... 94

Figure 3.9 Sensitivity of real-time fluorescent mRPA-CRISPR/Cas assay. a) RPA-CRISPR/Cas for tet(M). b) RPA-CRISPR/Cas for crassphage. c) RPA-CRISPR/Cas for tet(x3). Target concentrations are from $10^{4}$-$10^{-1}$ copies $\mu L^{-1}$. NC: negative control. The plotted curve is a mean of triplicates. ..... 96

Figure 3.10 Real-time fluorescent mRPA-CRISPR/cas assay on spiked surface and tap water samples. a), c) and e) are results of spiked tap water. b), d) and f) are results of spiked surface water. a) and b) are results of tet(M), c) and d) are of crassphage, and e) and f) are of tet(x3). Target concentrations are from $10^{6}$-$10^{-1}$ copies $\mu L^{-1}$. NC: negative control. The plotted curve is a mean of triplicates. ..... 100

Figure 4.1 Overview of mRPA-CRISPR/Cas based electrochemical and lateral flow assay detections ..... 106

Figure 4.2 Biosensing mechanism of the developed signal-off electrochemical based mRPA-CRISPR/Cas assay. a) The setup of the working electrode incubation for detection. b) Schematic illustration of electrode surfaces and SWV signals before and after reaction in the cases of positive and negative controls. ..... 109

Figure 4.3 Schematic representation of electrode immobilisation approaches. a) separate immobilisation. b) co-immobilisation. ..... 111

Figure 4.4 Schematic illustration of lateral flow strip assembly. a) The distribution of zones on backing card. b) Attachment of nitrocellulose membranes (printed with control and test lines) onto the backing card. c) Attachment of

sample pad which overlaps with the nitrocellulose membrane of 3 mm. d) Attachment of wick pad which overlaps with the nitrocellulose membrane of 3 mm. The assembled pad is finally cut to strips of 5 mm width. ..... 112

Figure 4.5 Biosensing mechanisms of the developed lateral flow strip. a) Composition of lateral flow assay. Streptavidin coated AuNP reporter was mixed with sample before test. b) Schematic illustration of on test and control lines capturing probes in the cases of positive and negative controls. .... 113

Figure 4.6 Optimisation of lateral flow assay reaction conditions. a) Selection of nitrocellulose membrane between MDI 70, MDI 90 and MDI 150 modified with test and control lines. b) optimisation of reporter concentration: 1 OD, 0.5 OD, and 0.1 OD streptavidin coated AuNP mixed with running buffer (n=3) c) Optimisation of reaction volume, 50 µL, 75 µL and 100 µL (n=3) d) BSA blocking effect on AuNP to prevent non-specific binding. Solid square marks the position of test lines while dashed square marks the position of control lines. ..... 116

Figure 4.7 Optimisation of probe concentration for LFA. a) Different concentrations (125 nM, 50 nM, 10 nM, 5 nM and 0 nM) of LFA probes added to 0.5 OD BSA-streptavidin-AuNP in running buffer. (n=3) b) Schematic illustration of control lines when 125 nM probe or 5 nM probe is added. Solid square marks the position of test lines while dashed square marks the position of control lines. ..... 118

Figure 4.8 Demonstration of LFA on developed mRPA-CRISPR/Cas using $10^5$ copies $\mu L^{-1}$ tet(x3) as example. a) LFA results of positive and negative controls. PC-1: positive control case 1. PC-2: positive control case 2. NC: negative control. b) Schematic illustration of streptavidin-AuNP bound probe. c) Reversely inserted LFA into the testing sample solution with taken off wick pads. Solid square marks the position of test lines while dashed square marks the position of control lines. ..... 119

Figure 4.9 Sensitivity of LFA based mRPA-CRISPR/Cas assay. a) LFA mRPA-CRISPR/Cas for tet(x3). b) LFA mRPA-CRISPR/Cas for crassphage. c) RPA-CRISPR/Cas for tet(M). 1: only BSA-streptavidin-AuNP. 2-7: 10-fold serial diluted target concentrations ranging from $10^5$-$10^0$ copies $\mu L^{-1}$. 8:

negative control. Experiments were conducted in triplicates with one shown as demonstration. Solid square marks the position of test lines while dashed square marks the position of control lines..... 120

Figure 4.10 Optimisation in immobilisation strategy of gold working electrode. a) Characteristic cyclic voltammogram of cleaned gold electrodes. b) Demonstration photo of electrodes incubated for different immobilisation strategies under sealed and dark conditions. GE3: separate immobilisation. GE1: co-immobilisation..... 121

Figure 4.11 Electrochemical measurements of GE1 (co-immobilisation). a) Cyclic voltammograms of different scan rates (50 mV $s^{-1}$, 100 mV $s^{-1}$, 150 mV $s^{-1}$, 200 mV $s^{-1}$, 250 mV $s^{-1}$, 300 mV $s^{-1}$, 350 mV $s^{-1}$, 400 mV $s^{-1}$, 450 mV $s^{-1}$, and 500 mV $s^{-1}$) recorded at equilibrium. Dashed box: Faradaic current. Solid box: capacitive current. b) Plot of scan rate versus peak currents of CV (both oxidation and reduction) with linear fits. c) square wave voltammograms of different frequencies (50 Hz, 100 Hz, 150 Hz, 200 Hz, 250 Hz, 300 Hz, 350 Hz, 400 Hz, 450 Hz, and 500 Hz) recorded at equilibrium. d) plot of frequencies versus peak currents of SWV with the linear fit. ..... 125

Figure 4.12 Electrochemical measurements of GE3 (separate immobilisation). a) Cyclic voltammograms of different scan rates (50 mV $s^{-1}$, 100 mV $s^{-1}$, 150 mV $s^{-1}$, 200 mV $s^{-1}$, 250 mV $s^{-1}$, 300 mV $s^{-1}$, 350 mV $s^{-1}$, 400 mV $s^{-1}$, 450 mV $s^{-1}$, and 500 mV $s^{-1}$) recorded at equilibrium. Dashed box: Faradaic current. Solid box: capacitive current. b) Plot of scan rate versus peak currents of CV (both oxidation and reduction) with linear fits. c) square wave voltammograms of different frequencies (50 Hz, 100 Hz, 150 Hz, 200 Hz, 250 Hz, 300 Hz, 350 Hz, 400 Hz, 450 Hz, and 500 Hz) recorded at equilibrium. d) plot of frequencies versus peak currents of SWV with the linear fit. ..... 127

Figure 4.13 Sensitivity of electrochemical based mRPA-CRISPR/Cas assay. a) Electrochemical mRPA-CRISPR/Cas for tet(x3). b) Electrochemical mRPA-CRISPR/Cas for crassphage. c) Electrochemical RPA-CRISPR/Cas for tet(M). Experiments were conducted in triplicates. ..... 127

Figure 4.14 Results of qPCR detection of target genes in the real water samples. a) Calculated DNA concentration for tet(M) and tet(x3) detection in four

drinking water samples. b) Calculated DNA concentration for crassphage detection in four drinking water samples c) Calculated DNA concentration for tet(M) and tet(x3) detection in ten wastewater samples d) Calculated DNA concentration for crassphage detection in ten wastewater samples. NC: negative control. Experiments were conducted in triplicates. ..... 129

Figure 4.15 Photo of LFA based mRPA-CRISPR/Cas assay on real water samples. NC: negative control. X: tet(x3). M: tet(M). C: crassphage. Experiments were conducted in triplicates with one shown as demonstration. Solid square marks the position of test lines while dashed square marks the position of control lines. ..... 130

Figure 4.16 Results of electrochemical detection of target genes in the real water samples. a) Measured current changes for three targets detection in four drinking water samples. b) Measured current changes for three targets detection in ten wastewater samples. NC: negative control. Experiments were conducted in triplicates. ..... 132

Figure 5.1 Scheme of antibiotics detection platform of hydrogel-based CRISPR/Cas assay. ..... 139

Figure 5.2 Chemical structure of kanamycin ..... 140

Figure 5.3 Overview of workflow for initiator release upon target binding with aptamer. The two colours of aptamers represent two different sequences of aptamers, as they were designed differently for the downstream reactions i.e., HCR, and CRISPR/Cas. ..... 142

Figure 5.4 Overview of workflow of hydrogel formation and characterisation with electrochemical measurement. The higher the extent of the hydrogel is cleaved, the more MB is leaked into the solution, and therefore the SWV electrochemical signal increases. ..... 145

Figure 5.5 Overview of workflow of in silico modelling of aptamer-target binding. ..... 147

Figure 5.6 Results of initiator release upon target binding to aptamer. a) gel electrophoresis image of subsequent HCR with released initiator. (n=3) Subsequent HCR was conducted in another triplicate. Lane L: 100 bp DNA

ladder. Lane 1-9: negative controls. Lane 10-18: positive controls. b) demonstrative photo of colorimetric assessment of aptamer binding to target. Left: 20 nm AuNP + 1M NaCl. Right: 20 nm AuNP + $ddH_2O$. c). Left: 20 nm AuNP + aptamer + 1M NaCl. Right: 20 nm AuNP + $ddH_2O$ + 1M NaCl. d) 1: 20 nm AuNP + aptamer + kanamycin + 1M NaCl. 2: 20 nm AuNP + aptamer - kanamycin + 1M NaCl. 3: 20 nm AuNP + $ddH_2O$ + kanamycin + 1M NaCl. 4: 20 nm AuNP + $ddH_2O$ - kanamycin + 1M NaCl. ..... 148

Figure 5.7 Gel electrophoresis image of HCR conducted in 5× SSC buffer at 50 °C for one hour. Land L: 1000 bp DNA ladder, Lane 1-3: negative control; Lane 4-6: positive controls (with initiator concentration equals to 1 μM). All experiments were conducted in triplicates. ..... 149

Figure 5.8 Gel electrophoresis images of HCR LOD evaluation experiments. a) reactions conducted in heat block. b) experiments conducted in Quant 3 Studio PCR machines. All experiments were conducted in triplicates. Land L: 100 bp DNA ladder. Lane 1-3: negative control; Lane 4-6: initiator concentration 0.1 nM; Lane 7-9: initiator concentration 1 nM; Lane 10-12: initiator concentration 10 nM; Lane 13-15: initiator concentration 100 nM; Lane 16-18: initiator concentration 1 μM. ..... 150

Figure 5.9 Schematic secondary structures of hairpins designed for HCR reactions (presented with the most stable form). a) HP1-a b) HP2-a c) HP1-b d) HP2-b. Figures were produced from mFold. ..... 151

Figure 5.10 HCR-CRISPR/Cas fluorescent plots. Before: HCR-CRISPR/Cas assay fluorescent plots when hairpins were pretreated with 30 min bench-top cooling from 95 °C. After: when hairpins were pretreated with 0.015 °C $s^{-1}$ Quant Studio 3 PCR machine cooling from 95 °C. PC: initiator added to HCR before CRISPR/Cas. NC: no initiators addec. H2O: $ddH_2O$ substituted HCR assay in subsequent CRISPR/Cas assay. All experiments were conducted in triplicates and the plot was a mean of them. ..... 153

Figure 5.11 Formation and characterisation of hydrogel wrapping MB inside. a) photo of hydrogel produced in triplicates following separate catalysts (APS and TEMED) addition (S) and altogether addition (A). b) SWV diagrams measuring 10-fold serial diluted MB solution, ranging from 10 nM to 10000

nM, as well as hydrogel with MB added to 0.01 M PBS solution. all: all hydrogels added (100 µL) 5: 5 µL of hydrogel added. All experiments were conducted in triplicates. ..... 154

Figure 5.12 predicted 3D structures of aptamers. a) original aptamer reported in literature (apori). b) modified aptamer sequence 1 (ap1). c) modified aptamer sequence 2 (ap2). Different colours represent different base pairs. Blue: guanine. Red: adenine. Yellow: cystine. Orange: thymine..... 156

Figure 5.13 Docked aptamer-target complex structure. a) apori b) ap1 c) ap2. ..... 156

Figure 5.14 Starting structures of aptamer-ligand complex in a dodecahedron box of water and ions for MD simulation. grey structures: kanamycin ligand. Coloured ribbons: DNA aptamer. small dots, balls and sticks: ions and water molecules. a) apori b) ap1 c) ap2. ..... 157

Figure 6.1 Schematic illustration of the relationships between faeces, antibiotics, and ARG in the environment. ..... 166

# List of Tables

Table 2.1 Summary of examples of AMR detection. ..... 40

Table 2.2 Summary of main features, advantages and disadvantages of the amplification methods. ..... 53

Table 2.3 Summary of examples of ARG detection. ..... 56

Table 2.4 Summary of examples of antibiotics detection. ..... 66

Table 3.1 Overview of RPA-CRISPR conditions and detection methods ..... 101

Table 4.1 Wicking time of different NC membranes ..... 116

Table 4.2 List of reduction peak potential, current, and area of cleaned working electrodes. ..... 122

Table 4.3 Summary of results of LFA based mRPA-CRISPR/Cas assay on real water sample detections ..... 131

Table 5.1 Thermodynamic data of hairpin sets designed. Data was calculated from mFold at 25 °C, 0.15 M NaCl and 0.02 M $Mg^{2+}$. ..... 151

Table 5.2 Summary of docked structure with calculated affinities. ..... 157

Table 5.3 Summary of MD simulation results of aptamer-ligand short range interaction energy. ..... 158

# List of Equations

Equation 1 ..... 82

Equation 2 ..... 158

# List of Abbreviations

| | |
|---|---|
| µPAD | paper-based microfluidic analytical device |
| A | adenine |
| AMR | antimicrobial resistance |
| APS | ammonium persulfate |
| ARB | antibiotic resistant bacteria |
| ARG | antibiotic resistance gene |
| AST | antimicrobial susceptibility testing |
| AuNP | gold nanoparticle |
| AURA | antimicrobial resistance use and resistance in Australia |
| BSA | bovine serum albumin |
| C | cystine |
| CARSS | Canadian antimicrobial resistance surveillance systems |
| cDNA | complementary DNA |
| CE | capillary electrophoresis |
| CRISPR | clustered regularly interspaced short palindromic repeats |
| CV | cyclic voltammetry |
| DNA | deoxyribonucleic acid |
| dsDNA | double-stranded DNA |
| EARS-Net | European antimicrobial resistance surveillance network |
| ECSA | electrochemical active surface area |
| EDTA | ethylenediaminetetraacetic acid |
| ELISA | enzyme-linked immunosorbent assay |
| EM | energy minimisation |

| | |
|---|---|
| EU | European Union |
| FDA | food and drug administration |
| FITC | fluorescein |
| G | guanine |
| GLASS | global antimicrobial resistance and use surveillance system |
| GPS | global positioning system |
| HCR | hybridisation chain reaction |
| HGT | horizontal gene transfer |
| HIC | high-income countries |
| HPLC | high-performance liquid chromatography |
| IoT | internet of things |
| LAMP | loop-mediated isothermal amplification |
| LC-MS | liquid chromatography mass spectroscopy |
| LFA | lateral flow assay |
| LMICs | low- and middle- income countries |
| LOD | limit of detection |
| LOQ | limit of quantification |
| MB | methylene blue |
| MD | molecular dynamics |
| MGE | mobile genetic element |
| MIC | minimal inhibitory concentration |
| mRPA | multiplexed RPA |
| MST | microbial source tracking |
| NAAT | nucleic acid amplification testing |

| | |
|---|---|
| NARMS | national antimicrobial resistance monitoring system for enteric bacteria |
| NC | nitrocellulose membrane |
| NGO | non-governmental organisation |
| OD | optical density |
| P | pathway |
| PBS | phosphate buffer saline |
| PDB | protein data bank |
| POU | point of use |
| qPCR | quantitative polymerase chain reaction |
| R | receptor |
| RNA | ribonucleic acid |
| RPA | recombinase polymerase amplification |
| RPP | ribosomal protection protein |
| S | source |
| SDGs | sustainable development goals |
| SELEX | Systematic Evolution of Ligands by EXponential enrichment |
| S-P-R | source-pathway-receptor |
| ssDNA | single-stranded DNA |
| SWV | square wave voltammetry |
| T | thymine |
| TAE | tris-acetate-EDTA |
| TEMED | N, N, N’,N’-tetramethylethylenediamine |
| U | uracil |
| UV | ultraviolet |

| | |
|---|---|
| WGS | whole-genome sequencing |
| WHO | World Health Organisation |
| WWTPs | wastewater treatment plants |

# Publications list

## Journal Articles

**Li W**, Coulon F, Singer A, Zhu YG & Yang Z. (2021). Paper-based devices as a new tool for rapid and on-site monitoring of "superbugs". Environmental Science and Technology, 55, 12133.

**Li W**, Ma X, Yong YC, Liu G & Yang Z. (2023). Review of paper-based microfluidic analytical devices for in-field testing of pathogens. Analytica Chimica Acta, 1278, 341614.

## Conference Presentations

**Li W**, Coulon F, Yang Z. (2022) A paper-based device integrating RPA-CRISPR assay for detecting antimicrobial resistance genes in the environmental water. Environmental Biotechnology Network (EBNET) - A BBSRC/EPSRC Networks in Industrial Biotechnology and Bioenergy Early Career Researcher conference (ECR22), Jubilee Conference Centre, Nottingham, UK, 12-14 September 2022.

**Li W**, Coulon F, Yang Z. (2023) A Dual Mode Paper-based RPA-CRISPR/Cas Biosensor for Detection of Antimicrobial Resistance Gene in Water. Sensing in Water 2023, Sensors for Water Interest Group (SWIG), Nottingham Belfry, UK, 27-28 September 2023.

## Book Chapters

**Li W**, Spatola Rossi C, Coulon F & Yang Z. (2023). Smartphone-based sensors for water quality In Comprehensive Analytical Chemistry (101). Elsevier. https://doi.org/10.1016/bs.coac.2023.02.006.

Pan Y, **Li W**, Hui Q & Yang Z. (2023). Biosensors for bacteria detection In Barhoum A & Altintas Z (eds), Advanced Sensor Technology: Biomedical, Environmental, and Construction Applications. Elsevier. https://doi.org/10.1016/B978-0-323-90222-9.00011-X.

Xu Q, Pan Y, **Li W** & Yang Z. (2023). Amperometric sensors In Barhoum A & Altintas Z (eds), Fundamentals of Sensor Technology: Principles and Novel Designs. Elsevier. https://doi.org/10.1016/B978-0-323-88431-0.00007-7.

# 1 Introduction

Antimicrobial resistance (AMR) occurs when microorganisms once susceptible to the antimicrobial agents are no longer sensitive to them, which can lead to severe infections that are difficult to treat. AMR is a global public health concern, resulting in 1.27 million deaths and 4.95 million associated deaths annually [1]. It was estimated that there would be 10 million deaths, alongside a cumulative economic cost of $100 trillion by 2050 [2].

To tackle the problem, World Health Organisation (WHO) established a Global Antimicrobial Resistance and Use Surveillance System (GLASS) in 2015 to foster standardised AMR surveillance and data collection worldwide [3]. Although most current data are collected under clinical context, there is an emerging recognition of the importance to embrace the 'One Health' concept which is an approach calling for 'the collaborative efforts of multiple disciplines working locally, nationally, and globally, to attain optimal health for people, animals and our environment', and more attention is drawn to the 'environment' and its role in AMR transmission [4].

On the microscale, AMR is caused by the expression of antimicrobial resistance genes (ARGs). ARGs can further relocate autonomously between cells or mobile genetic elements (MGEs) such as plasmids and even transmit to other hosts via horizontal gene transfer (HGT), and therefore ARGs spread, leading to extensive dissemination [5]. Since inappropriate use of antimicrobial agents act as selection pressure that prompt the antibiotic resistant bacteria (ARB) and ARG [6], the presence and quantity of antimicrobial agent should also be monitored. Hence, to further understand the transmission pathway, it is vital to carry out timely and effective surveillance for AMR, including both ARGs and antibiotics.

Conventional ARG detection approaches include polymerase chain reaction (PCR) or whole-genome sequencing (WGS) and as for antibiotics detection, conventional methods include liquid chromatography mass spectroscopy (LC-MS) [7] and high-performance liquid chromatography (HPLC) [8]. Although those methods can provide sensitive and selective determination of antimicrobial agents' level, most requires a laboratory set up, such as sophisticated and

expensive equipment, trained personnel, and time-consuming operation process [9,10]. Continuous efforts have been made to develop point-of-use (POU) bioassays for low-cost and rapid on-site measurement for both ARG and antibiotics. Currently, isothermal amplification of gene targets is extensively employed for gene detection with enhanced analytical performance and portability for POU. There is also an emerging trend of CRISPR/Cas applied in diagnostics [11–14], in both nucleic acid and non-nucleic acid detection, where the latter utilises aptamer to transfer from chemical signals to nucleic acid ones. However, most assays are designed for clinical purposes rather than for environmental detection, while the latter is more demanding in sensitivity and specificity due to the diluted concentration of target nucleic acids in complicated environmental matrices. There is an urgent need to evaluate and advance current detection techniques to provide timely surveillance of AMR in the environment. The data collected could therefore prompt timely intervention actions from relevant agencies, ensuring that necessary assistance reaches the affected populations and potentially saving lives. The advanced biosensing techniques not only provide a powerful tool for detection, but also address the urgent need for improved water monitoring and intervention strategies in low- and middle-income countries (LMICs). By facilitating in-time surveillance and response to AMR, it has the potential to significantly improve public health outcomes and contribute to saving resources in both human and economic terms, alleviating the social and economic burden.

## 1.1 Aims and Objectives

The aim of the PhD study is to advance the biosensing techniques for rapid, cost-effective, sensitive, and onsite ARG and antibiotic detection in regions with limited infrastructure. The specific research objectives of the study are to:

1) Identify research knowledge gap via critically review existing literature on environmental transmission routes of AMR and current POU biosensing techniques for AMR detection in water.
2) Assess a real-time fluorescent multiplexed RPA coupled CRISPR/Cas (mRPA-CRISPR/Cas) assay for ARG detection

3) Expand the use of developed ARG detection assay for lateral flow and voltametric end-point detections.
4) Investigate the biosensing techniques for rapid, cost-effective, and sensitive detection of antibiotics in water.

## 1.2 Thesis structure

The general structure of the entire thesis is described below, and a schematic illustration is as shown in Figure 1.1.

**Chapter 1 Introduction.** A brief background on AMR was illustrated, with a specific emphasis on the related public health crisis especially when embracing the 'One Health' concept. Challenges on tackling the issue were therefore assessed, followed by main contributions of this PhD study in resolving the issues. The aim of the PhD study was then clearly stated with specific objectives to achieve the general aim. Finally, a general outline on the thesis structure was presented.

**Chapter 2 Addressing Antimicrobial Resistance: Strategies, Technologies, and Future Prospects.** A critical review was carried out on AMR transmission routes in water, followed by evaluation of POU detection approaches of AMR including ARG and antibiotics. Finally, research gaps were identified and evaluated.

**Chapter 3 Enhanced Detection of Antibiotic Resistance Genes and Microbial Source Tracking Using Real-Time Fluorescent mRPA-CRISPR/Cas Assay: A Versatile Tool for Resource-Limited Settings.** Real-time fluorescent mRPA-CRISPR/Cas assay was investigated for detecting tetracycline resistance gene (tet(M)), tigecycline resistance gene (tet(x3)), and human source biomarker (crassphage). Reaction conditions were optimized, and analytical performances were evaluated in pristine samples. Then, the mRPA-CRISPR/Cas assay was effectively utilized for analysing real water samples, including spiked surface water and drinking water samples with a limit of detection of 1 copy $\mu L^{-1}$.

**Chapter 4 Enhancing Environmental Monitoring with Integrated Detection Approaches: Lateral Flow and Electrochemical Assays with mRPA-CRISPR/Cas.** The advanced ARG detection assay as described in Chapter 3 was further expanded to combine lateral flow and electrochemical detection approaches. Following optimisation of reaction conditions, both lateral flow and electrochemical assay were characterised in terms of sensitivity. Ten wastewater samples and four drinking water samples were finally employed to assess the robustness of the expanded ARG detection assay with results compared with those of qPCR.

**Chapter 5 Feasibility and Challenges in Hydrogel-based HCR-CRISPR/Cas Assay for Antibiotic Detection: A Path Forward.** A hybridisation chain reaction (HCR) coupled CRISPR/Cas based hydrogel assay was designed for antibiotics detection and kanamycin was employed as the model drug. Aptamers were designed for target binding, followed by the HCR assay for amplification and subsequent CRISPR/Cas assay for sequence specific detection. The construction of hydrogel was then validated by electrochemical measurement. In addition, current obtained results were assessed and analysed for future improvements. Potential reasons behind failures of capturing target with aptamers were investigated by computational modelling of aptamer-target affinity assessment.

**Chapter 6 Conclusions and Future Work.** The main findings and contributions of this PhD study were summarised and evaluated. Besides, the remaining works and potential future research topics were further assessed.

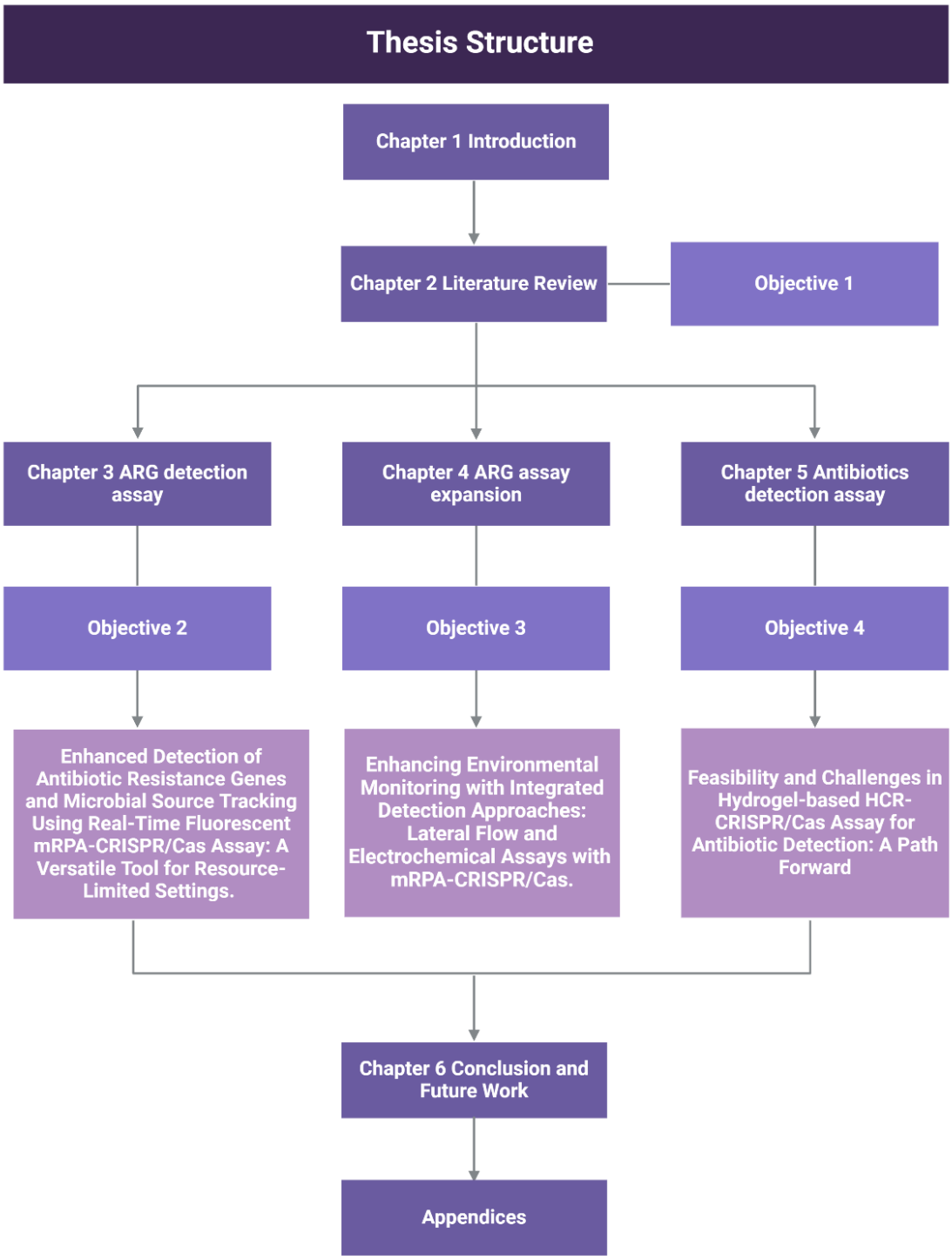


Figure 1.1 Flow chart of thesis structure with corresponding research objectives and expected outcomes.

# 2 Addressing Antimicrobial Resistance: Strategies, Technologies, and Future Prospects

## 2.1 Introduction

Antimicrobial resistance (AMR) represents a condition where microorganisms once susceptible to the antimicrobial reagents are no longer sensitive to them, which can lead to severe infections that are difficult to treat. It has been recognised as a global public health threat, with 1.27 million annual deaths attributed to AMR and 4.95 million deaths associated [1]. Moreover, if no action is taken, 10 million annual deaths is estimated, alongside a cumulative cost of $100 trillion, by 2050. AMR also threatens Sustainable Development Goals (SDGs) – it is estimated by World Bank that an extra 28 million people will be forced into extreme poverty by 2050 unless AMR is contained [2].

To tackle the problem, the WHO established a Global Antimicrobial Resistance and Use Surveillance System (GLASS) [15] in 2015 to foster standardised AMR surveillance and data collection worldwide, with subsequent establishment of national AMR monitoring programmes, such as the Canadian Antimicrobial Resistance Surveillance Systems (CARSS), the National Antimicrobial Resistance Monitoring System for Enteric Bacteria (NARMS), the Antimicrobial Use and Resistance in Australia (AURA) and the European Antimicrobial Resistance Surveillance Network (EARS-Net). Although most current data are collected under clinical context, there is an emerging recognition of the importance to embrace the ‘One Health’ concept (human-animal-environment) [4] and more attention is drawn to the ‘environment’ and its role in AMR transmission. To date, vast research has demonstrated the crucial role of water acting as reservoirs and pathway in AMR transmission. For example, wastewater treatment plants (WWTPs) are hotspots of AMR harbouring-microorganisms, disinfectants, antimicrobial reagents, and heavy metals, which are hard to completely remove even after treatment, and they gravely contribute to AMR selection and accumulation. With the effluent continuously released to nearby environment such as receiving rivers, AMR therefore disseminates to wider world, e.g., drinking water and recreational water, exposing to human and animals, leading

to risks of resistant microbial infections. However, most studies are only concerned with detection or quantifying AMR in discrete water environment, with a lack of research illustrating the fate of AMR transmission to describe the complete route.

Besides, to further understand the transmission routes and to tackle AMR, it is vital to carry out timely and effective surveillance for AMR. On the microscale, AMR is caused by the expression of antimicrobial resistance genes (ARGs). ARGs can further relocate autonomously between cells or mobile genetic elements (MGEs) such as plasmids and even transmit to other hosts via horizontal gene transfer (HGT), and therefore ARGs spread, leading to extensive dissemination. And the microbial hosts, in particular bacteria, that carry ARGs are called antibiotic resistant bacteria (ARB), which can physically transfer and transmit, and therefore leads to enlarged AMR spread [5]. Since inappropriate use of antimicrobial reagents act as selection pressure that prompt the ARB and ARG [6], the presence and quantity of antimicrobial reagent should also be monitored.

Currently, there are two mainstream approaches for AMR monitoring, phenotypic testing focusing on ARB detection (microbial culture method) and genotypic testing focusing on ARG detection (molecular testing) [16]. While phenotypic detection is of clinical importance especially in guiding treatment options, it is less suitable for environmental monitoring as it is more than difficult to isolate single species of bacteria in such complicated matrices with various bacteria present, which leaves molecular detection as a better approach to choose. However, most conventional molecular approaches such as polymerase chain reaction (PCR) are time- and labour-intensive, requiring for laboratory setup and trained personnel for operation and data analysis. With the advancement of biotechnology in nucleic acid detection, methods such as isothermal amplification have been developed for rapid and simple detection, but most still is laboratory-based and dependent on equipment and trained personnel [9].

As for antimicrobial reagent especially antibiotics detection, conventional approaches include liquid chromatography mass spectroscopy (LC-MS) [7,17], high performance liquid chromatography (HPLC) [8], capillary electrophoresis (CE) [18]. Although those methods can provide sensitive and precise determination of

antimicrobial reagents level, most require a centralised laboratory, such as sophisticated and expensive equipment, trained personnel, and time-consuming operation process.

Efforts have been made to develop simple, cost-effective, user-friendly, sensitive, specific, rapid and robust methods for AMR detection in resource-limited settings. There are various studies reporting assays targeting AMR with excellent performances, but most are conducted under clinical context, lacking those aimed to detect in the environment.

In this chapter, current evidence on the presence of AMR in different water environments is gathered, and key AMR transmission pathways are identified using the source-pathway-receptor (S-P-R) paradigm. Potential factors (e.g., COVID19 pandemic and microplastic pollution) that can influence AMR transmission events in water are also taken into consideration and their impacts are discussed. Furthermore, recent progresses on rapid AMR detection methods are summarised, with features of different methods, both merits and drawbacks are reviewed and analysed. Finally, by identifying key aspects that require further research and surveillance measurements, an insight on control strategy of AMR transmission in water could be provided.

## 2.2 AMR transmission routes in water

AMR transmission occurs when ARG carrying mobile genetic elements (MGEs), or its host spread and infect other hosts [19]. To clearly identify transmission routes, the S-P-R paradigm is employed, where source (S) is the reservoir of antimicrobial resistant organisms/genomes, pathway (P) is the media of the event and receptor (R) is what receives AMR transmission from source via pathway [20]. Besides, S-P-R paradigm should be highly non-linear as shown in Figure 2.1, as receptors could be the sources in different pathways and vice versa. To enhance understandings on the transmission mechanism and impacts of influencing factors, S-P-R loops are depicted to be linear processes.

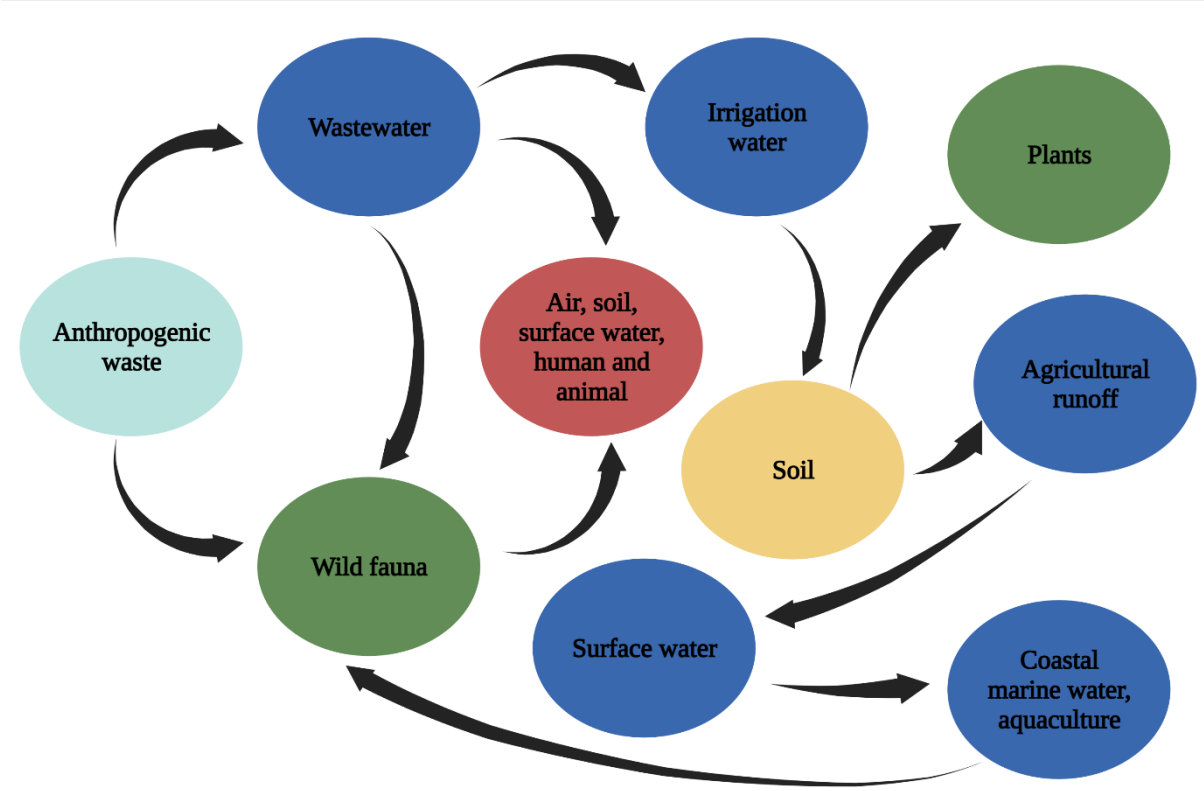


Figure 2.1 Illustration of loop shaped SPR paradigm.

External factors that can have an impact on AMR transmission routes are also discussed, which include disease pandemic (e.g., COVID19), and anthropogenic pollution (e.g., microplastics). To further understand the impacts, it is important to understand AMR dissemination mechanisms in the genetic levels [21,22]. Currently, there are three main ways including:

1) Classical mutation: an intrinsic spontaneous mechanism that modifies selected genes, resulting in alternative transcription of antibiotic targets and reduces the effects of antibiotics [23]. Also known as vertical gene transfer (mother cell to daughter cell). Reports also have shown that reactive oxygen species generated from sub-inhibitory concentrations of antibiotics can induce this mutagenesis [24].
2) Horizontal gene transfer (HGT): a phenomenon where ARGs are transferred between pathogens either via mobile genetic elements (MGEs) such as plasmids (conjugation) and phage (phage transduction) or via

direct uptake of exogenous DNA from the surrounding environment (transformation) [25].

3) Adaptive response: an intrinsic cellular property or regulatory circuit, where stressors in the environment (e.g., addition of antibiotics) can induce changes in stochastic properties such as permeability and gene expression [26].

External factors impact on the AMR dissemination by encouraging the mechanisms as mentioned above. Most external factors affect AMR transmission in one or two ways, such as overuse of disinfectants during pandemic encourages microorganisms to have adaptive response [5]. And there are examples where external factors influence AMR transmission in all three ways. Microplastics can enrich organic chemical compounds e.g., antimicrobial reagents as well as microorganism colonies, leading to the formation of 'plastisphere' and this phenomenon induces mutagenesis, contributes to HGT and changes the living environment and thus induces adaptive responses [21]. When considering AMR conditions in the environment, the S-P-R paradigm needs to be clearly identified and influencing factors should also be taken into account.

### 2.2.1 Fundamental SPR paradigms in the environment

#### 2.2.1.1 Main sources

It was found that higher human activities tend to result in higher AMR rates [27] e.g., rural antifungal resistance is much less detected than urban one [28] and commercial costal water (i.e., bathing beaches) tends to harbour a higher frequency of ARB than non-commercial one [29]. Studies have also found that higher population of human will result in higher load of both antimicrobial reagents and ARGs in the wastewater [30–32]. Since human wastes are mostly emitted to the environment in the form of wastewater, wastewater is then considered to be the main source of AMR transmission. Hospital effluents [33–35] also present to be sources of antimicrobial reagents and pathogens which might not have a consistent effect on AMR transmission in the environment after emitted. This is

possibly because AMR is already well developed in the wastewater treatment plants (WWTPs) and therefore no longer further develop during transmission [36].

Extreme weathers such as storms can lead to drain outfalls, can lead to leakages in wastewater pipes. Sewage can then leak and overflow into urban streams (estuaries) and finally discharge into bathing waters or even oceans [37], resulting in the dissemination of AMR [38]. Fortunately, ARB from fresh water and faeces are likely to die off rapidly in the marine environment [39]. As in the case of fresh water, the range and persistence of contamination is affected by flow rates, temperature, and other environmental conditions – Young et al. [40] found that ARGs from sewage spill tend to disappear from water and sediment in two weeks.

Untreated wastewater, if used as irrigation water, will transmit antimicrobial resistant microorganisms e.g., bacteria to soil [41]. On the other hand, during heavy rains, agricultural runoffs can in turn transmit AMR to surface water e.g., rivers.

Besides, it is worth mentioning that different treatment options of wastewater can have contrary effects on AMR. It seems that treatment methods with higher removal efficiency of antibiotic reagents tend to perform worse in case of removal of ARGs and vice versa [30].

#### 2.2.1.2 Pathways

Except for river confluence, wildlife presents to be an important pathway for AMR transmission. Close contact with human area predisposes the transmission of AMR genes to wildlife e.g., hedgehogs [42]. Wild fauna, e.g., cockroach, toads, rats and anoles, can spread AMR from WWTPs [43] and invertebrates such as earthworm from livestock manure [42] to the surrounding areas e.g., domestic animals [43]. Migratory wild birds, e.g., sedentary seagulls are thought to carry and spread resistant bacteria – although there is only limited evidence, it seems to be reasonable deduction [44]. Reynolds et al. [38] found that seagulls can contaminate bathing water (e.g., beaches) as well as coastal waters [45]. Besides, in areas which are less accessible by human, AMR transmission is still prompted by wildlife. Faecal samples of 49 wild rabbits were examined in Tunis and results

found that they contain multiple ARB, which could potentially contribute to AMR spread [46].

When considering AMR transmission in the environment, air is the least studied area as it is generally not suitable for bacterial growth [47], however, studies also show its potential acting as a non-negligible pathway e.g., via bioaerosol. In addition to wildlife, air can also disseminate AMR to the surrounding areas [43]. Research shows that broiler farms, especially the litter samples inside, contaminate the surrounding area through air pathway [47]. However, the bacterial load is affected by multiple factors: it decreases with distance to the farm, and season also plays an important role as it will impact on light exposure, temperature and dehydration status [47].

#### 2.2.1.3 Receptors

Other than water, soil also acts as a main AMR reservoir in the environment, especially those applied with manure which usually contains various enteric bacteria and ARGs. Plants can therefore acquire AMR from soil both through roots (internal pathway) and through aerosol (external pathway) [48]. The accumulated AMR can pass along food chain when plants are ingested by human and/or animals) [49]. Although some treatments e.g., land application [50] are available to remove ARGs from manure, the bioaerosols (i.e., airborne biological particles including fungi, bacteria etc.) generated during the process can concentrate ARGs, leading to their spread though air pathway, both upwind and downwind. Besides, with marine environment, ARB can infect human both via direct contact (recreational costal water) and via food chain when people consume seafood [39].

### 2.2.2 External factors influencing AMR transmission in the environment.

#### 2.2.2.1 COVID19 pandemic

The pandemic exacerbates the AMR situation, as the increase in empirical antibiotic use [51] as well as disinfectants, alcohol-based hand sanitisers, and

antiseptic hand wash [52] further select resistant bacteria. Besides, the abuse and inappropriate disposal of chemicals added on extra selection pressure to the environmental microorganisms.

Mis-prescribing of antibiotics to COVID patients was also reported during the early stage of the pandemic, which also accelerates the development of AMR [53]. Studies were also carried out to investigate faecal ARGs alterations in COVID-19 patients who were expose to empirical antibiotics [54], and the results showed that antibiotic treatment significantly increased the ARGs abundance in intestinal flora of COVID-19 patients, resulting in striking alterations of the ARG profiles composition.

#### 2.2.2.2 Anthropogenic pollution

Heavy metal pollution is considered as a co-selection factor of AMR, and studies have shown that increased AMR rate was observed with cattle continuously exposed to heavy metal contaminated water in the farm [55].

Plastic pollution has long been a big environmental concern. Microbial community can colonise on microplastic beads forming a biofilm which is termed ‘plastisphere’. Studies have shown that plastics associated with sewage pollution can facilitate survival and dissemination of bacteria and related ARGs when compared to naturally occurring substrates such as seaweeds and sand [56,57]. Besides, microplastics can escape from WWTPs while the effect of disinfection (ozone disinfection) is debatable - it promotes selection while it also reduces bacterial count. Galafassi et al. [58] found that the disinfection process through ozonation had no impact on the concentration and the characteristics of microplastics, the composition of the bacterial community of the plastisphere, and the ARGs abundances on microplastics.

In addition, microplastics can also persist in soil [59]. It is shown that microplastics can select the bacterial community colonised on them and enrich antimicrobial reagents to its pore surface, leading to higher rate of AMR compared to soil microbiota as HGT is encouraged [58].

## 2.3 Rapid detection methods of AMR in the environment

As aforementioned, there are various detection approaches for AMR, and they are mainly classified into two types: phenotypic and genotypic approaches. While the former focuses on the macro microorganism scale, the latter focuses on the detection on the gene level, i.e., ARGs. Phenotypic detection, also known as antimicrobial susceptibility testing (AST), confirms the resistance via bacterial growth in the presence of antibiotics. To quantitatively determine the susceptibility, the concept of minimal inhibitory concentration (MIC) was introduced, and it is defined as 'the lowest concentration of an antibacterial agent expressed in mg $L^{-1}$ which, under strictly controlled *in vitro* conditions, completely prevents visible growth of the test strain of an organism' [60]. MICs determination approaches include broth dilution [61], antimicrobial gradient [62], and disk diffusion tests [63]. With the advancement of technology, automated instrument system was enabled to reduce the labour, minimise manual errors and standardise end-point readings in a shorter time. [64] Besides, various commercial kits such as Etest® (BioMérieux) have been developed for easy and simple AST tests while compromising the flexibility in testing. These AST methods are featured by their cost-effectiveness, reproducibility in results, well-established results interpretation primarily from the European Committee on Antimicrobial Susceptibility Testing and the American Clinical and Laboratory Standards Institute [65]. However, they are also time- and labour-intensive, with no information/insights related to gene or AMR mechanisms given. Therefore, it is rarely used in the environmental samples – it would be even more tedious to isolate and culture one specific bacteria in the environmental samples which contain various microorganisms.

On the other hand, genotypic detections, also known as molecular detection approaches, could not only compensate for the phenotypic detections by providing information on ARGs and related mechanisms in shorter time, but also act as a more suitable approach for metagenomic detection [66]. Typically, molecular detection approaches of AMR include four different methods: nucleic acid amplification testing (NAAT), hybridisation, sequencing and immunoassays.

PCR has been regarded as gold standard of molecular detection due to its excellent robustness, sensitivity, and specificity [67]. However, expensive equipment and laboratory set-up is needed for PCR, and this limits its application in resource limited areas. Nevertheless, NAAT has its intrinsic flaws as genotypes do not always indicate to phenotypes, and only known genes or mutations can be detected: both of which limit its application in field [68]. However, the expression of ARGs (i.e., phenotypes) sometimes is not fully represented by the presence of genes. Furthermore, it is necessary to continuously update and adapt programs and related databases to understand the resistance mechanisms and characterize the possible AMR threats, which is not always feasible [68]. Under this circumstance, subsequent developments of isothermal amplification techniques such as loop-mediated isothermal amplification (LAMP) [69] and recombinase polymerase amplification (RPA) [70] offer rapid, simple, sensitive and specific detection approach for ARG detection, while still trained personnel is required to operate the assay and analyse the data. To better suit the POU purpose, in addition to NAATs, end-point detection approaches have advanced [71] e.g., by integrating with lateral flow strip [72].

Antimicrobial agents are widely used in agriculture, aquaculture, livestock farming, human and veterinary health centre, and clinics, resulting in its extensive pollution to the environment especially water [73]. Since antimicrobial reagent can prompt AMR development at concentrations as low as ng $mL^{-1}$ under laboratory conditions [74], it is also vital to tackling AMR. Conventional detection methods of antimicrobial reagent include microbial inhibition screening, chromatography/mass spectrometry, and immunoassay such as enzyme-linked immunosorbent assay (ELISA) [75–79]. While they are cost-effective and robust, they are time-consuming, with unsatisfying sensitivity and accuracy. Later-developed analytical instruments such as high-performance liquid chromatography (HPLC) and liquid chromatography mass spectrometry (LC-MS) offer ultrasensitive detection, but they require laboratory setups with expensive and sophisticated equipment [80–84].

With the advancement of analytical chemistry and biotechnology, there are various bioassays developed to realise POU detections for ARGs and antibiotics

in the environment. In addition to assays, microfluidics, first proposed in 1970s, is regarded to be a platform accommodating assays to address POU issue [85] and Figure 2.2 shows example schematics of microfluidic devices in AMR detection [86–88]. Microfluidic devices are able to be integrated with both phenotypic and genotypic AMR detection. By combining with microfluidic devices, the volume of reaction and assay turnaround time are significantly reduced [89]. In particular, single-cell-based AST has emerged as effective technology to combat AMR, as the direct analysis of single cell eliminates the need for culturing [90]. Most single-cell-based AST works by optically monitoring the morphological changes (e.g., cell area and shape) of cells under antibiotics, which involves the process of trapping cells on microfluidic chips. For example, Li et al. [91] reported an adaptable microfluidic chip which was suitable for different sizes of cells. This was achieved by the tuneable on-chip valves that were able to apply different pressures onto the parallel chambers. The proposed microfluidic chip was able to distinguish different bacterial pathogens in various sample matrices including urine, blood cultures and whole blood samples. Besides, a pilot study was conducted and results showed a sensitivity of 100% and specificity of 83.33% for pathogen classification and achieved 100% concordance for AST.

In addition to integrating with AST, microfluidic devices can also integrate with NAAT for ARG detection. For instance, Trick et al. [92] proposed a PCR-based portable magnetofluidic platform to detect *Neisseria gonorrhoeae* and its susceptibility to ciprofloxacin. As the rapid PCR could be achieved via elevated reaction kinetics (e.g., increased primer, DNA polymerase and $Mg^{2+}$ concentration) and optimized design of heat block geometry to reach quick temperature cycling, the developed microfluidic device was able to perform DNA extraction, PCR, results analysis within less than 15 mins. Finally, penile swab samples were collected from sexual health clinics in Baltimore, MD, USA and Kampala, Uganda, and the results demonstrated an overall sensitivity and specificity of 97.7% and 97.6%, respectively, as well as a 100% concordance with culture results for ciprofloxacin resistance.

Moreover, since the thermal cycling process requires much energy, isothermal amplification seems to be a better choice to integrate with POU microfluidic

devices. Ma et al. [93] reported a colorimetric LAMP-based self-driven microfluidic device that was portable, automated and user-friendly. The methicillin-resistant *Staphylococcus aureus* bacteria was employed as demonstration for bacteria detection, with a LOD of 30 CFU per reaction. The whole process was completed within 40 mins. Furthermore, Kalsi et al. [94] developed a fluorescent RPA-based programmable digital microfluidic assay to simultaneously detect three ARGs, CTX-M-15, KPC and NDM-1. Electronic control was utilised to mix the droplets of RPA assay in the microfluidic device. The turnaround time (i.e., 25 min) was significantly reduced to half of the time needed for benchtop assay, with a LOD of 10 copies.

Among all microfluidic devices, paper-based microfluidic analytical device (μPAD), e.g., lateral flow assay (LFA), stands out due to its ubiquitous and affordable paper substrate. Besides, there are also other merits. Paper is lightweighted, and therefore it is suitable for mass production and easy for transport and storage. The cellulose nature of paper results in its intrinsic capillary action, internally driving the movement of fluid without the need for extra energy source. Moreover, cellulose is also compatible for biomolecules (e.g., aptamers and antibodies) modification, allowing for extensive assays to be integrated. Furthermore, used paper can be disposed readily via combustion, without risks of biohazardous contamination [10,95,96]. Overall, the past two decades have witnessed the flourishment of μPAD in POU detection since its first report in 2007 [97]. μPAD has been reported to incorporate various detection methods, for example, fluorescence [98], colorimetry [99], Raman spectroscopy [100] and electrochemistry [101].

As a portable, rapid and simple device, there is an emerging trend of employing μPAD for onsite AMR testing, with lab and real samples detected to demonstrate its versatility and robustness even in complex matrices including both clinical and environmental samples. For example, He et al. [102] reported a laser-patterned μPAD for colorimetric detection and antimicrobial resistance susceptibility testing of four antibiotics i.e., amoxicillin, ciprofloxacin, gentamicin and nitrofurantoin against *Escherichia coli*. Artificial urine spiked with *E. coli* was employed as samples, and results showed comparable performance to conventional disk

diffusion susceptibility testing, demonstrating the robustness of this POU device. Besides, Boehle et al. [103] proposed a µPAD integrating a colorimetric detection of β-lactamase-producing *E. coli* in river water and sewage. The LOD was determined to be $3.8 \times 10^6$ CFU $mL^{-1}$. And the antimicrobial resistance in various species of bacterial isolates e.g., *Chromobacterium violaceum* was also identified, further illustrating the applicability of the developed device. Finally, all results were confirmed with reference to traditional culturing methods, AST, and PCR analysis.

In addition to phenotypic susceptibility testing, researchers also proposed µPADs to integrate with NAAT for ARG detections. Choopara et al. [104] reported a fluorometric LAMP-based µPAD for the detection of methicillin-resistant *Staphylococcus aureus* (MRSA) (i.e., *mecA* gene). The results showed an LOD of 10 ag (equivalent to 1 copy) of *mecA* as well as a specificity of 100% within 36−43 min in both pristine and clinical samples. Finally, the developed µPAD 35-day stability when storied at 25 °C. Furthermore, Mao et al. [105] reported a fluorescent and LFA based LAMP coupled CRISPR/Cas portable device for the rapid and visual detection of macrolide resistance gene *ermB* in wastewater. The LOD was $2.75 \times 10^3$ copies $\mu L^{-1}$. Besides, the real sample detection results of both fluorescent biosensor and LFA were verified with gold standard qPCR and showed 100% detection rate.

Table 2.1 below shows the examples of AMR detection mentioned in the previous text. Although most current research focuses on the application in clinical areas, there is an emerging recognition of applying the technology for environmental surveillance.

Table 2.1 Summary of examples of AMR detection.

| Detection approach | Target | Sensitivity | Matrices | Ref. |
|---|---|---|---|---|
| lateral flow immunoassay (LFIA) | VanA-producing *enterococci* | $6.3 \times 10^6$ CFU per test (MH plates) and | Buffer | [72] |

| | | | | |
|---|---|---|---|---|
| | | $4.9 \times 10^5$ CFU per test (ChromID VRE plate) | | |
| bead-based microfluidic device integrating fluorophore-labelled rolling circle amplification products | Influenza and Ebola RNA | < 0.5 fM | Buffer | [86] |
| Vacuum-loading microfluidic device for rapid screening for bacterial antibiotic susceptibility | *Escherichia coli* KRX cells | N/A | Urine sample | [87] |
| Fluorescent multi-volume microchamber-based microfluidic ($MVM^2$) platform | *E. coli* 541-15, ileal mucosa, bovine mastitis, the MCF-7 human breast cancer cell line and a *Saccharomyces cerevisiae* strain | N/A | Buffer | [88] |
| Single-cell based AST on | *S. epidermidis, M. bacteremicum, and E. coli* | N/A | Urine, blood cultures | [91] |

| | | | | |
|---|---|---|---|---|
| an adaptable microfluidic chip | | | and whole blood samples | |
| PCR-based portable magnetofluidic platform | *Neisseria gonorrhoeae* and its susceptibility to ciprofloxacin | 97.7% | Penile swab samples | [92] |
| Colorimetric LAMP-based self-driven microfluidic device | Methicillin-resistant *Staphylococcus aureus* bacteria | 30 CFU per reaction | Buffer | [93] |
| Fluorescent RPA-based programmable digital microfluidic assay | *CTX-M-15, KPC* and *NDM-1* | 10 copies | Buffer | [94] |
| Colorimetric laser-patterned µPAD | AST of amoxicillin, ciprofloxacin, gentamicin and nitrofurantoin against *Escherichia coli* | N/A | Spiked artificial urine sample | [102] |
| Colorimetric µPAD | β-lactamase-producing *E. coli* | $3.8 \times 10^6$ CFU $mL^{-1}$ | River water and sewage | [103] |
| Fluorometric LAMP-based µPAD | *mecA* | 1 copy | Buffer and clinical samples | [104] |

| | | | | |
|---|---|---|---|---|
| Fluorescent and LFA based LAMP coupled CRISPR/Cas | *ermB* | $2.75 \times 10^3$ copies $\mu L^{-1}$ | Wastewater | [105] |

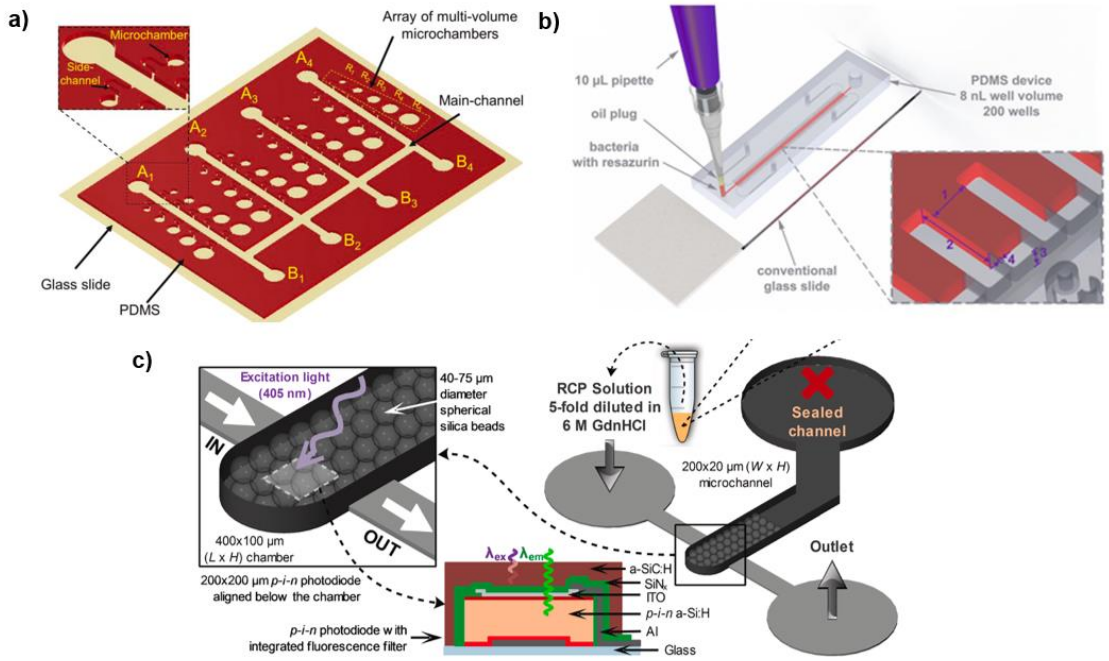


Figure 2.2 Schematics of AMR (including ARG and antibiotics) detection using different type of microfluidic devices. a) Biological small-molecule assays using gradient-based microfluidics b) Microfluidics for antibiotic susceptibility testing c) Silica bead-based microfluidic device with integrated photodiodes for the rapid capture and detection of rolling circle amplification (RCA) products in the femtomolar range. Reprinted from [86–88].

### 2.3.1 Antimicrobial resistant gene detection

Advancement in modern technology in biology, chemistry and materials has enabled NAAT to improve on performances and integrate with rapid end-point approaches e.g., µPAD for onsite testing of infectious diseases and AMR [106–109]. Besides, NAAT has been widely operated with reliable sensitivity and specificity[110].

PCR is the gold standard of NAAT detection of AMR, which has been employed by multiple studies especially in high throughput screening of ARGs in environmental samples [111–115]. In general, PCR is carried out in thermocyclers with multiple thermocycles e.g., 40, for target amplification. Briefly, in each cycle, there are three stages in PCR amplification: denaturation, annealing and extension, as shown in Figure 2.3. Firstly, the double stranded template is denatured to be two separate single strands at 95 ºC. Then, primers anneal to the single strands at a lower temperature, e.g., 55 ºC and finally the new DNA strands extend at a higher temperature, e.g., 72 ºC.

One of the key aspects of successful real-time quantitative PCR (RT-qPCR) assay is the design of primers and dual-labelled probes. Generally, the length of the primers is mainly from 15-30 nt, and the two primers should be of comparable length (difference < 3 nt). GC%, i.e., the percentage of guanine and cystine in the sequence, should be in the range of 40-60% to maintain a stable while kinetically active structure. Tm, i.e., the melting temperature of the primers should be between 50 ºC and 58 ºC for optimal thermodynamic performance, and the two primers in a pair should have a difference in Tm less than 5 ºC. As for the dual-labelled (fluorophore-quencher) probe, the length should be less than 30 nt, GC% from 40-60%, while its Tm should be 5-10 ºC higher than its paired primers. The amplicon size should be in the range of 70-200 bp with a GC% of 30-80% [116].

Dual-labelled probe is not the only method for PCR result characterisation, fluorescent DNA-binding dye such as EvaGreen (Fisher Scientific, UK) can also be used to fluorescently monitor PCR process. However, DNA-binding dye shows less specificity in sequence as it emits fluorescence when it intercalates with dsDNA, no matter what the sequence is; while dual-labelled probe only anneals to its complementary sequence and represents fluorescence, leading to improved false-positive issues.

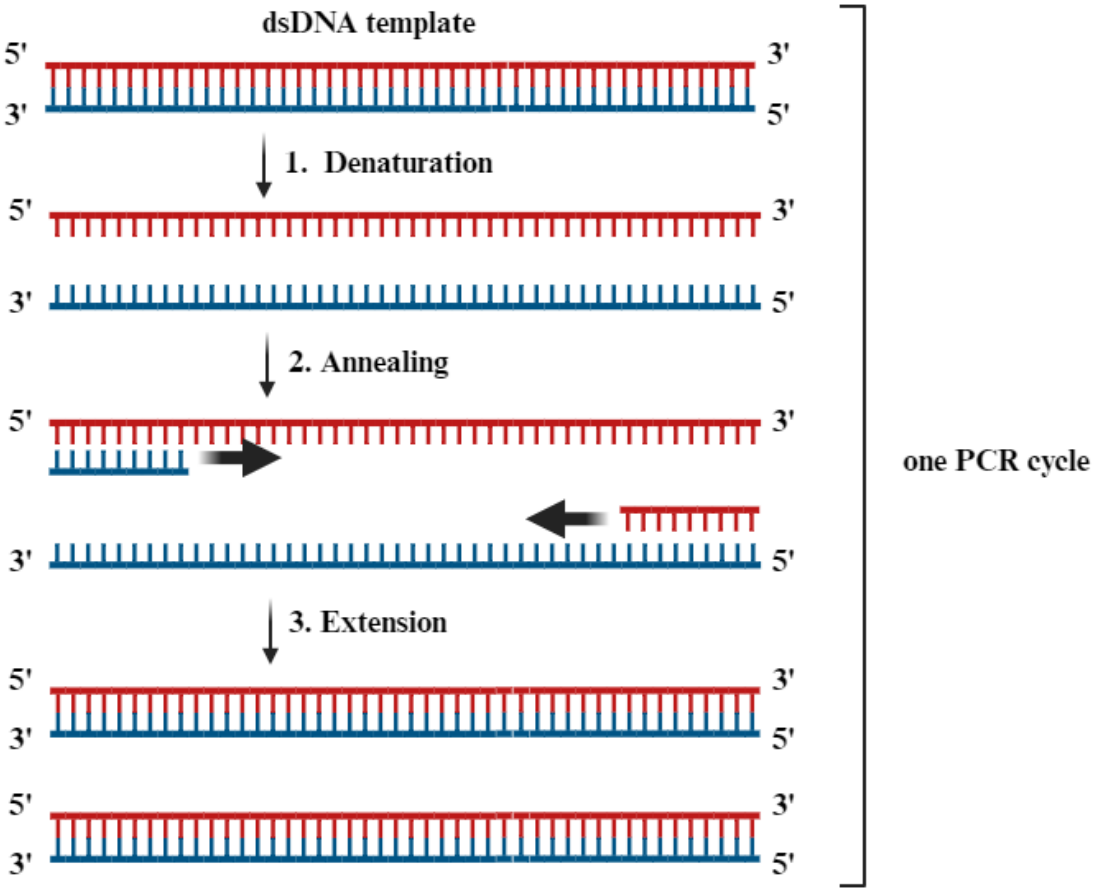


Figure 2.3 Schematic illustration of one PCR cycle.

On the other hand, isothermal amplification is more suitable for POU testing in resource-limited settings, as it only requires simple condition to perform without the need for complicated thermal cycling and expensive equipment [117]. Currently, there are a few isothermal amplification methods available including LAMP, RPA and rolling circle amplification (RCA).

LAMP, first proposed in 2008 [69], is one of the most employed isothermal amplification methods and has been discussed in various papers [117–120]. LAMP is performed via the employment of 4-6 different primers identifying 6-8 different regions of the target sequence, as well as a DNA polymerase which also has the displacement activity. The amplification mechanism of LAMP is as shown in Figure 2.4. Briefly, the whole process is composed of two phases, initial and cyclic amplification phase. During the initial phase, the strand displacement reaction is initiated by the hybridisation between F2 of FIP and F2c of template under the

presence of Bst DNA polymerase. With primer annealing and strand displacements, an intermediate structure (i.e., the dumbbell structure), of the template is formed. When progressing to the cyclic amplification phase, the previously formed dumbbell structure is further amplified by primers, leading to a mixture of DNAs of different lengths. This repeated expansion produces numerous dumbbell structured DNA sequences, resulting in the exponential amplification of the template DNA [118]. LAMP is therefore featured by its excellent specificity, sensitivity and amplification efficiency, with $10^9$ copies of the target sequence generated in less than 1 hour at 60 - 65 °C. The final products are stem-loop nucleic acids with different number of inverted targets repeats and could be detected either endpoint or real-time [96].

Despite LAMP being a sensitive, specific, and highly efficient isothermal amplification technique, the difficulty in LAMP primer design has long been a huge challenge. Although there are two main software for LAMP primer design, significant empirical primer optimisation is usually required [121].

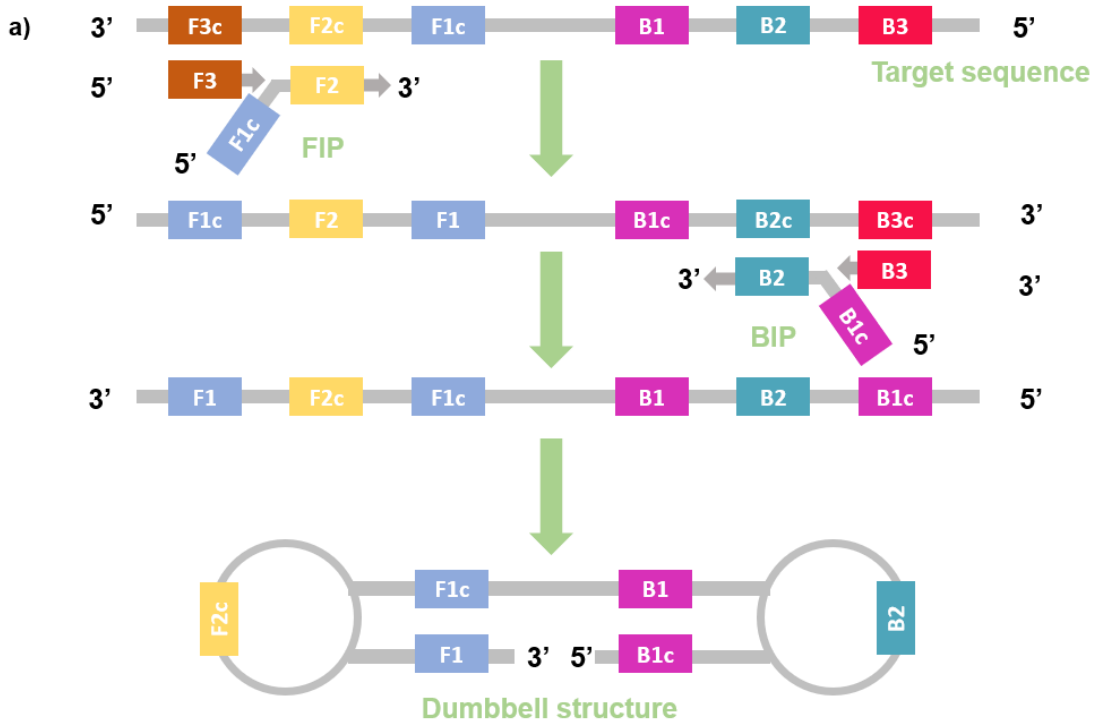

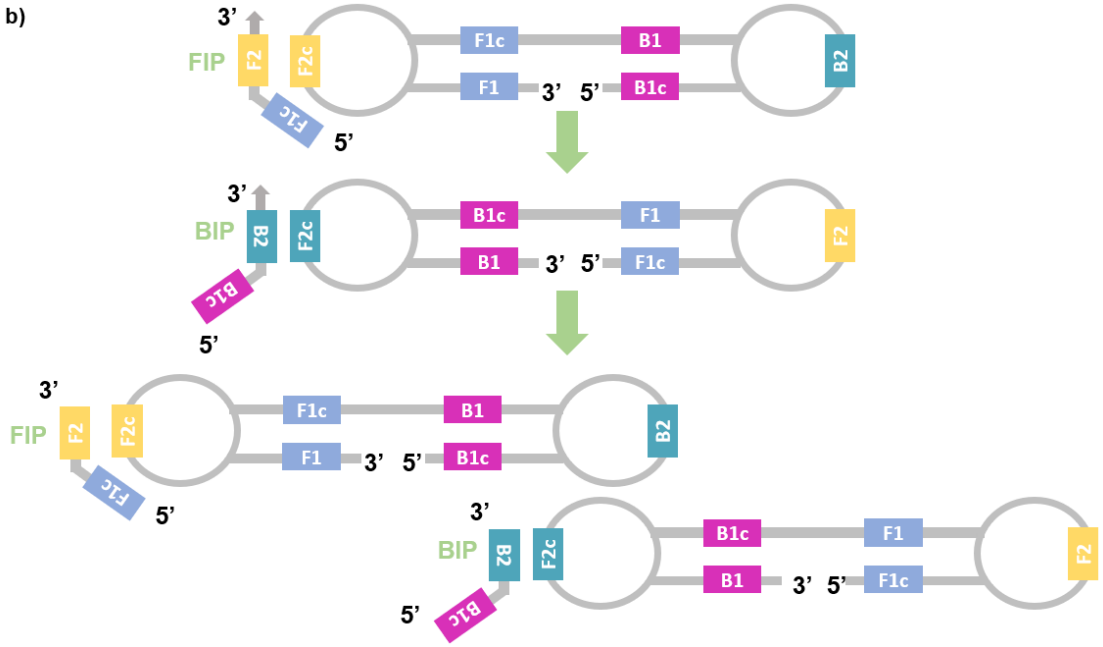


Figure 2.4 Schematics of LAMP amplification mechanisms. a) Initial phase where dumbbell structured intermediates are generated. b) Cyclic amplification phases where DNA template is exponentially amplified. F1c, F2c, B1c, B2c is complementary to F1, F2, B1, B2, respectively.

Stedtfled et al. [122] reported LAMP assays to quantify the mobile genetic element class 1 integron-integrase gene (intI1) against universal bacteria 16S rRNA gene. IntI1 is an indicator gene that could be used to represent multiple ARGs, and normalisation of target markers to 16S rRNA gene is a routine implementation for relative abundance calculation. Experiments were conducted in river and lake samples, and the results showed that there was a significant Pearson correlation between the intI1 gene LAMP assay and ARG relative abundance from qPCR results. This result remained even when experiments were performed by "untrained" personnel who were volunteer undergraduate students at a local community college using a hand-held real-time DNA analysis device - Gene-Z. Overall, the proposed LAMP assay was validated to perform excellent to onsite monitor environmental samples without specific pre-training.

In addition, LAMP is also widely integrated with device for ultrasensitive and specific detection. For example, Suea-Ngam et al. [123] developed an *in situ* colorimetric μPAD based on silver nanoplates integrated with LAMP for the

detection of Methicillin-resistant *Staphylococcus aureus* (target mecA gene). The visible colour change could be observed (red when targeting DNA amplicons present and yellow when absent), while quantitative analysis can also be achieved via a smartphone camera. The result could be obtained within 30 minutes with a LOD of a single copy. It showed the potential to be developed into a versatile field-deployable POU device for various infectious diseases. Besides, lateral flow assay can also integrate with LAMP for rapid and simple detection. Chen et al. [124] reported a multiplex LAMP integrated with nanoparticle-based lateral flow biosensor for the detection of all *S. aureus* species and identification of methicillin-resistant *Staphylococcus aureus*. The LOD of the multiple-LAMP assay for genes responsible for resistance i.e., femA and mecA detection was 100 fg per reaction with a 100% specificity. The whole process including template preparation and gene identification was completed within 80 mins without cross-reactions to non-*S. aureus* strains. Moreover, Meng et al. [125] reported a multiplex real-time LAMP-based microfluidic device which discriminated *Staphylococcus aureus*, *Staphylococcus epidermidis*, *Staphylococcus haemolyticus*, and *Staphylococcus hominis.* Their methicillin resistance was predicted by targeting the mecA and femA genes within 70 min. The LODs for *S. aureus*, *S. epidermidis*, *S. hominis*, and methicillin-resistant *S. aureus* were 20 CFU per reaction, and for *S. haemolyticus* was 200 CFU per reaction. A total of 102 positive cultures of cerebrospinal fluid and mixed cultures were tested and readily identified with the portable, rapid, accurate, and easy to use device. Except for nanoparticles, transition metal complexes have also been reported to integrate with LAMP. Hassan et al. [126] reported a colorimetric LAMP assay for detection of mcr-1, blaKPC (KPC-1 to KPC-4 alleles), blaOXA-48, blaOXA-23 and blaVIM (VIM-1 and VIM-2 alleles) genes from *Escherichia coli, Klebsiella, Salmonella enterica* and *Acinetobacter*, which was demonstrated with pond water samples. The developed assays were 100 % sensitive and specific with a LOD of 0.0625 µg $mL^{-1}$ and 10 CFU $mL^{-1}$ for genomic DNA and spiked bacterial cells, respectively, within 1 hour.

Moreover, there are also reports demonstrating the feasibility of RPA and RCA integrated POU detection of AMR. RPA is an isothermal NAAT whose

amplification mechanism is similar to that of PCR, as shown in Figure 2.5. While PCR utilises thermal cycling to achieve strand displacement, annealing, and extension, RPA reaction occurs at a constant temperature of 37 – 42 °C. In an RPA assay, to realise strand displacement at a temperature below melting point, a recombinase-primer complex under the condition of ATP and crowing agents (e.g., high molecular weight polyethylene glycol) is formed and invades into the double strand of the DNA template. In addition, the presence of single-stranded binding proteins that bind to the displaced strand further stabilises the denaturation step. Then the DNA polymerase binds to the primer and starts the strand extension after recombinase-primer complex disassembles. The whole process is finally repeated for exponential amplification. As most DNA amplification strategies, such as PCR and LAMP, magnesium ion ($Mg^{2+}$) plays a key role for amplification initiation. And in RPA, the concentration of $Mg^{2+}$ is a crucial parameter to optimise for improved amplification efficiency [127].

Basic RPA reactions are featured by DNA intercalating dye or gel electrophoresis, which either suffer from false positive results due to off-target binding or is labour- and time- intensive to carry out, and both limit RPA's application in multiplexing and rapid field tests [127]. RPA amplicons can be detected both in real-time and endpoint. Real-time fluorescent monitoring is achieved via DNA-intercalating dye e.g., EvaGreen as mentioned or via fluorescent probes. While the former is of the same principle as PCR, the latter requires an extra DNA repair enzyme Exonuclease III that cleaves the fluorescent probe at the dSpacer site, separating fluorophore and quencher, and therefore leading to the fluorescence emission. However, Exonuclease III can result in DNA degradation, and therefore the amplicons are not liable for gel electrophoresis for further validation. Other endpoint detections such as voltametric approaches [128] and lateral flow assays [129] are reported to be widely applied for RPA amplicon monitoring.

Due to the complexity of chemistry in RPA assays, limited research conducted on exploring its underlying chemistry and kinetics [130]. However, recent developments of RPA have evolved to expand its use in wide areas, e.g., pathogens of plants [131] and agricultural products [132], and rabies virus [133]. RPA has also been reported to conjugate with microfluidics for the POU purposes, and

its successful deployment in the Ebola outbreak [134] further validated its robustness in onsite measurements. With the advancements in biotechnology e.g., CRISPR/Cas, RPA-CRISPR/Cas integration is flourishing for potential higher sensitivity and specificity [11], and RPA was utilised as a preamplifier.

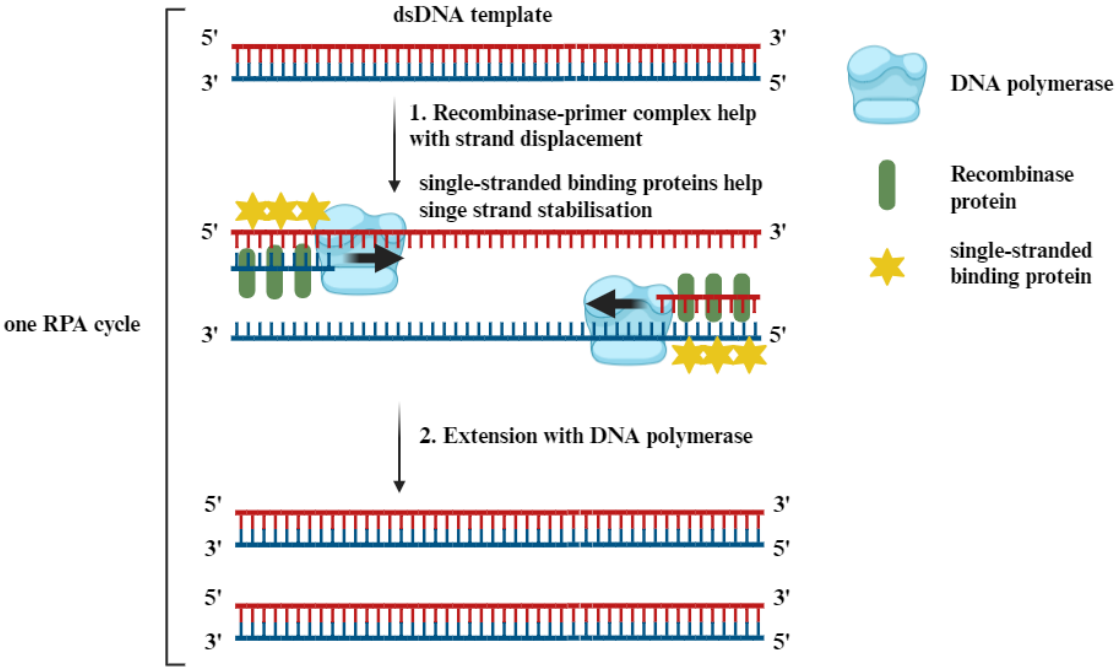


Figure 2.5 Schematic illustration of RPA working principle.

Lin et al. [135] reported an RPA assay integrated with fluorescent and lateral flow dipstick detections for identifying clinically relevant AMR genes retained by *S. aureus* isolates. Results showed an accuracy higher than 92% for 54 collected *S. aureus* isolates. Nakano et al. [136] developed a RPA integrated microbead dielectrophoresis based DNA detection method for bla(CTX-M-15) which is responsible for resistance to extended spectrum beta-lactam antibiotics. A LOD of 2 copies per reaction for pure plasmid and 50 copies per reaction for genomic DNA was reached with a dynamic range up to $10^5$ copies per reaction within 26 min. Solid phase RPA was also developed for ARG detection. Butterworth et al. [137] proposed a modified RPA assay coupled with electrochemical amperometric measurements for the detection of oxacillin genes in *Escherichia coli*. A LOD of 319 CFUs $mL^{-1}$ was reached within 60 min.

In addition, Sollweck et al. [138] reported a flow-based microarray chip to accommodate colony fusion RPA assay for ARG and their carrying species monitoring in surface water of River Lech within 1.5 h. The assay system discriminated *Escherichia coli* colonies between carrying blaCTX-M cluster 1 resistance genes and carrying blaCTX-M genes of other clusters, as well as other bacterial species carrying blaCTX-M resistance genes, such as *Klebsiella pneumoniae*.

As for RCA, it is an isothermal enzymatic process that usually composed of four components: DNA polymerase, a short primer, a circular DNA/RNA template, and dNTPs at 37$^{o}$C. The key of RCA is the formation of a circular DNA/RNA template (usually 15-200 nt) which is either synthesised enzymatically or chemically. The enzymatic formation takes place when a DNA or RNA primer is annealed to a ssDNA template, forming a circular complex, while the chemical one is through intramolecular ligation between phosphate and hydroxyl groups [139].

Based on the circular DNA template, linear DNA or RNA products can therefore further be generated with primer and the pre-made circle. In addition to linear DNA product formation, there are also strategies called 'multiprimed RCA' [140] and 'hyperbranched RCA' [141] , where DNA or RNA products are formed exponentially, as shown in **Figure 2.6**. Those two methods can be combined, and in this way, the detection limit can be further improved even to single molecule [140].

There are various detection approaches of RCA amplicons. End-point methods such as gel electrophoresis as well as real-time fluorescent detection including fluorophore-conjugated dNTP during RCA and hybridisation of fluorescent complementary probes are widely used [139]. Although RCA presented to be a highly sensitive isothermal detection approaches, it suffered from certain challenges. For example, due to its non-linear amplification kinetics and complicated DNA structure formation, the scalability of RCA is also an issue to be addressed [142]. Nonetheless, it remains to be an obstacle to obtain high-purity circular templates in large quantity, which inhibits the RCA efficiency. Besides, the storage of RCA products tends to be challenging as they might aggregate due to non-specific inter- and intra-molecular crosslinking [139].

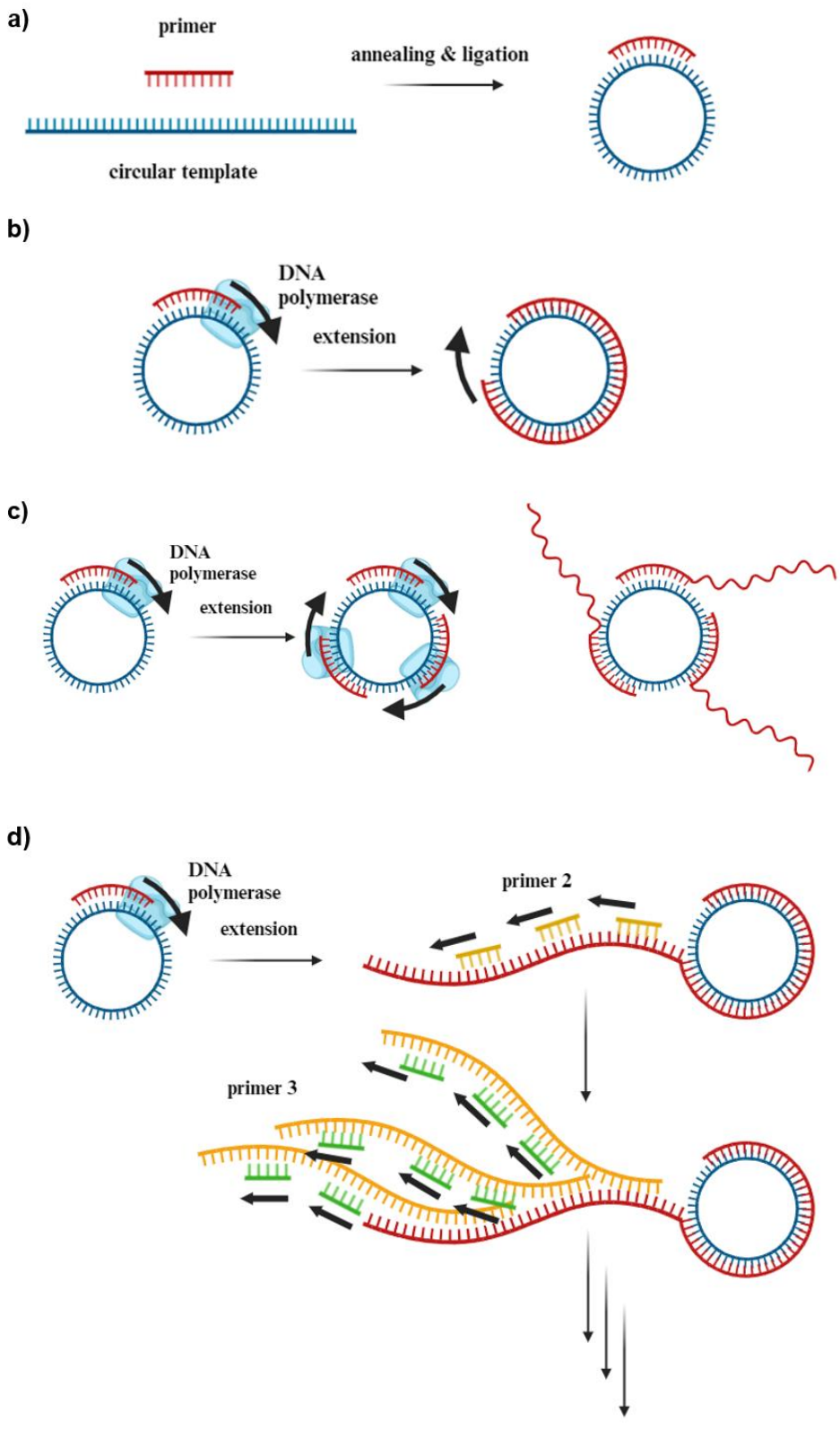


Figure 2.6 Schematic illustration of RCA working mechanism. a) Formation of circular DNA product via ligation between circular DNA template and primer. b) Linear DNA product formation from the circular DNA product and the primer with

the aid of DNA polymerase. c) multiprimed RCA where more than one primer can bind to the circular template. d) hyperbranched RCA where circular DNA product was employed as template for further amplification with different primer sets.

Jain et al. [143] reported a colorimetric-readouts platform that can be used in resource-limited settings. It was based on padlock probe rolling circle amplification and nuclease protection, with an end-point lateral flow detection. The assay provides a limit of detection of 1.1 pM target DNA.

Except for conventional optical and electrochemical detections, isothermal amplifications can also couple with sequencing to provide further genetic and mechanistic information. Gilddon et al. [144] proposed a genotyping workflow for *mycobacterium tuberculosis* using RPA and nanopore sequencing on MinION, achieving a sensitivity and specificity of rifampin resistance prediction of 96.3 % and 100%, respectively, and that of isoniazid resistance prediction were 100% and 100%, respectively. Besides, generally speaking, change in pH was also employed in ARG detection. Hu et al. [145] reported a thin-film transistor nanoribbon sensor integrating RPA for the detection of CTX-M and NDM, two genes that confer bacterial resistance to cephalosporins and carbapenems, respectively. Results showed that this sensor could detection < 10 copies of target genes from *E. coli* or *K. pneumoniae* clinical isolates within a few minutes. Moreover, the primer-dimer amplification effect was minimised through the design of a differential readout system. This device therefore held the potential to analyse genes in a cost-effective, portable, and real-time manner.

Table 2.2 shown below summaries the main features, as well as advantages and disadvantages of the four different amplification techniques that are frequently used in gene detection.

Table 2.2 Summary of main features, advantages and disadvantages of the amplification methods.

| Name | Main features | Advantages | Disadvantages |
|---|---|---|---|
| PCR | Each PCR cycle includes three stages | Gold standard for NAAT | Reaction process needs thermal cycling |

| | | | |
|---|---|---|---|
| | (denaturation, annealing, extension)<br>Each stage is conducted at a different temperature<br>Only two primers required | Sensitive<br>Specific<br>Compatible with multiple detection approaches | Limited application for field-based detections |
| LAMP | Formation of a dumbbell structure as an intermediate<br>Involving 6-8 primers per reaction<br>Constant reaction temperature ranging from 60 - 65 $^{o}$C | Isothermal reaction<br>Compatible with multiple detection approaches<br>Suitable for field-based detections | Complicated reaction mechanism<br>Difficulty in primer design and empirical primer optimisation |
| RPA | Recombinase protein complexes with primer to invade into double-stranded DNA under ATP and crowing agents<br>SSB protein stabilises the displaced strand<br>Involving two primers<br>Constant reaction temperature ranging from 37-42 $^{o}$C | Isothermal reaction<br>Simple reaction mechanism similar to that of PCR<br>Sensitive<br>Specific<br>Compatible with multiple detection approaches<br>Suitable for field-based detections | Unclear underlying reaction chemistry and kinetics |

| | | | |
|---|---|---|---|
| RCA | Formation of circular nucleic acid template (enzymatically or chemically)<br>Involving single primer<br>Constant reaction temperature at 37 $^{o}$C (optimal) | Isothermal reaction<br>Sensitive<br>Specific<br>Compatible with multiple detection approaches<br>Suitable for field-based detections | Difficulty in scalability<br>Hard to obtain high-purity circular template<br>Challenges in long-term storage of RCA products |

Advancements in biotechnology such as CRISPR/Cas also contributed to prompting ARG detection, even without amplification. CRISPR/Cas system, short for clustered regularly interspaced short palindromic repeats and CRISPR-associated system, was first found in prokaryotes as RNA-directed adaptive immune systems against invading of viruses or plasmids and was then developed as gene editing tools [146]. With the discovery of trans-cleavage activity of type V Cas enzymes such as Cas12a and cas13, its potential in biosensing and molecular diagnostics has been explored. Briefly, Cas12a enzyme recognise a T-rich protospacer-adjacent motif (PAM) which maturates the sequence-specific guide CRISPR RNA (crRNA), leading to a PAM-distal break on with staggered 5' and 3' end of target dsDNA (cis-cleavage). In the meantime, local ssDNA is non-specifically cleaved (trans-cleavage). Only when cis cleavage occurs, can trans-cleavage take place. Therefore, ssDNA can act as probes to mark the recognition and cleavage of a specific sequence by crRNA and Cas12a. For example, a fluorophore and a quencher can be tagged to 5' end and 3' end of the ssDNA, respectively, to achieve real-time fluorescence monitoring of CRISPR/Cas activity. A schematic illustration is shown in Figure 2.7.

Kasputis et al. [147] reported an affordable, highly specific and sensitive colorimetric CRISPR-Cas12a-based assay. ARGs were detected in washing water collected from a food processing plant. Three representative ARGs were detected with a LOD of 5 nM or lower without pre-amplification. In addition, the assay was able

to detect $10^3$ gene copies in washing water from a fruit washing facility which is a more complex medium. The results suggested that this method can be utilised to monitor and therefore prevent the immense AMR spread among the food supply chain. Deng et al. [148] proposed a one-pot CRISPR-integrated assay for instant and visual detection of *B. pseudomallei*. Reactions were completed in an all-in-one single tube in the hand within 30 minutes. The LODs reached 2.19 copy $\mu L^{-1}$ of plasmid DNA, 12.5 CFU $mL^{-1}$ of *B. pseudomallei*, and 61.5 CFU $mL^{-1}$ of bacteria in spiked blood samples, respectively. 100% accuracy was exhibited in clinical isolates and samples. The proposed system enables rapid and onsite detection of genes in resource-limited settings and is friendly to non-expert end users.

Table 2.3 below summaries the examples of ARG detection described in 2.3.1.

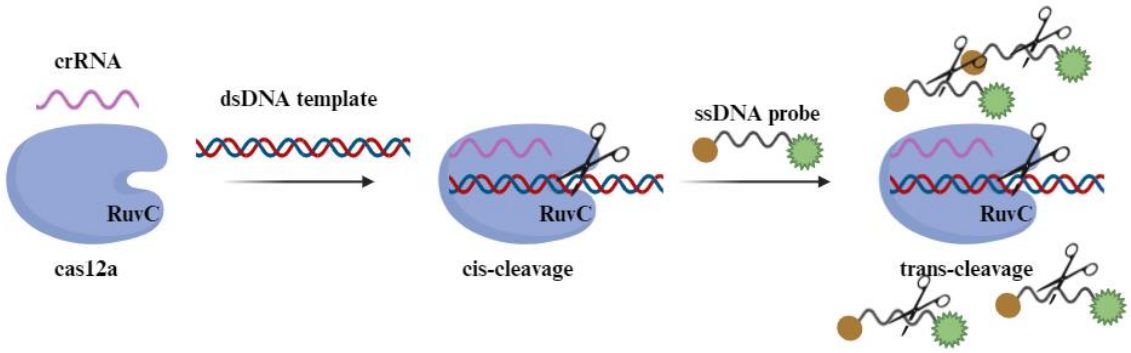


Figure 2.7 Schematic illustration of CRISPR/Cas working mechanism.

Table 2.3 Summary of examples of ARG detection.

| Detection approach | Target | Sensitivity | Matrices | Ref. |
|---|---|---|---|---|
| PCR and gel electrophoresis at 1.5% agarose | *LacZ, uidA* and *int1* genes | N/A | Drinking water from restaurants (n = 18), health center (n = 9), and residences (n = 4) located in Chattogram City, Bangladesh | [111] |

| | | | | |
|---|---|---|---|---|
| PCR and gel electrophoresis at 2% agarose | *csgA* and *iss* gene | N/A | samples (n=114) from dead birds (heart, liver, lungs, and cloacal swab) and surrounding environments such as feeder, drinker, litter, PVC pipe, water tank wall, feed, and water | [112] |
| PCR and gel electrophoresis at 1.5% agarose | *blaTEM , sul1, tetA(A), and aadA1* | N/A | *Aeromonas spp.* from wild Nile tilapia from Lake Manzala and the lake water | [113] |
| PCR and gel electrophoresis at 1.5% agarose | *spiC, pipD* and *int1* genes | N/A | 361 faecal (189), oral (100), environmental (soil (36) and water (27)) and feed (9) samples from different animals (cattle, sheep, goats, pigs, ducks and chickens) from Eastern Cape and KwaZulu-Natal Provinces in South Africa | [114] |

| | | | | |
|---|---|---|---|---|
| PCR and gel electrophoresis | *blaTEM, AmpC, blaGES, blaIMP, blaOXA-48, blaKPC, aadA, strA, aphA1, qnrVC, cmlA1 and catII* genes | N/A | different freshwater sheds in rustic milieu | [115] |
| LAMP assay | *intI1* gene | N/A | River and lake samples | [122] |
| colorimetric PAD based on AgNPls and LAMP | methicillin-resistant *Staphylococcus aureus* (MRSA) (mecA gene) | single target copy $\mu L^{-1}$ | Lysate from bacterialcolonies | [123] |
| multiplex LAMP linked to a nanoparticle-based lateral flow biosensor (m-LAMP-LFB) | femA and mecA genes | 100 fg of genomic DNA template per reaction | whole blood samples | [124] |
| a microfluidic device based on loop-mediated isothermal | mecA and femA genes | LOD of *S. aureus, S. epidermidis*, *S.* | cerebrospinal fluid (CSF) | [125] |

| | | | | |
|---|---|---|---|---|
| amplification (LAMP) | | *hominis*, and *methicillin-resistant S. aureus* were 20 CFU per reaction, and for *S. haemolyticus* was 200 CFU per reaction | | |
| Colorimetric LAMP | *mcr-1*, *blaKPC* (*KPC-1 to KPC-4* alleles), *blaOXA-48, blaOXA-23* and *blaVIM* (*VIM-1* and *VIM-2* alleles) genes | 0.0625 µg $mL^{-1}$ (genomic DNA) and 10 CFU $mL^{-1}$ (spiked bacterial cells) | Tap and pond water samples from a single site in Guildford, Surrey, United Kingdom. | 126 |
| Fluorescent and lateral flow RPA assay | *ermA, ermB, ermC, mecA, blaZ, tetK, tetM, msrA, aadD* | $10^1$ to $10^2$ copies $µL^{-1}$ | clinical samples from patients of the Second Affiliated Hospital of Shantou University Medical College | 135 |

| | | | | |
|---|---|---|---|---|
| microbead based RPA dielectrophoretic impedance measurement (DEPIM) | *blaCTX-M-15* | 2 copies per reaction (pure plasmid) and 50 copies per reaction (genomic DNA) | Buffer | [136] |
| direct-enzyme labelling based solid-phase chronoamperometric RPA | *blaOXA-1*, *tetA*, *aacA4*, *blaCTX-M-15* gemes | 319 CFUs $mL^{-1}$ | Buffer | [137] |
| colony-based fusion and heterogeneous asymmetry chemiluminescent RPA on a flow-based microarray chip | *blaCTX-M* genes | N/A | river water of the river Lech, Augsburg | [138] |
| RCA based lateral flow detection | Beta-lactamase resistance | 1.1 pM | Buffer and cacao leaf extract | [143] |
| RPA based nanopore sequencing workflow | drug resistant *M. tuberculosis* | 96.3% (rifampin resistance prediction) and 100% (isoniazid resistance prediction) | sputum samples of TB patients in KwaZulu Natal, South Africa | [144] |

| | | | | |
|---|---|---|---|---|
| RPA based thin-film transistor (TFT) nanoribbon (NR) sensor (pH change) | *CTX-M* and *NDM* | < 10 copies | human clinical sample from the National Collection of Type Cultures at Public Health England. | [145] |
| Colorimetric CRISPR/Cas assay | *ermB*, *sul1*, and *tetW* genes | $10^3$ gene copies | Washing water from a fruit washing facility | [147] |
| Fluorescent and colorimetric RPA based CRISPR/Cas assay | *B. pseudomallei* | 2.19 copy $\mu L^{-1}$ of plasmid DNA, 12.5 CFU $mL^{-1}$ of *B. pseudomallei,* and 61.5 CFU $mL^{-1}$ of bacteria in spiked blood samples | Spiked blood sample | [148] |

### 2.3.2 Antimicrobial reagent detection

The most common approach of detecting antimicrobial reagent is to employ aptamer or antibody as biorecognition element. Aptamer is a synthetic single stranded nucleic acid that can specifically bind to small molecules or macromolecules and is usually employed as a substitute of antibodies. For example, a paper-based fluorogenic RNA aptamer sensor was developed by Shaifiei et al. [149] to detect tetracycline. It was reported that a dynamic range of tetracycline, 0.1–0.8 mM, can induce 10%–90% of maximum fluorescence, as shown in Figure 2.8. In addition to its relatively high sensitivity, this device also presents high selectivity by distinguishing tetracycline from tobramycin, gentamicin, doxycycline, kanamycin, streptomycin, and ampicillin. It also

presented high specificity and stability after week-long storage at room temperature. Experiments were conducted in the RNase-free buffer, local tap water samples (Amherst, MA, USA) and surface water samples from Connecticut River, USA. Furthermore, Lin et al. [150] proposed a competitive fluorescent lateral flow immunoassay for ampicillin detection in hospital wastewater as shown in Figure 2.8. The limit of quantitation (LOQ) value under optimal condition could achieve 2.71 ng $L^{-1}$ with a more than 80.5% recovery, marking it as a promising tool for antibiotics detection in complicated wastewater matrices. Wang et al. [151] proposed a ratiometric paper-based platform for simultaneous detection of multiple aminoglycosides by adopting a digital fluorescence detector (DFD). As shown in Figure 2.8, the device is composed of five layers and four parallel channels. This design is based on the principle that the layers modified with aptamer/graphitic carbon nitride nanosheet could catalyse o-phenylenediamine to 2,3-diaminophenazine (DAP) when $H_2O_2$ is present. Once the aptamer is removed from the nanosheet via binding with its target, the DAP production will decrease due to the declined peroxidase-like activity of the nanosheet complex, and the change in signals could be recorded by the DFD. Linear range of target streptomycin (STR), tobramycin (TOB) and kanamycin (KAN) was reported to be 0.05−30 ng $mL^{-1}$, 0.1−150 ng $mL^{-1}$, and 0.05−150 ng $mL^{-1}$ with LODs of 0.023 ng $mL^{-1}$, 0.069 ng $mL^{-1}$, and 0.045 ng $mL^{-1}$, respectively. Successful simultaneous tests STR, TOB, and KAN in spiked river sample from Xiangjiang Rive using this assay were also demonstrated. Fernández-Gavela et al. [152] reported a rapid and cost-effective competitive photonic nano-immunosensor platform for onsite measurement of organic pollutants. An integrated asymmetric Mach-Zehnder interferometer of micro/nano dimensions based on silicon photonic technology was employed. The Mach-Zehnder interferometer is a competitive evanescent wave biosensor, where the binding of the analyte to the bioreceptor can lead to change of refractive index near the surface within an evanescent field (which is an oscillating electric and/or magnetic field that does not propagate as a wave but energy is spatially concentrated in the vicinity of the source). A four-channel microfluidic cell was designed, manufactured and incorporated in the miniaturized sensor for multiplexed detection. Besides,

automatic sample analysis was enabled by integrating a microfluidic delivery module. Tetracycline was detected as proof-of-concept with a LOD of 0.04 µg $L^{-1}$ which obeys the European legislation.

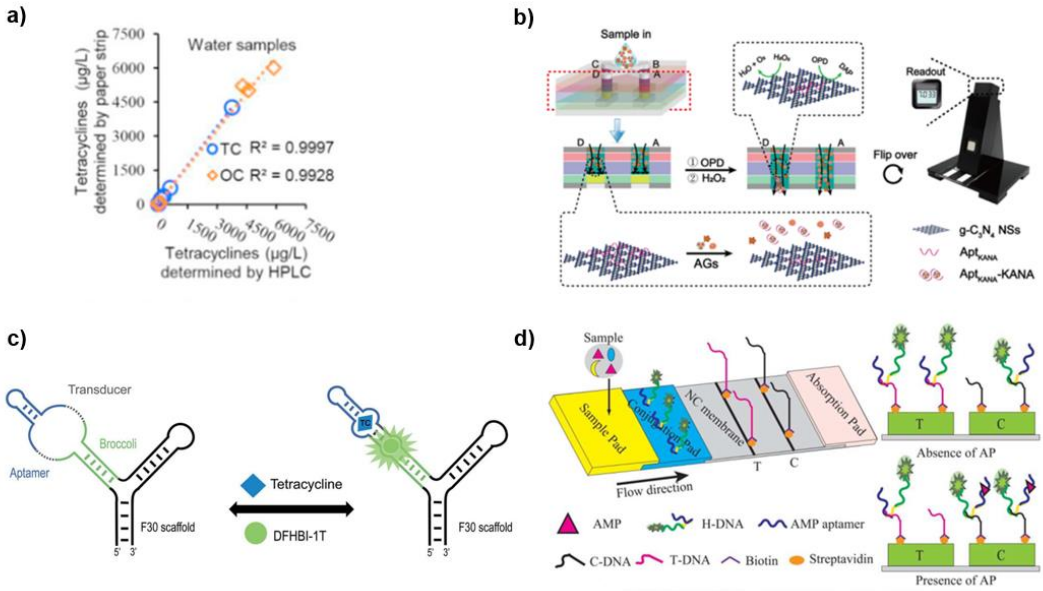


Figure 2.8. Schematics of antimicrobial detection using µPADs. a), b) and c) as mentioned in the main text. d) schematic lateral flow test design for ampicillin (AMP) detection. a) b) c) d) Reprinted from [149–151,153]

To further amplify the detection signal and therefore improve the detection sensitivity, isothermal amplification method of ssDNA such as hybridisation chain reaction (HCR) is employed. HCR was first developed by Dirks and Pierce in 2004 [154]. It is an enzyme-free DNA self-assembly process where two DNA hairpins (H1, H2) cascade react to form a nicked double-helix with repeated alternating H1 and H2 in the presence of a single stranded initiator, and therefore the signal of the initiator is amplified [155]. The working mechanism is as shown in Figure 2.9a. The reaction is driven by the open-up of two kinetically trapped nucleic acid hairpin probe via an initiator, and therefore the reaction can take place at a constant temperature. Once the HCR reaction is triggered, a chain reaction occurs, leading to double-stranded amplification polymers [154]. HCR sometimes suffers from false positive results, which could be a result of transit melting where hairpin stems open and bind to the toehold region of the other

hairpin. It is reported that this problem could be avoided via stringent design, compromising between thermodynamics (Gibbs free energy of hairpin structure < -16 kcal/mol) and kinetics. And there is minimal contribution from reaction time and ionic concentration [155]. Therefore, rational design of HCR hairpin pairs is vital for efficient and specific reaction. A hairpin is composed of three parts: toehold, stem, and loop, as shown in Figure 2.9b. There are some general design rules of a hairpin. The toehold is responsible for reaction initiation, therefore its length should be no longer than 12 nt, and GC% (the percentage of guanine and cystine in nucleic acid sequence) should be less than 30-40%, to enable fast kinetics. On the other hand, stem is in charge of the hairpin stability, so it should be longer than toehold and of a GC% more than 60% [156].

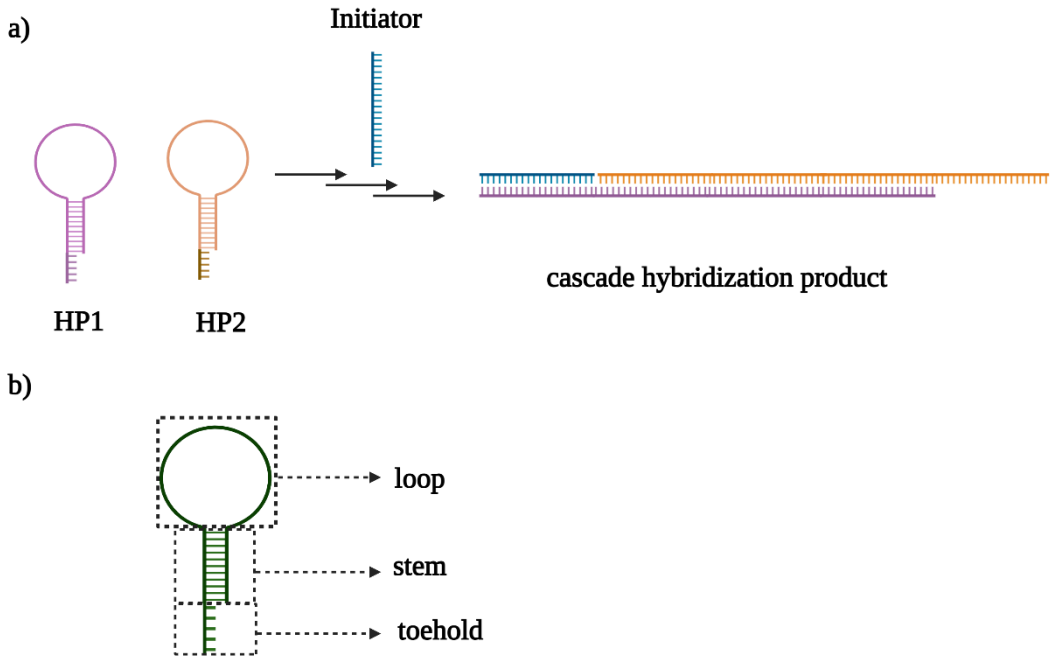


Figure 2.9 Illustration of HCR mechanisms. a) the process of exponential amplification of hairpins with the presence of the initiator b) structure of a hairpin, composed of a loop, a stem, and a toehold.

CRISPR/Cas system has been extensively applied in biosensing since its discovery due to its high base resolution and isothermal signal amplification. Although most current reports focus on its ability for nucleic acid detection, there is an emerging trend of applying CRISPR/Cas system for non-nucleic acid

detection [12]. Chen et al. [157] reported an onsite portable CRISPR/Cas integrated biosensor for kanamycin, based on a glucometer. Results showed that the linear range was from 1 pM to 100 nM with a LOD of 1 pM. No significant interference was observed from other antibiotics with kanamycin detection, and the recovery values were from 89-107.2 % for water samples and 86-106.5 % for milk samples (RSD < 5 %). Besides, Hu et al. [158] reported a metal tagged CRISPR/Cas12a bioassay for the detection of kanamycin, reaching a LOD of 4.06 pM within 30 minutes. *Pseudorasbora parva* samples from four different locations of Yangtze River were then analysed, as well as the bioaccumulation kinetics of kanamycin in serum, muscle, and liver tissues of *Pseudorasbora parva* in kanamycin-rich environments for 7 days.

To further improve analytical performance, conducting polymer polyaniline (PANI), a U-bent optical fibre-based immuno-sensing strategy has been developed for ciprofloxacin (CIP) detection in wastewater samples [159]. PANI was previously functionalised on a silica optical fibre where anti-CIP immunoglobulin G (IgG) was deposited. The result was detected via scanning electron microscopy and micro-Raman spectroscopy, with a linear range for CIP was from 0.01 to 10,000 ng $L^{-1}$. The detection limit was $3.30 \times 10^{-3}$ ng $L^{-1}$ with a LOQ of 0.01 ng $L^{-1}$. Real wastewater samples from Quebec (Canada) were examined and the results showed no significant difference when compared with reference method, indicating this new technique is selective, allowing a quantitative analysis of CIP in wastewater. In addition, Nguyen et al. [160] proposed a nanocomposite of graphene oxide and gold nanoparticles-based SERS microfluidic aptasensor for the detection of kanamycin with reduced blinking effects, achieving a LOD of 0.75 nM in a linear range of 1 nM to 100 nM.

In addition to optical detections, electrochemical sensors are also widely used in antimicrobial reagent detection. For example, Chinnappan et al. [161] reported a highly selective and sensitive competitive voltametric aptasensor for azlocillin detection with a limit of detection of 1.2 pg $mL^{-1}$ as well as remarkable selectivity against potential interfering agents, including amoxicillin, were achieved within 30-50 min. Over 90% recovery percentages were achieved when the sensor was applied to complex environments such as tap and wastewater. Efforts have also

been made for *in situ* and real-time detection. Chen et al. [162] proposed a miniaturized electronic antibiotic sensor based on field-effect transistor. An ultra-sensitivity to tobramycin with a LOD of 0.3 nM within 5 s was achieved, with a high specificity over other antibiotics such as kanamycin, streptomycin, ciprofloxacin, and tetracycline. In addition, sensing tests performed under controlled microfluidic flow conditions demonstrate its great potential in practical detection in environmental water.

Table 2.4 below summaries the examples of antibiotics detection described in 2.3.2.

Table 2.4 Summary of examples of antibiotics detection.

| Detection approach | Target | Sensitivity | Matrices | Ref. |
|---|---|---|---|---|
| Fluorogenic RNA aptamer μPAD | Tetracycline | dynamic range of 0.1–0.8 mM | RNase-free buffer, local tap water samples (Amherst, MA, USA) and surface water samples from Connecticut River, USA | [149] |
| Competitive fluorescent lateral flow immunoassay | Ampicillin | LOQ = 2.71 ng $L^{-1}$ | Hospital wastewater | [150] |
| Ratiometric fluorescent paper-based platform | Streptomycin (STR), tobramycin (TOB) and kanamycin (KAN) | 0.023 (STR), 0.069 (TOB), and 0.045 (KAN) ng $mL^{-1}$ | Spiked river sample from Xiangjiang River | [151] |

| | | | | |
|---|---|---|---|---|
| Competitive photonic nano-immunosensor microfluidic device | Tetracycline | 0.04 μg $L^{-1}$ | Real sea water | [152] |
| Whole-cell chromogenic paper strip biosensors | Tetracycline | 5.23 μg $L^{-1}$ | local fishponds in Nanjing (China) | [153] |
| CRISPR/Cas integrated glucometer | Kanamycin | 1 pM | Water and milk samples | [157] |
| Metal tagged CRISPR/Cas12a bioassay | Kanamycin | 4.06 pM | *Pseudorasbora parva* samples from Yangtze River | [158] |
| U-bent optical fibre-based (conducting polymer polyaniline (PANI)) immuno-sensor | Ciprofloxacin (CIP) | LOD = 3.30 × $10^{-3}$ ng $L^{-1}$ with a LOQ of 0.01 ng $L^{-1}$ | Real wastewater samples from Quebec (Canada) | [159] |
| Nanocomposite of graphene oxide and gold nanoparticles-based SERS microfluidic aptasensor | Kanamycin | 0.75 nM | Drinking water | [160] |
| Competitive voltametric aptasensor | Azlocillin | 1.2 pg $mL^{-1}$ | Spiked tap water and wastewater samples | [161] |

| | | | | |
|---|---|---|---|---|
| | | | collected in Riyadh city | |
| miniaturized electronic field-effect transistor | Tobramycin | 0.3 nM | Buffer | [162] |

## 2.4 Conclusion and perspectives

In this chapter, the AMR transmission routes in the environment following S-P-R paradigm were discussed. Wastewater was identified as the main source of AMR, with wild fauna and air as the pathway and food chain being the receptor. Efforts have been made to mitigate the risks of AMR in S-P-R paradigm, including improved wastewater treatment, regulatory measures, and public awareness campaigns. Incomplete metabolism and partial removal of AMR in WWTPs leads to its widespread in aquatic environment. Studies have been carried out evaluate the AMR removal efficiency of different treatment methods. Conventional biological wastewater treatment reduces the number of bacteria in the wastewater, but it cannot reduce the pathogenic potential of AMR in the bacteria [163]. Solid separation, e.g., membrane bioreactors, seems to provide an alternative for improved AMR removal [164]. The effectiveness of other treatment approaches, including UV irradiation, ozonation, and chlorination, is controversial, and highly dependent on factors e.g., treatment type, operational settings [165]. There is an urgent need to systematically review current wastewater treatment methods and combine advanced treatment procedures to improve AMR removal in WWTPs.

Legislation and regulatory measures have been issued to combat AMR, including 1) authorisation/registration of veterinary medicine products. Labelling, packaging, and advertising rules are clearly stated. Licensing rules on production, distribution, sale, and waste disposal are released. 2) Antibiotics are strictly restricted for non-therapeutic purposes. Rules are published for therapeutic reasons. The production waste and water disposal are highly regulated together with the remains of the antibiotics. Although AMR-relevant legislation and

regulation in the environmental sector is still underdeveloped, with the global awareness of One Health, it is promising to wait for its establishment.

Since early 1980s, the United Nation and the WHO have begun to implement global action of combating AMR in hospitals, i.e., the global assembly on AMR governance, followed by the establishment several national AMR monitoring systems of U.S. and other high-income countries (HICs). When progressing to the 2000s, with the escalating spread of AMR worldwide, global strategies of AMR monitoring further expanded to the areas of agriculture and the environment, as well as that in LMICs. Currently, AMR is recognised as not only a threat to human health, but also a huge burden to economic and social development. In this regard, several organisations including NGOs carry out public activities [166,167] e.g., holding sessions and workshops and publishing reports, to raise the public awareness and engagement. With all those efforts, lower volume of antibiotic consumption was reported in certain countries and the occurrence of AMR species also reduced [168]. However, the global use of antibiotics still rises and the situation in LMICs still persists [169]; therefore, more actions should take place to help.

Then we moved to detection approaches, summarising recent advancements of rapid molecular detection of AMR (i.e., ARGs) and antimicrobial reagent in environmental water, with an insight on the employment of microfluidics and μPADs. Recent developments on bioassays offer a promising low-cost, portable, and robust system integrating various molecular detection assays including NAATs. Devices accommodating bioassays such as lateral flow assay, in particular, is popular due to its ease of use, adequate sensitivity and selectivity, affordability, and its direct visual readout. Most methods are developed without the need for pre-training by specialists and enables rapid onsite detection, suggesting its applicability for in field measurement in resource-limited settings, e.g., LMICs. Since the global AMR surveillance programme now focuses on the environment and LMICs, POU assays hold the potential to be integrated into the system for rapid, simple, and sensitive detection. However, the development of POU assays suffers from a lack of scalable production methods, e.g., μPADs, resulting in most current studies only focus on novelty and resolution [170].

Therefore, it is calling for relevant stakeholders and or governmental bodies to implement these technologies for mass production.

Once commercialised, large-scaled data can be collected, and with the aid of smartphone, those data can be readily stored and exchanged. Smartphone has been regarded as a powerful sensing component since 2001 [171]. Due to its ubiquitous, operation simplicity and portable miniaturised computer nature, it is extensively integrated with sensors, leading to a wireless sensor network. Data can be collected by smartphone with its implemented sensors, e.g., camera [172]. With the built-in global positioning system (GPS), the data collected by smartphone is of location information, and therefore AMR abundance can be mapped. Eventually, a local, national, and global AMR profile can be built. With this AMR profile, the emergence of novel AMR and its transmission route are readily monitored, contributing to combat AMR, e.g., helps for clinical treatment of patients with specific travel history.

Furthermore, since computational sciences including deep learning and IoT are flourishing and in rapid growth, fundamental models can be built using data collected, and therefore the trend of AMR emergence and transmission can therefore be predicted with precision. Risks of sudden outbreaks of AMR can therefore be alleviated with timely and effective intervention from the warning. Although there is a lack of models built to predict AMR outbreaks at a regional wide, there are studies that show the power of integrating AMR detection techniques with computational approaches. Proposed in 2020, PARGT is a software tool to predict AMR in bacteria. Simulation results have shown that an accuracy of 87-90% was reached when PARGT predicted the AMR sequences for Gram-positive bacteria [173]. In addition to stand alone software, the development of algorithms is also crucial. An annotation method (pairwise comparative modelling) was developed and validated on the 3D structure basis of proteins. As a result, 6095 antimicrobial resistance determinants of 3.9 million proteins from the human intestinal microbiota were predicted [174]. Since the technology is translatable, work in computational based pathogen detection can initiate ideas as well. Sun et al. [175] proposed a deep-learning combined μPADs portable optoelectronic system for SARS-Cov-2 detection. Real-time data was

fed into neural networks for early prediction analysis. Results showed that the predicted accuracy, sensitivity and specificity reached 98.1%, 97.6%, and 98.6%, respectively. Besides, Duan et al. [176] proposed a deep learning-assisted smartphone based μPADs for protein biomarker detection. The proposed algorithm enabled elimination of ambient light influence and gave a >97% accuracy in rabbit IgG concentration quantification. More work is calling to further expand on this interdisciplinary area, contributing to facile AMR model predictions.

# 3 Enhanced Detection of Antibiotic Resistance Genes and Microbial Source Tracking Using Real-Time Fluorescent mRPA-CRISPR/Cas Assay: A Versatile Tool for Resource-Limited Settings

## 3.1 Introduction

Antimicrobial resistance (AMR) as introduced in 2.1, is a severe public health threat that leads to 1.27 million deaths each year [1]. Timely surveillance of AMR worldwide to track and confirm the resistance mechanisms can help to combat AMR, while most data collection is largely dependent on central laboratory set-ups, limiting its application in the point-of-use, preventing timely reflection on the local resistance profile where samples are collected. Besides, most research is focused on detection under clinical context. Therefore. it is urgently calling for the development of POU assay for environmental surveillance purposes.

Isothermal amplifications, including LAMP [118], RCA [177] and RPA [70], have been widely applied to POU assays, as they can amplify target genes in a high amplification efficiency at a constant temperature without the need of tedious thermal cycling process. Among all the reactions, RPA is featured by its simple assay construction (only two primers needed), low constant reaction temperature (37 – 42 ºC) and rapid reaction process (20 - 40 min) [127]. Much research has been conducted employing RPA for the detection of various genes. For example, Sollweck et al. [138] proposed a chip-based colony fusion RPA assay for blaCTX-M genes and their carrying species e.g., *E. coli* monitoring in surface water. And Ahn et al [178] reported a single step multiplexed RPA assay for simultaneous detection of foodborne pathogens.

Recently, CRISPR/Cas12a has been regarded as one of the options to improve the specificity of detection assays, as they can recognise a specific gene sequence (cis-cleavage, single turnover) and then triggers cuttings on nearby non-specific single-stranded DNA (trans-cleavage, multiple turnovers) [11,179]. CRISPR/Cas12a has been integrated with RPA reactions since 2018 [11], and subsequent studies [179–182] have been conducted to further improve the assay

performances. However, to date, most studies are still limited to the use of the assay under clinical context, lacking those aimed to be used for environmental samples, which are different matrices and therefore are demanding in assay sensitivity, specificity, and robustness.

Tetracycline is a family of antibiotics that works by inhibiting protein synthesis. It reversibly binds to the 30S ribosomal subunit of the bacteria, and thus hinders the binding of aminoacyl-tRNA to the adjacent ribosomal acceptor site, leading to bacteriostatic action [183,184]. And it was first discovered in 1948 in the form of chlortetracycline from *Streptomyces aureofaciens*. There are other naturally occurring tetracyclines (1st generation) such as oxytetracycline and tetracycline, as well as semi-synthetic ones (2nd generation) including minocycline and doxycycline. Moreover, there are 3rd generation drugs such as tigecycline and eravacycline [183]. Tetracycline family is featured by four linearly condensed benzene rings in a hydronaphtacene nucleus, as shown in Figure 3.1 with structures of tetracycline and tigecycline.

Resistance to tetracycline is generally mediated through one of the following mechanisms: overexpression of active efflux pumps, production of ribosomal protection proteins (RPPs), and enzymatic degradation [183,185]. Among them, overexpression of active efflux pumps efficiently decreases tetracycline concentration inside the bacterial cells, while the production of RPPs prevents the binding between tetracycline and its target ribosome. tet(M) is a one of the representative RPP coding genes, and it has been sequenced from several Gram-negative and gram-positive species [184]. And enzymatic degradation inactivates the functions of tetracycline by altering its chemical structure. Other mechanisms include target mutation where ribosomal protein genes and/or 16s subunit of rRNA genes mutate. The main resistance mechanisms are shown to confer resistance to most 1st and 2nd generations of tetracyclines, however, tigecycline, one of the last resort antibiotics, is reported to bypass most mechanisms due to its higher affinity with ribosome. Tigecycline is a synthetic derivative of minocycline (2nd generation) discovered in 1993 and approved by FDA in 2005. With its emerging use in clinics, the number of resistance cases is increasing, and it is reported that enzymatic degradation coded by tet(x) genes

confer resistance to tigecycline and tet(x3) is one of the recent discovered gene that presents high-level tigecycline resistance [186].

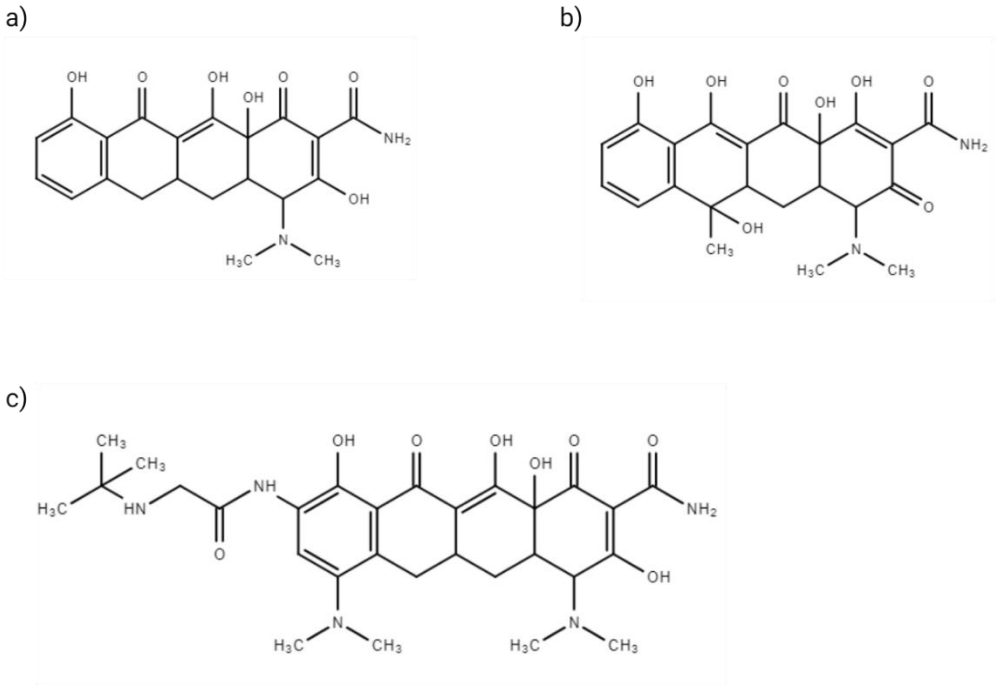


Figure 3.1 Chemical structures of a) tetracycline core structure b) tetracycline c) tigecycline.

In addition to ARGs, anthropogenic activities such as discharges of wastewater from wastewater treatment plants (WWTPs) [38] lead to the spread of AMR and antimicrobial agents from human to animals and the environment, and therefore microbial source tracking (MST) is employed to further understand the AMR transmission routes in the environment, especially the relative contribution of human. Crassphage, due to its abundance in human faecal samples worldwide, has been applied as human source biomarker to assess anthropogenic pollution [187].

Aquatic environments are regarded as one of the reservoirs and transmission routes of AMR dissemination [26,188], and drinking water and wastewater treatment processes are incapable of completely removing ARGs [189,190]. Therefore, the objective was to advance a molecular biological assay integrating RPA and CRISPR/Cas12a for rapid detection of ARGs in water. RPA was performed to

exponentially increase the copy numbers of the three target genes, tet(M), tet(x3) and crassphage, and the amplicons were detected by employing the trans-cleavage activity of the CRISPR/cas12a assay to further enhance the specificity and robustness of the assay. The LODs and robustness of the assay were investigated in pristine samples as well as different water samples (e.g., surface water and drinking water) were enriched, extracted, and finally detected fluorescently to further demonstrate the assay reliability.

## 3.2 Materials and Methods

### 3.2.1 Chemicals and apparatus

Quant Studio 3 Real-Time PCR System, Qubit 4 Fluorometer, SYBR Safe DNA Gel Stain, DNA Gel Loading Dye (6×), Qubit dsDNA HS Assay Kit from Thermo Fisher Scientific, UK. Syngene GBOX Gel-Doc system from Syngene, UK. TaqMan Fast Virus 1-step Master Mix (4×) was from Thermo Fisher Scientific, UK. EvaGreen, 20× in water, was from Cambridge BioScience (UK), while ethanol, agarose, double-distilled water (dd$H_2O$), syringes, syringe filters and swinnex filter holders were from Sigma Aldrich (UK). MagaZorb DNA Mini-Prep Kit and Zymoclean Gel DNA Recovery Kit were from Promega (UK) and Zymo Research (Germany), respectively. TwistAmp basic kit was from TwistDX, UK and EnGen Lba Cas12a (Cpf1) was from New England Biolabs, UK.

The detection target sequences were retrieved from National Library of Medicine with the NCBI reference number NZ_CP044485.1 (tet(M)), NC_024711.1 (crassphage), and NZ_CP045198.1 (tet(x3)). RPA and qPCR primers together with probes were designed using Primer-BLAST website and their sequenceslisted inTable **A.2** and Table A.3. They were synthesised by and purchased from Merck, UK. The 5’ end of the probes were modified with 6-FAM and 3’ end with BHQ-1. Amplification template of tet(x3) was synthesized and purchased from Eurofins Genomics, Germany, and those of tet(M) and crassphage were from the wastewater samples, gel purified and stored at -20 °C until use. 100 bp DNA Ladder were purchased from New England Biolabs (UK).

crRNA was designed on CRISPOR (http://crispr.tefor.net/) and purchased together with ssDNA probe (tagged with 6-FAM and BHQ-1) from Merck, UK. All chemicals were of analytical reagent grade and used without further purification. dd$H_2O$ was purified through a Millipore System (Millipore, USA, resistivity >18 MΩ). Each assay was repeated at least 3 times to ensure reproducibility.

### 3.2.2 DNA template concentration and extraction from wastewater

DNA template in pristine samples were extracted from wastewater samples collected from influents of Cranfield Wastewater Treatment Plant (capacity of 40,000 PE, Cranfield, UK). Three discrete 1 L wastewater samples were collected on 19/05/2022, 24/05/2022, and 26/05/2022. 40 mL wastewater samples were manually filtered and concentrated through 0.45 µm pore-sized membrane and DNAs were then extracted with Pro Magazorb kit following instructions. In brief, the whole process includes sample lysis, binding, washing and elution. 20 µL of well-mixed proteinase K solution was pipetted through the filter membrane followed by 200 µL well-mixed lysis buffer. The flow-through solution was pulse-vortexed for 15 seconds until a homogeneous mixture obtained, followed by an incubation in 56 ºC heat block for 10 minutes. After that, 500 µL of well-mixed binding buffer was added and pulse-vortexed for 15 seconds until a homogeneous mixture obtained. Following adding 20 µL well-mixed Magazorb Reagent (magnetic beads), the mixture was gently mixed and then incubated for 10 minutes at room temperature with occasional manual mixing every 2 minutes. Next, the mixture of Magazorb particles was placed onto a magnetic rack for 90 seconds. During the process, the magnet was inverted 3 times to rinse the tube cap while the tubes are tightly held onto the magnet. The supernatant was carefully removed without touching any Magazorb particles. Before adding 1 mL well-mixed wash buffer to the mixture, the tube was removed from the magnet. Then the mixture was vigorously vortexed followed by another sediment and aspiration as described above to remove the supernatant. The wash step was repeated once for clear supernatant. Finally, 200 µL well-mixed elution buffer was added to mixture which then through inverting and swirling. After incubating for 10 minutes at room temperature with occasional manual mixing every 2 minutes,

the Magazorb particles were separated with the magnetic rack. The extracted purified DNA was eventually transferred to a clean microcentrifuge tube and stored at -20 ºC for further use.

PCR amplifications were performed on the extracted DNA samples with 200 nM forward primer, 200 nM reverse primer, 1× Brilliant III QPCR Master Mix/Low ROX or TaqMan Fast Virus 1-step Master Mix and 1× EvaGreen in Quant Studio 3 PCR system. Subsequent gel electrophoresis was conducted to purify the amplicons. Gel DNA was recovered using Zymoclean Gel DNA Recovery kit following the kit guidelines. Before the recovery, Wash buffer was prepared by adding 104 mL 95% ethanol to the 24 mL DNA Wash Buffer concentrate, and the part of gel containing DNA fragments (i.e., where the band is) was excised from the gel using a scalpel. The gel was weighed and added into a tube before 3 volumes of ADB was added to each volume of DNA-contained gel, i.e., for 100 mg gel slice, 300 µL ADB was added. Then the mixture was incubated at 55 °C for 10 minutes until the gel was completely dissolved, followed by transferred to a Zymo-Spin Column in a Collection Tube. The tube was subsequently centrifuged for 1 minute with flow-through discarded. The wash step was conducted twice sequentially, by adding 200 µL DNA Wash Buffer to the column and the column was centrifuged for 1 minute. Finally, 100 µL DNA Elution Buffer was added to the column matrix, and the column was transferred to a 1.5 mL tube and centrifuged for 1 minute. The recovered DNA samples were measured in Qubit 4 Fluorometer and stored in -20 °C freezers for further use.

### 3.2.3 Quantification of nucleic acid concentration

Nucleic acid concentration was quantified using Qubit 4 Fluorometer (Thermo Fisher Scientific, UK) according to manufactures' guidance. Triplicate measurements were carried out for each sample. Generally, working solution was prepared by diluting assay Qubit Reagent 1:200 in Qubit Buffer. In principle, 200 µL working solution was prepared for each sample and standard measurement. Then, standards were set up by adding 190 µL well-mixed working solution with 10 µL well-mixed Qubit Standard, and the mixture was vortexed for 2-3 seconds. As for sample preparation, 195 µL well-mixed working solution were vortexed with

5 µL well-mixed DNA sample and the mixture was allowed to stand at room temperature for 2 minutes. Finally, the tubes were inserted into the Qubit 4 Fluorometer (standards before samples), and readings were taken by following the instructions shown on the Qubit screen.

### 3.2.4 RPA assay

Triplicates were conducted for all RPA assays. The RPA primers were designed using PrimerBlast with following principles: amplicon size, primer melting temperature, primer GC % and primer length. Briefly, amplicon size was aimed at 100 – 200 bp, with primer temperature at 50 – 100 °C, GC % in the range of 20-70%, and finally primer length of 30 – 36 nt.

TwistAmp basic kit was used for RPA reactions as per the manufacturer's instructions with slight modification. RPA Primer concentration is one of the optimisation parameters and it differs with different target. For crassphage, one 2× reaction mixture of 50 µL was prepared by adding 29.5 µL rehydration buffer, 2 µL EvaGreen, 1.125 µL 20 µM forward primer, 1.125 µL 20 µM reverse primer, and 9.75 µL dd$H_2O$, while that for tet(M) was 1.25 µL 20 µM forward/reverse primer and 9.5 µL dd$H_2O$, and for tet(x3) was 1.425 µL 20 µM forward/reverse primer and 9.15 µL dd$H_2O$.Then 43.5 µL primer solution was mixed with freeze-dried pellet provided along with the kit and then distributed into 2 reaction tubes, each was 21.75 µL. Then 1.25 µL of 280 mM magnesium acetate solution was added to each tube cap while 2 µL DNA sample was added and pipette mixed with the reaction mixture.

The reaction mix was then incubated at 39 °C for 40 min in a Quant Studio 3 real-time qPCR machine and the real-time amplification curves were recorded. Subsequently, gel electrophoresis was conducted by transferring the amplified products onto 2.4 % agarose gel stained with GoodView™ and visualized in a gel documentation system with 100 bp Plus DNA ladder. Primer concentration, Mg ion concentration, and reaction temperature were optimised to achieve the highest amplification efficiency.

The sensitivity of the optimised RPA assay for each target was investigated using 10-fold serial diluted target samples from $10^4$ copies $\mu L^{-1}$ to $10^{-1}$ copy $\mu L^{-1}$. The

real-time fluorescent curves were analysed, and 2.4 % agarose gel electrophoresis were run to further confirm the formation of amplicons. Since there were crowding agents and proteins in RPA assay, which led to smear of the DNA bands in gel, and therefore a pretreatment of DNA sample to clean before gel electrophoresis was required. ChargeSwitch PCR Clean-Up Kit (Invitrogen, UK) was then employed in the following steps: 25 µL Purification Buffer (N5) was added to 25 µL RPA samples and well-mixed, followed by the addition of 10 µL well-mixed ChargeSwitch Magnetic Beads and pipette mixed. The mixture was allowed to incubate for 1 minute at room temperature, before the tube was placed on the magnet for separation for another minute. Then the supernatant was discarded, and the tube was removed from the magnet before 150 µL Wash Buffer (W12) was added and pipette mixed. After that, the mixture again was placed on the magnet for separation with a final disposal of supernatant. The washing process was repeated once more before DNA elution, where 25 µL Elution Buffer (E5) was added and incubated for 1 minute at room temperature, followed by magnetic separation. Finally, the supernatant was ready for gel electrophoresis.

### 3.2.5 CRISPR/Cas assay

Triplicates were conducted for all CRISPR/Cas assays. CRISPR assays were optimised on reaction time, reaction temperature, ratio between CRISPR/cas12a enzyme and crRNA and ratio between CRISPR/cas12a enzyme and ssDNA probe, as shown in Figure 3.7. The optimised CRISPR assays (3 µL 10× NEB buffer, 1 µL 1 µM cas12a, 1 µL 1 µM crRNA, 2.5 µL 10 µM ssDNA probe, 2.5 µL dd$H_2O$) were then performed on RPA amplicons by adding the CRISPR/Cas mixture to the RPA solution. A sensitivity analysis was finally carried out as before on the 10-fold serial diluted target genes samples from $10^4$ copies $\mu L^{-1}$ to $10^{-1}$ copy $\mu L^{-1}$. Real-time fluorescent curves were recorded using the QuantStudio 3 real-time qPCR machine.

### 3.2.6 Multiplexed RPA (mRPA) integrated CRISPR/Cas assay

To better suit the purpose of POU testing, multiplex RPA with specific CRISPR/Cas detections were developed and triplicates were conducted for all

assays. The schematic illustration is shown in Figure 3.2. The 2× mRPA assay was 50 µL in total and prepared as stated in 3.2.4 with slight modification: 1.25 µL 20 µM forward/reverse primers (tet(M)), 1.425 µL 20 µM forward/reverse primers (tet(x3)), 1.125 µL 20 µM forward/reverse primers (crassphage), 29.5 µL rehydration buffer, 4.4 µL dd$H_2O$. Each 41.5 µL primer solution was added to the lyophilised pellet with subsequent equal separation to two reaction tubes. 1.25 µL 280 mM $Mg^{2+}$ was added to tube cap and 3 µL mixed DNA samples was added to each reaction assay. The reaction mix was then incubated at 39 °C for 40 min in a Quant Studio 3 real-time qPCR machine. Then CRISPR/Cas detection was conducted on the mRPA products as described in 3.2.5. A sensitivity investigation was then conducted as before on the 10-fold serial diluted target genes from $10^4$ copies $\mu L^{-1}$ to $10^{-1}$ copy $\mu L^{-1}$. Real-time fluorescent curves were recorded using the QuantStudio 3 real-time qPCR machine and the reaction was conducted in triplicates.

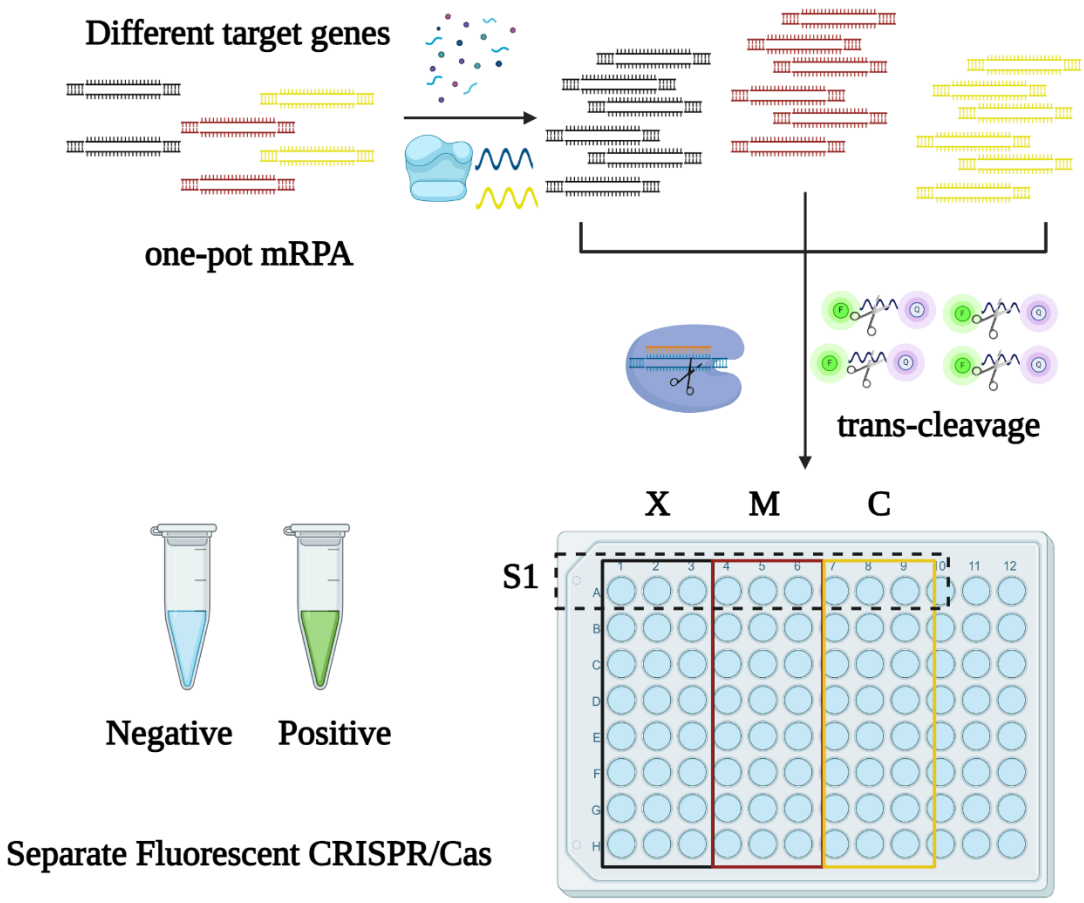


Figure 3.2 Schematic illustration of mRPA-CRISPR/Cas assay. X, tet(x3), M, tet(M), and C, crassphage. S1 represents sample one, and the first row of the 96-well plate indicates detection of X, M and C in sample 1 in triplicates.

### 3.2.7 Analytical performance evaluation in spiked water samples

The workflow of real sample detections is as shown in Figure 3.3. Spiked surface and drinking water samples were prepared by adding a volume of ARG solution of known concentration. DNA was then extracted using DNA extraction kit, followed by real-time fluorescent mRPA-CRISPR/Cas assay, and the results were compared with the known spiked concentration. Accuracy was calculated as detailed in 3.2.8 for performance evaluation.

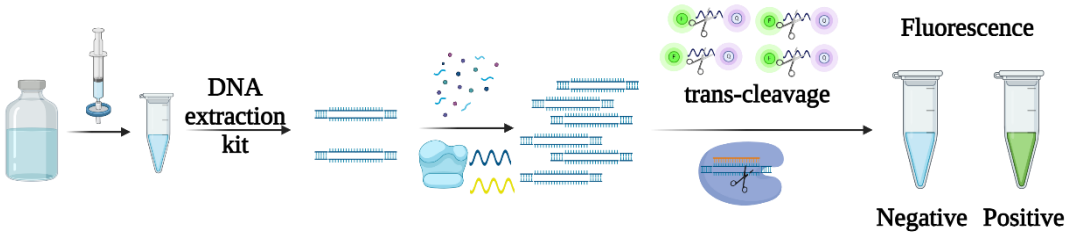


Figure 3.3 Workflow of ARG detection with fluorescent mRPA/CRISPR-Cas assay.

### 3.2.8 Data analysis and evaluation

Real-time fluorescent data was measured, retrieved, and exported from the QuantStudio 3 real-time qPCR machine. And all experiments were conducted in triplicates. $ddH_2O$ was employed as negative controls. The means of triplicates were calculated together with standard deviation for repeatability analysis. Standard deviation was calculated in the following equation:

$$Std = \sqrt{\frac{\sum(X-\alpha)^2}{n-1}}$$

Equation 1

where Std represents standard deviation, X represents each value, α represents the mean of values, and n represents number of replicates.

Data were treated and plotted using python3 Matplotilib. The threshold of positive assay was determined to be 10% of the maximum fluorescence recorded. Experiments were done on known positive samples (diluted target in pristine samples) and known negative samples ($ddH_2O$ as substitution of target gene), and the recorded signals of known negative samples (background noise) were always lower than 10% of the maximum fluorescence recorded. The accuracy was calculated as (true positives + true negatives)/(true positives + false negatives + true negatives + false positives) × 100. To evaluate the performance of the advanced mRPA-CRISPR/Cas assay, data were compared with other studies in the literature, as shown in Table 3.1.

It should be noted that $ddH_2O$ was used as negative controls

## 3.3 Results and discussion

### 3.3.1 Optimisation of RPA assay

To improve the sensitivity of RPA assay, optimisation of RPA assay conditions for ARG detection was conducted on tet(M), tet(x3), and crassphage on Quant Studio 3 thermal cycler. EvaGreen was employed as the real-time fluorescent indicator in the assay. tet(x3) template synthesised by and purchased from Eurofins, Germany, while tet(M) and crassphage templates prepared by wastewater extraction-PCR amplification-agarose gel purification and extraction procedure. Figure 3.4a showed the mean amplification curves of crassphage and tet(M) isolated from DNAs of extracted wastewater via PCR. Then gel electrophoresis was conducted on the PCR amplicons to further purify the isolated crassphage and tet(M) sequences. Subsequent DNA extraction from gel was carried out before final concentration determination using Qubit and 10-fold serial dilution to prepare the templates, as illustrated in schemes shown in Figure 3.4b.

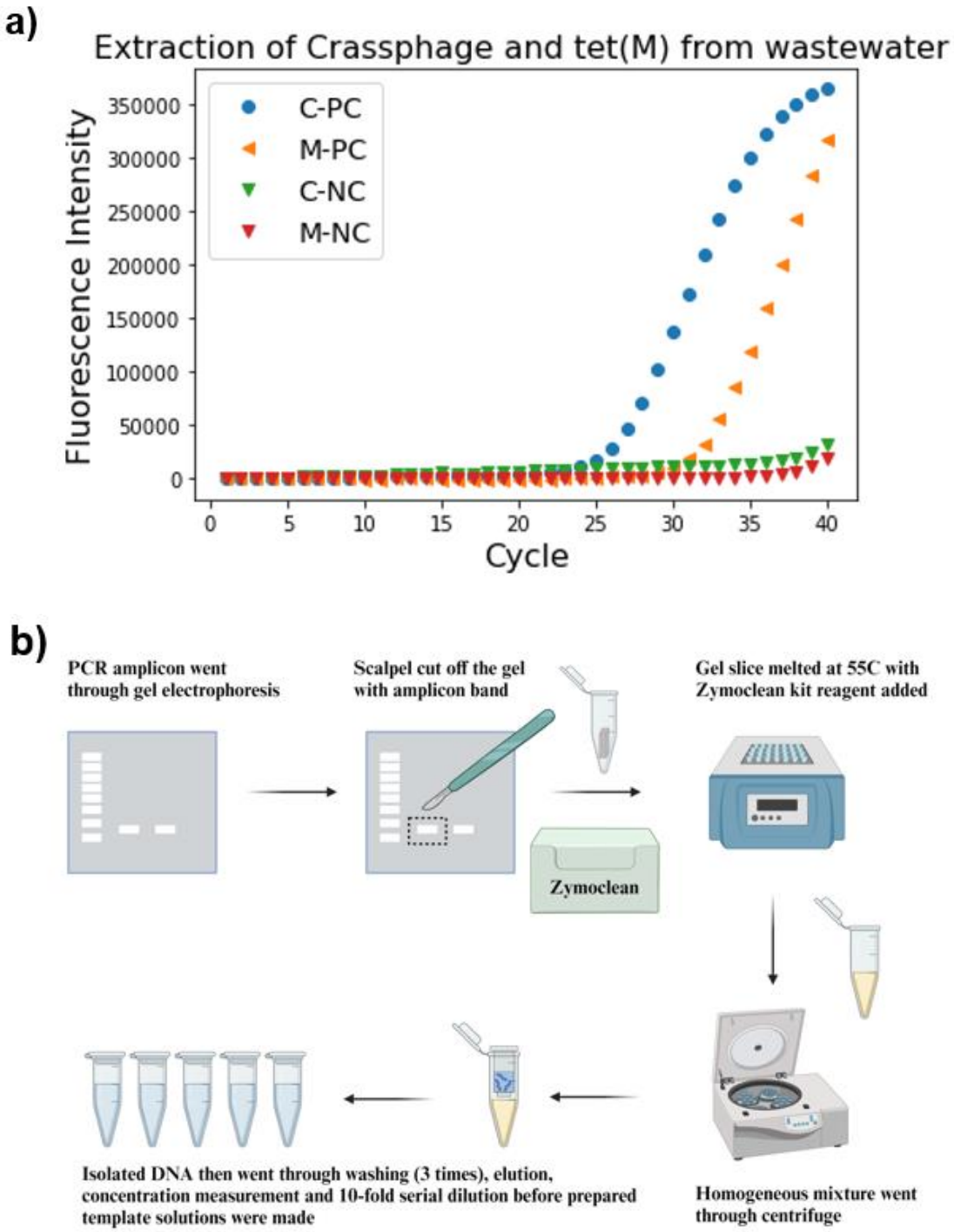


Figure 3.4 Preparation of templates of crassphage and tet(M). a) Mean amplification curves of crassphage and tet(M) from DNAs of extracted wastewater via PCR. Experiments were conducted in triplicates. PC: positive control. NC: negative control. b) schematic illustration of the workflow of preparation of templates from PCR amplicons isolated from wastewater DNA extracts.

The optimisation parameters include forward and reverse primer concentration, reaction temperature, reaction time, and Mg concentration. The optimal parameter set was selected based on a combination of fast kinetics (slope of real-time amplification curve) and minimal non-specific amplification. tet(x3) was employed as a model target for the parameter optimisation.

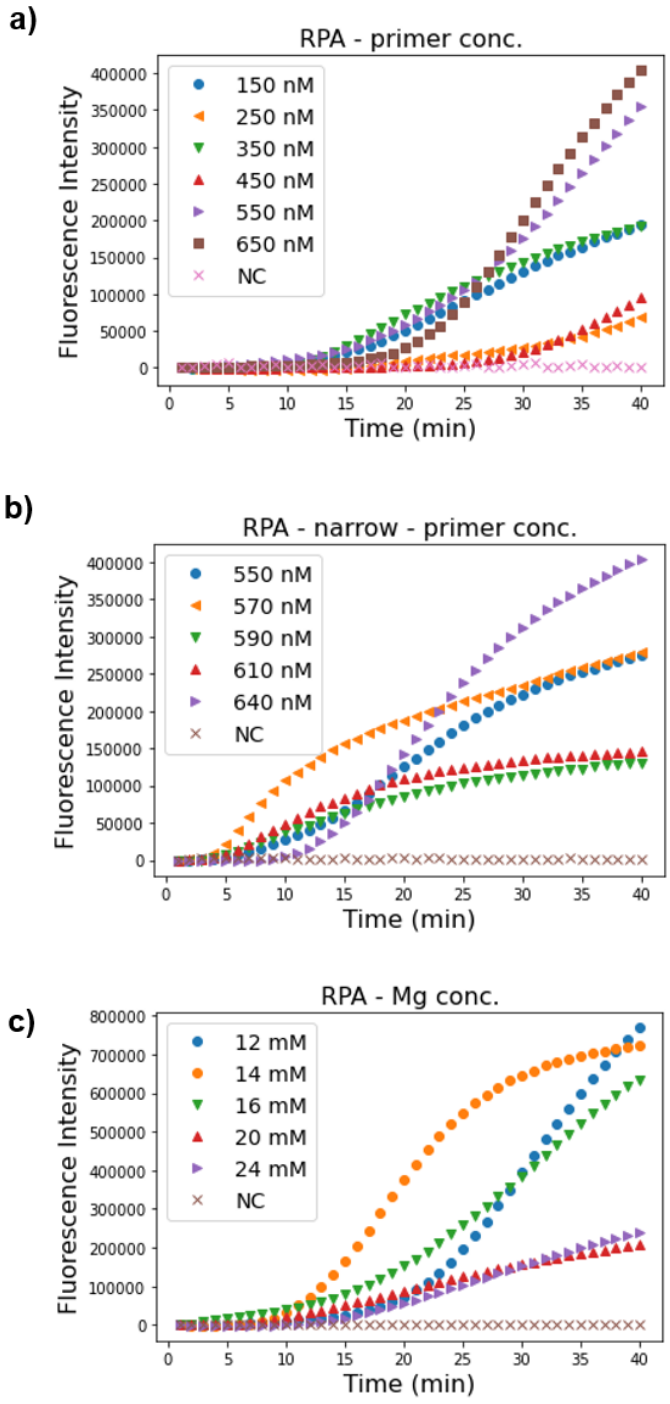

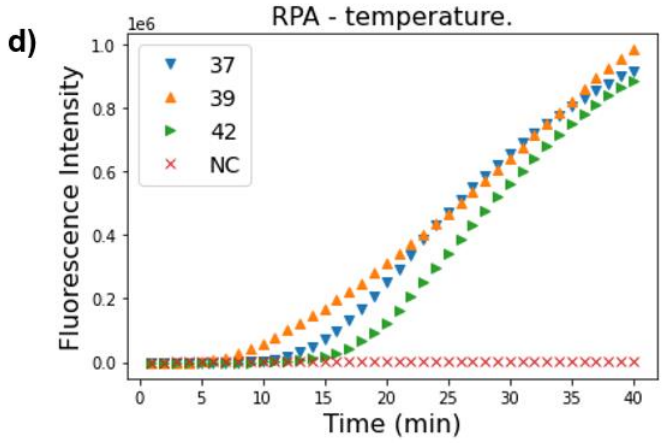


Figure 3.5 Optimisation of real-time fluorescent RPA assay. a) primer concentration with a broad range from 150 nM to 650 nM, and b) a narrower concentration range was then evaluated from 550 nM to 640 nM. (constant temperature at 39 °C and constant $Mg^{2+}$ concentration of 14 mM) c) $Mg^{2+}$ ion concentration ranging from 12 mM to 24 mM. (constant primer concentration at 570 nM and constant temperature at 39 °C) d) reaction temperature of 37 °C, 39 °C, 42 °C. (constant primer concentration at 570 nM and con constant $Mg^{2+}$ concentration of 14 mM) NC: negative control (dd$H_2O$ substituted template). All assays were repeated three times. The presented curve is a mean of triplicates.

$Mg^{2+}$ ion concentration is an important factor of RPA reactions, as it initiates the reaction and acts as the enzyme cofactors [70,134]. In this experiment, it was optimised from 12 mM to 24 mM. As can be seen from the Figure 3.5, 14 mM $Mg^{2+}$ ion concentration gave the fastest reaction kinetics and therefore it was chosen as the optimal $Mg^{2+}$ ion concentration, which is in line with manufacturer's guidance.

It is reported that RPA works at temperatures from 22 to 45°C with an optimal range of 37 to 42°C [127,138,178]. To determine the optimal reaction temperature, RPA assays were conducted at 37, 39, and 42°C with real-time fluorescent amplification curves recorded. From the Figure 3.5d, the fastest reaction kinetics was seen when reactions were performed at 39°C. Therefore, 39°C was chosen as the optimal reaction temperature.

Primer concentrations were finally optimised first with a broad range of 150 nM to 650 nM as advised by Twistdx RPA kit instructions. From the Figure 3.5a, it was noticed that the optimal tet(x3) primer concentration range laid between 550 nM to 650 nM, and therefore a smaller range of primer concentration was investigated. From the Figure 3.5b, the optimal primer concentration was determined to be 570 nM. Similar optimisation was carried out on other two targets, and the optimised primer concentration for tet(M) was 500 nM and that of crassphage was 450 nM.

It is worth noting that the real-time fluorescent curves in Figure 3.5 seemed to have different shapes. Some presented to have faster kinetics in the beginning of the reaction but with lower maximum fluorescence intensity (Figure 3.5b, curves of 570, 590, 610 nM), while others presented to have slower kinetics at the start but with higher overall fluorescence (Figure 3.5d). While the latter was the expected performance, the former might be due to the heterogeneity distribution of reagents which came from the high viscosity of the RPA solution. The high viscosity resulted from the crowing agents added that aimed to bring reagents together for more efficient amplification. However, if not mixed adequately, the high viscosity could also lead to higher local concentration which eventually resulted in faster kinetics but lower overall amplification. This lack of homogeneity also caused the variability between curves of the same reaction conditions (e.g., curves of 550 nM in Figure 3.5a and b). The difference in real-time fluorescence shape, to some extent, indicated that some reactions in the optimisation process might not in its homogeneous state, which introduced some human errors, and therefore weakened the robustness of optimisation on the primer concentration. On the other hand, real-time fluorescent curves of the $Mg^{2+}$ ion concentration and the reaction temperature showed similar shapes, and therefore their optimisation should be seen as valid.

To sum up, the optimised reaction parameters were as follows: reaction temperature 39°C, $Mg^{2+}$ ion concentration 14 mM, and primer concentration (tet(x3)) 570 nM, primer concentration (tet(M)) 500 nM, primer concentration (crassphage) 450 nM (as shown in Figure A.2).

The LOD was determined to be the lowest concentration that showed difference in signal comparing with negative controls. With the optimal assay conditions, the LODs of the RPA assays of the three targets, tet(M), tet(x3), and crassphage were evaluated. RPA was performed on 10-fold serial diluted target DNA sequences ($10^{4}$-$10^{-1}$ copies $\mu L^{-1}$) were prepared in pristine samples, and $ddH_2O$ was employed as the internal negative control. All RPA assays were conducted on a Quant Studio 3 Real-Time PCR system.

The amplifications across different concentrations basically initiated at similar time, around 5-10 minutes (tet(x3) and crassphage), while that of tet(M) was around 10-15 minutes (Figure 3.6). And a higher concentration could lead to a quicker reaction kinetics. The LODs of all three targets being 1 copy $\mu L^{-1}$. This result was further confirmed by agarose gel electrophoresis as illustrated in Figure 3.6. Lane L is the 100 bp DNA ladder, and lanes 1 – 5 represent target concentrations from $10^{4}$-$10^{0}$ copies $\mu L^{-1}$. The single band at target DNA length showed the formation of amplicons. It should be noted that the length of tet(M) target sequence was 108 bp, that of crassphage was 112 bp and that of tet(x3) was 108 bp.

From observing the plots as in Figure 3.6, it is worth noting that the RPA assay of $10^{-1}$ copies $\mu L^{-1}$ target sequences showed comparable curves as that of the negative control. The RPA assay might not be sensitive enough to detect the target of $10^{-1}$ copies $\mu L^{-1}$, while this could also be resulted from errors introduced in the serial dilution step. The $10^{-1}$ copies $\mu L^{-1}$ solution was prepared via 10-fold serial dilution by adding 10 µL well-mixed $10^{0}$ copies $\mu L^{-1}$ target solution to 90 µL $ddH_2O$. Although precautious actions including vortex mixture for 15 s were taken, the small quantity and highly diluted stock solution can lead to the probable heterogeneity distribution of target DNA in the $10^{-1}$ copies $\mu L^{-1}$ solution. Pipetting errors were also likely introduced during the process of dilution, resulting in the concentration less than $10^{-1}$ copies $\mu L^{-1}$, and even close to 0, which could explain that not any amplification could be observed from the real-time fluorescence curve.

Comparing with other studies, the proposed RPA assay exhibited better detection limits with comparable reaction time. Woo et al. [191] reported an RPA array chip

for the detection of DNA amplicons of respiratory pathogens including *S.pneumoniae*, *C.pneumoniae*, *H.influenzae*, *M.pneumoniae*, which reached LODs of 10, 10, $10^4$ and $10^3$ copies per reaction, respectively. Ge et al. [192] proposed an RPA-based photoelectrochemical assay for detecting *E. coli O157:H7* and *S. aureus* with LODs of 3 and 7 copies $\mu L^{-1}$, respectively. Geng et al. [193] reported an RPA assay to determine *Vibrio parahaemolyticus* concentration in seafood, reaching a LOD of 102 copies per reaction.

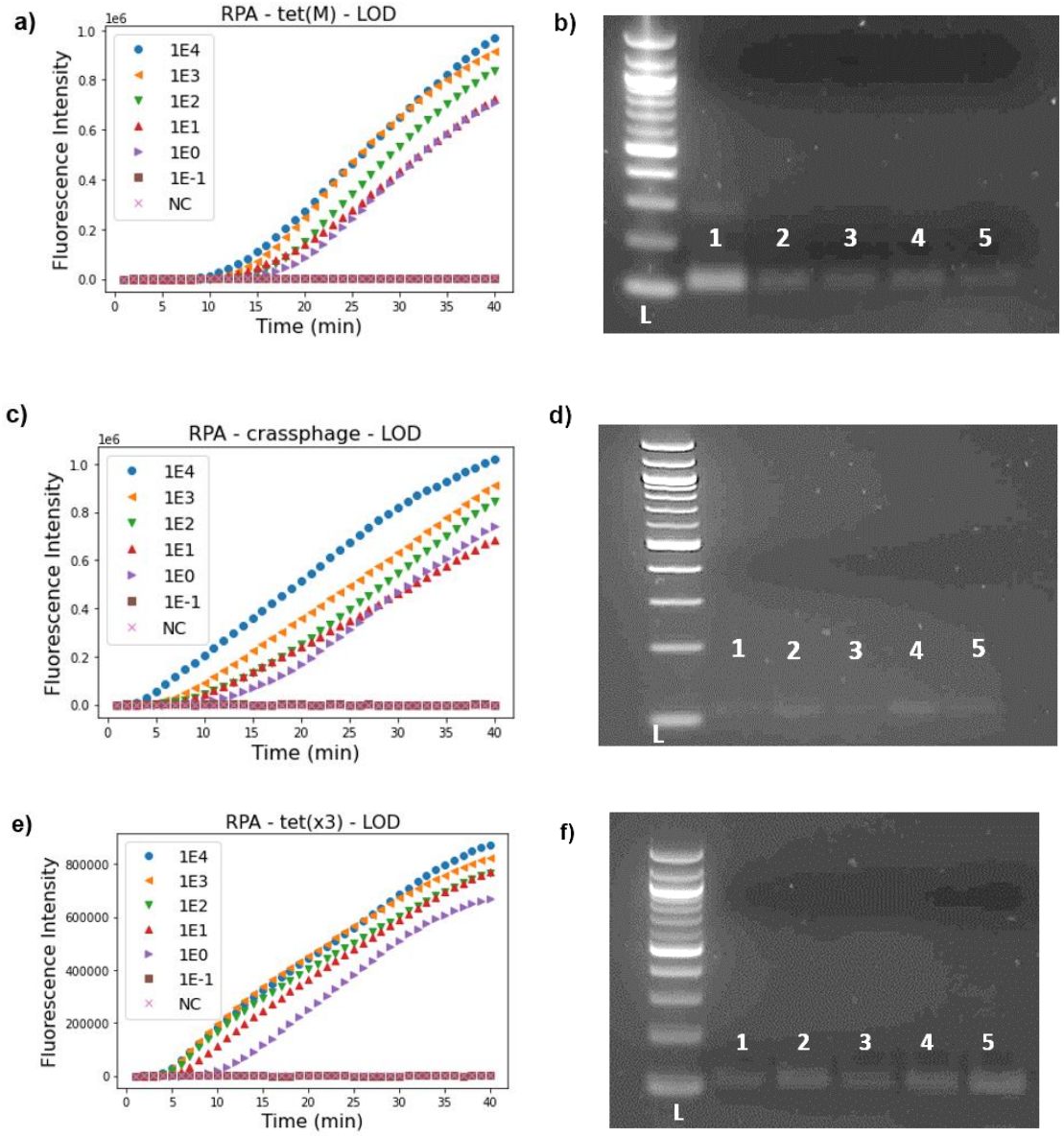


Figure 3.6 Sensitivity of RPA assay of a) and b) tet(M), c) and d) crassphage, and e) and f) tet(x3). a), b), c) represent the real-time fluorescent curves against time

under different concentration, ranging from $10^4$ copies $\mu L^{-1}$ to $10^{-1}$ copies $\mu L^{-1}$, while b), d) and f) represent the gel electrophoresis results of RPA assay. L represents 100 bp DNA ladder, Lane 1: $10^4$ copies $\mu L^{-1}$, Lane 2: $10^3$ copies $\mu L^{-1}$, Lane 3: $10^2$ copies $\mu L^{-1}$, Lane 4: $10^1$ copies $\mu L^{-1}$, Lane 5: $10^0$ copies $\mu L^{-1}$. NC: negative control. The presented curve is a mean of triplicates. The RPA assay conditions were the chosen ones as described above.

### 3.3.2 Optimisation of CRISPR/Cas assay

To improve the sensitivity of CRISPR/Cas assay, optimisation of assay conditions was conducted on RPA amplicons of tet(M), tet(x3), and crassphage on Quant Studio 3 thermal cycler. 6-FAM labelled ssDNA probe was employed as the real-time fluorescent indicator in the assay. The optimisation parameters include cas12a:crRNA ratio, cas12a:probe ratio, and reaction temperature. The optimal parameter set was selected based on a combination of fast kinetics and minimal non-specific amplification. Tet(x3) was employed as a model target for reaction parameter optimisation.

In principle, cas12a enzyme binds to crRNA in 1:1 ratio, and therefore experiments were conducted on testing the ratio between cas12a and crRNA from 1: 0.9, 1:1, and 1:1.2 as shown in Figure 3.7a. With similar reaction kinetics indicated by the real-time fluorescent amplification curves, the ratio of 1:1 showed an outstanding faster kinetics and therefore was chosen as the ratio used in subsequent experiments. Then, reaction temperature was optimised between 37 to 42°C. Reactions at 39 and 42°C both represented high reaction kinetics as shown in Figure 3.7b. While considering its integration with the pre amplification step of RPA, whose optimised reaction temperature was 39 °C, 39°C would be a better choice for CRISPR/cas reaction temperature due to assay simplicity. Finally, the ratio between cas12a and fluorescent ssDNA probe was optimised. Ratios of 1:15, 1:20, and 1:25 were investigated and 1:25 showed the fastest kinetics and the highest fluorescent signals, as shown in Figure 3.7c. Therefore, 1:25 was chosen to be the optimised ratio.

To sum up, the chosen CRISPR/Cas reaction conditions were as follows: reaction temperature at 39°C, cas12a: crRNA ratio equalled 1:1 and cas12a: probe ratio

1: 25. The amplification curves of the other two targets, tet(M) and crassphage, under the chosen reaction conditions were also shown as in Figure 3.7 d.

a)

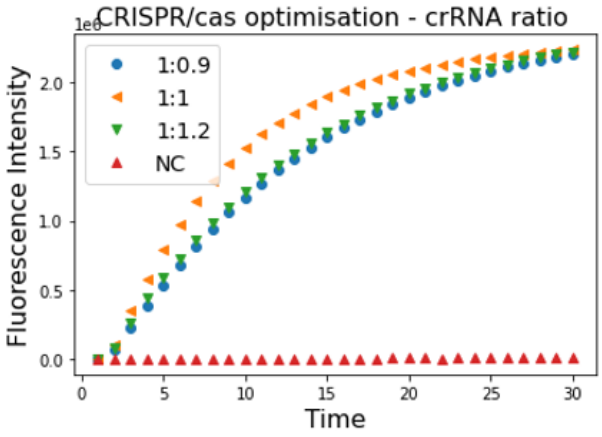
CRISPR/cas optimisation - crRNA ratio
1e6
Fluorescence Intensity
Time
1:0.9
1:1
1:1.2
NC

b)

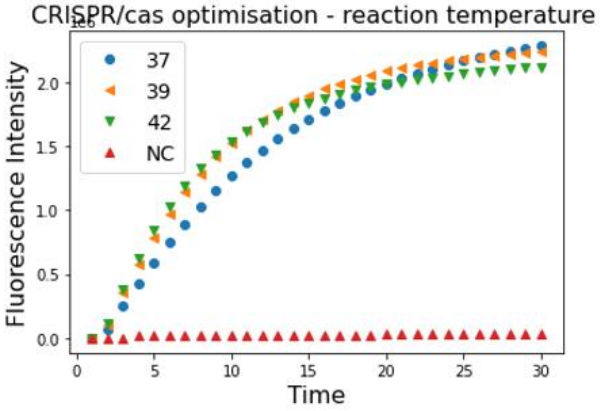
CRISPR/cas optimisation - reaction temperature
1e6
Fluorescence Intensity
Time
37
39
42
NC

c)

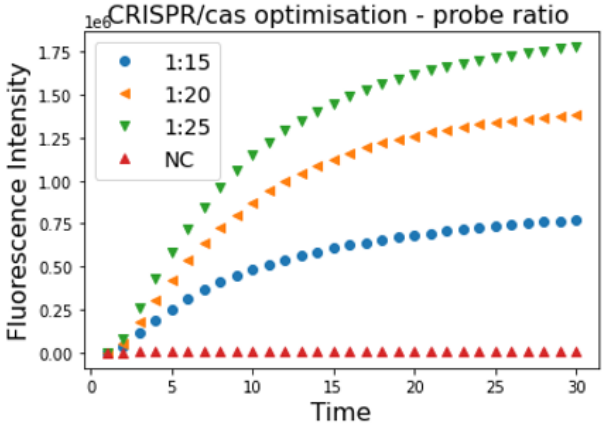
CRISPR/cas optimisation - probe ratio
1e6
Fluorescence Intensity
Time
1:15
1:20
1:25
NC

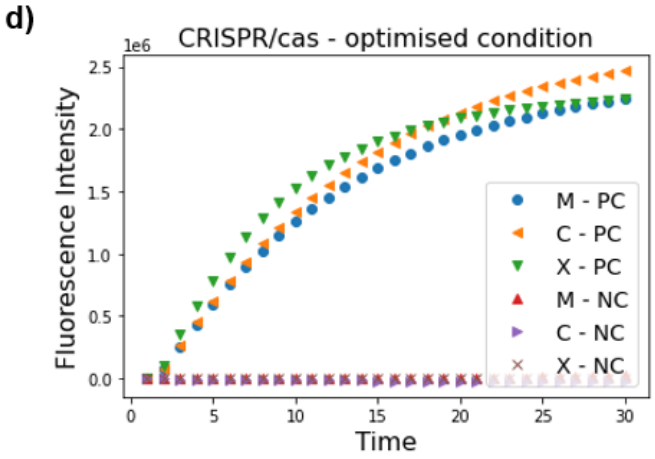


Figure 3.7 Optimisation of CRISPR/Cas assay using tet(x3) as a model target. a) cas12a: crRNA ratio optimisation b) reaction temperature optimisation c) cas12a: ssDNA probe ratio optimisation d) Real-time fluorescent RPA-CRISPR/Cas on all three targets, including tet(x3) (X). PC: positive control. NC: negative control. The presented curve is a mean of triplicates.

With the optimal assay conditions, the LODs of the RPA-CRISPR/Cas assays of the three targets, tet(M), tet(x3), and crassphage were evaluated. First, RPA was performed on 10-fold serial diluted target DNA sequences ($10^{4}$-$10^{-1}$ copies $\mu L^{-1}$) and $ddH_2O$ was employed as the internal negative control. All RPA assays were conducted on a Quant Studio 3 Real-Time PCR system. Subsequently, optimised CRISPR/Cas assay was carried out on the RPA amplicons of different initial concentrations, and again $ddH_2O$ was employed as the internal negative control. All subsequent CRISPR/Cas assays were conducted on a Quant Studio 3 Real-Time PCR system.

In Figure 3.8, the real-time fluorescent curves of all three targets were represented. Since the CRISPR/Cas reaction was performed on RPA amplicons, the reaction initiated at around 2 minutes for all targets where RPA reaction proceeded. And therefore, the LODs of CRISPR/Cas assays were the same as the RPA assays and were investigated to be 1 copy $\mu L^{-1}$ for all three targets.

Comparing to most reported CRISPR/Cas assays, the proposed assay showed better LODs and comparable analysis time. Wang et al. [194] proposed an RPA-CRISPR/Cas assay for *Enterocytozoon hepatopenaei* detection, reaching a LOD

of 10 copies, and Liu et al. [195] reported an RPA-CRISPR/Cas for *Staphylococcus aureus* detection, with an LOD of 5 copies per µL. And Li et al. [196] proposed a one-pot RPA-CRISPR/Cas assay for determining methicillin-resistant *Staphylococcus aureus* and it achieved an LOD of 10 copies per µL.

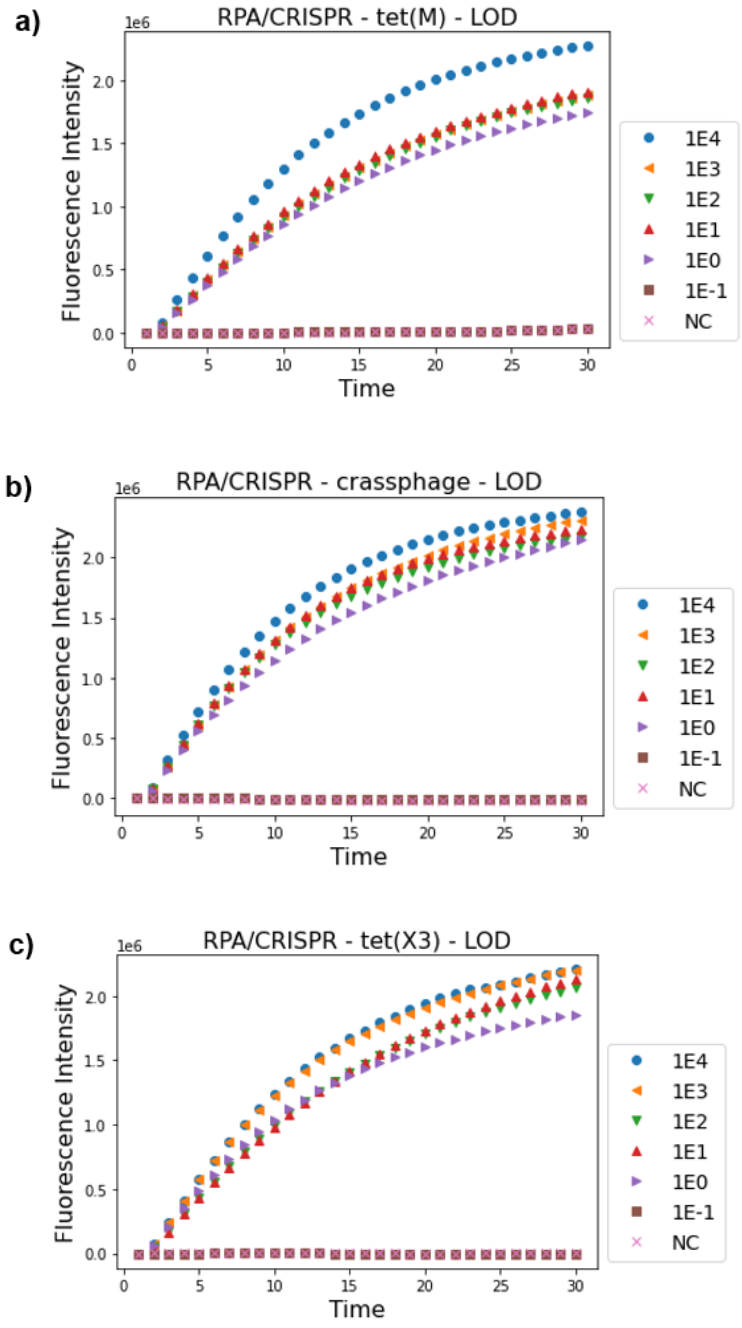


Figure 3.8 Sensitivity of real-time fluorescent RPA-CRISPR/Cas assay. a) RPA-CRISPR/Cas for tet(M). b) RPA-CRISPR/Cas for crassphage. c) RPA-

CRISPR/Cas for tet(x3). Target concentrations are from $10^{4}$-$10^{-1}$ copies $\mu L^{-1}$. NC: negative control. The plotted curve is a mean of triplicates.

### 3.3.3 Real-time fluorescent mRPA-CRISPR/Cas assay for ARG detections

#### 3.3.3.1 Analytical performance evaluation

The assay was further modified to be multiplexed, i.e., amplification of three targets simultaneously, with subsequent specific CRISPR/Cas detection. The LOD of the mRPA-CRISPR/Cas assay was investigated as stated above with slight modification. All three targets were mixed at equal concentration (i.e., 100 copies $\mu L^{-1}$ tet(M) mixed with 100 copies $\mu L^{-1}$ tet(x3) and 100 copies $\mu L^{-1}$ crassphage) to make DNA samples. 10-fold serial diluted target DNA sequences ($10^{4}$-$10^{-1}$ copies $\mu L^{-1}$) were amplified by the developed mRPA assay of three gene targets, respectively. As for internal negative controls, dd$H_2O$ was employed. All mRPA assays were conducted on a Quant Studio 3 Real-Time PCR system. Then specific CRISPR/Cas assay was applied on the mRPA product for detection, and again dd$H_2O$ was employed as the internal negative control. All subsequent CRISPR/Cas assays were conducted on a Quant Studio 3 Real-Time PCR system.

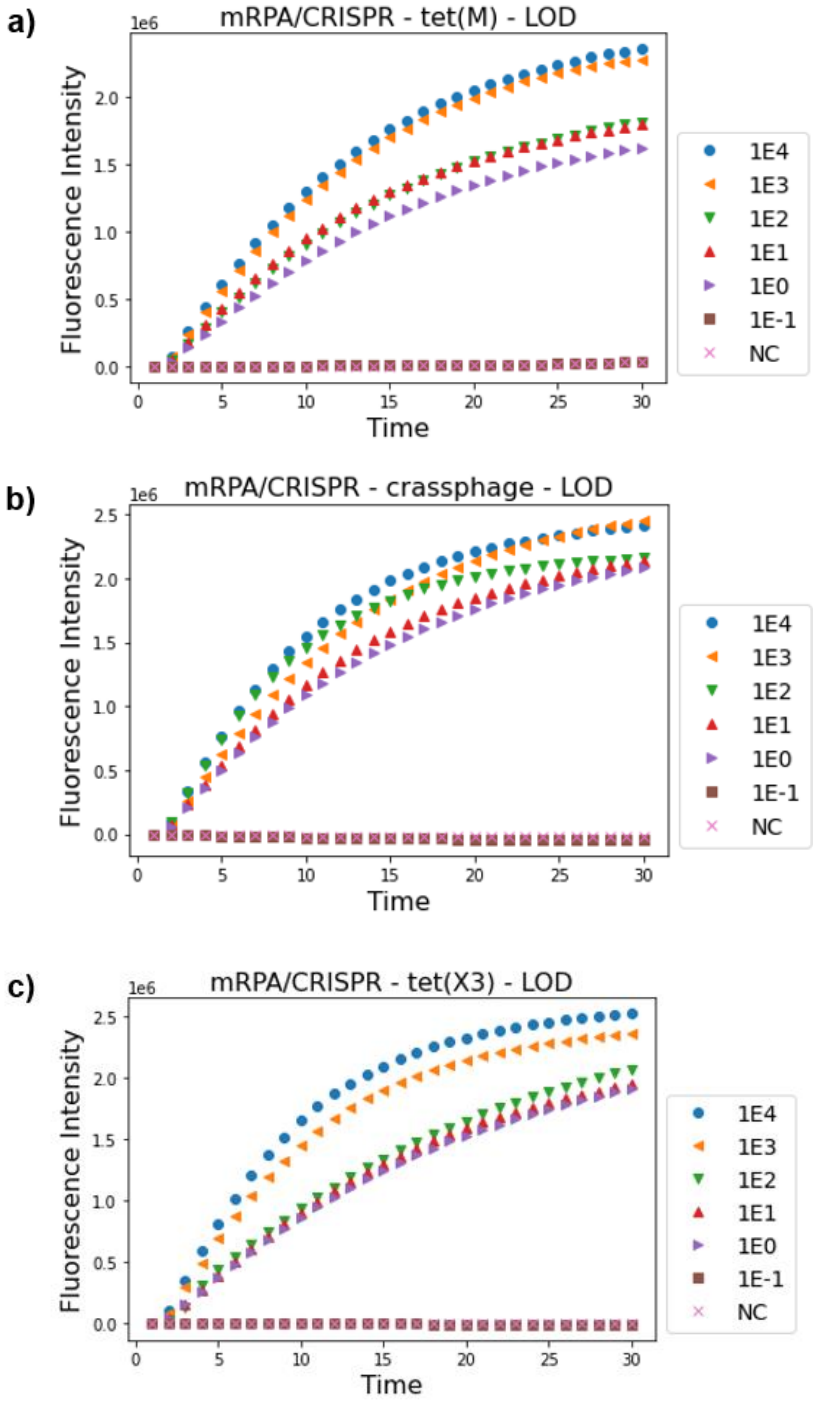


Figure 3.9 Sensitivity of real-time fluorescent mRPA-CRISPR/Cas assay. a) RPA-CRISPR/Cas for tet(M). b) RPA-CRISPR/Cas for crassphage. c) RPA-CRISPR/Cas for tet(x3). Target concentrations are from $10^{4}$-$10^{-1}$ copies $\mu L^{-1}$. NC: negative control. The plotted curve is a mean of triplicates.

As shown in Figure 3.9, the real-time fluorescent curves of mRPA-CRISPR/Cas assays were presented. It could be seen that the LODs of mRPA-CRISPR/Cas maintained to be 1 copy $\mu L^{-1}$ for all three targets. Besides, the CRISPR/Cas detection initiated still at around 2 minutes for all three targets at different temperatures, indicating the pre mRPA amplification maintained its amplification efficiency as the single target amplification with RPA. Besides, as shown in 3.3.1 and 3.3.2, the LOD of RPA, RPA-CRISPR/Cas and mRPA-CRISPR/Cas remained to be 1 copy $\mu L^{-1}$. This result indicated that the CRISPR/Cas assay had no effect on improving the overall sensitivity which was probably mainly contributed by the RPA assay. However, end-point RPA assay (e.g., gel electrophoresis or Eva Green fluorescent detection) alone can only offer non-sequence-specific detection, and therefore not suitable for multiplexed RPA assay. In this way, CRISPR/Cas was still required in order to be integrated with multiplexed RPA assay, since it served as an end-point detection approach that could distinguish different target sequences.

There was another observation that all three target genes shared the same LODs in terms of mRPA-CRISPR/Cas assay. Since the sensitivity was mainly determined by RPA assay as just discussed, the same LOD among three genes was probably due to the comparable efficiency of the RPA assay of the three targets. Since various RPA assay condition was tested for each gene target and the set of parameters that gave the best performance was chosen, it was reasonable to have same high sensitivity for all targets.

#### 3.3.3.2 Evaluation of analytical performance with spiked real water samples

The developed real-time fluorescent mRPA-CRISPR/Cas assay was finally validated with spiked real water samples to assess its field-testing applicability. Surface water samples collected from Willen Lake, Milton Keynes, UK and tap water from laboratories at Cranfield, UK, were spiked with purified DNA sequences of different known concentrations ($10^6$-$10^0$ copies $\mu L^{-1}$). Then the spiked water samples went through DNA extraction, followed by mRPA-

CRISPR/Cas assay with dd$H_2O$ employed as the internal negative control, on a Quant Studio 3 Real-Time PCR system.

The mRPA-CRISPR/Cas assay results of spiked surface water samples and spiked tap water samples of tet(M), crassphage, and tet(x3), respectively are shown in Figure 3.10. It could be seen that all reactions initiated at around 2 minutes as in pristine samples. And all reactions with target concentrations higher or equal to 1 copy $\mu L^{-1}$ proceeded, which was in line with that of pristine samples. When compared with the known spiked concentration, accuracy of the mRPA-CRISPR/Cas assay reached 100% on all three targets. Therefore, results illustrated that there were no inhibitors in surface water and tap water matrices, and the developed mRPA-CRISPR/Cas assay was ready to be tested and validated its applicability in real water samples.

a)

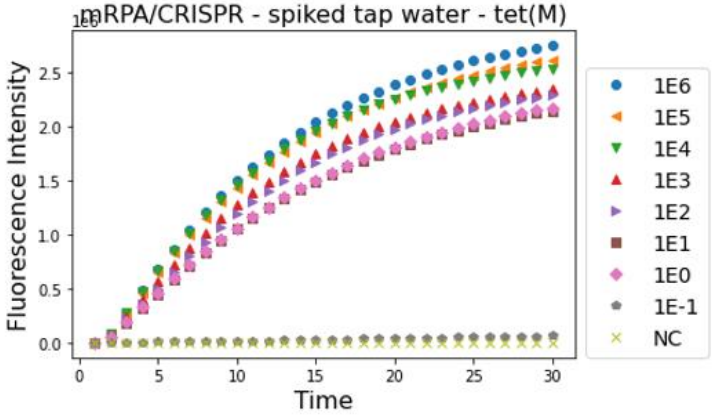
mRPA/CRISPR - spiked tap water - tet(M)
1e6
Fluorescence Intensity
Time
1E6
1E5
1E4
1E3
1E2
1E1
1E0
1E-1
NC

b)

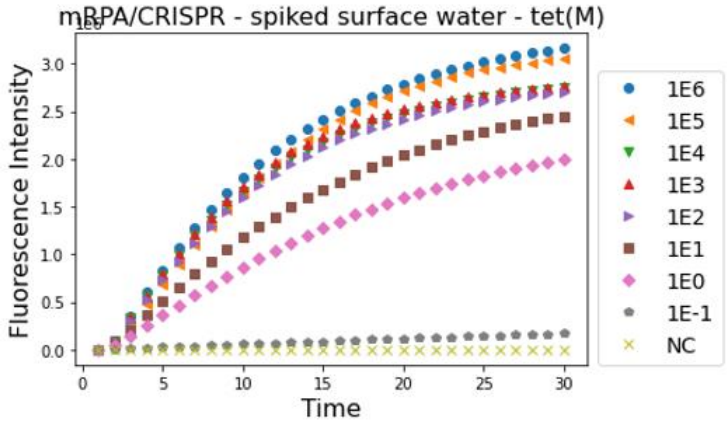
mRPA/CRISPR - spiked surface water - tet(M)
1e6
Fluorescence Intensity
Time
1E6
1E5
1E4
1E3
1E2
1E1
1E0
1E-1
NC

c)

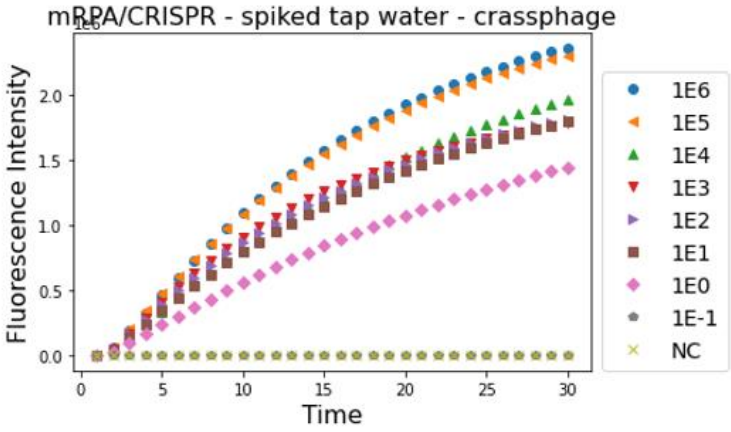
mRPA/CRISPR - spiked tap water - crassphage
1e6
Fluorescence Intensity
Time
1E6
1E5
1E4
1E3
1E2
1E1
1E0
1E-1
NC

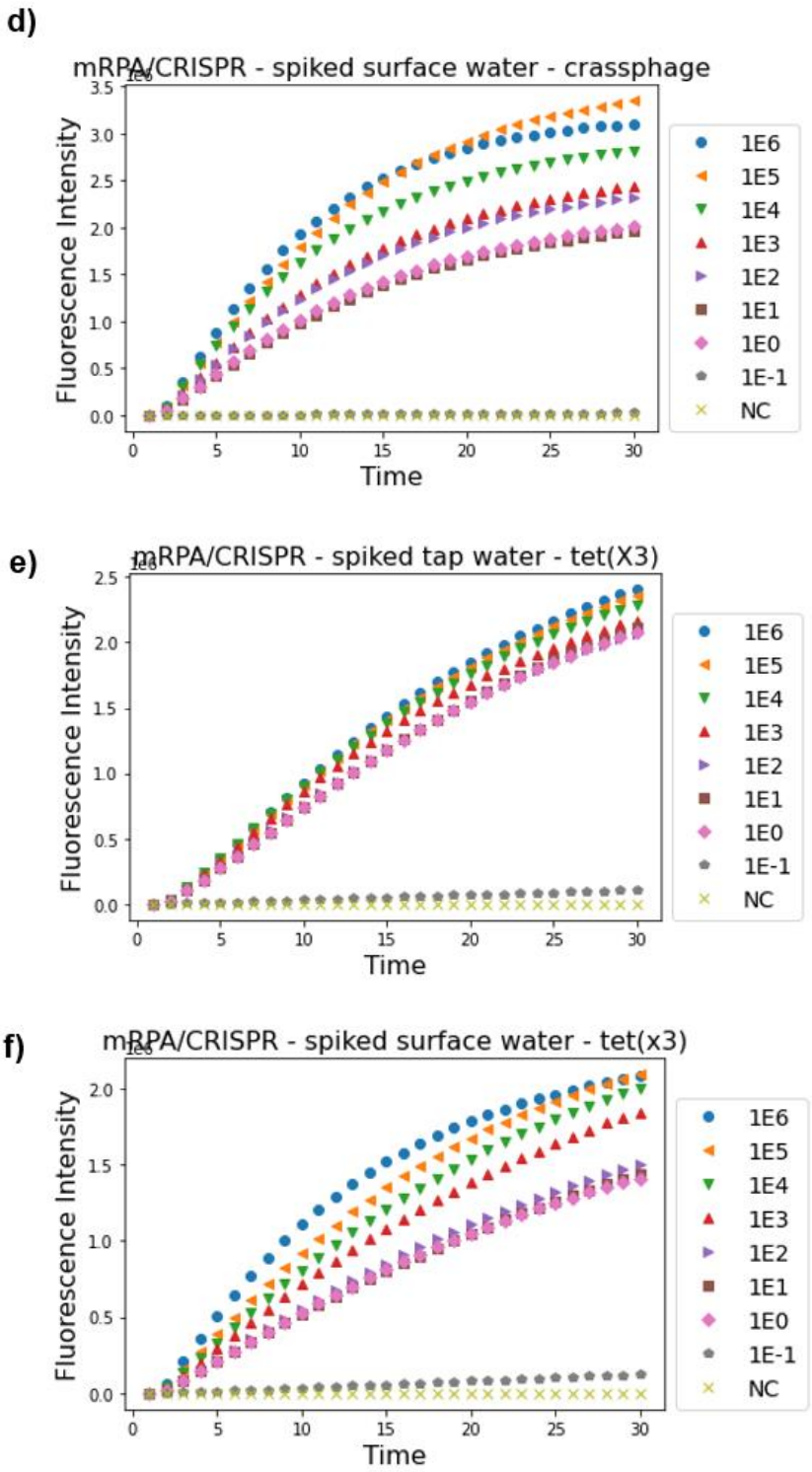


Figure 3.10 Real-time fluorescent mRPA-CRISPR/cas assay on spiked surface and tap water samples. a), c) and e) are results of spiked tap water. b), d) and f) are results of spiked surface water. a) and b) are results of tet(M), c) and d) are of crassphage, and e) and f) are of tet(x3). Target concentrations are from $10^{6}$-$10^{-1}$ copies $\mu L^{-1}$. NC: negative control. The plotted curve is a mean of triplicates.

Table 3.1 Overview of RPA-CRISPR conditions and detection methods

| Detection approaches | Detection target | Sensitivity | Matrices | Multiplex | Ref |
|---|---|---|---|---|---|
| Fluorescent, colorimetric, lateral flow | *Plasmodium* spp parasites | 1 copy $\mu L^{-1}$ (fluorescent and colorimetric), 10 copy $\mu L^{-1}$ (lateral flow) | Dried filter blood spots | N | [197] |
| Fluorescent | *Enterocytozoon hepatopenaei* | 10 gene copies per reaction | Shrimps | N | [194] |
| Fluorescent, lateral flow | *S. aureus* | 5 copies per reaction | Milk and water | N | [195] |
| Fluorescent, lateral flow | *Clostridioides difficile toxin genes* | 10 copies (tcdA) and 1 copy (tcdB) | Pristine and diarrhea samples | Y | [198] |
| Fluorescent | 14 respiratory infectious viruses | 2 copies $\mu L^{-1}$ | Pristine samples | Y | [199] |
| Fluorescent, electrochemical | *Brucella* spp. | 2 copies per reaction | Milk and blood samples | N | [200] |
| Electrochemical | human papillomavirus-16 | $6.022 \times 10^5$(1 pM) | vaginal swab samples | N | [201] |

## 3.4 Conclusions

The development of a real-time fluorescent mRPA-CRISPR/Cas assay enables rapid, sensitive, and efficient amplification and detection of different ARGs and MST gene under isothermal conditions, indicating its potential in versatile use in resource-limited area. Individual RPA reaction conditions were optimised and achieved a LOD of 1 copy $\mu L^{-1}$ for all three targets. The following optimisation of CRISPR/Cas assay allowed to achieve a LOD of 1 copy $\mu L^{-1}$ for all three targets. Finally, mRPA-CRISPR/Cas assay was developed with the LODs for all three targets remained 1 copy $\mu L^{-1}$.

Compared to other studies as demonstrated in Table 3.1the developed assay is more sensitive than most of them. Besides, the assay multiplexed amplified different targets, which most other studies lack. The multiplexing nature effectively simplifies the assay process and alleviates resource and human force burden. Besides, this developed assay filled the need that there is a lack of multiplexed RPA-CRISPR/Cas assay for ARG and source-tracking detection in the water. It contributed to the AMR monitoring in the environmental transmission.

Although current assays were completed in Quant Studio 3 PCR machines, it is for the need to real-time fluorescent curves observation for reaction monitoring. Its isothermal nature enables the assay to be carried out in portable hot water bath or dry heat block, and the fluorescent results reading could be achieved by portable fluorimeter, further enhancing its POU feature. Moreover, the developed mRPA-CRISPR/Cas assay is promising for onsite ARG detection, as the assay was demonstrated to be 100% accurate when tested in spiked surface water and tap water samples. In addition, the LODs of the developed assay in spiked real water samples were the same as those of pristine samples, indicating the assay holds high robustness and could overcome possible inhibitors in real water sample matrices that might affect assay performances.

Finally, the developed assay holds high potential for transferability. By simply changing RPA primers and crRNAs, the developed assay could be extensively applied to other gene targets for rapid, sensitive, and potential onsite detections.

In summary, the proposed fluorescent mRPA-CRISPR/Cas is a promising POU detection tool due to its simplicity, portability, rapid, and sensitive nature. It contributes to the development of multiplexing RPA without compromising reaction time and sensitivity while lowering the cost of the assay. Its potential in extending to other targets could contribute to universal AMR testing in environmental monitoring. Besides, building from this study, POU devices accommodating the developed assay are to be produced, enabling various detection and monitoring of gene biomarkers of AMR and pathogens not only in the field of environment, but also under clinical context and food safety area.

# 4 Enhancing Environmental Monitoring with Integrated Detection Approaches: Lateral Flow and Electrochemical Assays with mRPA-CRISPR/Cas

## 4.1 Introduction

AMR is a leading cause of morbidity and mortality worldwide [1]. National and global action plans have been established for ARG, ARB and antibiotics monitoring to address this global public health concern, however, most data are collected under clinical context. Recently, there has been an emerging trend on monitoring the AMR in the environment, especially in different water bodies e.g., surface waters. Municipal wastewater is one of the most critical AMR sources to the environment, and therefore it is necessary to monitor its level of ARGs.

As discussed in 3.1, isothermal amplification and CRISPR/Cas technology have been extensively applied in rapid gene detection, which suits the purpose of rapid and sensitive monitoring of ARGs at POU. Based on that, a real-time fluorescent mRPA-CRISPR/Cas for multiplexed amplification was developed with a detection of three target genes of LODs of 1 copy $\mu L^{-1}$. However, the developed mRPA-CRISPR/Cas assay requires trained personnel and sophisticated equipment, limiting its application for onsite measurements. There is an urgent need to call for other detection approaches for effective onsite readable result delivery.

Lateral flow assay (LFA) is an integrated device with biosensing assay accommodated, meeting the requirements of WHO REASSURED principles for POU devices, i.e., real-time connectivity, ease of specimen collection and environmental friendliness, affordability, sensitivity, specificity, user-friendliness, rapidity and robustness [202]. Generally, a LFA is composed of four parts, sample pad, where sample is dropped, conjugate pad, where labelled reporters combine with biorecognition elements, reaction membrane, where test line and control line are printed to bind with targets, and finally, wick pad, where waste is absorbed [203]. Colloidal gold is most widely employed as LFA labels. while there are other options, including carbon nanotubes and quantum dots [204]. Still, colloidal gold remains to be extensively employed due to their cost-effective development,

intense colour, high stability and naked eye inspection of results. Benefitted from its cellulose paper-based nature, LFA offers low-cost and sustainable manufacturing, and the capillary force of the porous paper provide equipment-free microfluidics [205]. The high compatibility to various samples leading to application of LFA covers clinics e.g., pregnancy tests and COVID19 monitoring [206], environment e.g., pesticides [207], and food safety e.g., pathogens [208].

While LFA presents to be a rapid and cost-effective POU tool, on the other hand, electrochemical detection holds the potential for quantification measurements. It measures the change in electrical signals on electrode surface during an electrochemical reaction involving electron transfer. Among all kinds of electrochemical sensors, the voltametric ones where current is recorded as a function of potential, including cyclic, square wave, and linear sweep, are widely used. Due to its ability in excluding interferences from non-Faradaic processes, SWV is regarded as a highly sensitive approach and is widely applied in environmental detections, especially pollutants in the water [209–212]. In addition, electrochemical based sensors are also highly efficient, executable, fast to operate, and cost-effective; they also hold the potential for future miniaturisation to form an integrated POU device.

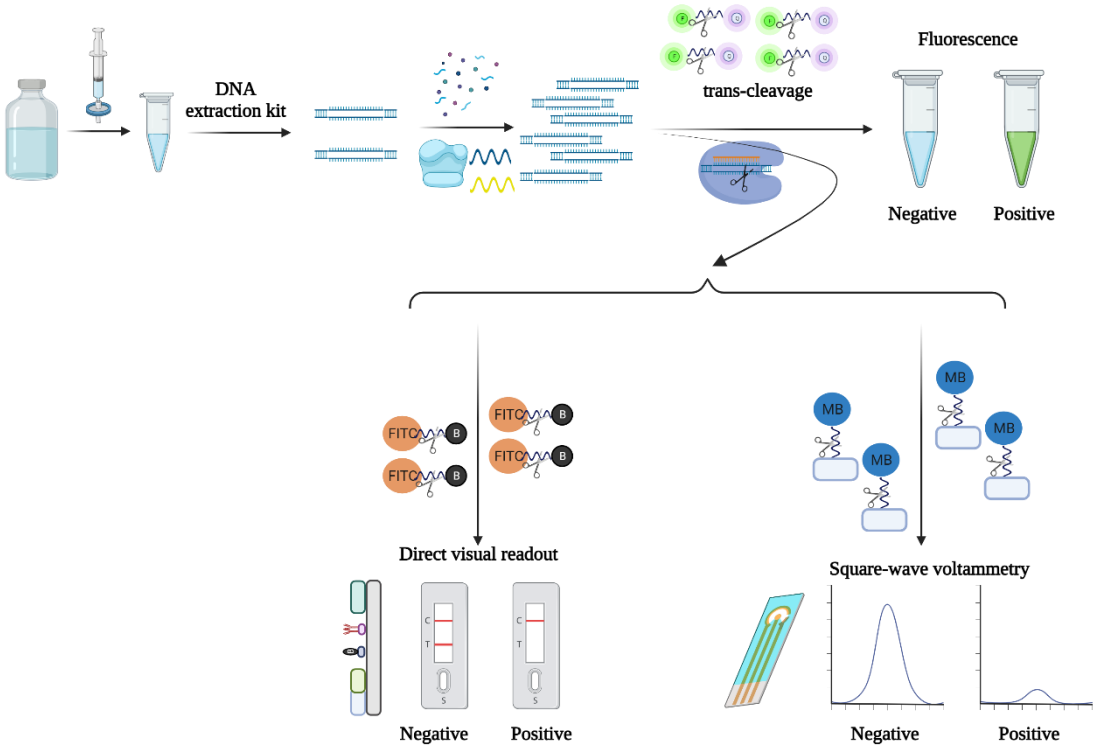


Figure 4.1 Overview of mRPA-CRISPR/Cas based electrochemical and lateral flow assay detections

The objective of this chapter is to expand the developed mRPA-CRISPR/Cas to two other detection approaches, i.e., electrochemical and lateral flow assay, for the rapid monitoring of ARGs (tet(M) and tet(x3)) and the MST gene (crassphage) at POU, as shown in Figure 4.1. The electrochemical assay was developed and the immobilisation strategy of probe onto the electrode was optimised, and the lateral flow assay was assembled from pads with nitrocellulose membrane optimised (they are of different pore size and thus wicking time). The analytical performance of both assays was evaluated with 10-fold serial diluted pristine samples of all three targets. For electrochemical detection, the sensitivity of all three targets reached 10 copies $\mu L^{-1}$, while for lateral flow assays, the sensitivity of tet(x3) and crassphage was 1 copy $\mu L^{-1}$ and that of tet(M) was 10 copies $\mu L^{-1}$. Both assays were applied for gene detection in wastewater samples and validated by comparing the result with that of qPCR.

## 4.2 Materials and Methods

### 4.2.1 Chemicals and apparatus

Quant Studio 3 Real-Time PCR System, and TaqMan Fast Virus 1-step Master Mix (4×) was from Thermo Fisher Scientific, UK. EvaGreen, 20× in water, was from Cambridge BioScience (UK), while ethanol, ddH2O, were from Sigma Aldrich (UK). TwistAmp basic kit was from TwistDX, UK and EnGen Lba Cas12a (Cpf1), 10× NEB Buffer, and cas12a diluent solution were from New England Biolabs, UK. BioReady Material Starter Kit for Lateral Flow, 40 nm BioReady Gold Nanospheres – Streptavidin and anti-FITC antibody were from Stratech, UK. BSA-biotin conjugate, sucrose, PBS tablet, Triton X-100, NaCl, BSA were from Merck, UK. PK-4 Electrode Polishing Kit is from Alvatek, UK. Forced air oven StableTemp is from Cole-Parmer, UK.

The working electrodes were gold electrodes (code BASMF2014-1EA, Sigma Aldrich, UK), auxiliary ones were made of platinum wire (code BASi MW-1032, Alvatek, UK) and reference ones were Ag|AgCl (code BASi MF-2052, Alvatek, UK). All the measurements were conducted under room temperature, via Multi Autolab/M204 (Metrohm, UK), and data was collected and analysed with Nova 2.1(Metrohm, UK).

RPA and qPCR primers together with probes were designed using Primer-BLAST website and their sequences listed in Table **A**.**2** and Table A.3. They were synthesised by and purchased from Merck, UK. The 5' end of the probes were modified with 6-FAM and 3' end with BHQ-1. crRNA was designed on CRISPOR (http://crispr.tefor.net/) and purchased together with ssDNA probe (tagged with 6-FAM and BHQ-1) from Merck, UK. Amplification template of tet(x3) was synthesized and purchased from Eurofins Genomics, Germany, and those of tet(M) and crassphage were from the wastewater samples, gel purified and stored at -20°C until use. Electrochemical reporter probe modified with MB and -SH group and the lateral flow assay reporter, modified with FITC and biotin were from Merck, UK. All chemicals were of analytical reagent grade and used without further purification. dd$H_2O$ was purified through a Millipore System (Millipore,

USA, resistivity >18 MΩ). Each assay was repeated at least 3 times to ensure reproducibility.

### 4.2.2 DNA template extraction from wastewater samples and quantification

DNA templates in pristine samples were extracted from wastewater samples and prepared as detailed previously in 3.2.2. The concentration of extracted DNAs was measured by Qubit 4 Fluorimeter as described previously in 3.2.3. Finally, the resulting DNA samples were stored at – 20 °C freezer until use.

### 4.2.3 mRPA-CRISPR/Cas assay

The mRPA-CRISPR/Cas assay was conducted as described in 3.2.6. Briefly, the 2× mRPA assay was 50 µL in total and prepared as stated in 3.2.4 with slight modification: 1.25 µL forward/reverse primers (tet(M)), 1.425 µL forward/reverse primers (tet(x3)), 1.125 µL forward/reverse primers (crassphage), 29.5 µL rehydration buffer, 4.4 µL dd$H_2O$. Each 41.5 µL primer solution was added to the lyophilised pellet with subsequent equal separation to two reaction tubes. 1.25 µL 280 mM $Mg^{2+}$ was added to tube cap and 3 µL mixed DNA samples was added to each reaction assay. The reaction mix was then incubated at 39 °C for 40 min in a Quant Studio 3 real-time qPCR machine. Then CRISPR/Cas detection was conducted on the mRPA products as described in 3.2.5 with slight modification to suit for downstream electrochemical/lateral flow assay detection, as detailed in the following sections. A sensitivity investigation was then conducted as before on the 10-fold serial diluted target genes for both detection methods.

### 4.2.4 Electrochemical detection

Electrochemical detection is also widely employed for rapid and onsite detection of environmental pollutants. The designed biosensing mechanism is as shown in Figure 4.2. In brief, the mRPA-CRISPR/Cas is conducted as described previously, while the ssDNA probe in CRISPR/Cas assay is changed to thiol conjugated ssDNA with the other end tagged with electrochemical active redox reporter methylene blue (MB). The probe is subsequently immobilised onto working electrode surface due to gold-thiol interactions. Then the SWV signal of the

immobilised electrode is measured before the electrode is immersed into mRPA-CRISPR/Cas assay solution and incubated at 39 °C for 30 min. If targets are present and thus probes cleaved, leading to the dissociation of MB, then the electrochemical signal is reduced. While targets are absent, MB is still conjugated with probes and therefore bound to the electrode surface, the electrochemical signals will remain the same as before the reaction. It is worth mentioning that before each SWV measurement, the working electrode was carefully rinsed with ultrapure water to minimise non-specific adsorption of MB. Several SWV measurements were conducted, and the SWV signals were only recorded once a stable peak current and peak shape of SWV were obtained, which usually took less than one minute.

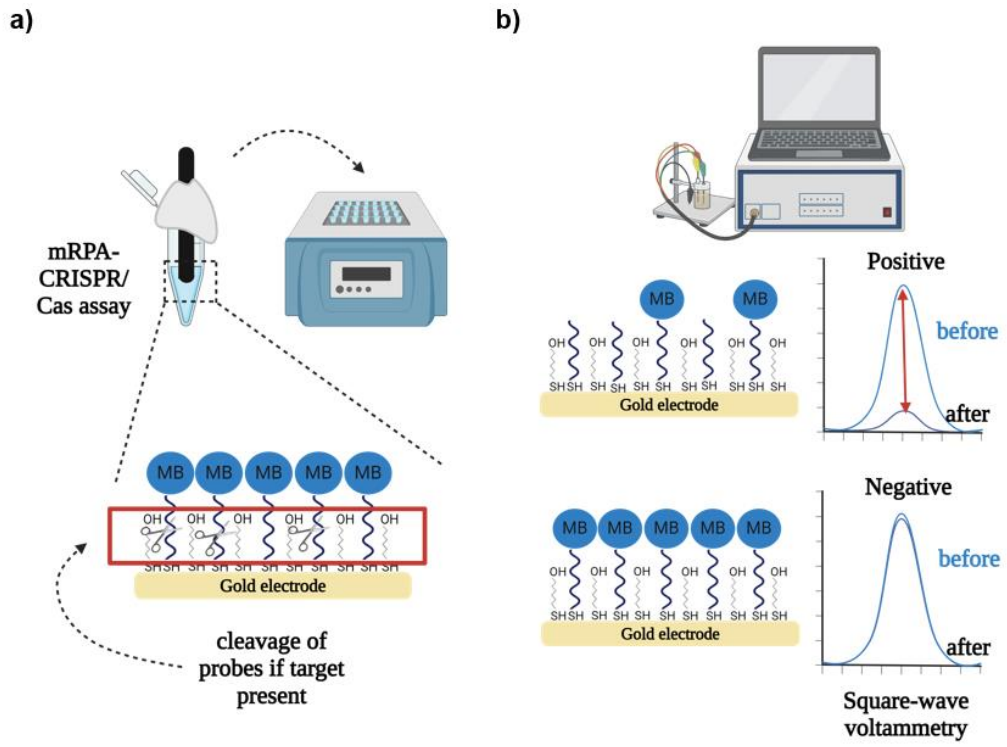


Figure 4.2 Biosensing mechanism of the developed signal-off electrochemical based mRPA-CRISPR/Cas assay. a) The setup of the working electrode incubation for detection. b) Schematic illustration of electrode surfaces and SWV signals before and after reaction in the cases of positive and negative controls.

All the measurements were conducted in triplicates under room temperature, via Multi Autolab/M204 (Metrohm, UK), and data was collected and analysed with Nova 2.1(Metrohm, UK) on a laptop. Gold electrode (code BASMF2014-1EA, Sigma Aldrich, UK), platinum wire (code BASi MW-1032, Alvatek, UK)) and Ag/AgCl (3 M NaCl) (code BASi MF-2052, Alvatek, UK) were, respectively, employed as working electrode, auxiliary electrode and reference electrode. The phosphate buffered saline (PBS, 0.01 M $Na_2HPO_4$-$NaH_2PO_4$-KCl, pH 7.4) was prepared from PBS tablets from Sigma-Aldrich (UK). Gold electrode was cleaned by polish kit and CV (potential range -0.25V – 1.6 V) in 0.5 M $H_2SO_4$ solution, rinsed with ultrapure water and dried under $N_2$ gas before immobilisation. Besides, the thiolated CRISPR/Cas electrochemical reporter probe (**Table A.8**) was reduced by adding TCEP in 100 × excess, e.g., 30 mM tris(2-carboxyethyl)phosphine (TCEP) to 300 µM probe, for 2 hours at room temperature. The reduced probes are stored in -20 °C until use.

As for the immobilisation, two different methods were employed to compare, as shown in Figure 4.3. One (separate immobilisation) was to immerse the gold electrode in 150 µL 1 µM reduced ssDNA probe solution for 2 hours at room temperature in a sealed and dark environment, followed by immersing in 150 µL 10 mM 6-mercapto-1-hexanol (MCH) solution sealed and dark overnight at room temperature to backfill any space left on the surface. In addition, the other (co-immobilisation, modified from Yang et al. [213] was to mix the electrochemical reporter with MCH resulting in a 150 µL solution of 1 µM reporter with 10 µM MCH before immersing the gold electrode overnight in a sealed and dark environment, and in the subsequent step, the immersed electrode was dipped into 150 µL 1 mM MCH solution sealed and dark for one hour. Finally, the electrode is stored in 0.01M PBS solution sealed and dark in 4 °C until use.

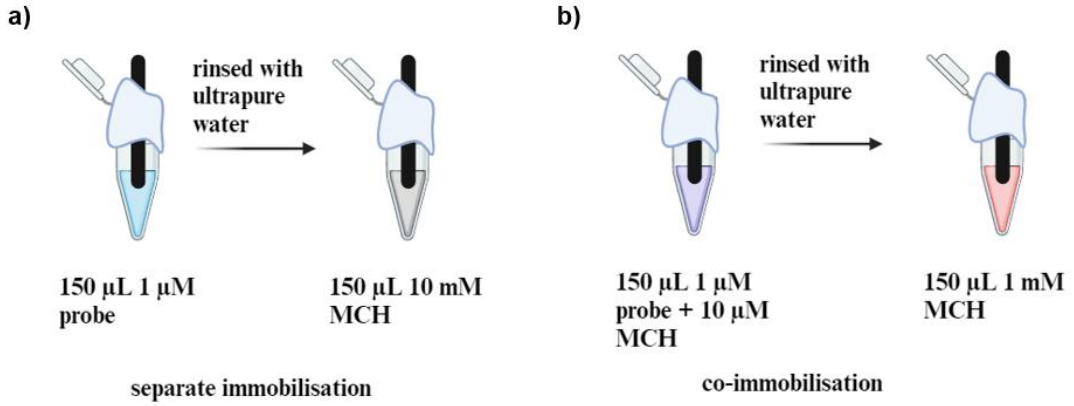


Figure 4.3 Schematic representation of electrode immobilisation approaches. a) separate immobilisation. b) co-immobilisation.

Square wave voltammetry (SWV) experiments of the electrode before and after mRPA-CRISPR/Cas assay for all three targets were completed in buffer solution of 0.01M PBS solution. The potential range of SWV is -0.5 V to 0 V, with a step of 1 mV and frequency of 150 Hz. 10-fold serial diluted purified targets ($10^5$ copies $\mu L^{-1}$to 1 copy $\mu L^{-1}$) of all three genes, (tet(x3), tet(M), and crassphage) went through electrochemical mRPA-CRISPR/Cas assay for the determination of sensitivity. All experiments were conducted in triplicates.

### 4.2.5 Lateral flow strips detection

Lateral flow strips were assembled before detection. The sample pads (8950 glass fibre, Ahlstrom) and wick pads (grade 222, Ahlstrom) were cut to strips of 18 mm width before use. Optimisation on nitrocellulose membrane selection was conducted among MDI 70, 90, 150. Before assembly, 1 mg $mL^{-1}$ anti-FITC antibody (Stratech, UK) in 0.01 M sodium phosphate, 0.25 M NaCl, and 1 mg $mL^{-1}$ BSA-biotin (Sigma Aldrich, UK) in 0.01M PBS with 5% sucrose were pipetted (in 1.3 µL drops) onto the nitrocellulose membranes to make the control and test lines, respectively, with a 5 mm distance in between the two lines. Then the membrane with pipetted test and control lines was dried in 37 °C forced air oven overnight. Then the LFAs were assembled according to manufacturers' instructions. Briefly, as shown in Figure 4.4, the nitrocellulose membranes were first attached to the backing cards, followed by the sample pad, with an overlap

with membrane of 3 mm, and then the wick pad was attached, with another overlap with membrane of 3 mm. Finally, the cards were cut to strips of 5 mm width and ready to be used.

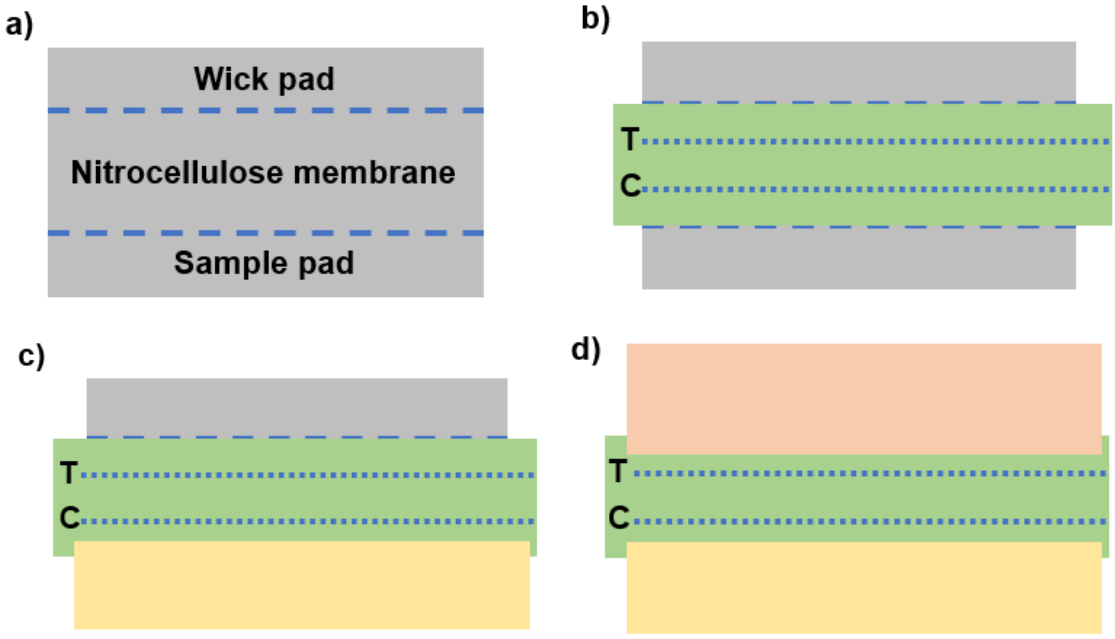


Figure 4.4 Schematic illustration of lateral flow strip assembly. a) The distribution of zones on backing card. b) Attachment of nitrocellulose membranes (printed with control and test lines) onto the backing card. c) Attachment of sample pad which overlaps with the nitrocellulose membrane of 3 mm. d) Attachment of wick pad which overlaps with the nitrocellulose membrane of 3 mm. The assembled pad is finally cut to strips of 5 mm width.

The biosensing mechanism of the developed lateral flow strip is presented in Figure 4.5. Briefly, the strip is made up of three pads: a sample pad, a nitrocellulose membrane, and a wick pad. Control lines (anti-FITC antibody) are printed closer to the sample pad than test line (BSA conjugated biotin) with a 5 mm distance in between. mRPA-CRISPR/Cas reaction is carried out as described in 4.2.3 but the ssDNA probe is changed from the fluorescent one to the designed lateral flow one, with ssDNA tagged with FITC antibody and biotin. Streptavidin coated AuNP is chosen as the colorimetric reporter and mixed with mRPA-CRISPR/Cas products before dropped onto sample pad. Running buffer is added to the mixture to help with the wicking of analytes. To sum up, the LFA

mRPA-CRISPR/Cas mixture contains the CRISPR/Cas solution with LFA probe, mRPA amplicons, streptavidin coated AuNP and running buffer when dropping onto the sample pad and tested by LFA. If the target is absent, the mRPA-CRISPR/Cas will not be triggered and therefore, the probe remains complete. Once they conjugate with colorimetric reporter, only the control lines will show colour and the test lines remain blank. On the other hand, if the target is present, triggering the mRPA-CRISPR/Cas reaction, the probes will be cleaved to different extend depending on the target concentration. Thus, the cleaved parts where colorimetric reporters conjugated are captured by the test lines, leading to colour on test lines while less or no colour shown on control lines.

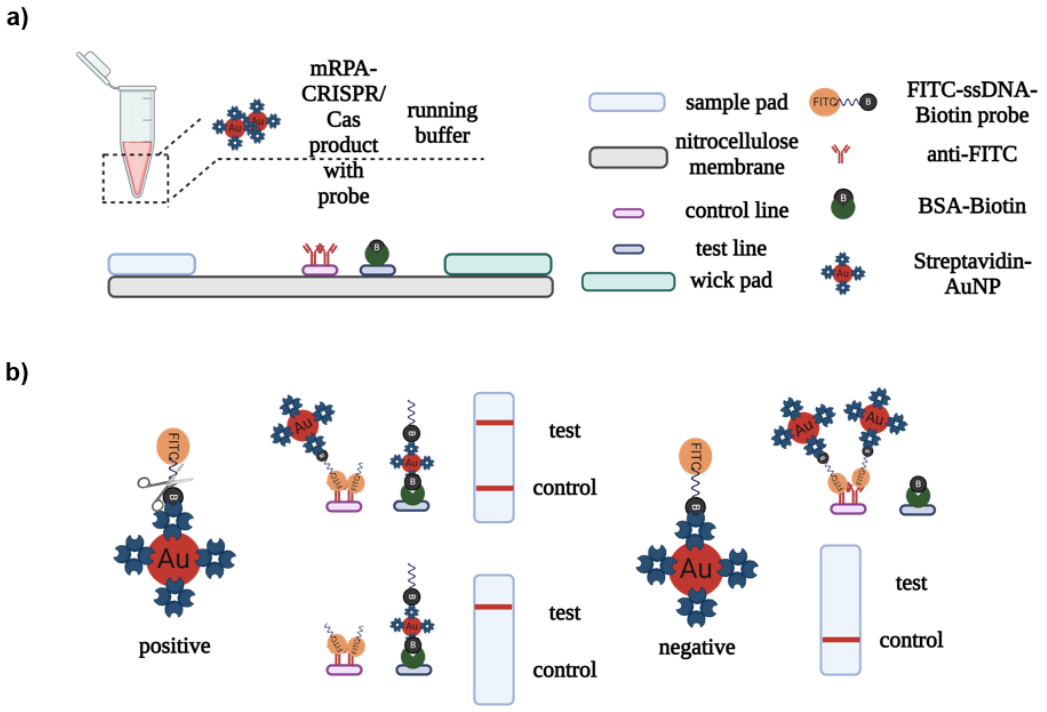


Figure 4.5 Biosensing mechanisms of the developed lateral flow strip. a) Composition of lateral flow assay. Streptavidin coated AuNP reporter was mixed with sample before test. b) Schematic illustration of on test and control lines capturing probes in the cases of positive and negative controls.

For detection, samples were mixed with BSA coated gold nanosphere-streptavidin composites and running buffer, with a final volume of 75 µL and a final concentration of gold nanosphere of 0.5 OD. The gold nanosphere-streptavidin composites were blocked with BSA in the following steps: first, the

gold composites were mixed with 1% (w/v) BSA solution for 30 minutes at 4 °C. Then the mixture was centrifuged, and the supernatant was discarded. Finally, the collected pellet was resuspended in 1% BSA and 3% sucrose in 0.01M PBS solution and stored in dark at 4 °C until use. The LFA strip was then vertically inserted into the mixture of running buffer, CRISPR/Cas solution and mRPA products. The results were read in 15 minutes. Running buffer was 0.1% Triton X-100 and 1 % NaCl in ultrapure water. To determine the LFA sensitivity, mRPA-CRISPR/Cas based lateral flow assay was performed on 10-fold serial diluted purified targets ($10^5$ copies $\mu L^{-1}$ to 1 copy $\mu L^{-1}$) of all three genes, (tet(x3), tet(M), and crassphage). All experiments were conducted in triplicates.

### 4.2.6 Real sample validation

The workflow of real sample detections is as shown in Figure 4.1. Ten wastewater samples collected from Cranfield Wastewater Treatment Plant, Cranfield, UK; and four drinking water samples including two from Nigera and two from potable water tap of private water supplies in Aberdeenshire, Scotland, UK were used in the experiment. Triplicates were conducted for each sample and each gene. 40 mL water samples as mentioned were filtered through 0.45 µm pore-sized membrane and DNAs were then extracted with Pro Magazorb kit following its instructions, resulting in 200 µL eluted DNA samples. The extracted DNA samples were stored in -20°C freezers for further use.

As reference, qPCR experiments (total volume of each assay 20 µL) were performed on all three genes as follows (per assay): 5 µL 4× TaqMan mastermix, 500 nM forward primer, 500 nM reverse primer, 250 nM TaqMan probe.

Both electrochemical and lateral flow measurements were conducted on the extracted DNA samples and the results were compared with qPCR results for assay performance evaluation.

### 4.2.7 Data analysis and evaluation

All electrochemical measurements were conducted in triplicates under room temperature, via Multi Autolab/M204 (Metrohm, UK), and data was collected and

analysed with Nova 2.1(Metrohm, UK) on a laptop. Means and standard deviations of data were determined as previously described in 3.2.8. Threshold to distinguish positives and negatives was determined to be 0.04 μA. Data were treated and plotted using python3 Matplotilib.

All lateral flow detections were conducted in triplicates under room temperature, and photos were taken with iPhone 12 pro max. The threshold for determining positive and negative was conducted by naked eye and comparison of colorimetric intensity between test strips and negative controls.

The accuracy was calculated as (true positives + true negatives)/(true positives + false negatives + true negatives + false positives) × 100.

## 4.3 Results and discussion

### 4.3.1 Optimisation of lateral flow assay (LFA)

The development of LFA requires optimisation after assembly to improve its analytical performance. The choice of nitrocellulose (NC) membrane is vital for LFA development, and NC membrane should be chosen based on the size of the analyte and sample type. As the pore size of NC membrane increases, the flow rate of sample increases (i.e., wicking time decreases), and thus leaves less time for test lines and control lines to capture the probes in the sample, leading to reduced sensitivity. In addition, the concentration of colorimetric reporter is also important for result visualisation.

As shown in Figure 4.6a, test lines and control lines are pipetted in 1.3 μL drops onto three different NC membranes, MDI 70, MDI 90, and MDI 150. The reported wicking time of each NC membrane is as stated in Table 4.1. The modified NC membranes were dried in forced air oven at 37 °C overnight before assembled into LFA strips to use. Running buffer was then mixed with streptavidin-AuNP for different final concentrations, 1 OD, 0.5 OD and 0.1 OD, before assembled LFA strips were immersed into the solutions, as shown in Figure 4.6b. In this experiment, 1 OD of the employed 40 nm AuNP equals to $10^{-10}$ M according to manufacturers' instruction. From observing the results, 0.5 OD streptavidin-AuNP showed the most intense colour in control lines with less background, and MDI

90 showed the most uniform colour. Therefore, MDI 90 was selected as NC membrane to be used and 0.5 OD streptavidin-AuNP was determined to be the optimal reporter concentration. Reaction volume of LFA, on the other hand, can also affect assay sensitivity. The higher the reaction volume is, the quicker the sample flows through the NC membrane. As shown in Figure 4.6c, 50 µL, 75 µL, and 100 µL running buffer with 0.5 OD streptavidin-AuNP were tested on MDI 90 strips. The resulting bands showed similar performances, and therefore 100 µL was chosen to meet the rapid testing purpose, as it showed the quickest flow among the three.

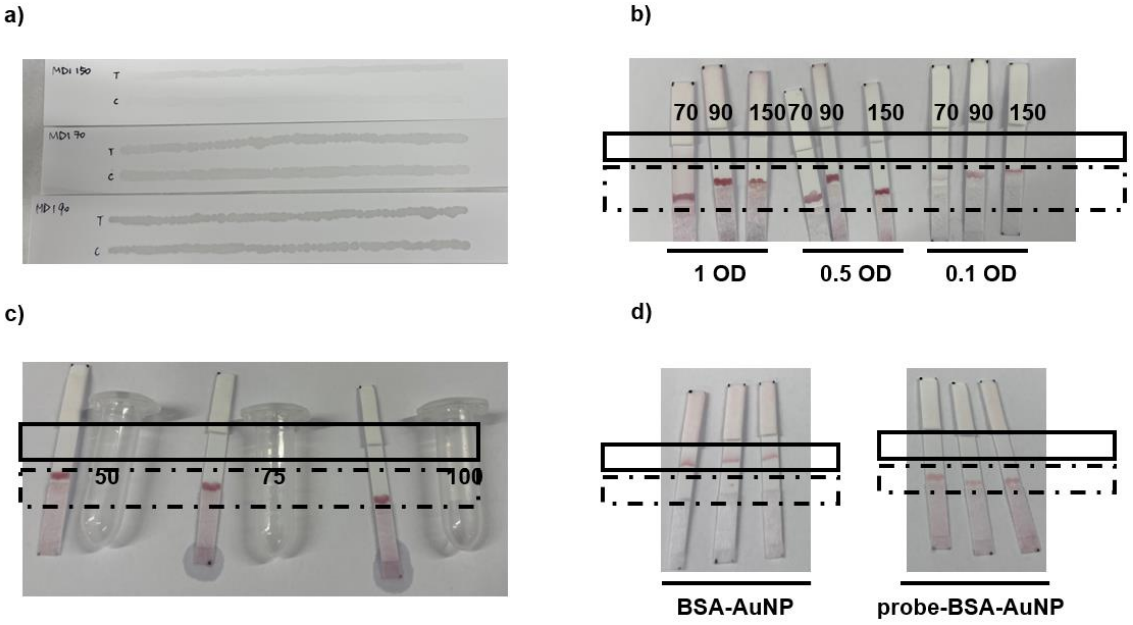


Figure 4.6 Optimisation of lateral flow assay reaction conditions. a) Selection of nitrocellulose membrane between MDI 70, MDI 90 and MDI 150 modified with test and control lines. b) optimisation of reporter concentration: 1 OD, 0.5 OD, and 0.1 OD streptavidin coated AuNP mixed with running buffer (n=3) c) Optimisation of reaction volume, 50 µL, 75 µL and 100 µL (n=3) d) BSA blocking effect on AuNP to prevent non-specific binding. Solid square marks the position of test lines while dashed square marks the position of control lines.

Table 4.1 Wicking time of different NC membranes

| Type | Wicking Time (s) |
|---|---|

| | |
|---|---|
| MDI 70 | 70±12 |
| MDI 90 | 90±15 |
| MDI 150 | 150±20 |

However, a problem rises from the results as colour is only shown on control lines. In principle, streptavidin coated AuNP should not bind with control lines, as there are only anti-FITC antibodies deposited; but should bind with test lines where BSA-biotin is printed. One possible reason is that AuNPs can non-specifically bind to proteins. To solve this problem, BSA is coated onto the streptavidin-AuNP as mentioned in 4.2.5. As shown in Figure 4.6d, BSA coated streptavidin-AuNP no longer binds to the control line binds to the test line. When the LFA probe is added, BSA-streptavidin-AuNP is completely conjugated to the probe, and therefore captured by control lines rather than the test lines.

The next step is to determine the concentration of LFA probe that should be added to the 0.5 OD BSA-streptavidin-AuNP and running buffer mixture. 125 nM, 50 nM, 10 nM, 5 nM and 0 nM LFA probe were added, respectively, and the results are as shown in Figure 4.7a. From the results, 5 nM probe is adequate to capture all colorimetric reporter without any leakage to the test lines. However, there was an anti-intuitive observation that the band intensity decreased with increasing probe concentrations. One possible explanation is that, as illustrated in Figure 4.7b, the LFA probe is more than enough to capture all colorimetric reporters. Therefore, increasing overall probe concentrations in the LFA detection led to decreasing concentration of ‘colorimetric reporter bound probe’. Since the intensity of the band is only dependent on the concentration of the ‘colorimetric reporter bound probe’ rather than that of the ‘overall prove’. In this case, higher overall probe concentration leads to diluted concentration of ‘reporter bound probe’ captured by the control lines. Thus, the intensity of control line decreases with increasing overall probe concentration.

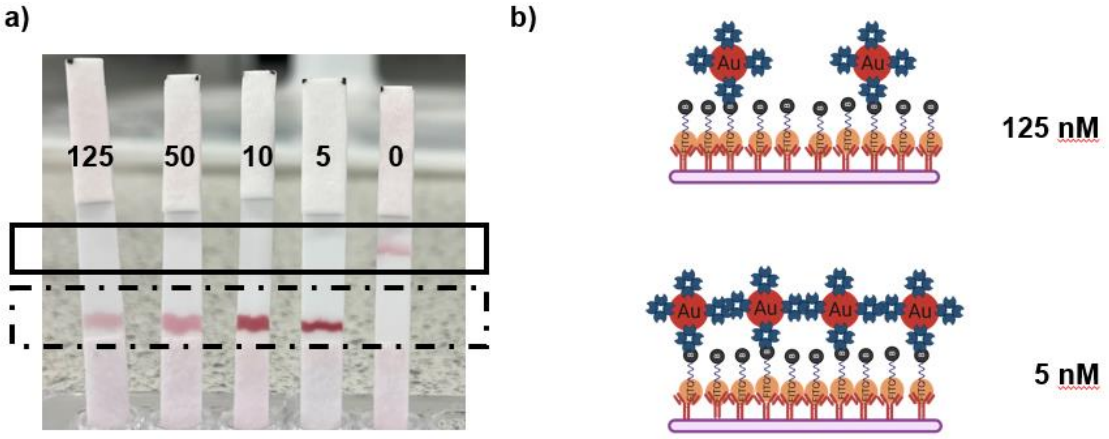


Figure 4.7 Optimisation of probe concentration for LFA. a) Different concentrations (125 nM, 50 nM, 10 nM, 5 nM and 0 nM) of LFA probes added to 0.5 OD BSA-streptavidin-AuNP in running buffer. (n=3) b) Schematic illustration of control lines when 125 nM probe or 5 nM probe is added. Solid square marks the position of test lines while dashed square marks the position of control lines.

After optimisation, the first attempt to test the feasibility of developed LFA on mRPA-CRISPR/Cas products was carried out, using $10^5$ copies $\mu L^{-1}$ tet(x3) as a case study. The results are as shown in Figure 4.8a. While the performance of negative controls was in line with prediction, an unexpected circumstance occurs in the positive controls. The test lines did not show intense colour bands but only show blank or vague bands (PC-1 and PC-2). As illustrated in Figure 4.8b, one AuNP can bind to several streptavidin, and one streptavidin possesses four binding sites with biotin. Therefore, in principle, even if binding with AuNP takes up two sites of streptavidin, and one site is needed to bind with the LFA probe, there is still one site left for cleaved reporter to bind with biotin on the test line. However, experimental results suggested that binding to LFA probe and AuNP changes the conformation of streptavidin, making it less prevalent to binding with biotin on the test line. To eliminate the effect of control lines in the issue of test line not showing, the LFA strips were then reversely (upside down) immersed into the sample solutions with the wick pads taken off. As shown in Figure 4.8c, the results suggested that the issue of test line not showing (i.e., non-binding

between cleaved ssDNA-biotin-streptavidin AuNP complex and test line) was not interfered by the presence control lines.

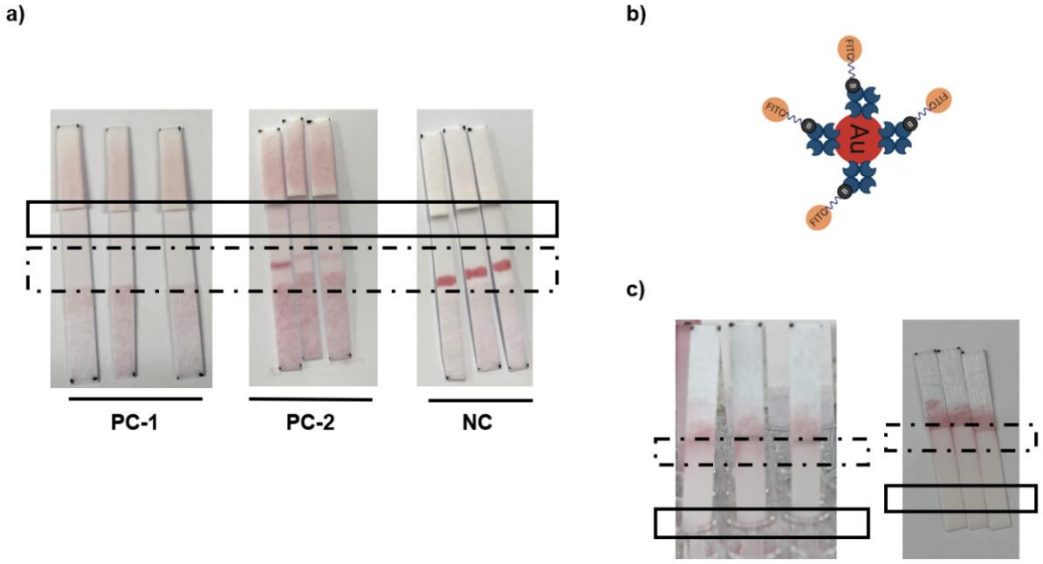


Figure 4.8 Demonstration of LFA on developed mRPA-CRISPR/Cas using $10^5$ copies $\mu L^{-1}$ tet(x3) as example. a) LFA results of positive and negative controls. PC-1: positive control case 1. PC-2: positive control case 2. NC: negative control. b) Schematic illustration of streptavidin-AuNP bound probe. c) Reversely inserted LFA into the testing sample solution with taken off wick pads. Solid square marks the position of test lines while dashed square marks the position of control lines.

Although the test lines are not working as expected, due to the working principle of the LFA (shown in 错误!未找到引用源。), the control line itself might be adequate to demonstrate the presence of the targets. Since the test line captures the cleaved part of the probe while the control line captures the remaining one, in principle, band intensity change either on control line or test line should be able to illustrate the cleavage of the probe, i.e., the presence of the targets. If negative controls are conducted individually and independently together with test samples on the same batch of the lateral flow strips, the developed LFA can still determine the presence of the targets by only observing the intensity of control line bands. However, even if the lateral flow strips were produced from the same batch of pads and membranes, there are risks that each strip does not perform the same

as expected. In this way, the results of the lateral flow tests and the negative control might not stand solidly. More efforts should still be carried out to further explore the reason behind the 'not showing' test lines, aiming to restore the lateral flow strip as a standalone gene test device with internal controls.

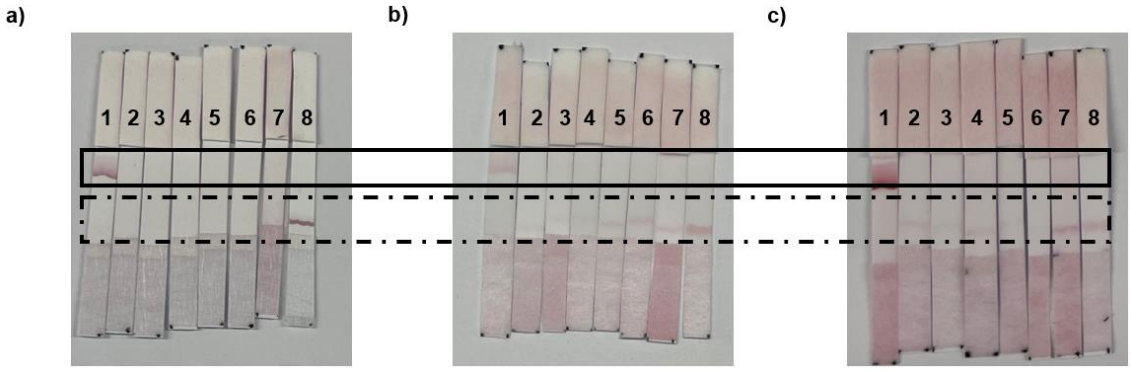


Figure 4.9 Sensitivity of LFA based mRPA-CRISPR/Cas assay. a) LFA mRPA-CRISPR/Cas for tet(x3). b) LFA mRPA-CRISPR/Cas for crassphage. c) RPA-CRISPR/Cas for tet(M). 1: only BSA-streptavidin-AuNP. 2-7: 10-fold serial diluted target concentrations ranging from $10^5$-$10^0$ copies $\mu L^{-1}$. 8: negative control. Experiments were conducted in triplicates with one shown as demonstration. Solid square marks the position of test lines while dashed square marks the position of control lines.

With all LFA reaction parameters optimised and problem solved, the exploration of LFA sensitivity was carried out. As shown in Figure 4.9, 10-fold serial diluted pristine target samples were employed with a concentration range of $10^5$-$10^0$ copies $\mu L^{-1}$, and a negative control was conducted each time. Vague control lines can be observed due to the incomplete cleavage of LFA probes. Positive and negative results were therefore determined by comparing the intensity of control lines with the negative controls. In this way, from visual readings, the LODs of LFA based mRPA-CRISPR/Cas assay for tet(x3), crassphage, and tet(M) were 1 copy $\mu L^{-1}$, 1 copy $\mu L^{-1}$, and 10 copies $\mu L^{-1}$, respectively.

### 4.3.2 Optimisation of electrochemical assay

To integrate the developed mRPA-CRISPR/Cas assay with electrochemical detection, the CRISPR/Cas probe is immobilised on the working gold electrode

surface. Before immobilisation, the gold working electrode was cleaned with polish kit and subsequent electrochemical cleaning by CV in 0.5 M sulphuric acid solution until characteristic gold cyclic voltammograms are shown, as in Figure 4.10a. The peaks of CVs are due to the reduction of gold oxide on the gold electrode surface. Then different immobilisation strategies were tried for optimal reaction conditions. Co-immobilisation and separate immobilisation strategies were conducted as described in 4.2.4, and a photo for demonstration is as shown in Figure 4.10b.

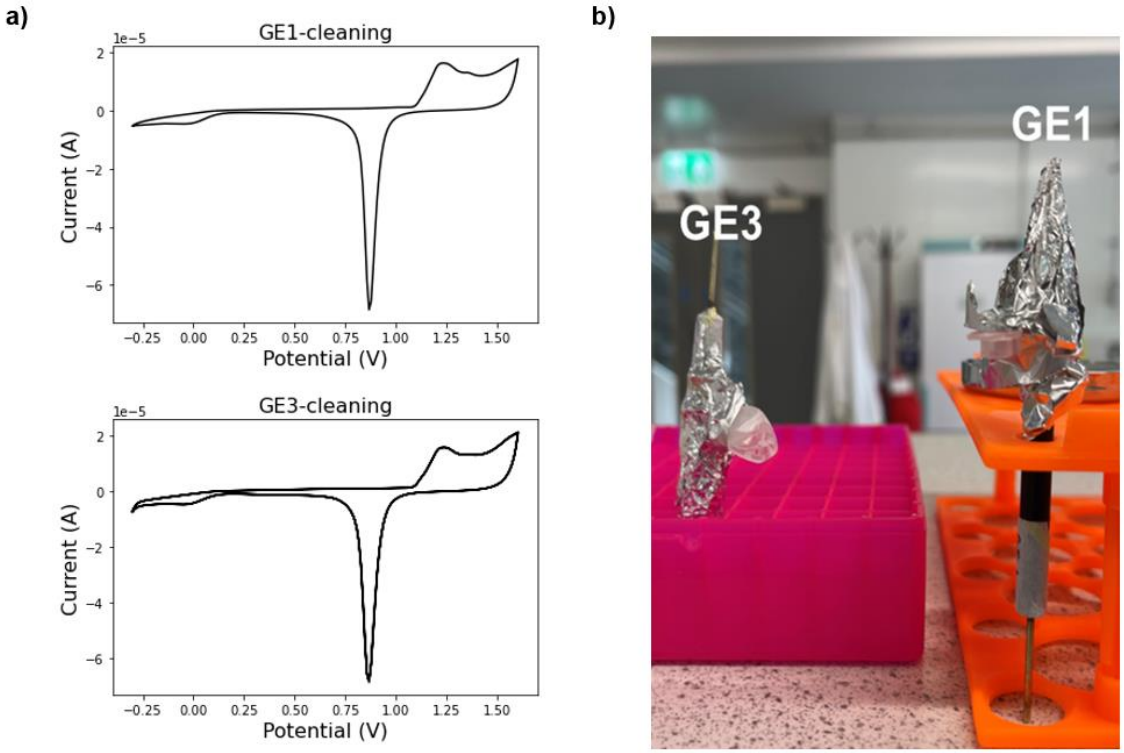


Figure 4.10 Optimisation in immobilisation strategy of gold working electrode. a) Characteristic cyclic voltammogram of cleaned gold electrodes. b) Demonstration photo of electrodes incubated for different immobilisation strategies under sealed and dark conditions. GE3: separate immobilisation. GE1: co-immobilisation.

Table 4.2 List of reduction peak potential, current, and area of cleaned working electrodes.

| | Peak potential (V) | Peak current (A) | Peak area (C) | ECSA ($cm^2$) |
|---|---|---|---|---|
| GE1 | 0.86609 | -6.82E-05 | 5.96E-06 | 0.015 |
| GE3 | 0.86609 | -6.80E-05 | 6.34E-06 | 0.016 |

Figure 4.10a shows the cyclic voltammogram of cleaned gold electrode, where reduction peak data were obtained, and the data are as shown in

Table 4.2. The electrochemical active surface area (ECSA) of gold working electrode could therefore be calculated by integrating the charge required for reducing the gold oxide, assuming the charge density for gold oxide reduction is 390 μC $cm^{-2}$ [214]. As shown in

Table 4.2, the two working electrodes had comparable ECSA, and therefore there was an almost the same starting point for immobilisation.

After immobilisation, the immobilised electrodes were characterised with CV and SWV. Figure 4.11 and Figure 4.12 represented the CV and SWV results of electrodes immobilised in different methods. As can be seen from Figure 4.11b, Figure 4.11d and Figure 4.12b, Figure 4.12d, peak currents were linearly proportional to scan rate and frequency, indicating that there were surface adsorbed behaviours, and therefore both of the immobilisations were successful. However, as can be seen from Figure 4.11a and Figure 4.12a, separate immobilisation clearly presented less capacitive current, resulting in less background noises. This was further confirmed by the comparison between Figure 4.11c and Figure 4.12c, where the SWV peak currents of separate immobilisation were higher, suggesting higher immobilised probe concentration and thus better signals.

Once the immobilisation strategy was optimised, the next step would be to explore the sensitivity of this electrochemical based mRPA-CRISPR/Cas assay. mRPA-CRISPR/Cas assay was conducted on 10-fold serial diluted pristine target samples before the mRPA products were incubated with CRISPR/Cas assay and probe-immobilised electrode as previously described. The current change before and after mRPA-CRISPR/Cas assay was measured and calculated, and the results were as presented in Figure 4.13. It could be seen that the LODs for all three targets were 10 copies $\mu L^{-1}$. Besides, from Figure 4.13, the absolute current change for different targets were varied, decreasing from tet(x3), to Crassphage and finally to tet(M). The possible reason accounting for this observation is that the CRISPR/Cas incubation and measurements were conducted sequentially from tet(x3), to Crassphage and finally to tet(M). Therefore, the probe density on the electrode surface decreased with cleavage, leading to the reduced value of current change.

a)

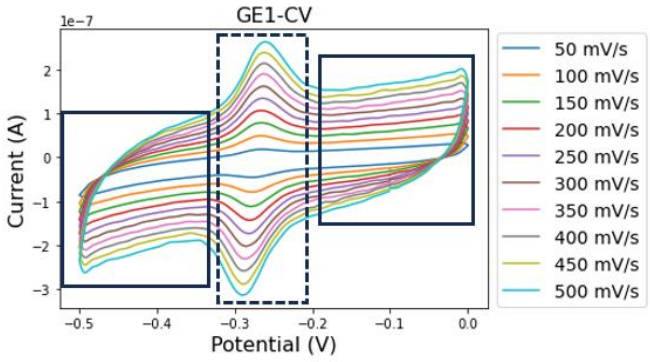
GE1-CV
1e−7
Current (A)
Potential (V)
50 mV/s
100 mV/s
150 mV/s
200 mV/s
250 mV/s
300 mV/s
350 mV/s
400 mV/s
450 mV/s
500 mV/s

b)

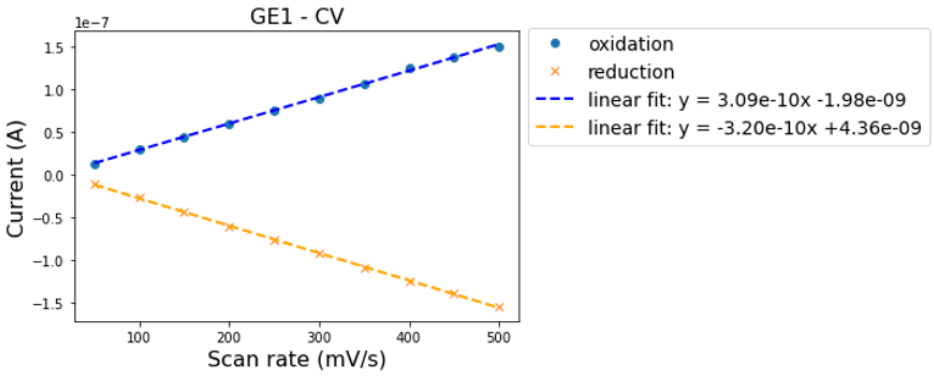
GE1 - CV
1e−7
Current (A)
Scan rate (mV/s)
oxidation
reduction
linear fit: y = 3.09e-10x -1.98e-09
linear fit: y = -3.20e-10x +4.36e-09

c)

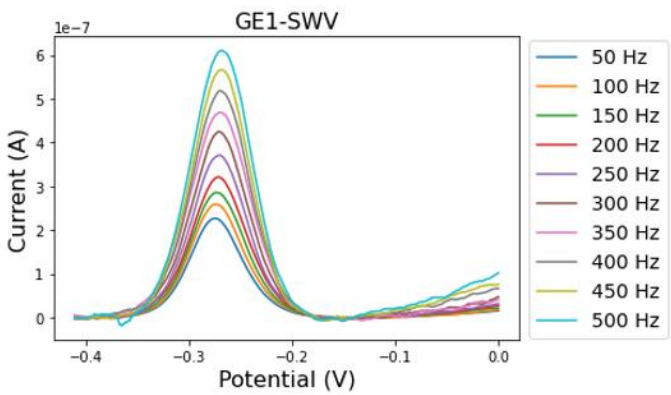
GE1-SWV
1e−7
Current (A)
Potential (V)
50 Hz
100 Hz
150 Hz
200 Hz
250 Hz
300 Hz
350 Hz
400 Hz
450 Hz
500 Hz

d)

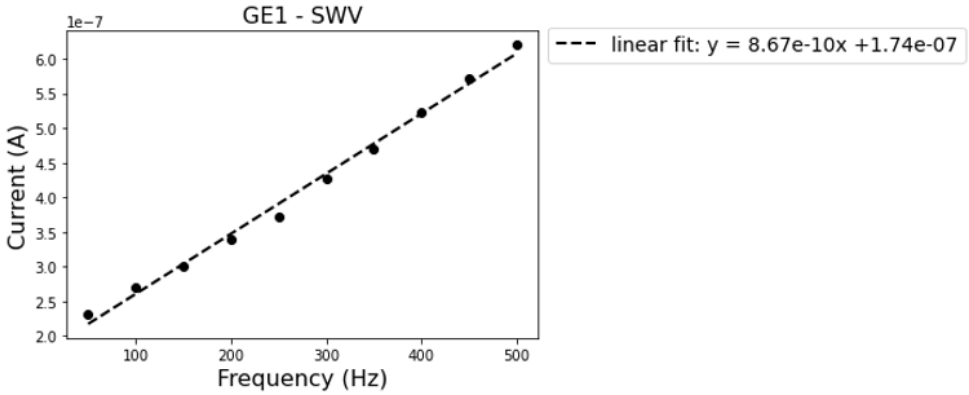
GE1 - SWV
1e−7
Current (A)
Frequency (Hz)
linear fit: y = 8.67e-10x +1.74e-07

Figure 4.11 Electrochemical measurements of GE1 (co-immobilisation). a) Cyclic voltammograms of different scan rates (50 mV $s^{-1}$, 100 mV $s^{-1}$, 150 mV $s^{-1}$, 200 mV $s^{-1}$, 250 mV $s^{-1}$, 300 mV $s^{-1}$, 350 mV $s^{-1}$, 400 mV $s^{-1}$, 450 mV $s^{-1}$, and 500 mV $s^{-1}$) recorded at equilibrium. Dashed box: Faradaic current. Solid box: capacitive current. b) Plot of scan rate versus peak currents of CV (both oxidation and reduction) with linear fits. c) square wave voltammograms of different frequencies (50 Hz, 100 Hz, 150 Hz, 200 Hz, 250 Hz, 300 Hz, 350 Hz, 400 Hz, 450 Hz, and 500 Hz) recorded at equilibrium. d) plot of frequencies versus peak currents of SWV with the linear fit.

a)

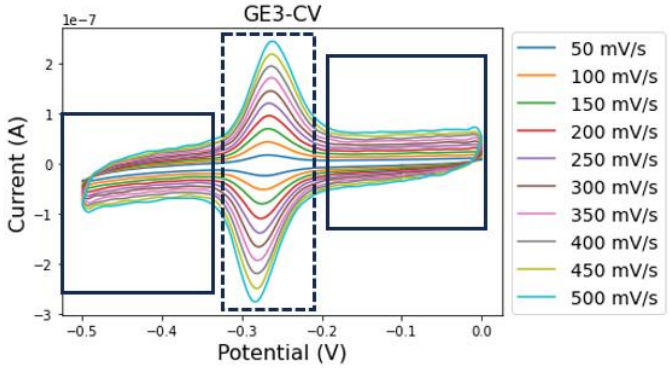
GE3-CV
1e−7
Current (A)
Potential (V)
50 mV/s
100 mV/s
150 mV/s
200 mV/s
250 mV/s
300 mV/s
350 mV/s
400 mV/s
450 mV/s
500 mV/s

b)

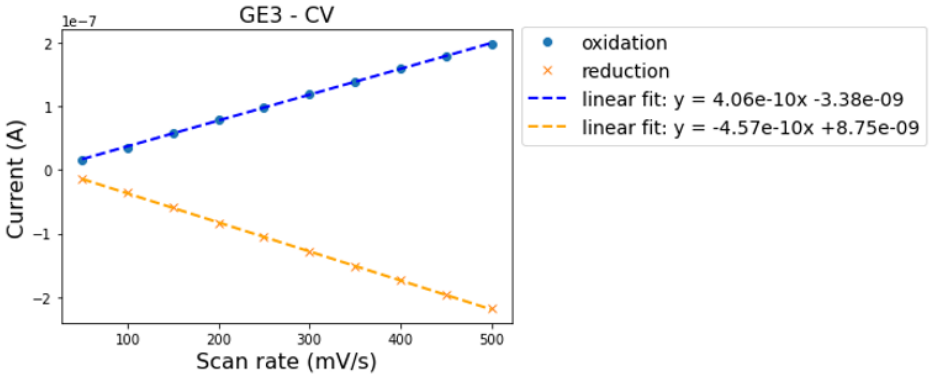
GE3 - CV
1e−7
Current (A)
Scan rate (mV/s)
oxidation
reduction
linear fit: y = 4.06e-10x -3.38e-09
linear fit: y = -4.57e-10x +8.75e-09

c)

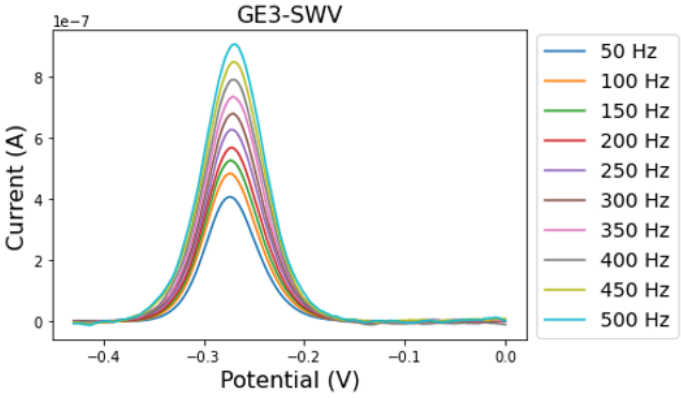
GE3-SWV
1e−7
Current (A)
Potential (V)
50 Hz
100 Hz
150 Hz
200 Hz
250 Hz
300 Hz
350 Hz
400 Hz
450 Hz
500 Hz

d)

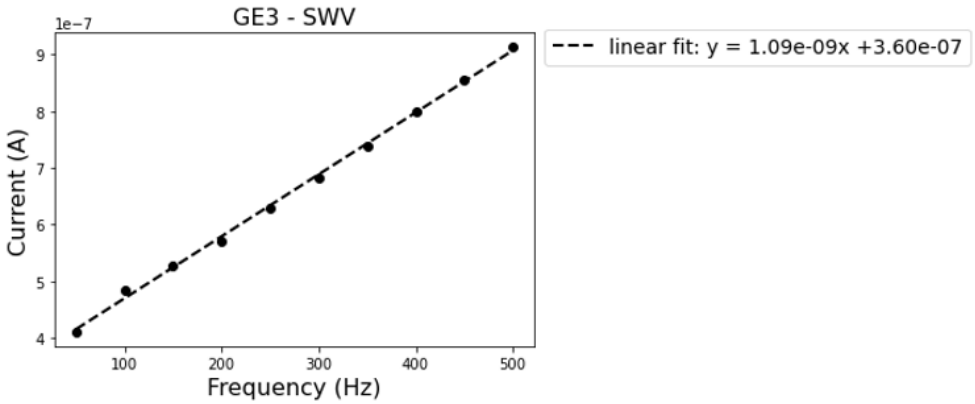
GE3 - SWV
1e−7
Current (A)
Frequency (Hz)
linear fit: y = 1.09e-09x +3.60e-07

Figure 4.12 Electrochemical measurements of GE3 (separate immobilisation). a) Cyclic voltammograms of different scan rates (50 mV $s^{-1}$, 100 mV $s^{-1}$, 150 mV $s^{-1}$, 200 mV $s^{-1}$, 250 mV $s^{-1}$, 300 mV $s^{-1}$, 350 mV $s^{-1}$, 400 mV $s^{-1}$, 450 mV $s^{-1}$, and 500 mV $s^{-1}$) recorded at equilibrium. Dashed box: Faradaic current. Solid box: capacitive current. b) Plot of scan rate versus peak currents of CV (both oxidation and reduction) with linear fits. c) square wave voltammograms of different frequencies (50 Hz, 100 Hz, 150 Hz, 200 Hz, 250 Hz, 300 Hz, 350 Hz, 400 Hz, 450 Hz, and 500 Hz) recorded at equilibrium. d) plot of frequencies versus peak currents of SWV with the linear fit.

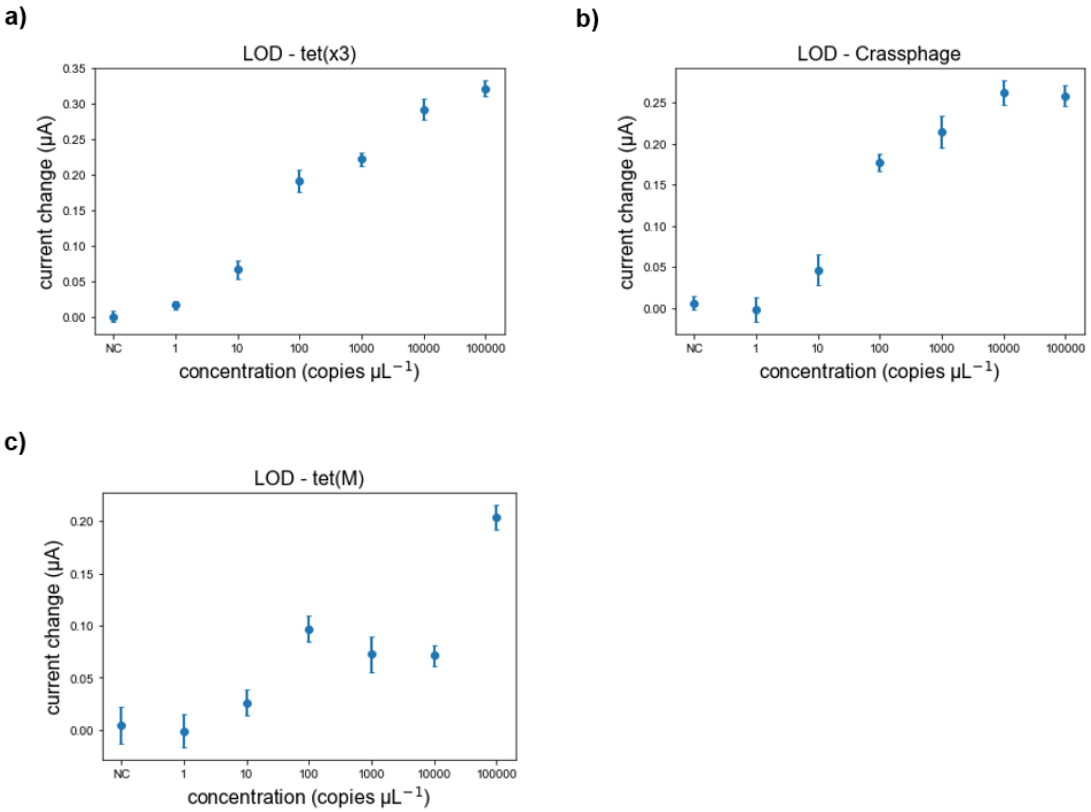


Figure 4.13 Sensitivity of electrochemical based mRPA-CRISPR/Cas assay. a) Electrochemical mRPA-CRISPR/Cas for tet(x3). b) Electrochemical mRPA-CRISPR/Cas for crassphage. c) Electrochemical RPA-CRISPR/Cas for tet(M). Experiments were conducted in triplicates.

### 4.3.3 mRPA-CRISPR/Cas lateral flow for ARG detection in real samples

To validate the feasibility and field-testing applicability of the developed LFA for ARG detection, wastewater and drinking water samples were extracted and tested. Wastewater samples were collected from influents of the Cranfield Wastewater Treatment Plant, Cranfield, UK. Drinking water samples were from Nigera and potable water tap of private water supplies in Aberdeenshire, Scotland, UK. DNAs were extracted from wastewater samples, went through mRPA-CRISPR/Cas assay, and finally detected by the developed LFA. qPCR was employed as a 'gold standard' technique to quantify the target concentrations in the samples and the results were used as references in this experiment.

Before target concentration quantification in samples, qPCR assays were carried out on 10-fold serial diluted target pristine samples, as shown inFigure **A**.**1**. In this way, the standard plots as shown in Figure **A**.**1**and were employed as references for unknown sample target concentration calculations. The sensitivity of qPCR assays for three targets were 1 copies $\mu L^{-1}$ for both crassphage and tet(x3), and 10 copies $\mu L^{-1}$ for tet(M).

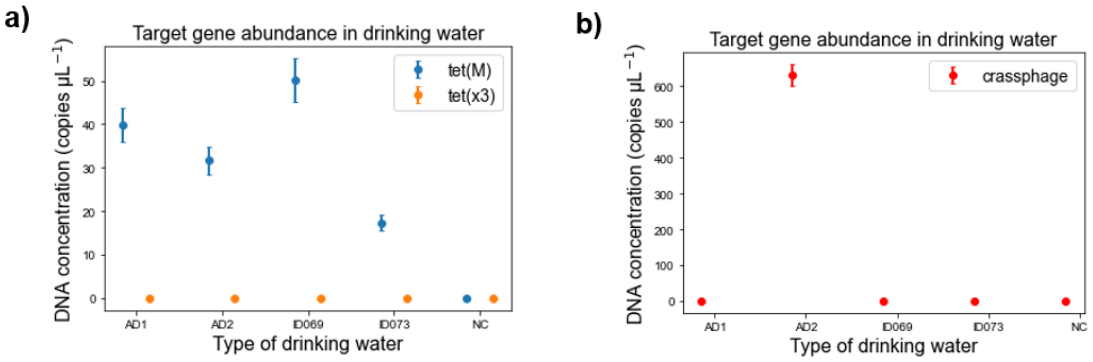

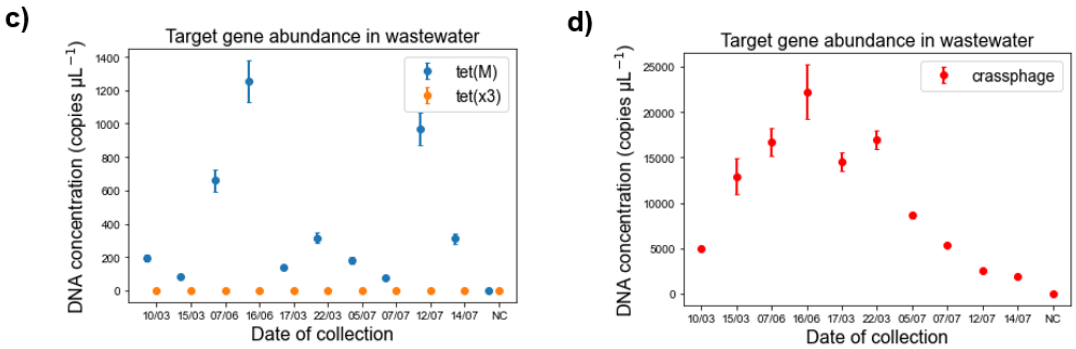


Figure 4.14 Results of qPCR detection of target genes in the real water samples. a) Calculated DNA concentration for tet(M) and tet(x3) detection in four drinking water samples. b) Calculated DNA concentration for crassphage detection in four drinking water samples c) Calculated DNA concentration for tet(M) and tet(x3) detection in ten wastewater samples d) Calculated DNA concentration for crassphage detection in ten wastewater samples. NC: negative control. Experiments were conducted in triplicates.

Then, qPCR detections were carried out on extracted wastewater and drinking water samples. AD1 and AD2 were drinking water samples from Africa, and ID069 and ID073 were drinking water samples from Scotland, UK. Wastewater samples were named after the date of collection, e.g., 10/03/22 was the sample collected on 10$^{th}$ March 2022. In total, four drinking water samples and ten wastewater samples were collected, extracted, and tested by qPCR assay. 错误! 未找到引用源。 shows the results of target concentrations in the samples.

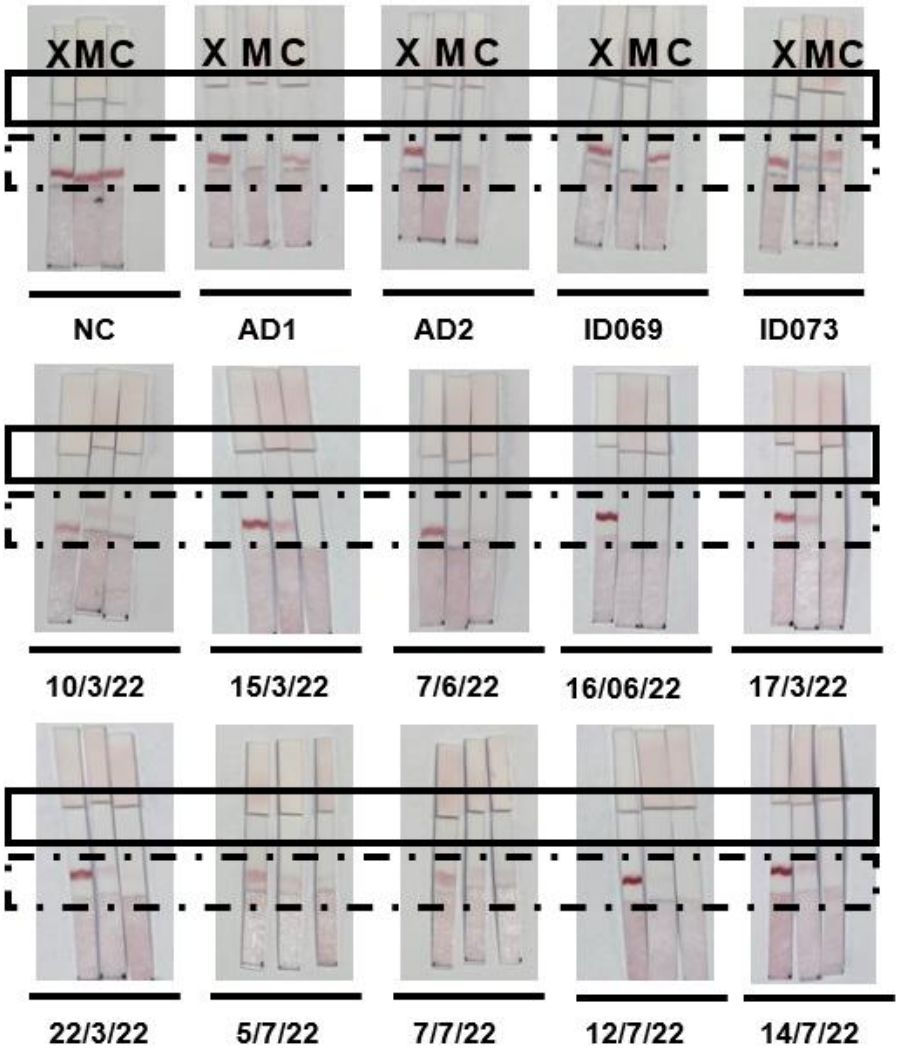


Figure 4.15 Photo of LFA based mRPA-CRISPR/Cas assay on real water samples. NC: negative control. X: tet(x3). M: tet(M). C: crassphage. Experiments were conducted in triplicates with one shown as demonstration. Solid square marks the position of test lines while dashed square marks the position of control lines.

Then, LFA based mRPA-CRISPR/Cas detections were carried out on the extracted real water samples, and the results are as demonstrated as photos in Figure 4.15. A summary of qualitative observed results is presented in Table 4.3. By comparing with the qPCR results, the LFA based mRPA-CRISPR/Cas

reached 100% accuracy, indicating the good robustness of the developed LFA detection of DNA extracted from complicated matrices.

Table 4.3 Summary of results of LFA based mRPA-CRISPR/Cas assay on real water sample detections

| | Tet(x3) | Tet(M) | Crassphage |
|---|---|---|---|
| AD1 | N | P | N |
| AD2 | N | P | P |
| ID069 | N | P | N |
| ID073 | N | P | N |
| 5/7/2022 | N | P | P |
| 7/7/2022 | N | P | P |
| 7/6/2022 | N | P | P |
| 10/3/2022 | N | P | P |
| 17/3/2022 | N | P | P |
| 22/3/2022 | N | P | P |
| 15/3/2022 | N | P | P |
| 12/7/2022 | N | P | P |
| 14/7/2022 | N | P | P |
| 16/6/2022 | N | P | P |

### 4.3.4 mRPA-CRISPR/Cas electrochemical ARG detection in real samples

After the optimisation and analytical performance analysis of the electrochemical based detection, the next step is to test its robustness in real water samples. As mentioned in 4.3.3, the same DNAs extracted from four drinking water and ten wastewater ones were employed to validate the feasibility of this developed electrochemical mRPA-CRISPR/Cas assay. In brief, the peak current of SWV of the immobilised electrode was recorded before and after each CRISPR/Cas

incubation with mRPA amplicons, and the current change was calculated and used to determine the presence of targets in the samples.

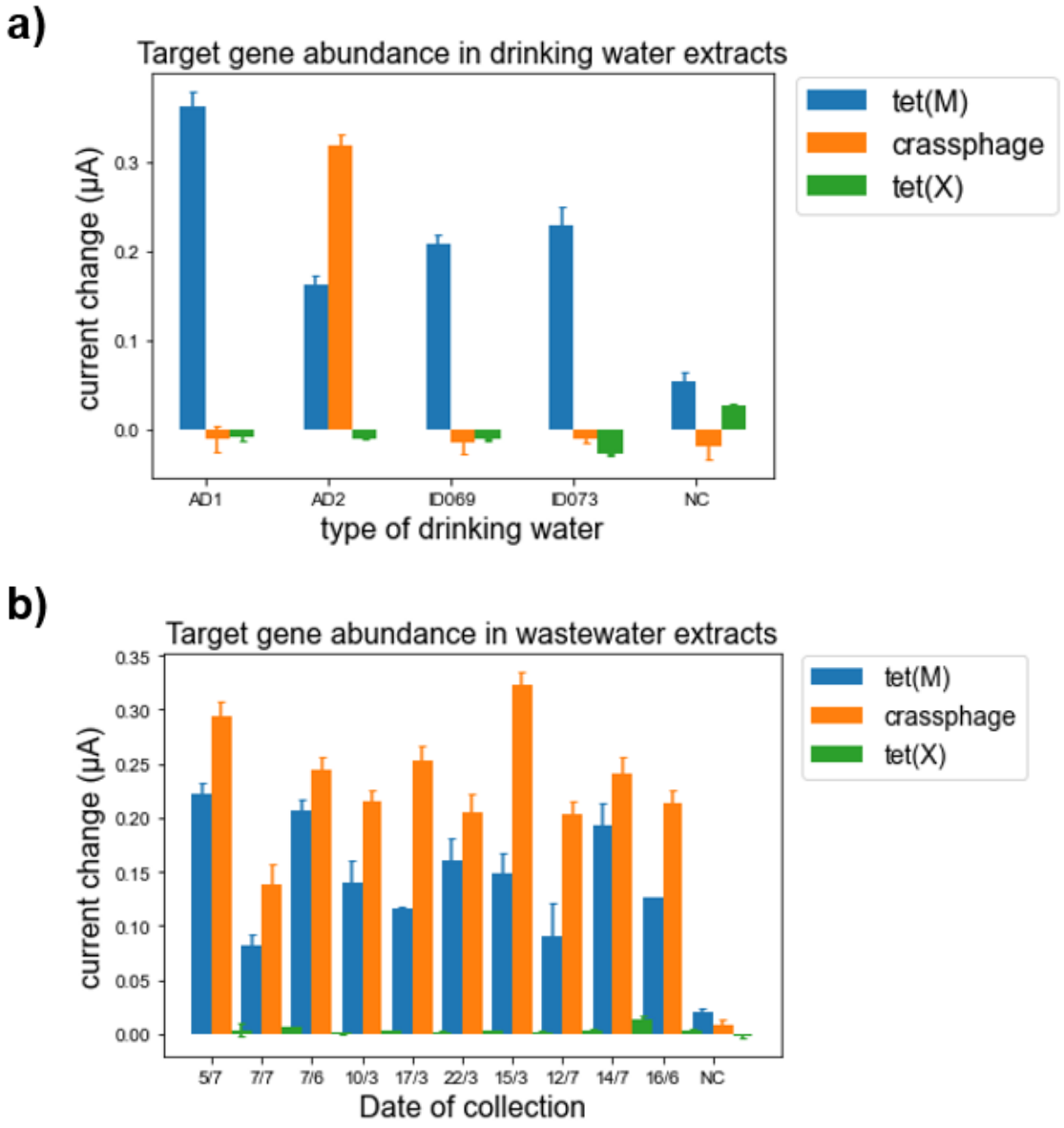


Figure 4.16 Results of electrochemical detection of target genes in the real water samples. a) Measured current changes for three targets detection in four drinking water samples. b) Measured current changes for three targets detection in ten wastewater samples. NC: negative control. Experiments were conducted in triplicates.

Figure 4.16 shows the results of electrochemical detection in the 14 real water samples. The slight negative and/or positive current changes were normal

fluctuations of peak currents, suggesting that there was minimal current change before and after incubation, and thus minimal targets in the sample. By comparing the obtained results with qPCR ones (as shown Figure A.1 qPCR results for quantifying three targets. real-time fluorescent amplification curves of 10-fold serial diluted a) tet(M c) crssphage e) tet(x3) ranging from 108 – 100 copies µL-1. standard plot of b) tet(M) d) crassphage f) tet(x3) with linear fit. Experiments were done in triplicates. NC: negative control.

), the accuracy of the assay achieved 100%, and the robustness of the developed electrochemical detection was validated, implying that the assay holds potentials to be employed for detections of DNA extracted from complex matrices, and therefore could be utilised for onsite detections.

Overall, the proposed LFA exhibited more sensitive performance and comparable reaction time through comparison with literature. Su et al. [215] proposed a multiplexed reverse transcriptase-RPA coupled CRISPR/Cas LFA for the detection of COVID19, reaching a LOD of 10 copies per test. And Li et al. [216] reported an RPA-CRISPR/Cas based LFA to detect *Vibrio* species carrying the pVA1 plasmid which is responsible for acute hepatopancreatic necrosis disease in shrimps. The LOD reached 200 copies $\mu L^{-1}$. Besides, Lei et al. [217] proposed an LFA accommodating RPA-CRISPR/Cas assay for determination of *Toxoplasma gondii* in the environment, with a LOD of 3.3 copies $\mu L^{-1}$. As for the electrochemical method, there is limited studies reporting RPA-CRISPR/Cas based voltametric detections. Xu et al. [200] reported a dual sensing mode RPA-CRISPR/Cas detection assay to electrochemically determining the Brucella spp. load in the blood and milk samples, with a LOD of 2 copies per reaction. Although this LOD is lower, it lacks the multiplexability that enables simultaneous determination of different targets, which was realised in our proposed assay. And. del Río et al. [218] proposed a solid phase RPA based electrochemical approach for the detection of *Piscirickettsia salmonis*. The LOD reached $10^2$ copies $\mu L^{-1}$, and our approach is more sensitive due to the signal amplification by CRISPR/Cas assay.

## 4.4 Conclusions

Lateral flow and electrochemical based detection approaches were integrated with the developed mRPA-CRISPR/Cas assay in Chapter 3 via simple modification of the CRISPR/Cas probe. Optimisation of LFA were conducted to reach LODs of 1 copy $\mu L^{-1}$ for tet(x3) and crassphage, and 10 copies $\mu L^{-1}$ for tet(M). And electrochemical based mRPA-CRISPR/Cas assay was also optimised and achieved LODs of 10 copies $\mu L^{-1}$ for all targets. Both of the assay was tested against DNA extracted from real water samples including four drinking water (two from Nigera while other two from Scotland, UK) and ten wastewater samples (from influents of WWTPs, Cranfield, UK). The accuracy when compared with the gold standard qPCR results reached 100% for both detection approaches, indicating its robustness in different complicated matrices and its potential for onsite detection. In summary, this proposed LFA and electrochemical mRPA-CRISPR/Cas assay provides an economical, rapid, sensitive, and POU detection approach for environmental monitoring. While electrochemical detections hold the potential for quantification of targets with the aid of calibration curves, only qualitative measurements were conducted in this experiment. Further efforts could therefore be devoted to optimising the electrochemical assay, for example, to maximise the MB probe density on the electrode surface and therefore improve the signal amplitude, so that quantification of targets might be realised.

Besides, the developed mRPA-CRISPR/Cas assay proved its compatibility with various detection approaches, including fluorescence, LFA and electrochemistry, via simple change of CRISPR/Cas probe. There are potentials of the assay to be integrated with other methods, e.g., chemiluminescence, surface-enhanced Raman spectroscopy.

Due to the transferability of the techniques, the developed LFA and electrochemical assay could be extended to other gene targets, offering potentials in various environmental pollutants monitoring, e.g., pathogens and viruses. While further efforts could be devoted to involving portable

electrochemical workstations as well as chip-based electrode systems in the electrochemical-based assay, LFA is already a portable POU device for sample detection and is readily available to be employed for onsite measurement. Besides, smartphone-based sensing technologies could be combined with the developed system and contribute to simple data visualisation, storage, and transport.

# 5 Feasibility and Challenges in Hydrogel-based HCR-CRISPR/Cas Assay for Antibiotic Detection: A Path Forward

## 5.1 Introduction

Antimicrobial resistance (AMR) as mentioned in the previous chapters, is a severe public health threat worldwide, and is calling for attention.[1] Overuse and abuse of antimicrobial reagents have been regarded as the main factor that exacerbates AMR widespread. Therefore, timely surveillance of AMR, especially antimicrobial agents, could be feasible to explore more opportunities and thus to tackle this public health concern [6]. Conventional testing methods such as LC-MS, can provide sensitive and precise determination of antimicrobial reagents level, while most requires a laboratory set up. Therefore, there is an urgent need in rapid, simple, low-cost, and specific method for the effective onsite detection of antimicrobial reagent.

Aptamers are synthetic single-stranded oligonucleotides which selectively bind to the targets with high affinity and high specificity. They are selected via an *in vitro* iterative process called SELEX (Systematic Evolution of Ligands by EXponential enrichment). As alternatives to antibodies, they are featured by ease of synthesis, modification, storage and transportation, versatile applications, biodegradability in biological environments, cost effectiveness, and tuneable stability [219]. Therefore, aptamers have been widely applied as biorecognition elements in diagnostics [220] (e.g., wearable biosensors), therapeutics [220] (e.g., targeted drug delivery) and environment monitoring [221] (e.g., water quality).

As stated in 2.3.2, HCR reaction is widely employed to improve the sensitivity of the aptamer detection assays. As it might suffer from false positive results, it is vital to design hairpin carefully. NUPACK (https://www.nupack.org/) is a software suite that analyse and design nucleic acid secondary structures. It was employed in this project for the hairpin design, and analysis of thermodynamics of ensemble resulted from different strands.[222]

Benefitting from its simplicity in assay composition, high sensitivity and controllable kinetics, HCR has been widely used in biosensing [223–225].

In recent years, hydrogels, especially the target-responsive ones (i.e., smart hydrogel) that are constructed by DNA, have attracted increasing attention in its application of point-of-use (POU) detection. Studies have been conducted on development of smart DNA hydrogels to build detection platforms. Zhu et al. (2010) [226] first proposed a colorimetric agent-caging hydrogel built from DNA grafted polyacrylamide and target-specific aptamer as a novel visual detection platform, and 20 ng cocaine was detected in 10 minutes, demonstrating the feasibility of hydrogel in detection. To better suit the purpose of POU, in 2013, Yang group [227] combined DNA hydrogels with commercial glucometer to detect non-glucose reagents. Following studies [228–231] have been done to further improve the analytical performance of smart DNA hydrogel-based sensing platform and its potential in POU. With the advancements in nano- and material technology, smart DNA hydrogels have been coupled with *de novo* metallic nanoparticles which act either as reporter or catalytic reagents, pushing the limit of detection and improving sensor performance [232–235]. However, in most cases, a high concentration of external stimuli is required to trigger fast and sensitive response [236].

CRISPR/Cas system has been regarded as a promising toolbox to complement smart hydrogel detection for improved limit of detection [236]. It was first found in prokaryotes as RNA-directed adaptive immune systems against invading of viruses or plasmids and was then developed as gene editing tools. With the discovery of trans-cleavage activity of type V Cas enzymes such as Cas12a and cas13, its potential in biosensing and molecular diagnostics has been explored and research has been conducted for the development of various detection platforms such as SHERLOCK [237] and DETECTR [11]. In 2019, English et al. [238] employed CRISPR/Cas12a to precisely control properties of smart DNA hydrogels, and therefore realised the controlled release of small hydrogel cargoes containing small molecules, enzymes, nanoparticles, and live cells. Besides, the control over electronic devices, and detection of viruses with

microfluidic devices were also realised. This reported programmable CRISPR/Cas responsive DNA hydrogels convert biological information into changes in material properties with programmable readouts, and thus can be applied in tissue engineering, molecular diagnostics, and bioelectronic interfaces. Subsequently, there are studies [239,240] reporting DNA hydrogel-CRISPR/Cas based optical detection (fluorescent and colorimetric) of small molecules and proteins (creatine kinase MB, estradiol (E2) and prostate-specific antigen (PSA)), as well as those that based on electrochemical detections [241].

To date, there is still a lack of studies exploring the potential of modulating smart hydrogel with CRISPR/Cas technology especially for improving analytical performances of POU devices. A hydrogel-CRISPR/Cas platform for ultrasensitive detection of non-nucleic acid small molecule was therefore designed and the scheme is as shown in Figure 5.1. Briefly, the aptamers of kanamycin were first immobilised onto magnetic beads and locked the initiator via DNA complementary base pair interactions. Once the target kanamycin was present, the aptamers would tend to bind with kanamycin and therefore released the initiator to the solution. Then magnetic separation was carried out and the supernatant containing initiators was mixed with HCR hairpins, initiating the HCR reactions. Finally, the HCR products were recognised by the CRISPR/Cas system, trans cleaving the ssDNA linkers of the DNA hydrogels, leading to MB leakage and therefore electrochemical signals.

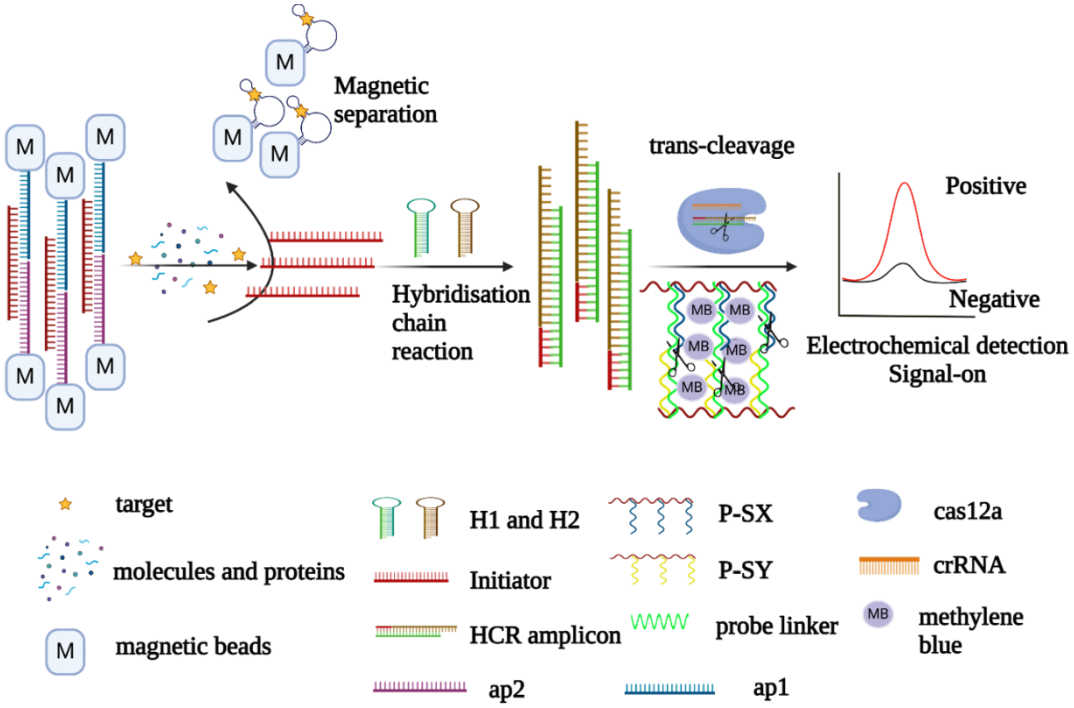


Figure 5.1 Scheme of antibiotics detection platform of hydrogel-based CRISPR/Cas assay.

Kanamycin was chosen to demonstrate the feasibility of the developed platform. It is an aminoglycoside, and the structure is as shown in Figure 5.2. It is mainly used in animal husbandry for disease prevention and treatment and for animal growth promotion. It works by inhibiting protein synthesis during the amino acid transfer from aminoacyl-tRNA to ribosomes [242]. Kanamycin only hydrolyses in water when the temperature reaches 100 °C [243], and therefore they accumulate and spread in the environment, leading to oto- and nephrotoxicity [244]. As a result, it is of great importance to monitor kanamycin concentration in water.

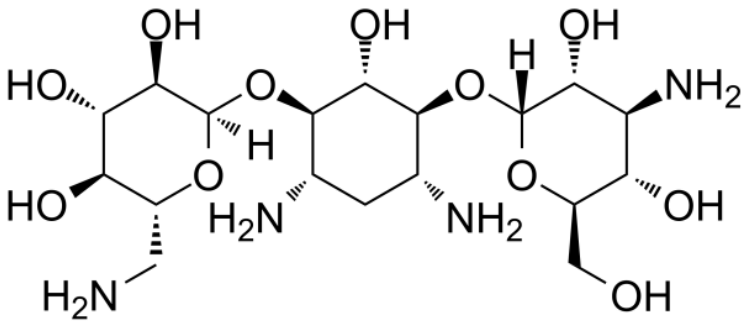


Figure 5.2 Chemical structure of kanamycin

Electrochemical detection was employed for determination of target molecules. The presence of hydrogel prevents methylene blue from exchanging electrons with electrodes, and thus lowers the current measured via SWV. When the target presents and is recognised by the aptamer, triggering subsequent amplification and CRISPR/Cas assay, the ssDNA linker of the hydrogel is then cleaved, leading to the leakage of methylene blue and restore the current.

The aim of this experiment was to develop a novel electrochemical bioassay for antibiotics detection; however, some unexpected obstacles was encountered, and the time was constrained. Therefore, this experiment was not completed. As a result, current achievements and potential reasons for the failure which is supported by computational predictions and simulations were discussed in this Chapter.

## 5.2 Materials and Methods

### 5.2.1 Chemicals and apparatus

Acrylamide, ammonium persulfate (APS), N, N, N′, N′-Tetramethyl ethylenediamine (TEMED), methylene blue (MB), and magnesium acetate ($Mg(CH_3COO)_2$), Tris-HCl (pH 7.5), EDTA, NaCl, PBS tablet, and bis-acrylamide were bought from Merck Life Science UK Limited (Sigma Aldrich, USA). EnGen Lba Cas12a, 10× NEB Buffer, and cas12a diluent solution were provided by New England Biolabs (Hitchin, UK). Oligonucleotides were purchased from Integrated DNA Technologies (Leuven, Belgium) and from Merck Life Science UK Limited

(Sigma Aldrich, USA). Their sequences and modifications were listed in Table S2. 50× TAE buffer and 100 bp DNA Ladder were purchased from New England Biolabs (UK).

Working electrodes were gold electrodes (code BASMF2014-1EA, Sigma Aldrich, UK), auxiliary ones were made of platinum wire (code BASi MW-1032, Alvatek, UK) and reference ones were Ag|AgCl (code BASi MF-2052, Alvatek, UK). All the measurements were conducted under room temperature, via Multi Autolab/M204 (Metrohm, UK), and data was collected and analysed with Nova 2.1(Metrohm, UK).

Quant Studio 3 Real-Time PCR System, Qubit 4 Fluorometer, SYBR Safe DNA Gel Stain, DNA Gel Loading Dye (6×), Qubit ssDNA Assay Kit and Dynabeads™ MyOne™ Streptavidin C1 are from Thermo Fisher Scientific, UK. Syngene GBOX Gel-Doc system from Syngene, UK. All chemicals were of analytical reagent grade and used without further purification. ddH2O was purified through a Millipore System (Millipore, USA, resistivity >18 MΩ). Each assay was repeated at least 3 times to ensure reproducibility.

### 5.2.2 Initiator release from target binding

Biotinylated aptamers were modified on magnetic beads according to the instructions provided by the manufacturer (Dynabeads™ MyOne™ Streptavidin C1). 2× washing buffer (10 mM Tris-HCl (pH 7.5), 1 mM EDTA, and 2 M NaCl) was prepared beforehand. The initial washing step was carried out to transfer the magnetic beads from stock solutions to the washing buffer. The provided magnetic beads were then washed as follows: A volume of resuspended beads was transferred to a tube, followed by addition of 1 mL 1× washing buffer and resuspension. The tube was then placed on a magnet for 1 minute before supernatant was discarded. Then the tube was removed from magnet and the washed beads were resuspended in a volume of washing buffer equal to the initial volume of beads taken from the vial. The washing step was repeated for a total of 3 washes. Then the beads were ready for the immobilisation procedure. First, the washed beads were resuspended in 2 × washing buffer to a final concentration of 5 μg $\mu L^{-1}$, followed by an addition of equal volume of biotinylated

aptamer diluted in DNase free water. Then the mixture was incubated for 15 minutes at room temperature with gentle rotation, before it was separated using a magnet for 3 minutes. Then the coated beads were washed 3 times with 1× washing buffer as described above. Finally, the aptamer coated beads were resuspended in DNase free water and stored at 4 °C fridge until further use.

The aptamer of kanamycin was derived from previous report [245]. Magnetic beads labelled aptamer (500 µL, 1 mg $mL^{-1}$) and excessive complementary oligonucleotide (initiator) solution were hybridized at 37°C for 30 min to obtain magnetic beads bound Apt-cDNA complex. Unreacted cDNAs were removed by magnetic separation, followed by resuspension to a volume of 50 µL. Then, 5 µL of the target (kanamycin) standard solution (1 mM), and 5 µL of magnetic beads bound Apt-cDNA complex, were incubated at 37°C for 1 h. Subsequently, the dissociated cDNA (8 µL) was collected by magnetic separation. Figure 5.3 shows the workflow of the process described above.

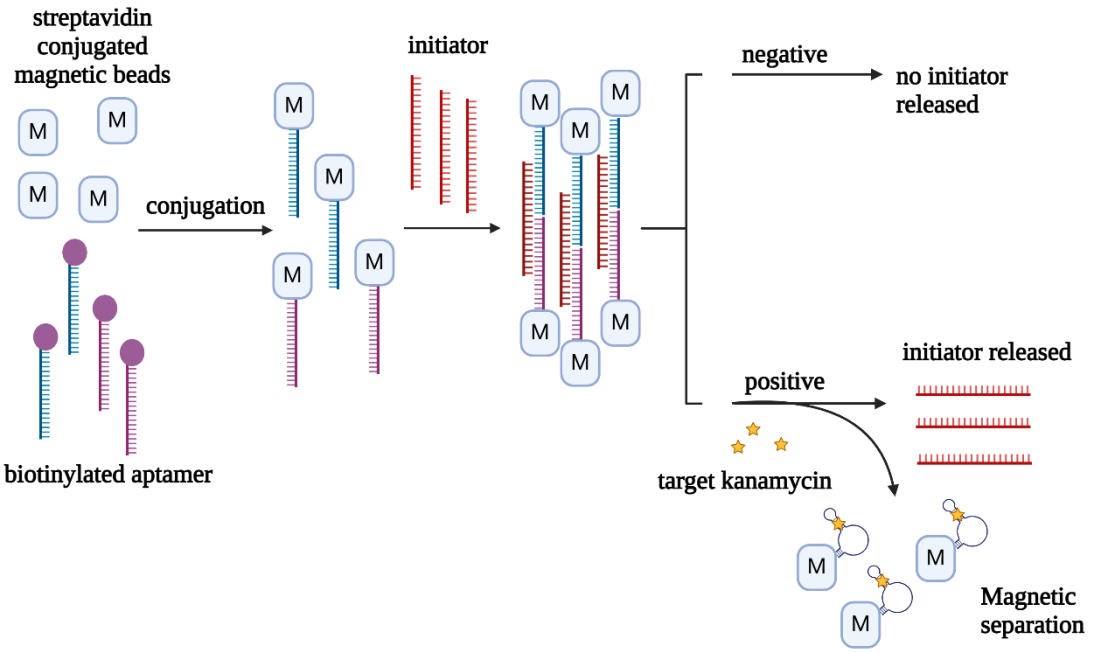


Figure 5.3 Overview of workflow for initiator release upon target binding with aptamer. The two colours of aptamers represent two different sequences of aptamers, as they were designed differently for the downstream reactions i.e., HCR, and CRISPR/Cas.

### 5.2.3 HCR assay

Hairpins were designed using NUPACK suites [222] and purchased from Merck, UK. The HCR assays were performed in different buffer solution, different reaction temperature (25 °C, 37 °C, and 50 °C), and different reaction time (1 hour, 4 hours, and overnight). Buffer solutions include 1 × SPSC buffer (1 M NaCl, 50 mM $Na_2HPO_4$; pH 7.5), 5× SSC buffer (600 mM NaCl, 60 mM sodium citrate), pure DNase free water, 1× PBS7 (10 mM phosphate, 1 M NaCl).

The pretreatment of each hairpin probe included snap-cooling and slow cooling. HCR reactions were conducted in different equipment, including Quant Studio 3 Real-Time PCR System, Biometra TProfessional Basic Thermocycler and Techne digital Dri-Block heaters DB200/3/230V. Snap cooling procedure was to heat two hairpins separately to 95 ºC for 2 minutes and immediately freeze them in -20 °C for 30 minutes, while slow cooling was to heat two hairpins separately to 95 ºC for 2 minutes and gradually cool them to room temperature before use. 1 µM hairpins were mixed different concentrations of initiators.

The total volume of reaction solution varied corresponding to each assay, including 10 µL to 100 µL. The results were validated using agarose-gel electrophoresis: the 2% agarose gel was prepared using 1 × TAE buffer. The gel was allowed to run at 100 V for 50 mins. Finally, the results were displayed using the Syngene GBOX Gel-Doc system. All experiments were conducted in triplicates.

### 5.2.4 CRISPR/Cas assay

1 µM cas12a and 1 µM crRNA was preincubated in 10 × NEBuffer 2.1 at 37 ºC for 1 hour, before 2 µL 1 µM 6-FAM labelled ssDNA probe and all HCR amplicons were added. In each HCR-CRISPR/Cas assay, a total volume of 16 µL include 1 µL 1 µM cas12a, 1 µL 1 µM crRNA, 2 µL 10 × NEBuffer 2.1, 2 µL 1 µM 6-FAM labelled ssDNA probe and 10 µL HCR amplicons. All experiments were conducted in triplicates.

### 5.2.5 Hydrogel formation

Preparation of DNA hydrogel was performed by following the previous literature with slight modifications [226,241]. 20 µL of 10 µM acrydite-modified X and Y were, respectively, mixed with 5 µL of 40% acrylamide in 25 µL of TAE/Mg buffer (pH 8.0, 20 mM acetic acid, 40 mM Tris, 12.5 mM $Mg(CH_3COO)_2$, 2 mM EDTA) solution. Then, the mixture was vacuumed in a pump-connected desiccator for 10 min. Next, APS (10%, 0.7µL) solution and TEMED (5%, 1.4 µL) solution were added to the above mixture to react under vacuum in the desiccator for 18 min to form the polyacrylamide-DNA complexes PA-X and PA-Y. To form the gel, the above PA-X and PA-Y were mixed with methylene blue (MB) (1.2 mM, 10 µL) and probe linker (probe L) (10 µM, 20 µL) and left at bench for 30 minutes.

### 5.2.6 Electrochemical detection

All the measurements were conducted under room temperature, via Multi Autolab/M204 (Metrohm, UK), and data was collected and analysed with Nova 2.1(Metrohm, UK) on a laptop. Gold electrode (code BASMF2014-1EA, Sigma Aldrich, UK), platinum wire (code BASi MW-1032, Alvatek, UK)) and Ag/AgCl (3 M NaCl) (code BASi MF-2052, Alvatek, UK) were, respectively, employed as working electrode, auxiliary electrode and reference electrode. The phosphate buffered saline (PBS, 0.01 M $Na_2HPO_4$-$NaH_2PO_4$-KCl, pH 7.4) was prepared from PBS tablets from Sigma-Aldrich (UK). Gold electrode was cleaned by polish kit and CV in 0.5 M sulphuric acid before use. Square wave voltammetry (SWV) experiments were completed in buffer solution of 0.01M PBS solution.

The current of 10-fold serial diluted methylene blue solution (10 nM – 10 µM) was measured by SWV and the voltammograms were recorded. Then 100 µL and 5 µL hydrogel with MB wrapped inside were detected in 0.01M PBS solution with SWV. All experiments were conducted in triplicates. An overview of the workflow from hydrogel formation and electrochemical characterisation is presented as shown in Figure 5.4.

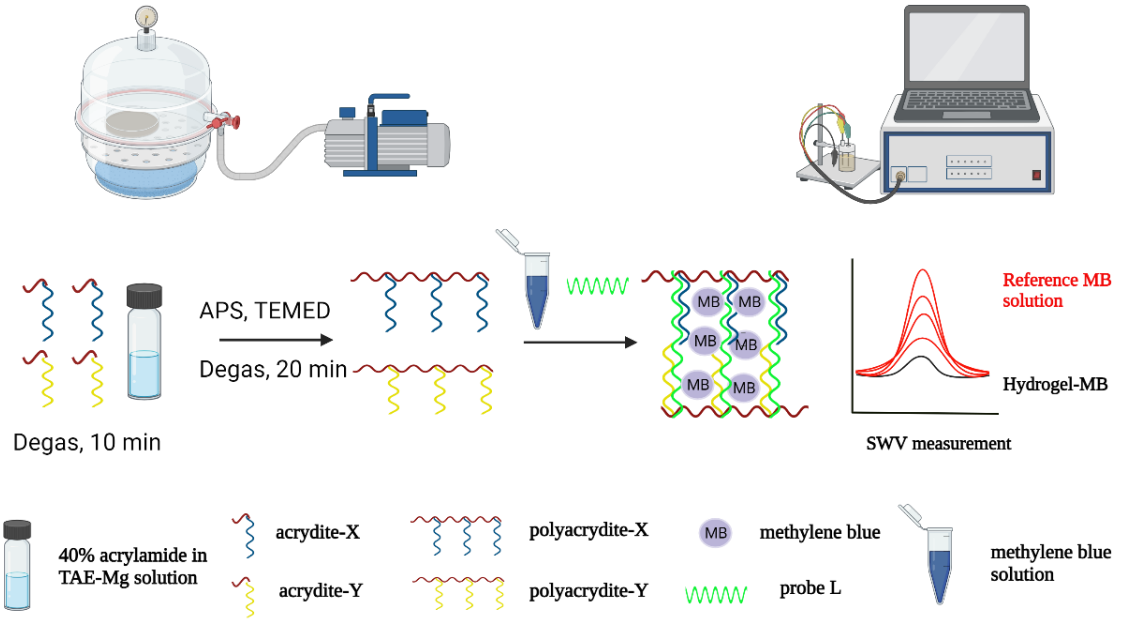


Figure 5.4 Overview of workflow of hydrogel formation and characterisation with electrochemical measurement. The higher the extent of the hydrogel is cleaved, the more MB is leaked into the solution, and therefore the SWV electrochemical signal increases.

### 5.2.7 Molecular dynamics simulation

The sequence of ap1 and ap2 was modified from kanamycin aptamer reported by Song et al. [245]. The secondary structures were predicted by mFold [246] with parameters of 0.15 M $Na^+$, 0.02 M $Mg^{2+}$, at 25 °C. Then the 3D structures of ap1, ap2, and originally reported aptamer were predicted by RNAComposer [247,248] and mutated back to DNA via 1) change ribonucleic acids to deoxynucleic acid by Discovery Studio 2021, and 2) modify all uracil (U) to thymine (T) via pymol [249–251]. Then energy minimisation (EM) was conducted by GROMACS 2023 [252] with CHARMM36 force field [253].

Ligand structure (i.e., kanamycin) was downloaded from PDB website and energy minimised before docking in Autodock Vina [254,255]. The docked pose was ranked according to affinity, and the one with the highest binding affinity was chosen for the subsequent complex molecular dynamic simulation. Ligand topology was generated in CGenFF [256,257] and combined with aptamer. The complex structures

were centred in a dodecahedron box with 10 Å distance from the box edges, before the box was filled with TIP3P water (model of water implemented in CHARMM forcefield, a three-site rigid water molecule with charges and Lennard-Jones parameters assigned to each of the three atoms) and 0.15 M NaCl. EM and subsequent equilibration of NVT (fixed molecule numbers, volume and temperature) and NPT (fixed molecule numbers, pressure and temperature) (equilibrium ensembles, bring the system to expected temperature and pressure) were conducted in GROMACS 2023[252]. Energy minimisation (EM)was carried out using the steepest descent method with a maximum step size of 0.01 nm and a tolerance of 1000 kJ $mol^{-1}$ $nm^{-1}$, followed by NVT ensemble equilibration at 300 K for 100 ps and then NPT equilibration at 298 K and 1 bar using Parrinello-Rahman pressure coupling for another 100 ps. Finally, a production run of 20 ns molecular dynamics (MD) simulation was conducted on the lowest energy complex with a time step of 2 fs. Constraints were applied on hydrogen bonds using the LINCS algorithm, and periodic boundary conditions (PBC) were applied in three directions (xyz). Particle mesh Ewald (PME) method with a grid spacing of 1.6 Å was employed for the long-range electrostatic interactions. V-rescale thermostat was for temperature coupling at 300 K while Parrinello-Rahman barostat was for pressure coupling. Trajectories were saved every 10 ps for further analysis. The workflow is as described in Figure 5.5 and is carried out on ap1, ap2 and originally reported aptamer sequences (apori).

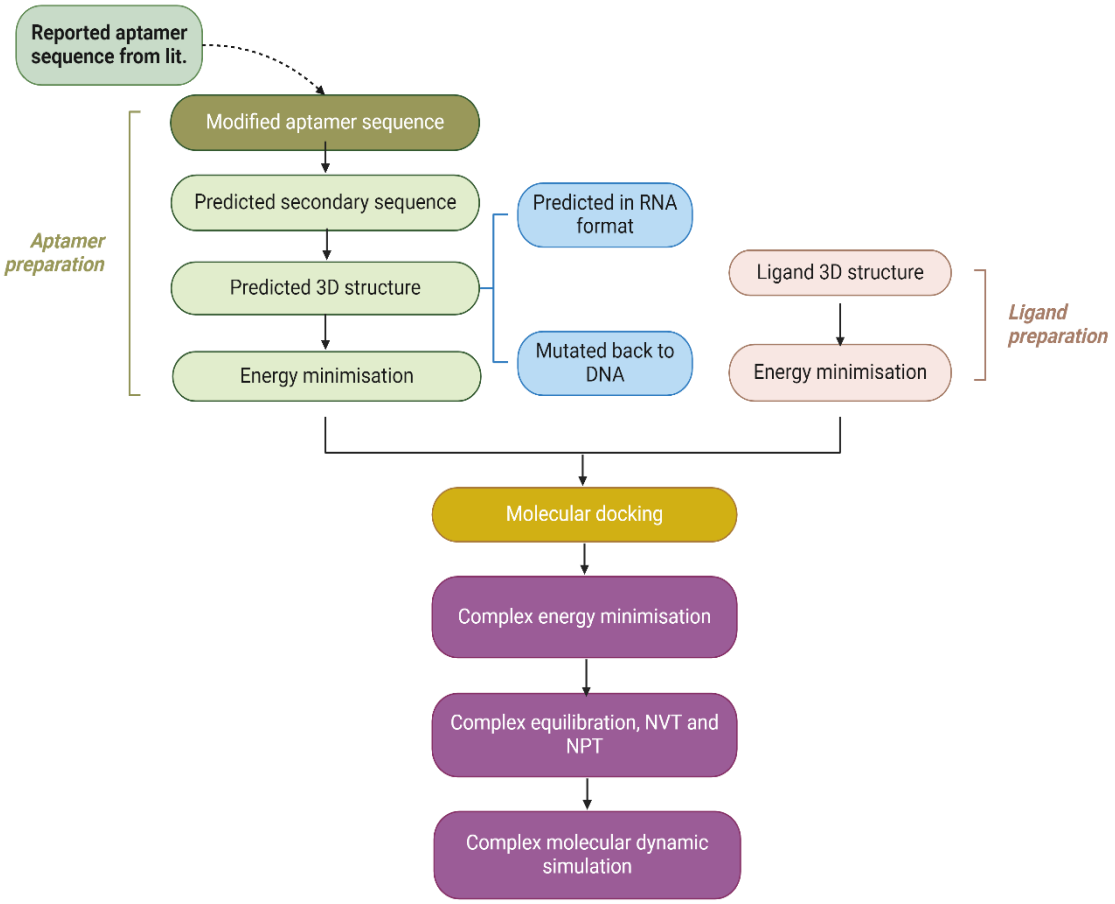


Figure 5.5 Overview of workflow of in silico modelling of aptamer-target binding.

## 5.3 Results and discussion

### 5.3.1 Initiator release

As shown in Figure 5.3, the initiator in principle was released upon binding of target kanamycin with aptamer. Magnetic beads conjugated aptamer 1 and 2 lock initiator in ratio of 4 µL: 4 µL: 2 µL (all at 10 µM) (final initiator concentration up to 2 µM). To assess the feasibility of the designed step, subsequent HCR amplification of the released initiator was conducted, and the results were visualised using gel electrophoresis as shown in Figure 5.6a. All experiments were conducted in triplicates. While lane 1-9 represents negative controls, lane 10-18 are the positive ones. However, no clear trend of successful HCR amplification could be identified from the gel results, indicating two possible

reasons behind: 1) unbound initiators are not properly eliminated via magnetic separation 2) designed aptamers do not bind with target effectively.

To explore and solve this issue, subsequent experiments were conducted, employing 20 nm bare AuNP as the colorimetric indicator. It was reported that ssDNA absorbed on the surface of AuNP and acted as stabiliser when in high salt concentration, preventing AuNPs from aggregating [258]. As shown in Figure 5.6b and c, when in 1 M NaCl solution, 20 nm AuNP aggregated in the absence of aptamer, but remained dispersed when aptamers were present. When target kanamycin was added, it in theory should bind with aptamers, leading to the dissociation of aptamers from AuNP surface, and therefore the AuNP would aggregate in high salt concentration. However, as indicated by Figure 5.6d, there was no obvious colour difference before and after kanamycin was added. As a result, it seemed that the designed aptamer would not effectively bind with the target, leading to the inefficient release of initiators. To validate this reason, a further *in silico* modelling of aptamer-target was carried out as in detailed in 5.3.5.

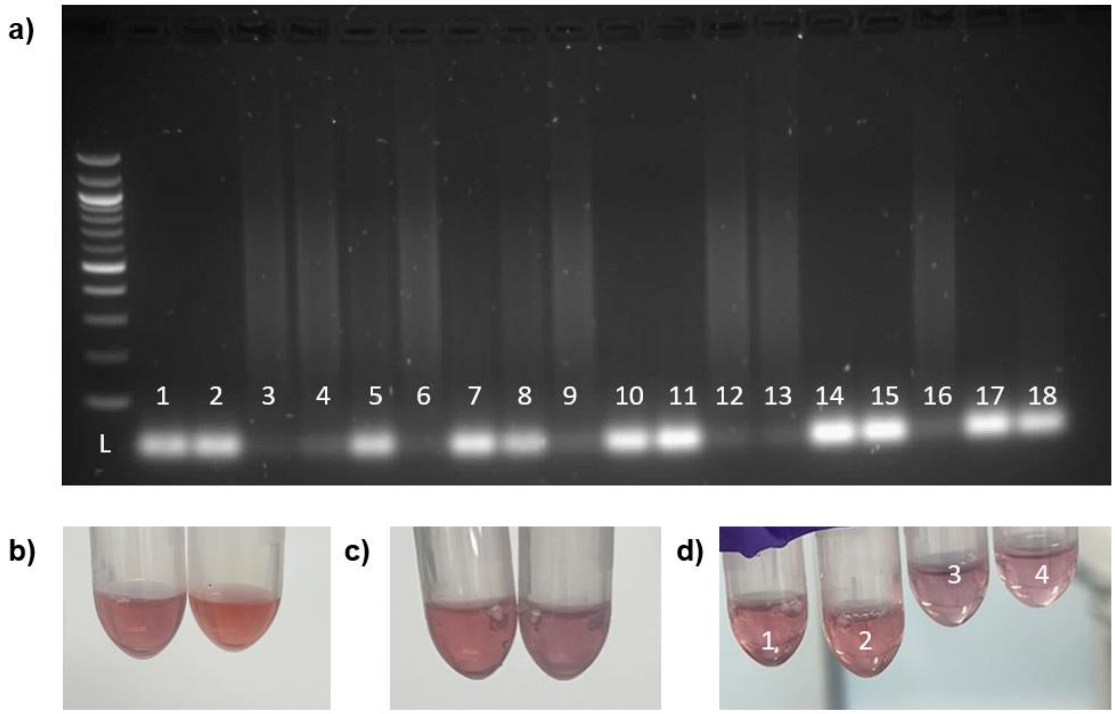


Figure 5.6 Results of initiator release upon target binding to aptamer. a) gel electrophoresis image of subsequent HCR with released initiator. (n=3) Subsequent HCR was conducted in another triplicate. Lane L: 100 bp DNA ladder.

Lane 1-9: negative controls. Lane 10-18: positive controls. b) demonstrative photo of colorimetric assessment of aptamer binding to target. Left: 20 nm AuNP + 1M NaCl. Right: 20 nm AuNP + $ddH_2O$. c). Left: 20 nm AuNP + aptamer + 1M NaCl. Right: 20 nm AuNP + $ddH_2O$ + 1M NaCl. d) 1: 20 nm AuNP + aptamer + kanamycin + 1M NaCl. 2: 20 nm AuNP + aptamer - kanamycin + 1M NaCl. 3: 20 nm AuNP + $ddH_2O$ + kanamycin + 1M NaCl. 4: 20 nm AuNP + $ddH_2O$ - kanamycin + 1M NaCl.

### 5.3.2 Optimisation of HCR assay

HCR is an enzyme-free DNA polymerase process, driven by the open-up of two kinetically trapped nucleic acid hairpin probe via an initiator. Different reaction condition, including reaction time (1 hour, 2 hour and overnight), reaction temperature (room temperature and 50 °C), and buffer composition, were tested for optimisation (minimal leakage and most efficient polymerisation). Gel electrophoresis was conducted to assess the HCR results. Finally, HCR carried out in 5× SSC buffer at 50 °C for one hour was regarded to be the optimal combination and the results were as shown in Figure 5.7.

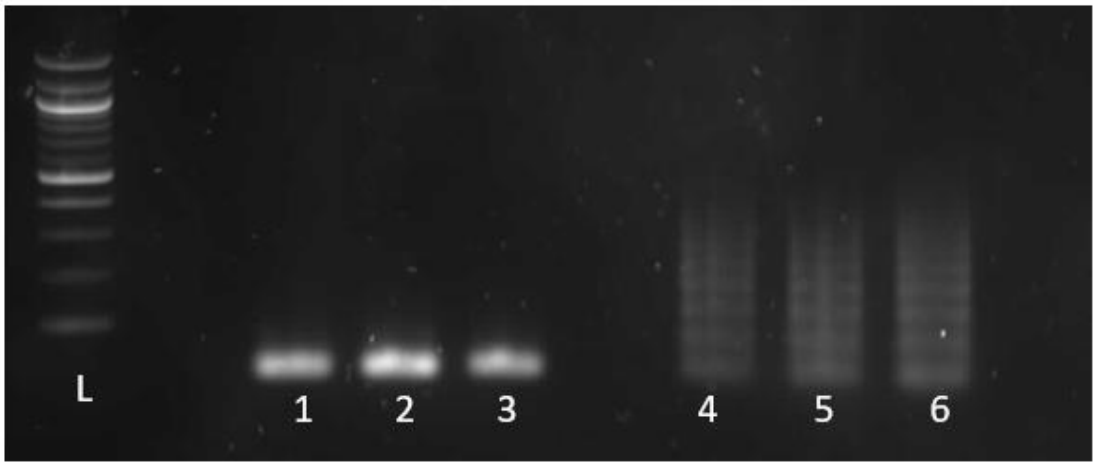


Figure 5.7 Gel electrophoresis image of HCR conducted in 5× SSC buffer at 50 °C for one hour. Land L: 1000 bp DNA ladder, Lane 1-3: negative control; Lane 4-6: positive controls (with initiator concentration equals to 1 μM). All experiments were conducted in triplicates.

Once the HCR reaction conditions were determined, the next step would be to explore the LOD of initiator in HCR assay. As shown in Figure 5.8, initiator concentrations from 0.1 nM and 1 μM was evaluated. Unfortunately, assays either conducted in heat block or in Quant Studio 3 PCR machine (where temperature control was more precise) only showed amplification with the highest initiator concentration (i.e., 1 μM). This experimental LOD was far from satisfactory, and therefore, the design of hairpins was evaluated to explore the reason.

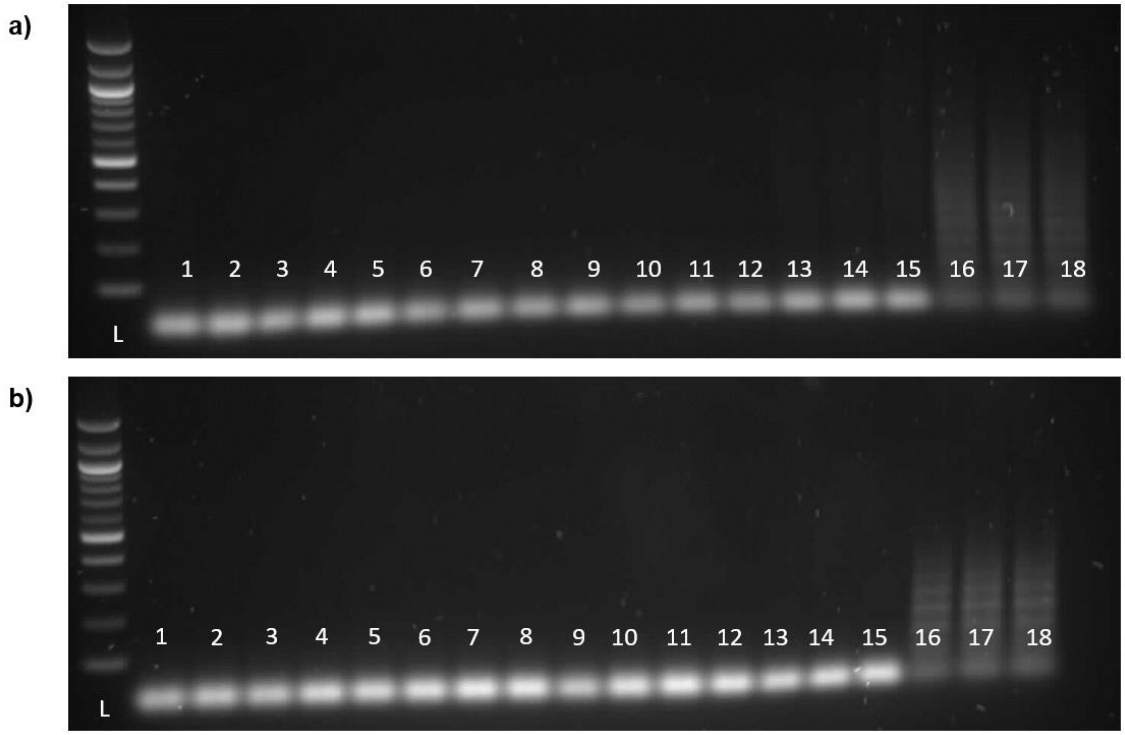


Figure 5.8 Gel electrophoresis images of HCR LOD evaluation experiments. a) reactions conducted in heat block. b) experiments conducted in Quant 3 Studio PCR machines. All experiments were conducted in triplicates. Land L: 100 bp DNA ladder. Lane 1-3: negative control; Lane 4-6: initiator concentration 0.1 nM; Lane 7-9: initiator concentration 1 nM; Lane 10-12: initiator concentration 10 nM; Lane 13-15: initiator concentration 100 nM; Lane 16-18: initiator concentration 1 μM.

The secondary structure of designed HP1-a and HP2-a are presented as hairpins (Figure 5.9), and their thermodynamic data are listed in Table 5.1. By comparing

with hairpins HR1 and HR2 reported in literature [155], HP1-a and HP2-a were too stable to be opened. And therefore, only when initiators were of high concentrations, could the HCR assay successfully conduct, which resulted in the unsatisfactory LOD of the HCR assay tested.

To solve this problem, a new set up hairpins, HP1-b and HP2-b, were designed as shown in Figure 5.9c and d. Their thermodynamic properties of this new set were also summarised in Table 5.1, which were comparable with those of literature [155], suggesting that there was higher chance to improve the LOD by enhancing the HCR reaction dynamics.

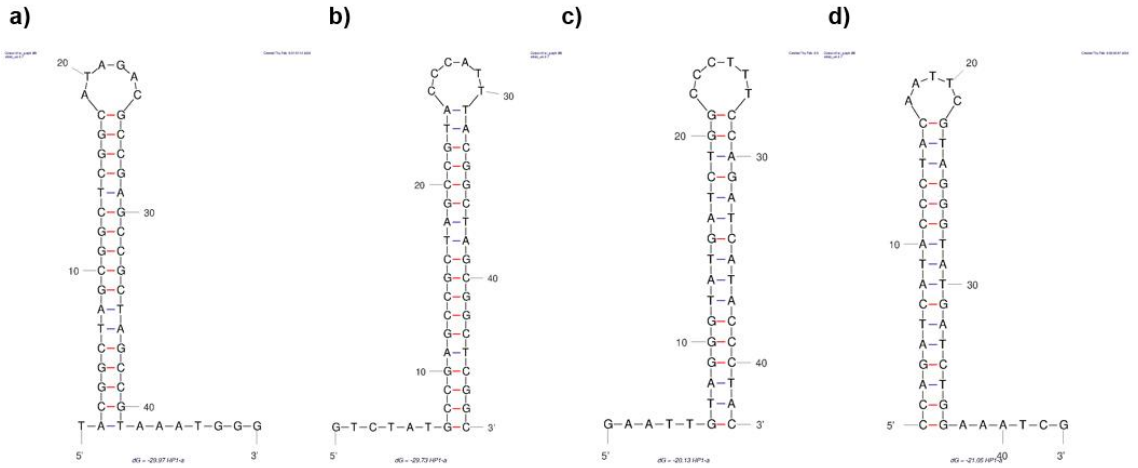


Figure 5.9 Schematic secondary structures of hairpins designed for HCR reactions (presented with the most stable form). a) HP1-a b) HP2-a c) HP1-b d) HP2-b. Figures were produced from mFold.

Table 5.1 Thermodynamic data of hairpin sets designed. Data was calculated from mFold at 25 °C, 0.15 M NaCl and 0.02 M $Mg^{2+}$.

| Hairpin name | ΔG (kcal $mol^{-1}$) | ΔH (kcal $mol^{-1}$) | ΔS (cal $K^{-1}$ $mol^{-1}$) | $T_m$ (°C) |
|---|---|---|---|---|
| HP1-a | -29.97 | -205.10 | -587.3 | 76 |
| HP2-a | -29.73 | -202.20 | -578.4 | 76.3 |
| HP1-b | -20.13 | -171.30 | -507 | 64.7 |
| HP2-b | -21.05 | -173.20 | -510.3 | 66.2 |
| HR1[155] | -18.69 | -154.2 | -454.5 | 66.1 |

| | | | | |
|---|---|---|---|---|
| HR2[155] | -20.39 | -162 | -474.9 | 67.9 |

### 5.3.3 Optimisation of CRISPR/Cas assay

HCR-CRISPR/Cas was designed to recognise the formation of HCR products and trigger the cleavage of DNA hydrogels for result detection. However, the CRISPR/Cas experiments suffered from significant false positive results, and the signals were even higher than the actual positive ones, as shown in Figure 5.10a. While 'PC' means 'initiator added to HCR before CRISPR/Cas' and 'NC' means 'no initiators added', the 'H2O' means that dd$H_2O$ was employed to substitute HCR products in CRISPR/Cas assay, to eliminate the interference of CRISPR/Cas assay solution.

Eliminating carry-over contamination and changing different CRISPR/Cas assay composition (as in Figure A7) did not solve the problem. As suggested by literature [155], the reason of this severe false positive signals could be due to HCR leakage. HCR leakage is caused by transit melting of hairpins, where stems open up and bind to the complementary toehold of the other hairpin. The leakage is mostly due to the improper design of hairpins. It is reported that the hairpins should be designed to have a free energy smaller than -16 kcal $mol^{-1}$ with a stem length longer than 16 bp, while reaction time and ionic concentration of buffer has only minimal effect. The design of HP1-a and HP2-a fell into the criteria for minimal HCR leakage (as in Table 5.1), then the technical operation should be taken into consideration.

Snap cooling and slow cooling of hairpin pretreatment could also play a role for HCR leakage. While snap cooling prompts intramolecular interactions and more secondary structures will form, slow cooling encourages intermolecular interactions as it allows more time for strands to find the real-matched sequences.

In the previous experiments, hairpins were pretreated by heating up to 95 °C followed by bench cooling for half hour before HCR. Although it was slower than leaving hairpins in freezers, the decreasing temperature speed was incontrollable. To precisely control the decreasing speed of temperature during cooling, Quant Studio 3 PCR machine was used to conduct the pretreatment. 0.015 °C $s^{-1}$ was set to cool the hairpins from 95 °C to 25 °C, before HCR and subsequent

CRISPR/Cas assay. The results were as shown in Figure 5.10b. Although there were still false positive signals, the intensity of negative controls reduced and fell below that of the positive controls. Figure 5.10c showed the comparison between signals before and after this technical improvement. The signal intensity of positive controls increased while that of negative controls decreased, suggesting that precise control of slow cooling using Quant Studio 3 PCR machine contributed to alleviating the false positive issue. Further work needs to be conducted to fully eliminate the background noise.

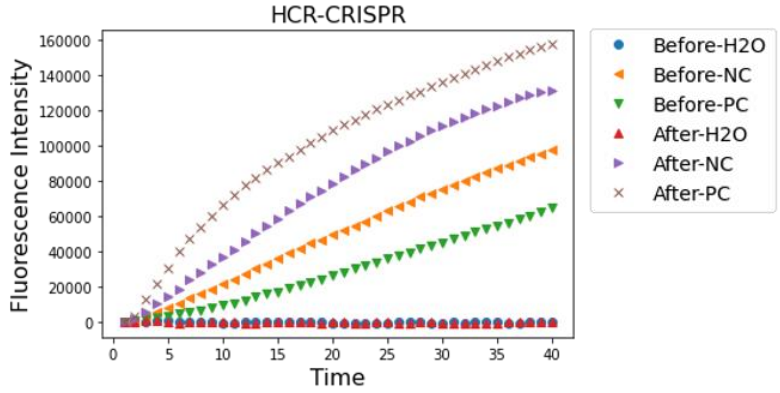


Figure 5.10 HCR-CRISPR/Cas fluorescent plots. Before: HCR-CRISPR/Cas assay fluorescent plots when hairpins were pretreated with 30 min bench-top cooling from 95 °C. After: when hairpins were pretreated with 0.015 °C $s^{-1}$ Quant Studio 3 PCR machine cooling from 95 °C. PC: initiator added to HCR before CRISPR/Cas. NC: no initiators addec. H2O: dd$H_2O$ substituted HCR assay in subsequent CRISPR/Cas assay. All experiments were conducted in triplicates and the plot was a mean of them.

### 5.3.4 Hydrogel formation

DNA hydrogel formation was divided into two steps. First, the acrydite conjugated to ssDNA strands X and Y polymerised first to polyacrylamide X (PA-X) and Y (PA-Y) under catalysts of APS and TEMED. Then, the formed PA-X and PA-Y bound with complementary linker L under room temperature to form hydrogels. To wrap MB particles inside, MB solution was added during the second step. Figure 5.11a showed the photos of hydrogels formed with different addition

strategy of catalyst. A represents adding APS and TEMED at the same time while S represents adding APS and TEMED in sequential order.

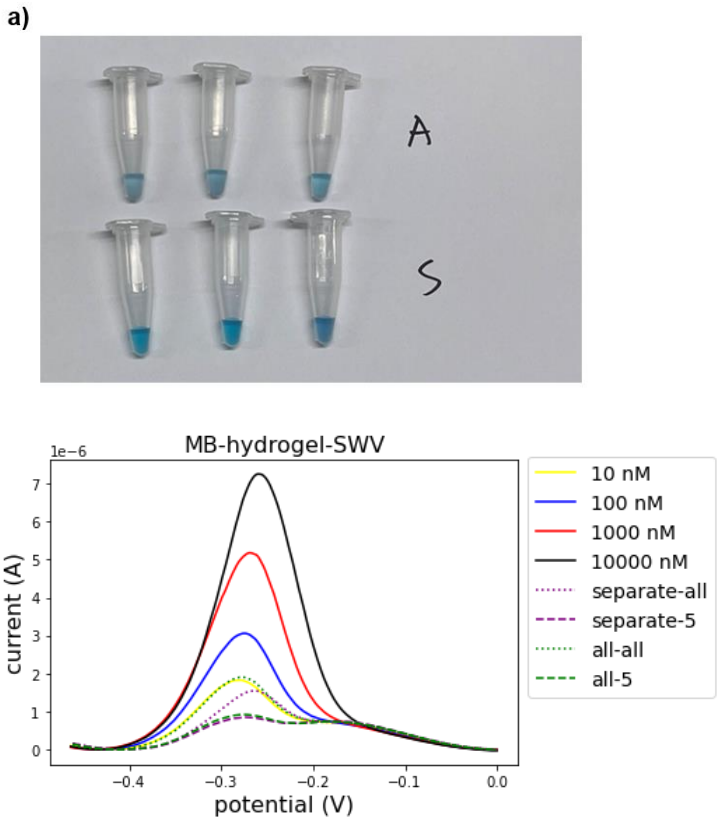


Figure 5.11 Formation and characterisation of hydrogel wrapping MB inside. a) photo of hydrogel produced in triplicates following separate catalysts (APS and TEMED) addition (S) and altogether addition (A). b) SWV diagrams measuring 10-fold serial diluted MB solution, ranging from 10 nM to 10000 nM, as well as hydrogel with MB added to 0.01 M PBS solution. all: all hydrogels added (100 µL) 5: 5 µL of hydrogel added. All experiments were conducted in triplicates.

Since PA-X, PA-Y and L were at µM level, it was hard to observe any physical form change upon hydrogel formation. Therefore, electrochemical measurement was employed to assess the electroactive MB signal. 10 µL 1.2 mM MB solution was used in hydrogel formation, indicating that 100 µL hydrogel in 10 mL 0.01 M PBS solution obtained 800 nM, and 5 µL hydrogel in 10 mL 0.01 M PBS solution obtained 40 nM MB.

As shown in Figure 5.11b, different concentrations of MB solutions were measured by SWV as reference. All (i.e., 100 µL) and 5 µL hydrogel with MB inside was measured by SWV in 0.01M PBS. The results were as shown in Figure 5.11b. The intensities of 100 µL hydrogel added were comparable (all) or lower than (separate) that of 10 nM MB solutions, and those of 5 µL added were much lower than that of 10 nM MB solutions, implying that hydrogels were successfully produced as the MB particles were prevented to have redox reactions on the working electrode surface. As for the catalysts adding strategy, the 5 µL of hydrogels were of comparable intensities, while 100 µL of separate addition had slightly lower intensities, suggesting that separate addition might perform better in producing hydrogels that could inhibit MB from having electrochemical reactions.

### 5.3.5 Molecular dynamics simulation for evaluation

To better understand the reason behind inefficient binding of designed aptamers and target kanamycin and shed light on future aptamer design validation, *in silico* experiments were conducted to explore the affinities between the capturing aptamer and target. Secondary structures were calculated from sequences, which subsequently contributed to the building of 3D DNA models. Since there are limited direct DNA 3D model building programs and algorithms, DNA 3D models are generally constructed through its RNA analogue with subsequent mutations back to DNAs [259]. Figure 5.12 showed the predicted aptamer 3D structures with base pairs annotated in different colours.

It was reported that the functional structure (i.e., the binding site) of kanamycin aptamer was in the loop of TTGAGGCTAA [260]. Therefore, docking of kanamycin was conducted with box set up in the loop. The docking results were ranked in the order of affinity, and Figure 5.13 showed the docked positions of aptamer with its corresponding docked ligand of the highest affinity. Table 5.2 showed a summary of calculated affinities of aptamer-ligand complex. Although the affinities were comparable in value, suggesting that the modified aptamer sequences (ap1 and ap2) should perform similar to the originally reported one (apori), docking is only a reflection of static view of complex, and the results

should be validated by molecular dynamic simulations where dynamic structural information of the interactions could be provided [261].

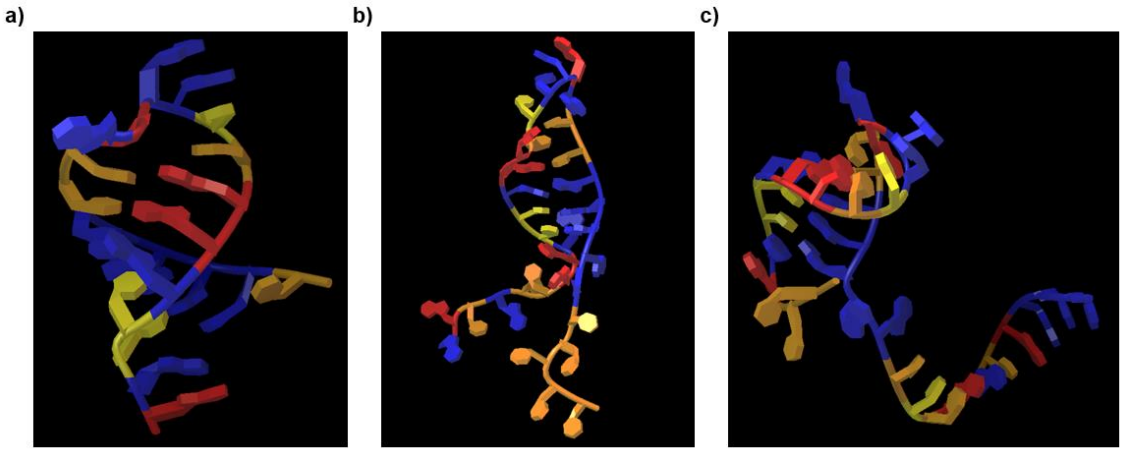


Figure 5.12 predicted 3D structures of aptamers. a) original aptamer reported in literature (apori). b) modified aptamer sequence 1 (ap1). c) modified aptamer sequence 2 (ap2). Different colours represent different base pairs. Blue: guanine. Red: adenine. Yellow: cystine. Orange: thymine.

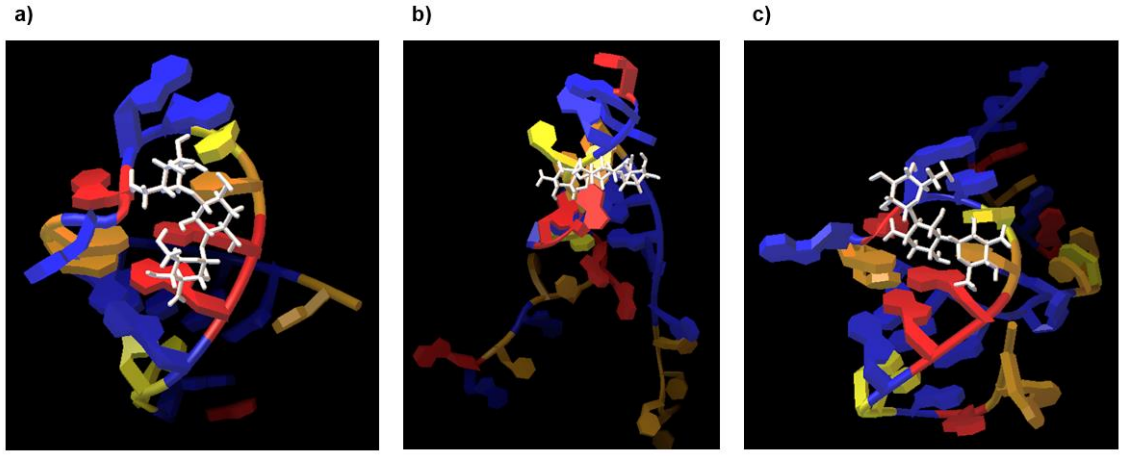


Figure 5.13 Docked aptamer-target complex structure. a) apori b) ap1 c) ap2.

Molecular dynamic simulation was then conducted with the docked complexes in a box filled with TIP3P water and $Na^+$ ions after energy minimisation, NVT and NPT equilibration. The starting structures of simulation were as shown in Figure 5.14. The simulation was conducted for 20 ns with trajectories recorded per 10 ps for further analysis.

Table 5.2 Summary of docked structure with calculated affinities.

| Complex name | Affinity (kJ $mol^{-1}$) |
|---|---|
| apori-kanamycin | -27.99 |
| ap1-kanamycin | -23.26 |
| ap2-kanamycin | -23.38 |

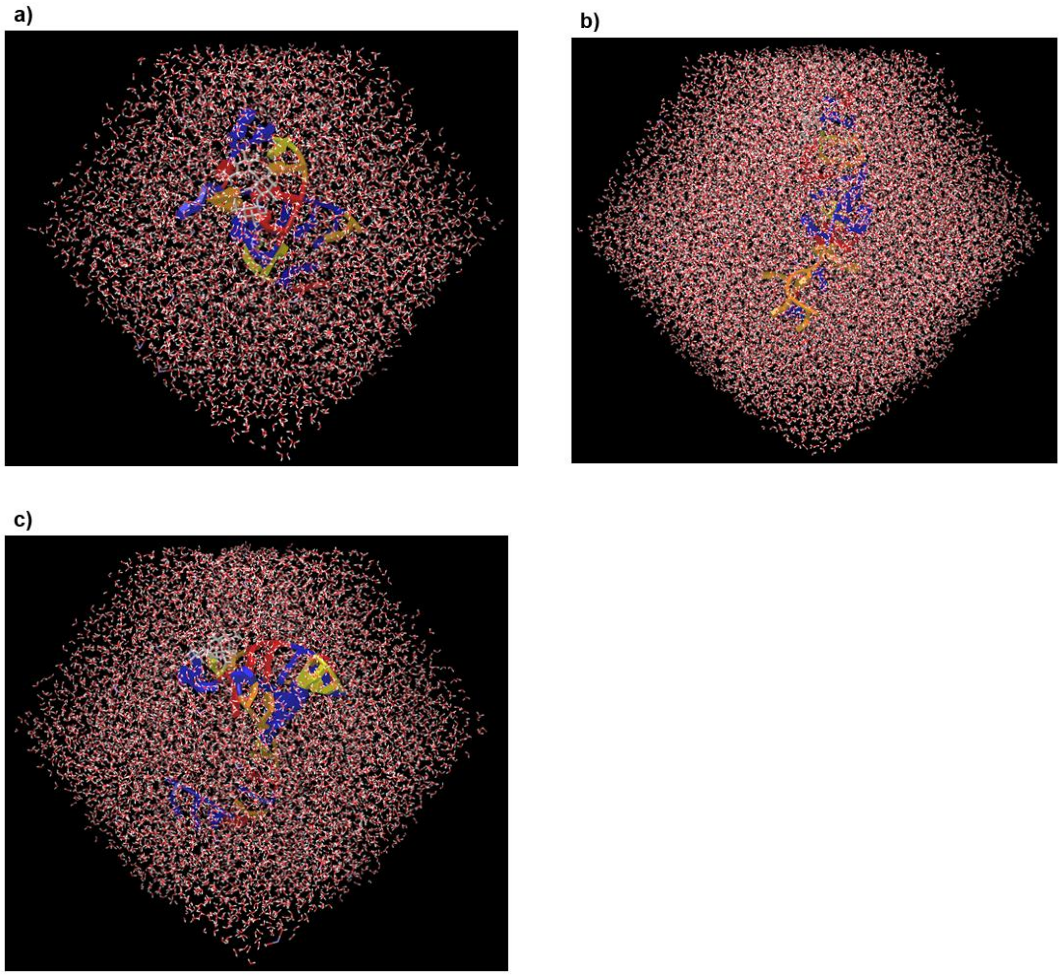


Figure 5.14 Starting structures of aptamer-ligand complex in a dodecahedron box of water and ions for MD simulation. grey structures: kanamycin ligand. Coloured ribbons: DNA aptamer. small dots, balls and sticks: ions and water molecules. a) apori b) ap1 c) ap2.

After MD simulation, the interaction energy between aptamer and ligand could be calculated using GROMACS 2023 [252]. While Lennard Jones potential describes

the potential between non-bonding atoms and molecules, coulombic potential describes the interaction between electrons based on their distance of separation, and the sum of them could be regarded as an approximation to estimate the total interaction energy between aptamer and the ligand. Table 7 summarises the simulation results of short-range Coulombic and Lennard-Jones aptamer-ligand interaction energy, with total interaction calculated as the following equation.

$$\boldsymbol{Total\ interaction = sum\ of\ variance \pm \sqrt{sum\ of\ standard\ deviation}}$$

Equation 2

As can be seen from Table 5.3, the original aptamer-kanamycin complex was far more stable than the designed aptamer complexes. This evidence supported and validated the proposed reason of failed initiator release experiments in 5.3.1, that the designed aptamers lack efficient binding ability with the target kanamycin. A possible solution to this problem would be to redesign/remodify the aptamers to have higher affinities.

Table 5.3 Summary of MD simulation results of aptamer-ligand short range interaction energy.

| Aptamer type | Coulombic interaction (kJ $mol^{-1}$) | Lennard-Jones interaction (kJ $mol^{-1}$) | Total interaction (kJ $mol^{-1}$) |
|---|---|---|---|
| apori | -52.36±17 | -36.71±13 | -89.07±5.477 |
| ap1 | -3.228±3 | -1.323±1.2 | -4.552±2.0493 |
| ap2 | -18.38±7.9 | -12.01±4.4 | -30.4005±3.507 |

## 5.4 Conclusions

A novel hydrogel-based HCR-CRISPR/Cas bioassay was designed for kanamycin detection. The first step of initiator release from aptamer upon target binding failed and potential reasons were investigated and validated through computational modelling. The binding between aptamer and target was double assessed via molecular docking and subsequent molecular dynamic simulations. By comparing interaction energies between designed and reported aptamers, it seemed that the failure of initiator release was due to the lack of effective aptamer

binding to the target. For future work, once capturing aptamers are designed, it would be helpful to assess their affinity work through modelling before wet lab works. Then the HCR assay was conducted and optimised but suffered from unsatisfactory LOD. The possible reasons could be that the improper design of HCR hairpins resulted in them too stable to react with initiators by comparing with literature studies. Although subsequent CRISPR/Cas assay was affected by significant false positive signals initially, the optimisation in technical operation between snap cooling and slow cooling partially solved the issue, while further efforts were required to eliminate the background noise. Finally, the hydrogels wrapping MB particles were successfully synthesised and characterised through SWV measurement with 10-fold diluted MB solution as reference.

Due to unexpected circumstances and time constraints, this antibiotic detection platform was not developed in full as planned. However, current data basically illustrates the feasibility of this assay as most steps were conducted. Although some obstacles were encountered during the development process, possible reasons and potential solutions were provided to solve the problems. Further efforts could be devoted to 1) redesign aptamers of higher affinity to targets 2) employ redesigned hairpins of less negative Gibbs free energy to conduct HCR to improve its sensitivity 3) eliminate CRISPR/Cas background noises by e.g., shorten crRNA length 4) combine the whole workflow to conduct kanamycin detection both in pristine samples and real water samples. Once the detection workflow is established, a non-labelled CRISPR/Cas modulated hydrogel system enabling rapid, sensitive, and POU detection of non-nucleic acid targets, i.e., antibiotics could be developed, allowing for onsite antibiotics pollution monitoring. Real water samples are to be tested with conventional HPLC results as validation. In addition, the workflow could be further modified by changing contents wrapped in hydrogel to suit other detection approaches, e.g., colorimetric detections, to meet different needs in resource limited settings. Besides, by combining the data of ARG and antibiotics concentration collected in the same area, it is possible to analyse the selective effects of antibiotics on ARGs and contribute to fundamental mechanistic studies.

Moreover, this platform also contributes to adopting CRISPR/Cas technology for small molecules detection rather than oligonucleotides. Since the techniques building up assay are transferrable, this platform is readily available to transfer to other small-molecule pollutants monitoring in the environment, i.e., pesticides, via the simple change of the capturing aptamer.

# 6 Conclusions and Future Work

## 6.1 Conclusions

This PhD study aimed to enhance the real-time fluorescent detection of ARGs through an innovative approach. By integrating multiplexed RPA and CRISPR/Cas methods, a remarkable LOD of 1 copy $\mu L^{-1}$ for all three gene targets, tet(M), tet(x3), and crassphage was reached. The assay demonstrated 100% accuracy in detecting ARGs in both spiked surface and tap water samples, indicating its robustness in complex matrices and therefore its potential for field applications.

To better suit the POU applications, the assay was expanded to LFA and electrochemical detections through simple modification of CRISPR/Cas probes. Following optimisation, the LODs reached 1 copy $\mu L^{-1}$ for tet(x3) and crassphage, and 10 copies $\mu L^{-1}$ for tet(M) for LFA, while electrochemical detection achieved 10 copies $\mu L^{-1}$ for all three targets. Testing real water samples, including four drinking water samples (2 from Nigeria and 2 from Scotland) and ten wastewater samples (influent from Cranfield WWTP, UK) yielded 100% accuracy compared to the gold standard qPCR, confirming, and validating the assay robustness, and reliability for onsite environmental monitoring. Overall, the PhD study provides a way forward to develop an economical, rapid, sensitive ARG detection assay that integrates three different end-point detection methods, with performances equivalent or better than existing ones. Such strategy can be particularly beneficial for implementation in low- and middle-income countries (LMICs) or remote regions with limited access to analytical infrastructures.

In addition to ARGs detection, antibiotic bioassay was using a hydrogel-based HCR-CRISPR/Cas assay with kanamycin as the model antibiotic. While encountering challenges during the development process, the underlying reasons and potential solutions were investigated using molecular docking and dynamic simulations. The aptamers were modified based on the sequence reported in the literature to suit the downstream HCR reactions. Although modified aptamers showed comparable affinity to target kanamycin, the results of MDS demonstrated a much smaller interaction energy between aptamer and

target for the modified ones. It indicated that the modified aptamers were less effective in capturing target, resulting in the minimal efficiency in initiator release. Besides, the hairpins design was reevaluated by 2D structure *in silico* prediction, and their high stability possibly inhibited the open up of hairpin structures, leading to the unsatisfying sensitivity of HCR. Although significant false positive signals were encountered for the CRISPR/Cas assay, improvements in hairpins pretreatment from snap cooling to slow cooling showed promise in reducing the background noise. The steps in the designed workflow and current data suggest the feasibility of this non-labelled HCR-CRISPR/Cas modulated hydrogel detection system, highlighting avenues for future research and refinements of ARGs detection in water samples.

## 6.2 Future Work

AMR is regarded as a public health challenge worldwide, resulting in millions of deaths each year [1]. The mobilisation of ARG between and within species leads to the expanded transmission of AMR, and the selection pressure from misused and abused antibiotics exacerbates the situation [4,5]. Therefore, ARGs and antibiotics level surveillance in the environment is vital to understanding the transmission process and potentially contributing to alleviate the AMR burden. The two assays designed and developed in this thesis aimed to determine the level of ARG and antibiotics in the environment, however, due to time constraints and unexpected circumstances, more work is required to be done to fully realise the goal. In the case of the antibiotic detection assay, as detailed in 5.4, the target specific aptamer is to be designed and assessed to maximise the target antibiotic capture and initiator release. Then, the redesigned hairpin sequences are to be employed for optimal HCR amplification performance. Once the background noise of CRISPR/Cas is tackled, the designed workflow is to be tested against pristine samples for sensitivity and specificity determination. Large scale real water samples are finally to be analysed by the developed workflow, with conventional HPLC results as gold standard reference.

On the other hand, in the case of ARG assay, the current results demonstrated the assay feasibility of sensitively and simultaneously detecting multiple ARG

from DNAs extracted from different real water matrices, including drinking water and wastewater. Besides, its compatibility with different endpoint detection approaches (fluorescent, electrochemical and lateral flow) was also shown. While current detection results only presented to be qualitative, the quantification of the ARG level in the environment is more of significance when guiding actions. Therefore, it is vital to further improve the current ARG detection to be quantitative.

Efforts should be made to improve the developed ARG detection assay from qualitative to quantitative. Currently, digital nucleic acid detection approach that enables absolute quantification of target nucleic acids has drawn much attention. Digital isothermal amplification method, in particular, digital RPA (dRPA), absolutely quantifies nucleic acid via sample compartmentalisation i.e., equally dividing reagents into thousands of reaction units before amplification. The amplification result of each unit then reflects the amount of target nucleic acids present in the sample, and the absolute number can be calculated using Poisson statistics. In addition to absolute target quantification, dRPA exhibits higher sensitivity, higher resolution (i.e., higher signal to background ratio), and higher tolerance to inhibitors when compared to traditional RPA [262].

Studies of dRPA quantifiying target nucleic acids have been reported. For example, Yang et al.[263] proposed a sample-in-digital-answer-out (SIDAO) diagnostic system that combines DNA extraction and dRPA. A simple single-layer PDMS microfluidic device was fabricated to realise fully automated sample extraction, partition and detection, and the whole process only took 70 min. However, same as traditional RPA, dRPA suffers from non-specific amplification due to its relatively low reaction temperature. Digital CRISPR/Cas system was therefore integrated with dRPA to address the problem. For example, Park et al. [264] for the first time reported a one-step dRPA coupled digital CRISPR/Cas assay called digitalisation enhanced CRISPR/Cas assisted one pot virus detection (deCOViD). Due to the specificity of crRNA and target sequence, the effect of non-specific amplification to the final detection results remained minimal. By comparing with traditional RPA-CRISPR/Cas detection in bulk solution, the proposed digital method showed better performances in detection time, signal to background ratio, dynamic range and sensitivity.

Therefore, it is worth devoting efforts to developing current mRPA-CRISPR/Cas detection approach to be digital, for improved analytical performances as well as absolute quantification of targets.

To achieve real-time monitoring, continuous efforts have been made to develop rapid and POU assays. However, most methods focused on detections under clinical context, lacking those aimed to be used in the environment, which is more demanding in assay analytical performance. Besides, to validate the robustness and feasibility, the developed POU assays require to test large scales of environmental aquatic samples from different locations. In addition, a fully automated portable device which is in line with the WHO REASSURED [202] framework should be developed to accommodate the assay to achieve onsite real time detections. Further work could be devoted into the development of POU devices that are affordable, sensitive, specific, user-friendly, rapid, and robust, and are of real-time connectivity, ease of specimen collection and environmental friendliness. µPAD, for example, is a promising POU platform for onsite detections especially in the resource limited area. It offers various merits including its cost-effectiveness, ease of transport and storage, biocompatibility, and suitability for mass production. Besides, its intrinsic capillary actions eliminate the need for external energy sources [96,265–267]. The advancement of µPAD has been flourishing since the initial work published in 2007 [97], and various applications were reported [10,98,100,101,265,268], indicating the great promise that µPAD holds in field testing in the environment. It is therefore worth devoting efforts to integrate the developed ARG or antibiotics assay with a µPAD to realise rapid and onsite measurements.

In addition to detection assay, the step of sample preparation before testing also plays a key role in acquiring accurate detection results [269]. Sample preparation affects the accuracy, sensitivity, and specificity of the detection assays, and continuous efforts have been made to address the challenges during method development and device integration. Conventional sample preparation step (isolation and DNA extraction) for NAAT, including lysis and subsequent liquid and solid phase extraction, is time- and labour-intensive. A central laboratory

setup and trained personnel are usually required, limiting its field-based applicability.

With the advancement of technologies, paper-based sample preparation has flourished and offers an alternative approach for rapid and user-friendly DNA isolation and extraction which can be carried out onsite. For example, Yang *et al.* [270] proposed a paper-origami device for cell lysis and DNA extraction. In the experiment, paper acted as a filtration substrate and glass fibre was employed to capture the lysed DNAs. By folding and flipping, the extracted and purified DNAs were eluted into the amplification chamber, realising gene detection on a POU device. Moreover, Lee *et al.* [271] employed mixed cellulose ester paper for DNA binding via ionic interaction. Capillary forces of cellulose drove the fluid transport via wicking, and the crowding effect of poly(ethylene) glycol-based (PEG) reagents concentrated the DNAs at the bottom of the paper. Finally, the bottom section with DNAs on was snapped off using the cap of a PCR tube and used as templates of the amplification. In addition to separate sample preparation and detection devices, Seok *et al.* [272] designed and developed a 3D-printed cassette that enables nucleic acid isolation, extraction and LAMP detection. Chitosan treated fibre glass membrane was employed for nucleic acid separation. A slider was utilized to realise complete integration from sample preparation to detection, presenting a from sample-to-answer POU device.

Other than paper-based sample preparation, Rodriguez-Mateos *et al.* [273] reported a lap-on-a-chip platform that integrates DNA extraction, purification and LAMP detection on a single polymethyl methacrylate (PMMA) based device. DNA was extracted via silica paramagnetic particles (PMP), with subsequent purification conducted through water-oil immiscible chambers.

Based on current research, potential future work could be to further develop a paper-based DNA isolation and extraction assay that integrates the POU detection device. Different chambers could be designed for different functions (i.e., DNA isolation and extraction, detection reaction, and detection result readout chamber) with channels in between to connect.

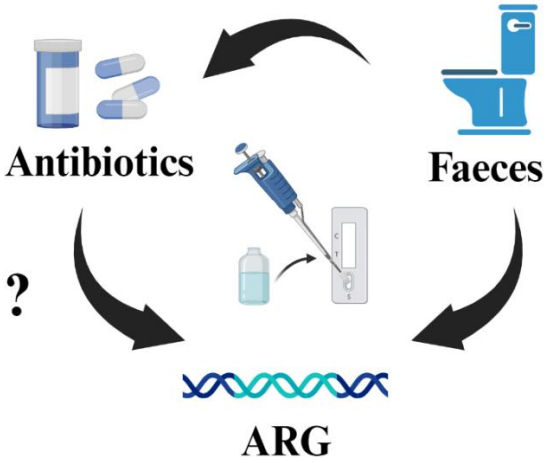


Figure 6.1 Schematic illustration of the relationships between faeces, antibiotics, and ARG in the environment.

Moreover, the real-time monitoring of ARG and antibiotics could also contribute to the fundamental understanding of AMR transmission mechanisms. As shown in Figure 6.1, the relationship between antibiotics and ARG of AMR transmission in the environment remains unclear. Studies have shown that in theory even transient exposure to sub-inhibitory concentration of antimicrobial agents can select for antimicrobial resistant microorganisms that possess survival advantages [274,275], i.e., those with antimicrobial resistance related genes (ARGs). However, evidence on the antibiotic selection consequences on AMR spread is controversial [276–278]. While some studies demonstrate that significant effect of selective agents such as antibiotics on AMR [279], most of them is concerned with mechanistic research and is in pristine condition [280], lacking those performed in complicated real samples. Besides, there are also various studies show that antibiotic selection does not significantly impact on AMR. Although some studies observed that higher antibiotic agent concentrations are in line with higher ARG abundances, it could also be largely explained by the faecal pollution in the sampled area, as faeces contain both ARG and antibiotic residues. In fact, studies have also shown there are correlations between ARG abundances and faecal contamination but not between antibiotic residue concentration [281], and most correlations between antibiotic and ARG abundance are results of same origin not causation [282], however, it has been difficult to measure the contribution

of both factors. As there is no widely agreed protocol to fully illustrate the problem, future work could be dedicated to tease apart the two effects, selection pressure and same origin, from each other regarding the selection pressure during AMR transmission in the environment.

# References

(1) Murray, C. J.; Ikuta, K. S.; Sharara, F.; Swetschinski, L.; Robles Aguilar, G.; Gray, A.; Han, C.; Bisignano, C.; Rao, P.; Wool, E.; Johnson, S. C.; Browne, A. J.; Chipeta, M. G.; Fell, F.; Hackett, S.; Haines-Woodhouse, G.; Kashef Hamadani, B. H.; Kumaran, E. A. P.; McManigal, B.; Agarwal, R.; Akech, S.; Albertson, S.; Amuasi, J.; Andrews, J.; Aravkin, A.; Ashley, E.; Bailey, F.; Baker, S.; Basnyat, B.; Bekker, A.; Bender, R.; Bethou, A.; Bielicki, J.; Boonkasidecha, S.; Bukosia, J.; Carvalheiro, C.; Castañeda-Orjuela, C.; Chansamouth, V.; Chaurasia, S.; Chiurchiù, S.; Chowdhury, F.; Cook, A. J.; Cooper, B.; Cressey, T. R.; Criollo-Mora, E.; Cunningham, M.; Darboe, S.; Day, N. P. J.; De Luca, M.; Dokova, K.; Dramowski, A.; Dunachie, S. J.; Eckmanns, T.; Eibach, D.; Emami, A.; Feasey, N.; Fisher-Pearson, N.; Forrest, K.; Garrett, D.; Gastmeier, P.; Giref, A. Z.; Greer, R. C.; Gupta, V.; Haller, S.; Haselbeck, A.; Hay, S. I.; Holm, M.; Hopkins, S.; Iregbu, K. C.; Jacobs, J.; Jarovsky, D.; Javanmardi, F.; Khorana, M.; Kissoon, N.; Kobeissi, E.; Kostyanev, T.; Krapp, F.; Krumkamp, R.; Kumar, A.; Kyu, H. H.; Lim, C.; Limmathurotsakul, D.; Loftus, M. J.; Lunn, M.; Ma, J.; Mturi, N.; Munera-Huertas, T.; Musicha, P.; Mussi-Pinhata, M. M.; Nakamura, T.; Nanavati, R.; Nangia, S.; Newton, P.; Ngoun, C.; Novotney, A.; Nwakanma, D.; Obiero, C. W.; Olivas-Martinez, A.; Olliaro, P.; Ooko, E.; Ortiz-Brizuela, E.; Peleg, A. Y.; Perrone, C.; Plakkal, N.; Ponce-de-Leon, A.; Raad, M.; Ramdin, T.; Riddell, A.; Roberts, T.; Robotham, J. V.; Roca, A.; Rudd, K. E.; Russell, N.; Schnall, J.; Scott, J. A. G.; Shivamallappa, M.; Sifuentes-Osornio, J.; Steenkeste, N.; Stewardson, A. J.; Stoeva, T.; Tasak, N.; Thaiprakong, A.; Thwaites, G.; Turner, C.; Turner, P.; van Doorn, H. R.; Velaphi, S.; Vongpradith, A.; Vu, H.; Walsh, T.; Waner, S.; Wangrangsimakul, T.; Wozniak, T.; Zheng, P.; Sartorius, B.; Lopez, A. D.; Stergachis, A.; Moore, C.; Dolecek, C.; Naghavi, M. Global Burden of Bacterial Antimicrobial Resistance in 2019: A Systematic Analysis. *The Lancet* **2022**, *399* (10325), 629. https://doi.org/10.1016/S0140-6736(21)02724-0.

(2) Tackling Antimicrobial Resistance 2019 to 2024. **2022**. assets.publishing.service.gov.uk/media/6261392d8fa8f523bf22ab9e/UK_AMR_5_year_national_action_plan.pdf

(3) WHO, Global Antimicrobial Resistance Surveillance System (GLASS) Molecular Methods for Antimicrobial Resistance (AMR) Diagnostics to Enhance the Global Antimicrobial Resistance Surveillance System. **2019,** Global Antimicrobial Resistance Surveillance System (GLASS). Molecular methods for antimicrobial resistance (AMR) diagnostics to enhance the Global Antimicrobial Resistance Surveillance System (who.int)

(4) Hernando-Amado, S.; Coque, T. M.; Baquero, F.; Martínez, J. L. Defining and Combating Antibiotic Resistance from One Health and Global Health Perspectives. *Nature Microbiology*. **2019**, *4*, 1432. https://doi.org/10.1038/s41564-019-0503-9.

(5) Larsson, D. G. J.; Flach, C. F. Antibiotic Resistance in the Environment. *Nature Reviews Microbiology*, **2022**, *20*, 257. https://doi.org/10.1038/s41579-021-00649-x.

(6) Cabello, F. C.; Godfrey, H. P.; Tomova, A.; Ivanova, L.; Dölz, H.; Millanao, A.; Buschmann, A. H. Antimicrobial Use in Aquaculture Re-Examined: Its Relevance to Antimicrobial Resistance and to Animal and Human Health. *Environmental Microbiology* **2013**, *15* (7), 1917. https://doi.org/10.1111/1462-2920.12134.

(7) Duelge, K. J.; Nishshanka, U.; De Alwis, H. G. An LC–MS/MS Method for the Determination of Antibiotic Residues in Distillers Grains. *Journal of Chromatography B* **2017**, *1053*, 81. https://doi.org/10.1016/J.JCHROMB.2017.03.037.

(8) Oyedeji, A. O.; Msagati, T. A. M.; Williams, A. B.; Benson, N. U. Detection and Quantification of Multiclass Antibiotic Residues in Poultry Products Using Solid-Phase Extraction and High-Performance Liquid Chromatography with Diode Array Detection. *Heliyon* **2021**, *7* (12), e08469. https://doi.org/10.1016/J.HELIYON.2021.E08469.

(9) Zhou, C.; Pan, Y.; Ge, S.; Coulon, F.; Yang, Z. Rapid Methods for Antimicrobial Resistance Diagnosis in Contaminated Soils for Effective Remediation Strategy. *TrAC Trends in Analytical Chemistry* **2021**, *137*, 116203. https://doi.org/10.1016/j.trac.2021.116203.

(10) Pan, Y.; Mao, K.; Hui, Q.; Wang, B.; Cooper, J.; Yang, Z. Paper-Based Devices for Rapid Diagnosis and Wastewater Surveillance. *TrAC Trends in Analytical Chemistry* **2022**, *157*, 116760. https://doi.org/10.1016/j.trac.2022.116760.

(11) Chen, J. S.; Ma, E.; Harrington, L. B.; Da Costa, M.; Tian, X.; Palefsky, J. M.; Doudna, J. A. CRISPR-Cas12a Target Binding Unleashes Indiscriminate Single-Stranded DNase Activity. *Science,* **2018**, *360* (6387), 436. https://doi.org/10.1126/SCIENCE.AAR6245/SUPPL_FILE/AAR6245_CHEN_SM.PDF.

(12) Xiong, Y.; Zhang, J.; Yang, Z.; Mou, Q.; Ma, Y.; Xiong, Y.; Lu, Y. Functional DNA Regulated CRISPR-Cas12a Sensors for Point-of-Care Diagnostics of Non-Nucleic-Acid Targets. *J. Am. Chem. Soc.* **2020**, *142* (1), 207. https://doi.org/10.1021/jacs.9b09211.

(13) Dai, Y.; Somoza, R. A.; Wang, L.; Welter, J. F.; Li, Y.; Caplan, A. I.; Liu, C. C. Exploring the Trans-Cleavage Activity of CRISPR-Cas12a (Cpf1) for the Development of a Universal Electrochemical Biosensor. *Angewandte Chemie - International Edition*. **2019**, *58*, 17399. https://doi.org/10.1002/anie.201910772

(14) Yang, Y.; Wang, D.; Lü, · Peng; Ma, S.; Chen, K. Research Progress on Nucleic Acid Detection and Genome Editing of CRISPR/Cas12 System. *Molecular Biology Reports 2023* **2023**, *1*, 1. https://doi.org/10.1007/S11033-023-08240-8.

(15) *Global Antimicrobial Resistance and Use Surveillance System (GLASS)*. https://www.who.int/initiatives/glass (accessed 2023-03-05).

(16) Vasala, A.; Hytönen, V. P.; Laitinen, O. H. Modern Tools for Rapid Diagnostics of Antimicrobial Resistance. *Front Cell Infect Microbiol* **2020**, *10*, 308. https://doi.org/10.3389/FCIMB.2020.00308/BIBTEX.

(17) Rehm, S.; Rentsch, K. M. LC-MS/MS Method for Nine Different Antibiotics. *Clinica Chimica Acta* **2020**, *511*, 360. https://doi.org/10.1016/J.CCA.2020.11.001.

(18) García-Campaña, A. M.; Gámiz-Gracia, L.; Lara, F. J.; Del Olmo Iruela, M.; Cruces-Blanco, C. Applications of Capillary Electrophoresis to the Determination of Antibiotics in Food and Environmental Samples. *Analytical and Bioanalytical Chemistry* **2009**, *395* (4), 967. https://doi.org/10.1007/S00216-009-2867-9.

(19) Ikhimiukor, O. O.; Odih, E. E.; Donado-Godoy, P.; Okeke, I. N. A Bottom-up View of Antimicrobial Resistance Transmission in Developing Countries. *Nature Microbiology 2022 7:6* **2022**, *7* (6), 757. https://doi.org/10.1038/s41564-022-01124-w.

(20) A Perspective of Environmental Pollution. M. W. Holdgate. *Cambridge University Press*. *International Relations* **1980**, *6* (5), 850. https://doi.org/10.1177/004711788000600518.

(21) Kaur, K.; Reddy, S.; Barathe, P.; Oak, U.; Shriram, V.; Kharat, S. S.; Govarthanan, M.; Kumar, V. Microplastic-Associated Pathogens and Antimicrobial Resistance in Environment. *Chemosphere* **2022**, *291*, 133005. https://doi.org/10.1016/J.CHEMOSPHERE.2021.133005.

(22) Amos, G. C. A.; Ploumakis, S.; Zhang, L.; Hawkey, P. M.; Gaze, W. H.; Wellington, E. M. H. The Widespread Dissemination of Integrons throughout Bacterial Communities in a Riverine System. *International Society for Microbial Ecology* **2018**, *12* (3), 681. https://doi.org/10.1038/s41396-017-0030-8.

(23) Andersson, D. I.; Hughes, D. Antibiotic Resistance and Its Cost: Is It Possible to Reverse Resistance? *Nature Review Microbiology* **2010**, *8* (4), 260. https://doi.org/10.1038/nrmicro2319.

(24) Kohanski, M. A.; DePristo, M. A.; Collins, J. J. Sublethal Antibiotic Treatment Leads to Multidrug Resistance via Radical-Induced Mutagenesis. *Molecular and Cellular Biology* **2010**, *37* (3), 311. https://doi.org/10.1016/j.molcel.2010.01.003.

(25) Aminov, R. I. Horizontal Gene Exchange in Environmental Microbiota. *Frontiers in Microbiology* **2011**, *2*. 1. https://doi.org/10.3389/fmicb.2011.00158.

(26) Karkman, A.; Do, T. T.; Walsh, F.; Virta, M. P. J. Antibiotic-Resistance Genes in Waste Water. *Trends in Microbiology* **2018**, *26* (3), 220. https://doi.org/10.1016/j.tim.2017.09.005.

(27) Amato, M.; Dasí, D.; González, A.; Ferrús, M. A.; Castillo, M. Á. Occurrence of Antibiotic Resistant Bacteria and Resistance Genes in Agricultural Irrigation Waters from Valencia City (Spain). *Agricultural Water Management,* **2021**, *256*, 107097. https://doi.org/10.1016/j.agwat.2021.107097.

(28) Barber, A. E.; Riedel, J.; Sae-Ong, T.; Kang, K.; Brabetz, W.; Panagiotou, G.; Deising, H. B.; Kurzai, O. Effects of Agricultural Fungicide Use on Aspergillus Fumigatus Abundance, Antifungal Susceptibility, and Population Structure. **2020**. *11,* e02213. https://doi.org/10.1128/mBio.

(29) Peter Moore, by J.; Rao, J. R.; Cherie Millar, B.; Goldsmith, C. E.; Coulter, W. A.; Moore, J. E.; Moore, J. A. Antimicrobial Resistance to 14 Antimicrobials in Marine Coastal Waters around Northern Ireland: Use of the Novel Relative Resistance Index as a Marker of Ecological Status; *Journal of Marine Research*, **2013**, 71, 1.

(30) Castrignanò, E.; Kannan, A. M.; Proctor, K.; Petrie, B.; Hodgen, S.; Feil, E. J.; Lewis, S. E.; Lopardo, L.; Camacho-Muñoz, D.; Rice, J.; Cartwright, N.; Barden, R.; Kasprzyk-Hordern, B. (Fluoro)Quinolones and Quinolone Resistance Genes in the Aquatic Environment: A River Catchment Perspective. *Water Research* **2020**, *182,* 1. https://doi.org/10.1016/j.watres.2020.116015.

(31) Leroy-Freitas, D.; Machado, E. C.; Torres-Franco, A. F.; Dias, M. F.; Leal, C. D.; Araújo, J. C. Exploring the Microbiome, Antibiotic Resistance Genes, Mobile Genetic Element, and Potential Resistant Pathogens in Municipal Wastewater Treatment Plants in Brazil. *Science of The Total Environment* **2022**, *842*, 156773. https://doi.org/10.1016/J.SCITOTENV.2022.156773.

(32) Mathys, D. A.; Mollenkopf, D. F.; Feicht, S. M.; Adams, R. J.; Albers, A. L.; Stuever, D. M.; Grooters, S. V.; Ballash, G. A.; Daniels, J. B.; Wittum, T. E. Carbapenemase-Producing Enterobacteriaceae and Aeromonas Spp. Present in Wastewater Treatment Plant Effluent and Nearby Surface Waters in the US. *PLoS One* **2019**, *14* (6), e0218650. https://doi.org/10.1371/journal.pone.0218650.

(33) Deguenon, E.; Dougnon, V.; Houssou, V. M. C.; Gbotche, E.; Ahoyo, R. A.; Fabiyi, K.; Agbankpe, J.; Mousse, W.; Lougbegnon, C.; Klotoe, J. R.; Tchobo, F.; Bankole, H.; Boko, M. Hospital Effluents as Sources of Antibiotics Residues, Resistant Bacteria and Heavy Metals in Benin. *SN Applied Science* **2022**, *4* (8), 206. https://doi.org/10.1007/S42452-022-05095-9.

(34) Mapipa, Q.; Digban, T. O.; Nnolim, N. E.; Nwodo, U. U. Antibiogram Profile and Virulence Signatures of Pseudomonas Aeruginosa Isolates Recovered from Selected Agrestic Hospital Effluents. *Scientific Report* **2021**, *11* (1), 11800. https://doi.org/10.1038/s41598-021-91280-6.

(35) Mapipa, Q.; Digban, T. O.; Nnolim, N. E.; Nontongana, N.; Okoh, A. I.; Nwodo, U. U. Molecular Characterization and Antibiotic Susceptibility Profile of Acinetobacter Baumannii Recovered from Hospital Wastewater Effluents. *Current Microbiology* **2022**, *79* (4), 123. https://doi.org/10.1007/S00284-022-02815-7.

(36) Harris, S.; Morris, C.; Morris, D.; Cormican, M.; Cummins, E. Antimicrobial Resistant Escherichia Coli in the Municipal Wastewater System: Effect of Hospital Effluent and Environmental Fate. *Science of the Total Environment* **2014**, *468*, 1078. https://doi.org/10.1016/j.scitotenv.2013.09.017.

(37) Montezzi, L. F.; Campana, E. H.; Corrêa, L. L.; Justo, L. H.; Paschoal, R. P.; Da Silva, I. L. V. D.; Souza, M. D. C. M.; Drolshagen, M.; Picão, R. C. Occurrence of Carbapenemase-Producing Bacteria in Coastal Recreational Waters. *International Journal of Antimicrobial Agents* **2015**, *45* (2), 174. https://doi.org/10.1016/j.ijantimicag.2014.10.016.

(38) Reynolds, L. J.; Sala-Comorera, L.; Martin, N. A.; Nolan, T. M.; Stephens, J. H.; Gitto, A.; O'Hare, G. M. P.; O'Sullivan, J. J.; Meijer, W. G. Correlation between Antimicrobial Resistance and Faecal Contamination in Small Urban Streams and Bathing Waters. *Science of the Total Environment* **2020**, *739*, 140242. https://doi.org/10.1016/j.scitotenv.2020.140242.

(39) Sala-Comorera, L.; Nolan, T. M.; Reynolds, L. J.; Venkatesh, A.; Cheung, L.; Martin, N. A.; Stephens, J. H.; Gitto, A.; O'Hare, G. M. P.; O'Sullivan, J. J.; Meijer, W. G. Bacterial and Bacteriophage Antibiotic Resistance in Marine Bathing Waters in Relation to Rivers and Urban Streams. *Frontiers in Microbiology* **2021**, *12*, 1. https://doi.org/10.3389/fmicb.2021.718234.

(40) Young, S.; Nayak, B.; Sun, S.; Badgley, B. D.; Rohr, J. R.; Harwood, V. J. Vancomycin-Resistant Enterococci and Bacterial Community Structure Following a Sewage Spill into an Aquatic Environment. *Applied Environmental Microbiology* **2016**, *82* (18), 5653. https://doi.org/10.1128/AEM.01927-16.

(41) Raseala, C. M.; Ekwanzala, M. D.; Momba, M. N. B. Shared Extended-Spectrum β-Lactamase-Producing Salmonella Serovars between Agricultural and Aquatic Environments Revealed through Inva Amplicon Sequencing. *Microorganisms* **2020**, *8* (12), 1. https://doi.org/10.3390/microorganisms8121898.

(42) Garcias, B.; Aguirre, L.; Seminati, C.; Reyes, N.; Allepuz, A.; Obón, E.; Molina-lopez, R. A.; Darwich, L. Extended-Spectrum β-Lactam Resistant Klebsiella Pneumoniae and Escherichia Coli in Wild European Hedgehogs (Erinaceus Europeus) Living in Populated Areas. *Animals* **2021**, *11* (10), 2837. https://doi.org/10.3390/ani11102837.

(43) Pot, M.; Guyomard-Rabenirina, S.; Couvin, D.; Ducat, C.; Enouf, V.; Ferdinand, S.; Gruel, G.; Malpote, E.; Talarmin, A.; Breurec, S.; Reynaud, Y. Dissemination of Extended-Spectrum-b-Lactamase-Producing Enterobacter Cloacae Complex from a Hospital to the Nearby Environment in Guadeloupe (French West Indies): ST114 Lineage Coding for a Successful IncHI2/ST1 Plasmid; *Antimicrobial chemotherapy*, **2021**. *65*, 1. https://journals.asm.org/journal/aac.

(44) Monticelli, L. S.; Decembrini, F.; Bergamasco, A.; Caruso, G. Water Quality Assessment of Transitional and Coastal Marine Sicilian Waters (Italy): Ecological and Epidemiological Significance of Multiple Antimicrobial Resistant Enterococcus Spp. *Estuarine Coastal Shelf Science* **2019**, *217*, 173. https://doi.org/10.1016/j.ecss.2018.11.021.

(45) Moura, A.; Araújo, S.; Alves, M.; Henriques, I.; Pereira, A.; Correia, A. C. M. The Contribution of Escherichia Coli from Human and Animal Sources to the Integron Gene Pool in Coastal Waters. *Frontiers in Microbiology* **2014**, *5*, 419. https://doi.org/10.3389/fmicb.2014.00419.

(46) Ben Said, L.; Jouini, A.; Fliss, I.; Torres, C.; Klibi, N. Antimicrobial Resistance Genes and Virulence Gene Encoding Intimin in Escherichia Coli and Enterococcus Isolated from Wild Rabbits (Oryctolagus Cuniculus) in Tunisia. *Acta Veterinaria Hungarica* **2019**, *67* (4), 477. https://doi.org/10.1556/004.2019.047.

(47) Sanz, S.; Olarte, C.; Hidalgo-Sanz, R.; Ruiz-Ripa, L.; Fernández-Fernández, R.; García-Vela, S.; Martínez-álvarez, S.; Torres, C. Airborne Dissemination of Bacteria (Enterococci, Staphylococci and Enterobacteriaceae) in a Modern Broiler Farm and Its Environment. *Animals* **2021**, *11* (6), 1783. https://doi.org/10.3390/ani11061783.

(48) Zhang, Y. J.; Hu, H. W.; Chen, Q. L.; Singh, B. K.; Yan, H.; Chen, D.; He, J. Z. Transfer of Antibiotic Resistance from Manure-Amended Soils to Vegetable Microbiomes. *Environmental International* **2019**, *130*. 104912. https://doi.org/10.1016/j.envint.2019.104912.

(49) Blaak, H.; van Hoek, A. H. A. M.; Veenman, C.; Docters van Leeuwen, A. E.; Lynch, G.; van Overbeek, W. M.; de Roda Husman, A. M. Extended Spectrum SS-Lactamase- and Constitutively AmpC-Producing Enterobacteriaceae on Fresh Produce and in the Agricultural Environment. *International Journal of Food Microbiology* **2014**, *168*, 8. https://doi.org/10.1016/j.ijfoodmicro.2013.10.006.

(50) Gao, M.; Qiu, T.; Sun, Y.; Wang, X. The Abundance and Diversity of Antibiotic Resistance Genes in the Atmospheric Environment of Composting Plants. *Environmental International* **2018**, *116*, 229. https://doi.org/10.1016/j.envint.2018.04.028.

(51) Schouten, J.; De Waele, J.; Lanckohr, C.; Koulenti, D.; Haddad, N.; Rizk, N.; Sjövall, F.; Kanj, S. S. Antimicrobial Stewardship in the ICU in COVID-19 Times: The Known Unknowns. *Int J Antimicrob Agents* **2021**, *58* (4), 106409. https://doi.org/10.1016/j.ijantimicag.2021.106409.

(52) Lu, J.; Guo, J. Disinfection Spreads Antimicrobial Resistance. *Science* **2021**, *371* (6528), 474. https://doi.org/10.1126/science.abg4380.

(53) Zhuo, C.; Wei, X.; Zhang, Z.; Hicks, J. P.; Zheng, J.; Chen, Z.; Haldane, V.; Walley, J.; Guan, Y.; Xu, H.; Zhong, N. An Antibiotic Stewardship Programme to Reduce Inappropriate Antibiotic Prescribing for Acute Respiratory Infections in Rural Chinese Primary Care Facilities: Study Protocol for a Clustered Randomised Controlled Trial. *Trials* **2020**, *21* (1), 394. https://doi.org/10.1186/s13063-020-04303-4.

(54) Kang, Y.; Chen, S.; Chen, Y.; Tian, L.; Wu, Q.; Zheng, M.; Li, Z. Alterations of Fecal Antibiotic Resistome in COVID-19 Patients after Empirical Antibiotic Exposure. *International Journal of Hygiene and Environmental Health* **2022**, *240*. 113882. https://doi.org/10.1016/j.ijheh.2021.113882.

(55) Gaeta, N. C.; Bean, E.; Miles, A. M.; Carvalho, D. U. O. G. de; Alemán, M. A. R.; Carvalho, J. S.; Gregory, L.; Ganda, E. A Cross-Sectional Study of Dairy Cattle Metagenomes Reveals Increased Antimicrobial Resistance in Animals Farmed in a Heavy Metal Contaminated Environment. *Frontiers in Microbiology* **2020**, *11*. 1. https://doi.org/10.3389/fmicb.2020.590325.

(56) Metcalf, R.; White, H. L.; Moresco, V.; Ormsby, M. J.; Oliver, D. M.; Quilliam, R. S. Sewage-Associated Plastic Waste Washed up on Beaches Can Act as a Reservoir for Faecal Bacteria, Potential Human Pathogens, and Genes for Antimicrobial Resistance. *Marine Pollution Bulletin* **2022**, *180*. 113766. https://doi.org/10.1016/j.marpolbul.2022.113766.

(57) Laganà, P.; Caruso, G.; Corsi, I.; Bergami, E.; Venuti, V.; Majolino, D.; La Ferla, R.; Azzaro, M.; Cappello, S. Do Plastics Serve as a Possible Vector for the Spread of Antibiotic Resistance? First Insights from Bacteria Associated to a Polystyrene Piece from King George Island (Antarctica). *International Journal of Hygiene and Environmental Health* **2019**, *222* (1), 89. https://doi.org/10.1016/J.IJHEH.2018.08.009.

(58) Galafassi, S.; Di Cesare, A.; Di Nardo, L.; Sabatino, R.; Valsesia, A.; Fumagalli, F. S.; Corno, G.; Volta, P. Microplastic Retention in Small and Medium Municipal Wastewater Treatment Plants and the Role of the Disinfection. *Environmental Science and Pollution Research International* **2022**, *29* (7), 10535. https://doi.org/10.1007/S11356-021-16453-2.

(59) Zhu, D.; Ma, J.; Li, G.; Rillig, M. C.; Zhu, Y. G. Soil Plastispheres as Hotpots of Antibiotic Resistance Genes and Potential Pathogens. *International Society for Microbial Ecology Journal* **2022**, *16* (2), 521–532. https://doi.org/10.1038/S41396-021-01103-9.

(60) Methods for the Determination of Susceptibility of Bacteria to Antimicrobial Agents. Terminology. *Clinical Microbiology and Infection* **1998**, *4* (5), 291–296. https://doi.org/10.1111/j.1469-0691.1998.tb00061.x.

(61) Marroki, A.; Bousmaha-Marroki, L. Antibiotic Resistance Diagnostic Methods for Pathogenic Bacteria. In *Encyclopedia of Infection and Immunity*; Elsevier, **2022;** 320. https://doi.org/10.1016/B978-0-12-818731-9.00133-6.

(62) Balouiri, M.; Sadiki, M.; Ibnsouda, S. K. Methods for in Vitro Evaluating Antimicrobial Activity: A Review. *Journal of Pharmaceutical Analysis* **2016**, *6* (2), 71. https://doi.org/10.1016/j.jpha.2015.11.005.

(63) Christenson, J. C.; Korgenski, E. K.; Relich, R. F. Laboratory Diagnosis of Infection Due to Bacteria, Fungi, Parasites, and Rickettsiae. In *Principles and Practice of Pediatric Infectious Diseases*; Elsevier, **2018**; *1422*, e3. https://doi.org/10.1016/B978-0-323-40181-4.00286-3.

(64) Jorgensen, J. H.; Ferraro, M. J. Antimicrobial Susceptibility Testing: A Review of General Principles and Contemporary Practices. *Clinical Infectious Diseases* **2009**, *49* (11), 1749. https://doi.org/10.1086/647952/2/49-11-1749-FIG003.GIF.

(65) Khan, Z. A.; Siddiqui, M. F.; Park, S. Current and Emerging Methods of Antibiotic Susceptibility Testing. *Diagnostics* **2019**, *9* (2), 49. https://doi.org/10.3390/diagnostics9020049.

(66) Banerjee, R.; Patel, R. Molecular Diagnostics for Genotypic Detection of Antibiotic Resistance: Current Landscape and Future Directions. *JAC Antimicrob Resist* **2022**, *5* (1), dlad018. https://doi.org/10.1093/JACAMR/DLAD018.

(67) Rohde, A.; Hammerl, J. A.; Boone, I.; Jansen, W.; Fohler, S.; Klein, G.; Dieckmann, R.; Al Dahouk, S. Overview of Validated Alternative Methods for the Detection of Foodborne Bacterial Pathogens. *Trends Food Sci Technol* **2017**, *62*, 113. https://doi.org/10.1016/J.TIFS.2017.02.006.

(68) Galhano, B. S. P.; Ferrari, R. G.; Panzenhagen, P.; de Jesus, A. C. S.; Conte-Junior, C. A. Antimicrobial Resistance Gene Detection Methods for Bacteria in Animal-Based Foods: A Brief Review of Highlights and Advantages. *Microorganisms* **2021**, *9* (5), 923. https://doi.org/10.3390/MICROORGANISMS9050923.

(69) Tomita, N.; Mori, Y.; Kanda, H.; Notomi, T. Loop-Mediated Isothermal Amplification (LAMP) of Gene Sequences and Simple Visual Detection of Products. *Nature Protocol* **2008**, *3* (5), 877. https://doi.org/10.1038/nprot.2008.57.

(70) Piepenburg, O.; Williams, C. H.; Stemple, D. L.; Armes, N. A. DNA Detection Using Recombination Proteins. *PLoS Biology* **2006**, *4* (7), 1115. https://doi.org/10.1371/journal.pbio.0040204.

(71) Liu, P.; Meagher, R. J.; Light, Y. K.; Yilmaz, S.; Chakraborty, R.; Arkin, A. P.; Hazen, T. C.; Singh, A. K. Microfluidic Fluorescence in Situ Hybridization and Flow Cytometry (MFlowFISH). *Lab on a Chip* **2011**, *11* (16), 2673. https://doi.org/10.1039/C1LC20151D.

(72) Oueslati, S.; Volland, H.; Cattoir, V.; Bernabeu, S.; Girlich, D.; Dulac, D.; Plaisance, M.; Laroche, M.; Dortet, L.; Simon, S.; Naas, T. Development and Validation of a Lateral Flow Immunoassay for Rapid Detection of VanA-Producing Enterococci. *Journal of Antimicrobial Chemotherapy* **2021**, *76* (1), 146. https://doi.org/10.1093/JAC/DKAA413.

(73) Liu, C.; Li, B.; Liu, M.; Mao, S. Demand, Status, and Prospect of Antibiotics Detection in the Environment. *Sensors and Actuators B Chemical* **2022**, *369*, 132383. https://doi.org/10.1016/J.SNB.2022.132383.

(74) Parthasarathy, R.; Monette, C. E.; Bracero, S.; Saha, M. S. Methods for Field Measurement of Antibiotic Concentrations: Limitations and Outlook. *FEMS Microbiology Ecology* **2018**, *94* (8), 105. https://doi.org/10.1093/FEMSEC/FIY105.

(75) Wang, Q.; Zhao, W. M. Optical Methods of Antibiotic Residues Detections: A Comprehensive Review. *Sens Actuators B Chem* **2018**, *269*, 238. https://doi.org/10.1016/J.SNB.2018.04.097.

(76) Pollap, A.; Kochana, J. Electrochemical Immunosensors for Antibiotic Detection. *Biosensors* **2019**, *9* (2), 61. https://doi.org/10.3390/BIOS9020061.

(77) Kao, W. C.; Belkin, S.; Cheng, J. Y. Microbial Biosensing of Ciprofloxacin Residues in Food by a Portable Lens-Free CCD-Based Analyzer. *Anal Bioanalytical Chemistry* **2018**, *410* (4), 1257. https://doi.org/10.1007/S00216-017-0792-X/TABLES/1.

(78) Wei, D.; Meng, H.; Zeng, K.; Huang, Z. Visual Dual Dot Immunoassay for the Simultaneous Detection of Kanamycin and Streptomycin in Milk. *Analytical Methods* **2018**, *11* (1), 70. https://doi.org/10.1039/C8AY02006J.

(79) Wang, X.; Gong, J.; Yuan, B.; Chen, Z.; Jiang, J. Sensitive and Multiplexed Detection of Antibiotics Using a Suspension Array Platform Based on

Silica-Agarose Hybrid Microbeads. *Journal of Hazardous Material* **2019**, *373*, 115. https://doi.org/10.1016/J.JHAZMAT.2019.03.081.

(80) Chung, H. H.; Lee, J. Bin; Chung, Y. H.; Lee, K. G. Analysis of Sulfonamide and Quinolone Antibiotic Residues in Korean Milk Using Microbial Assays and High Performance Liquid Chromatography. *Food Chemistry* **2009**, *113* (1), 297. https://doi.org/10.1016/J.FOODCHEM.2008.07.021.

(81) González De La Huebra, M. J.; Bordin, G.; Rodríguez, A. R. A Multiresidue Method for the Simultaneous Determination of Ten Macrolide Antibiotics in Human Urine Based on Gradient Elution Liquid Chromatography Coupled to Coulometric Detection (HPLC–ECD). *Analytica Chimica Acta* **2004**, *517*, 53. https://doi.org/10.1016/J.ACA.2004.04.042.

(82) Bohm, D. A.; Stachel, C. S.; Gowik, P. Validation of a Multi-Residue Method for the Determination of Several Antibiotic Groups in Honey by LC-MS/MS. *Analytical and Bioanalytical Chemistry* **2012**, *403* (10), 2943. https://doi.org/10.1007/S00216-012-5868-Z/FIGURES/6.

(83) Moudgil, P.; Bedi, J. S.; Aulakh, R. S.; Gill, J. P. S.; Kumar, A. Validation of HPLC Multi-Residue Method for Determination of Fluoroquinolones, Tetracycline, Sulphonamides and Chloramphenicol Residues in Bovine Milk. *Food Analytical Methods* **2019**, *12* (2), 338. https://doi.org/10.1007/S12161-018-1365-0/TABLES/1.

(84) Gros, M.; Rodríguez-Mozaz, S.; Barceló, D. Rapid Analysis of Multiclass Antibiotic Residues and Some of Their Metabolites in Hospital, Urban Wastewater and River Water by Ultra-High-Performance Liquid Chromatography Coupled to Quadrupole-Linear Ion Trap Tandem Mass Spectrometry. *Journal of Chromatography A* **2013**, *1292*, 173. https://doi.org/10.1016/J.CHROMA.2012.12.072.

(85) Terry, S. C.; Herman, J. H.; Angell, J. B. A Gas Chromatographic Air Analyzer Fabricated on a Silicon Wafer. *IEEE Trans Electron Devices* **1979**, *26* (12), 1880. https://doi.org/10.1109/T-ED.1979.19791.

(86) Soares, R. R. G.; Neumann, F.; Caneira, C. R. F.; Madaboosi, N.; Ciftci, S.; Hernández-Neuta, I.; Pinto, I. F.; Santos, D. R.; Chu, V.; Russom, A.;

Conde, J. P.; Nilsson, M. Silica Bead-Based Microfluidic Device with Integrated Photodiodes for the Rapid Capture and Detection of Rolling Circle Amplification Products in the Femtomolar Range. *Biosensors and Bioelectronics* **2019**, *128*, 68. https://doi.org/10.1016/j.bios.2018.12.004.

(87) Grigorov, E.; Peykov, S.; Kirov, B. Novel Microfluidics Device for Rapid Antibiotics Susceptibility Screening. *Applied Sciences* **2022**, *12* (4), 2198. https://doi.org/10.3390/app12042198.

(88) Azizi, M.; Davaji, B.; Nguyen, A. V.; Mokhtare, A.; Zhang, S.; Dogan, B.; Gibney, P. A.; Simpson, K. W.; Abbaspourrad, A. Biological Small-Molecule Assays Using Gradient-Based Microfluidics. *Biosensors and Bioelectronics* **2021**, *178*, 113038. https://doi.org/10.1016/j.bios.2021.113038.

(89) Shanmugakani, R. K.; Srinivasan, B.; Glesby, M. J.; Westblade, L. F.; Cárdenas, W. B.; Raj, T.; Erickson, D.; Mehta, S. Current State of the Art in Rapid Diagnostics for Antimicrobial Resistance. *Lab on a Chip* **2020**, *20* (15), 2607. https://doi.org/10.1039/D0LC00034E.

(90) Song, Y.; Yin, J.; Huang, W. E.; Li, B.; Yin, H. Emerging Single-Cell Microfluidic Technology for Microbiology. *TrAC Trends in Analytical Chemistry* **2024**, *170*, 117444. https://doi.org/10.1016/j.trac.2023.117444.

(91) Li, H.; Torab, P.; Mach, K. E.; Surrette, C.; England, M. R.; Craft, D. W.; Thomas, N. J.; Liao, J. C.; Puleo, C.; Wong, P. K. Adaptable Microfluidic System for Single-Cell Pathogen Classification and Antimicrobial Susceptibility Testing. *Proceedings of the National Academy of Sciences* **2019**, *116* (21), 10270. https://doi.org/10.1073/pnas.1819569116.

(92) Trick, A. Y.; Melendez, J. H.; Chen, F.-E.; Chen, L.; Onzia, A.; Zawedde, A.; Nakku-Joloba, E.; Kyambadde, P.; Mande, E.; Matovu, J.; Atuheirwe, M.; Kwizera, R.; Gilliams, E. A.; Hsieh, Y.-H.; Gaydos, C. A.; Manabe, Y. C.; Hamill, M. M.; Wang, T.-H. A Portable Magnetofluidic Platform for Detecting Sexually Transmitted Infections and Antimicrobial Susceptibility. *Science Translational Medicine* **2021**, *13,* 593. https://doi.org/10.1126/scitranslmed.abf6356.

(93) Ma, Y.-D.; Li, K.-H.; Chen, Y.-H.; Lee, Y.-M.; Chou, S.-T.; Lai, Y.-Y.; Huang, P.-C.; Ma, H.-P.; Lee, G.-B. A Sample-to-Answer, Portable Platform for Rapid Detection of Pathogens with a Smartphone Interface. *Lab on a Chip* **2019**, *19*, 3804. https://doi.org/10.1039/C9LC00797K.

(94) Kalsi, S.; Sellars, S.; Turner, C.; Sutton, J.; Morgan, H. A Programmable Digital Microfluidic Assay for the Simultaneous Detection of Multiple Anti-Microbial Resistance Genes. *Micromachines (Basel)* **2017**, *8* (4), 111. https://doi.org/10.3390/mi8040111.

(95) Mahadeva, S. K.; Walus, K.; Stoeber, B. Paper as a Platform for Sensing Applications and Other Devices: A Review. *ACS Applied Material Interfaces* **2015**, *7* (16), 8345. https://doi.org/10.1021/acsami.5b00373.

(96) Mao, K.; Min, X.; Zhang, H.; Zhang, K.; Cao, H.; Guo, Y.; Yang, Z. Paper-Based Microfluidics for Rapid Diagnostics and Drug Delivery. *Journal of Controlled Release* **2020**, *322*, 187. https://doi.org/10.1016/j.jconrel.2020.03.010.

(97) Martinez, A. W.; Phillips, S. T.; Butte, M. J.; Whitesides, G. M. Patterned Paper as a Platform for Inexpensive, Low-Volume, Portable Bioassays. *Angewandte Chemie International Edition* **2007**, *46* (8), 1318. https://doi.org/10.1002/anie.200603817.

(98) Arai, M. S.; de Camargo, A. S. S.; Carrilho, E. Fluorescent Paper-Based Analytical Devices. *Paper-based Analytical Devices for Chemical Analysis and Diagnostics* **2022**, 183. https://doi.org/10.1016/B978-0-12-820534-1.00002-5.

(99) Sriram, G.; Bhat, M. P.; Patil, P.; Uthappa, U. T.; Jung, H. Y.; Altalhi, T.; Kumeria, T.; Aminabhavi, T. M.; Pai, R. K.; Madhuprasad; Kurkuri, M. D. Paper-Based Microfluidic Analytical Devices for Colorimetric Detection of Toxic Ions: A Review. *TrAC - Trends in Analytical Chemistry* **2017**, *93*, 212. https://doi.org/10.1016/J.TRAC.2017.06.005.

(100) Marques, A. C.; Águas, H.; Martins, R.; Costa-Silva, B.; Sales, M. G.; Fortunato, E. Surface-Enhanced Raman Scattering Paper-Based Analytical Devices. *Paper-based Analytical Devices for Chemical Analysis*

*and Diagnostics* **2022**, 117. https://doi.org/10.1016/B978-0-12-820534-1.00001-3.

(101) Mettakoonpitak, J.; Boehle, K.; Nantaphol, S.; Teengam, P.; Adkins, J. A.; Srisa-Art, M.; Henry, C. S. Electrochemistry on Paper-Based Analytical Devices: A Review. *Electroanalysis* **2016**, *28* (7), 1420. https://doi.org/10.1002/ELAN.201501143.

(102) He, P. J. W.; Katis, I. N.; Kumar, A. J. U.; Bryant, C. A.; Keevil, C. W.; Somani, B. K.; Mahobia, N.; Eason, R. W.; Sones, C. L. Laser-Patterned Paper-Based Sensors for Rapid Point-of-Care Detection and Antibiotic-Resistance Testing of Bacterial Infections. *Biosensors and Bioelectronics* **2020**, *152*, 112008. https://doi.org/10.1016/j.bios.2020.112008.

(103) Boehle, K. E.; Gilliand, J.; Wheeldon, C. R.; Holder, A.; Adkins, J. A.; Geiss, B. J.; Ryan, E. P.; Henry, C. S. Utilizing Paper‐Based Devices for Antimicrobial‐Resistant Bacteria Detection. *Angewandte Chemie International Edition* **2017**, *56* (24), 6886. https://doi.org/10.1002/anie.201702776.

(104) Choopara, I.; Suea-Ngam, A.; Teethaisong, Y.; Howes, P. D.; Schmelcher, M.; Leelahavanichkul, A.; Thunyaharn, S.; Wongsawaeng, D.; deMello, A. J.; Dean, D.; Somboonna, N. Fluorometric Paper-Based, Loop-Mediated Isothermal Amplification Devices for Quantitative Point-of-Care Detection of Methicillin-Resistant *Staphylococcus Aureus* (MRSA). *ACS Sensors* **2021**, *6* (3), 742. https://doi.org/10.1021/acssensors.0c01405.

(105) Mao, K.; Zhang, H.; Ran, F.; Cao, H.; Feng, R.; Du, W.; Li, X.; Yang, Z. Portable Biosensor Combining CRISPR/Cas12a and Loop-Mediated Isothermal Amplification for Antibiotic Resistance Gene ErmB in Wastewater. *Journal of Hazardous Material* **2024**, *462*, 132793. https://doi.org/10.1016/J.JHAZMAT.2023.132793.

(106) Trinh, T. N. D.; Lee, N. Y. Nucleic Acid Amplification-Based Microfluidic Approaches for Antimicrobial Susceptibility Testing. *Analyst* **2021**, *146* (10), 3101. https://doi.org/10.1039/D1AN00180A.

(107) Sadiq, S. T.; Mazzaferri, F.; Unemo, M. Rapid Accurate Point-of-Care Tests Combining Diagnostics and Antimicrobial Resistance Prediction for Neisseria Gonorrhoeae and Mycoplasma Genitalium. *Sexually Transmitted Infections* **2017**, *93* (S4), S65. https://doi.org/10.1136/SEXTRANS-2016-053072.

(108) Magro, L.; Escadafal, C.; Garneret, P.; Jacquelin, B.; Kwasiborski, A.; Manuguerra, J. C.; Monti, F.; Sakuntabhai, A.; Vanhomwegen, J.; Lafaye, P.; Tabeling, P. Paper Microfluidics for Nucleic Acid Amplification Testing (NAAT) of Infectious Diseases. *Lab on a Chip* **2017**, *17* (14), 2347. https://doi.org/10.1039/C7LC00013H.

(109) Boutal, H.; Moguet, C.; Pommiès, L.; Simon, S.; Naas, T.; Volland, H. The Revolution of Lateral Flow Assay in the Field of AMR Detection. *Diagnostics (Basel)* **2022**, *12* (7), 1744. https://doi.org/10.3390/DIAGNOSTICS12071744.

(110) Kang, T.; Lu, J.; Yu, T.; Long, Y.; Liu, G. Advances in Nucleic Acid Amplification Techniques (NAATs): COVID-19 Point-of-Care Diagnostics as an Example. *Biosensors and Bioelectronics* **2022**, *206*, 114109. https://doi.org/10.1016/j.bios.2022.114109.

(111) Chowdhury, A. M. M. A.; Mina, S. A.; Hossain, A. K. M. Z.; Debnath, P.; Hasan, M. Z. Screening and Identification of Antibiotic Resistant Gene Int1 in Coliforms Isolated From Drinking Water. *Air, Soil and Water Research* **2022**, *15*, 1. https://doi.org/10.1177/11786221221084715/ASSET/IMAGES/LARGE/10.1177_11786221221084715-FIG3.JPEG.

(112) Grakh, K.; Mittal, D.; Prakash, A.; Jindal, N. Characterization and Antimicrobial Susceptibility of Biofilm-Producing Avian Pathogenic Escherichia Coli from Broiler Chickens and Their Environment in India. *Veterinary Research Communications* **2022**, *46* (2), 537. https://doi.org/10.1007/s11259-021-09881-5.

(113) Eid, H.; El-Mahallawy, H.; Elsheshtawy, H.; Shalaby, A.; Shetewy, M.; Eidaroos, N. Antimicrobial Resistance and Virulence-associated Genes of

Aeromonads Isolated From Lake Manzala Water and Wild Nile Tilapia: Implications to Public Health and The Lake Microbial Community. *Slovenian Veterinary Research*. **2022**, *59*. 1. https://doi.org/10.26873/SVR-1348-2022.

(114) Mthembu; Zishiri; Zowalaty. Detection and Molecular Identification of Salmonella Virulence Genes in Livestock Production Systems in South Africa. *Pathogens* **2019**, *8* (3), 124. https://doi.org/10.3390/pathogens8030124.

(115) Gxalo, O.; Digban, T. O.; Igere, B. E.; Olapade, O. A.; Okoh, A. I.; Nwodo, U. U. Virulence and Antibiotic Resistance Characteristics of Vibrio Isolates From Rustic Environmental Freshwaters. *Frontiers in Cellular and Infection Microbiology* **2021**, *11*, 1. https://doi.org/10.3389/fcimb.2021.732001.

(116) Lorenz, T. C. Polymerase Chain Reaction: Basic Protocol Plus Troubleshooting and Optimization Strategies. *Journal of Visualized Experiments* **2012**, *63*, 1. https://doi.org/10.3791/3998.

(117) Zhao, Y.; Chen, F.; Li, Q.; Wang, L.; Fan, C. Isothermal Amplification of Nucleic Acids. *Chemical Reviews* **2015**, *115* (22), 12491. https://doi.org/10.1021/acs.chemrev.5b00428.

(118) Notomi, T. Loop-Mediated Isothermal Amplification of DNA. *Nucleic Acids Research* **2000**, *28* (12), 63. https://doi.org/10.1093/nar/28.12.e63.

(119) Chen, J.-W.; Lau, Y. Y.; Krishnan, T.; Chan, K.-G.; Chang, C.-Y. Recent Advances in Molecular Diagnosis of Pseudomonasaeruginosa Infection by State-of-the-Art Genotyping Techniques. *Frontiers in Microbiology* **2018**, *9,* 1. https://doi.org/10.3389/fmicb.2018.01104.

(120) Zhang, H.; Xu, Y.; Fohlerova, Z.; Chang, H.; Iliescu, C.; Neuzil, P. LAMP-on-a-Chip: Revising Microfluidic Platforms for Loop-Mediated DNA Amplification. *TrAC Trends in Analytical Chemistry* **2019**, *113*, 44. https://doi.org/10.1016/j.trac.2019.01.015.

(121) Moehling, T. J.; Choi, G.; Dugan, L. C.; Salit, M.; Meagher, R. J. LAMP Diagnostics at the Point-of-Care: Emerging Trends and Perspectives for

the Developer Community. *Expert Review of Molecular Diagnostics* **2021**, *21* (1), 43. https://doi.org/10.1080/14737159.2021.1873769.

(122) Stedtfeld, R. D.; Stedtfeld, T. M.; Waseem, H.; Fitschen-Brown, M.; Guo, X.; Chai, B.; Williams, M. R.; Shook, T.; Logan, A.; Graham, A.; Chae, J. C.; Sul, W. J.; VanHouten, J.; Cole, J. R.; Zylstra, G. J.; Tiedje, J. M.; Upham, B. L.; Hashsham, S. A. Isothermal Assay Targeting Class 1 Integrase Gene for Environmental Surveillance of Antibiotic Resistance Markers. *Journal of Environmental Management* **2017**, *198*, 213. https://doi.org/10.1016/j.jenvman.2017.04.079.

(123) Suea-Ngam, A.; Choopara, I.; Li, S.; Schmelcher, M.; Somboonna, N.; Howes, P. D.; deMello, A. J.; Suea-Ngam, A.; Li, S.; Howes, P. D.; deMello, A. J.; Choopara Program in Biotechnology, I.; Schmelcher, M.; Somboonna, N. In Situ Nucleic Acid Amplification and Ultrasensitive Colorimetric Readout in a Paper-Based Analytical Device Using Silver Nanoplates. *Advanced Healthcare Materials* **2021**, *10* (7), 2001755. https://doi.org/10.1002/ADHM.202001755.

(124) Chen, X.; Ma, K.; Yi, X.; Xiong, L.; Wang, Y.; Li, S. The Rapid and Visual Detection of Methicillin-Susceptible and Methicillin-Resistant Staphylococcus Aureus Using Multiplex Loop-Mediated Isothermal Amplification Linked to a Nanoparticle-Based Lateral Flow Biosensor. *Antimicrobial Resistance and Infection Control* **2020**, *9* (1), 111. https://doi.org/10.1186/s13756-020-00774-x.

(125) Meng, X.; Zhang, G.; Sun, B.; Liu, S.; Wang, Y.; Gao, M.; Fan, Y.; Zhang, G.; Shi, G.; Kang, X. Rapid Detection of MecA and FemA Genes by Loop-Mediated Isothermal Amplification in a Microfluidic System for Discrimination of Different Staphylococcal Species and Prediction of Methicillin Resistance. *Frontiers in Microbiology* **2020**, *11*, 1487. https://doi.org/10.3389/FMICB.2020.01487/BIBTEX.

(126) Hassan, M. M.; van Vliet, A. H. M.; Higgins, O.; Burke, L. P.; Chueiri, A.; O'Connor, L.; Morris, D.; Smith, T. J.; La Ragione, R. M. Rapid Culture-Independent Loop-Mediated Isothermal Amplification Detection of Antimicrobial Resistance Markers from Environmental Water Samples.

*Microbial Biotechnology* **2023**, *16*, 977, https://doi.org/10.1111/1751-7915.14227.

(127) Lobato, I. M.; O'Sullivan, C. K. Recombinase Polymerase Amplification: Basics, Applications and Recent Advances. *TrAC Trends in Analytical Chemistry* **2018**, *98*, 19. https://doi.org/10.1016/j.trac.2017.10.015.

(128) Suprun, E. V.; Khmeleva, S. A.; Duskaev, I. F.; Ptitsyn, K. G.; Kurbatov, L. K.; Shershov, V. E.; Kuznetsova, V. E.; Lapa, S. A.; Chudinov, A. V.; Radko, S. P. Combining Recombinase Polymerase Amplification with Tyrosine Modified 2′-Deoxyuridine-5′-Triphosphate for Direct Voltammetric Detection of Double-Stranded DNA: Application to Potato Pathogen Dickeya Solani. *Talanta* **2024**, *273*, 125841. https://doi.org/10.1016/j.talanta.2024.125841.

(129) Salazar, A.; Ochoa-Corona, F. M.; Talley, J. L.; Noden, B. H. Recombinase Polymerase Amplification (RPA) with Lateral Flow Detection for Three Anaplasma Species of Importance to Livestock Health. *Scientific Report* **2021**, *11* (1), 15962. https://doi.org/10.1038/s41598-021-95402-y.

(130) Munawar, M. A. Critical Insight into Recombinase Polymerase Amplification Technology. *Expert Review of Molecular Diagnostics*. **2022**, *22*(7), 725. https://doi.org/10.1080/14737159.2022.2109964.

(131) Lau, H. Y.; Wang, Y.; Wee, E. J. H.; Botella, J. R.; Trau, M. Field Demonstration of a Multiplexed Point-of-Care Diagnostic Platform for Plant Pathogens. *Analytical Chemistry* **2016**, *88*, 16. https://doi.org/10.1021/acs.analchem.6b01551.

(132) Liu, H. Bin; Du, X. J.; Zang, Y. X.; Li, P.; Wang, S. SERS-Based Lateral Flow Strip Biosensor for Simultaneous Detection of Listeria Monocytogenes and Salmonella Enterica Serotype Enteritidis. *Journal of Agricultural Food Chemistry* **2017**, *65* (47), 1. https://doi.org/10.1021/acs.jafc.7b03957.

(133) Faye, M.; Abd El Wahed, A.; Faye, O.; Kissenkötter, J.; Hoffmann, B.; Sall, A. A.; Faye, O. A Recombinase Polymerase Amplification Assay for Rapid

Detection of Rabies Virus. *Scientific Report* **2021**, *11* (1), 1. https://doi.org/10.1038/s41598-021-82479-8.

(134) Faye, O.; Faye, O.; Soropogui, B.; Patel, P.; El Wahed, A. A.; Loucoubar, C.; Fall, G.; Kiory, D.; Magassouba, N.; Keita, S.; Kondé, M. K.; Diallo, A. A.; Koivogui, L.; Karlberg, H.; Mirazimi, A.; Nentwich, O.; Piepenburg, O.; Niedrig, M.; Weidmann, M.; Sall, A. A. Development and Deployment of a Rapid Recombinase Polymerase Amplification Ebola Virus Detection Assay in Guinea in 2015. *Eurosurveillance* **2015**, *20* (44), 1. https://doi.org/10.2807/1560-7917.ES.2015.20.44.30053.

(135) Lin, C.; Zeng, Y.; Zhu, Z.; Liao, J.; Yang, T.; Liu, Y.; Wei, H.; Li, J.; Ma, J.; Wu, X.; Lin, G.; Lin, L.; Chen, L.; Huang, H.; Chen, W.; Wang, J.; Wen, F.; Lin, M. A Rapid Antimicrobial Resistance Diagnostic Platform for Staphylococcus Aureus Using Recombinase Polymerase Amplification. *Microbiology Spectrum* **2023**, *11* (2), 1. https://doi.org/10.1128/spectrum.04476-22.

(136) Nakano, M.; Kalsi, S.; Morgan, H. Fast and Sensitive Isothermal DNA Assay Using Microbead Dielectrophoresis for Detection of Anti-Microbial Resistance Genes. *Biosensors and Bioelectronics* **2018**, *117*, 1. https://doi.org/10.1016/j.bios.2018.06.063.

(137) Butterworth, A.; Pratibha, P.; Marx, A.; Corrigan, D. K. Electrochemical Detection of Oxacillin Resistance Using Direct-Labeling Solid-Phase Isothermal Amplification. *ACS Sensors* **2021**, *6,* 1. https://doi.org/10.1021/acssensors.1c01688.

(138) Sollweck, K.; Streich, P.; Elsner, M.; Seidel, M. A Chip-Based Colony Fusion Recombinase Polymerase Amplification Assay for Monitoring of Antimicrobial Resistance Genes and Their Carrying Species in Surface Water. *ACS Environmental Science and Technology Water* **2021**, *1* (3), 584. https://doi.org/10.1021/ACSESTWATER.0C00110/ASSET/IMAGES/LARGE/EW0C00110_0006.JPEG.

(139) Ali, M. M.; Li, F.; Zhang, Z.; Zhang, K.; Kang, D.-K.; Ankrum, J. A.; Le, X. C.; Zhao, W. Rolling Circle Amplification: A Versatile Tool for Chemical Biology, Materials Science and Medicine. *Chemical Society Review* **2014**, *43* (10), 3324. https://doi.org/10.1039/c3cs60439j.

(140) Hutchison, C. A.; Smith, H. O.; Pfannkoch, C.; Venter, J. C. Cell-Free Cloning Using Φ29 DNA Polymerase. *Proceedings of the National Academy of Sciences* **2005**, *102* (48), 17332. https://doi.org/10.1073/pnas.0508809102.

(141) Lizardi, P. M.; Huang, X.; Zhu, Z.; Bray-Ward, P.; Thomas, D. C.; Ward, D. C. Mutation Detection and Single-Molecule Counting Using Isothermal Rolling-Circle Amplification. *Nature Genetics* **1998**, *19* (3), 225. https://doi.org/10.1038/898.

(142) Zhu, Z.; Yang, L. Recent Progress in Molecular Diagnostics: The Synergy of Rolling Circle Amplification and CRISPR/Cas Systems (2018–2024) – A Concise Review. *TrAC Trends in Analytical Chemistry* **2024**, *180*, 117902. https://doi.org/10.1016/j.trac.2024.117902.

(143) Jain, S.; Dandy, D. S.; Geiss, B. J.; Henry, C. S. Padlock Probe-Based Rolling Circle Amplification Lateral Flow Assay for Point-of-Need Nucleic Acid Detection. *Analyst* **2021**, *146* (13), 4340. https://doi.org/10.1039/D1AN00399B.

(144) Gliddon, H. D.; Frampton, D.; Munsamy, V.; Heaney, J.; Pataillot-Meakin, T.; Nastouli, E.; Pym, A. S.; Steyn, A. J. C.; Pillay, D.; McKendry, R. A. A Rapid Drug Resistance Genotyping Workflow for Mycobacterium Tuberculosis, Using Targeted Isothermal Amplification and Nanopore Sequencing. *Microbiology Spectrum* **2021**, *9* (3), 1. https://doi.org/10.1128/Spectrum.00610-21.

(145) Hu, C.; Kalsi, S.; Zeimpekis, I.; Sun, K.; Ashburn, P.; Turner, C.; Sutton, J. M.; Morgan, H. Ultra-Fast Electronic Detection of Antimicrobial Resistance Genes Using Isothermal Amplification and Thin Film Transistor Sensors. *Biosensors and Bioelectronics* **2017**, *96*, 1. https://doi.org/10.1016/j.bios.2017.05.016.

(146) Hsu, P. D.; Lander, E. S.; Zhang, F. Development and Applications of CRISPR-Cas9 for Genome Engineering. *Cell,* **2014** *157*(6):1262. https://doi.org/10.1016/j.cell.2014.05.010.

(147) Kasputis, T.; Hilaire, S. S.; Xia, K.; Chen, J. Colorimetric Detection of Antimicrobial Resistance from Food Processing Facilities Using a CRISPR System. *ACS Food Science and Technology* **2023**, *3* (1), 17. https://doi.org/10.1021/ACSFOODSCITECH.2C00302.

(148) Deng, L.; He, X.; Liu, K.; Li, Y.; Xia, H.; Qian, H.; Lu, X.; Mao, X.; Xiang, Y. One-Pot RPA-Cas12a Assay for Instant and Visual Detection of Burkholderia Pseudomallei. *Analytica Chimica Acta* **2023**, *1252*, 341059 https://doi.org/10.1016/j.aca.2023.341059.

(149) Shafiei, F.; McAuliffe, K.; Bagheri, Y.; Sun, Z.; Yu, Q.; Wu, R.; You, M. Paper-Based Fluorogenic RNA Aptamer Sensors for Label-Free Detection of Small Molecules. *Analytical Methods* **2020**, *12* (21), 2674. https://doi.org/10.1039/D0AY00588F.

(150) Lin, H.; Fang, F.; Zang, J.; Su, J.; Tian, Q.; Kankala, R. K.; Lin, X. A Fluorescent Sensor-Assisted Paper-Based Competitive Lateral Flow Immunoassay for the Rapid and Sensitive Detection of Ampicillin in Hospital Wastewater. *Micromachines* **2020**, *11* (4), 431. https://doi.org/10.3390/MI11040431.

(151) Wang, L.; Zhu, F.; Zhu, Y.; Xie, S.; Chen, M.; Xiong, Y.; Liu, Q.; Yang, H.; Chen, X. Intelligent Platform for Simultaneous Detection of Multiple Aminoglycosides Based on a Ratiometric Paper-Based Device with Digital Fluorescence Detector Readout. **2019**, *16*, 47. https://doi.org/10.1021/acssensors.9b01845.

(152) Fernández-Gavela, A.; Herranz, S.; Chocarro, B.; Falke, F.; Schreuder, E.; Leeuwis, H.; Heideman, R. G.; Lechuga, L. M. Full Integration of Photonic Nanoimmunosensors in Portable Platforms for On-Line Monitoring of Ocean Pollutants. *Sensors and Actuators B Chemical* **2019**, *297*, 126758. https://doi.org/10.1016/J.SNB.2019.126758.

(153) Ma, Z.; Liu, J.; Sallach, J. B.; Hu, X.; Gao, Y. Whole-Cell Paper Strip Biosensors to Semi-Quantify Tetracycline Antibiotics in Environmental Matrices. *Biosensors and Bioelectronics* **2020**, *168*. 1112528. https://doi.org/10.1016/J.BIOS.2020.112528.

(154) Dirks, R. M.; Pierce, N. A. Triggered Amplification by Hybridization Chain Reaction. *Proceedings of the National Academy of Sciences of the United States of America* **2004**, *101* (43), 15275. https://doi.org/10.1073/PNAS.0407024101/ASSET/B86174D6-86E5-49CA-8212-4BA2A737F118/ASSETS/GRAPHIC/ZPQ0450463730002.JPEG.

(155) Li, S.; Li, P.; Ge, M.; Wang, H.; Cheng, Y.; Li, G.; Huang, Q.; He, H.; Cao, C.; Lin, D.; Yang, L. Elucidation of Leak-Resistance DNA Hybridization Chain Reaction with Universality and Extensibility. *Nucleic Acids Research* **2020**, *48* (5), 2220. https://doi.org/10.1093/nar/gkaa016.

(156) Ang, Y. S.; Yung, L.-Y. L. Rational Design of Hybridization Chain Reaction Monomers for Robust Signal Amplification. *Chemical. Communications.* **2016**, *52* (22), 4219. https://doi.org/10.1039/C5CC08907G.

(157) Chen, J.; Shi, G.; Yan, C. Portable Biosensor for On-Site Detection of Kanamycin in Water Samples Based on CRISPR-Cas12a and an off-the-Shelf Glucometer. *Science of the Total Environment* **2023**, *872*. 162279. https://doi.org/10.1016/j.scitotenv.2023.162279.

(158) Hu, J.; Song, H.; Zhou, J.; Liu, R.; Lv, Y. Metal-Tagged CRISPR/Cas12a Bioassay Enables Ultrasensitive and Highly Selective Evaluation of Kanamycin Bioaccumulation in Fish Samples. *Analytical Chemistry* **2021**, *93* (42), 14214. https://doi.org/10.1021/acs.analchem.1c03094.

(159) Lamarca, R. S.; Franco, D. F.; Nalin, M.; De Lima Gomes, P. C. F.; Messaddeq, Y. Label-Free Ultrasensitive and Environment-Friendly Immunosensor Based on a Silica Optical Fiber for the Determination of Ciprofloxacin in Wastewater Samples. *Analytical Chemistry* **2020**, *92* (21), 14415. dx.doi.org/10.1021/acs.analchem.0c02355

(160) Nguyen, A. H.; Ma, X.; Park, H. G.; Sim, S. J. Low-Blinking SERS Substrate for Switchable Detection of Kanamycin. *Sensors and Actuators B Chemical* **2019**, *282*, 765. https://doi.org/10.1016/J.SNB.2018.11.037.

(161) Chinnappan, R.; Eissa, S.; Alotaibi, A.; Siddiqua, A.; Alsager, O. A.; Zourob, M. In Vitro Selection of DNA Aptamers and Their Integration in a Competitive Voltammetric Biosensor for Azlocillin Determination in Waste Water. *Analytica Chimica Acta* **2020**, *1101*, 149. https://doi.org/10.1016/J.ACA.2019.12.023.

(162) Chen, X.; Liu, Y.; Fang, X.; Li, Z.; Pu, H.; Chang, J.; Chen, J.; Mao, S. Ultratrace Antibiotic Sensing Using Aptamer/Graphene-Based Field-Effect Transistors. *Biosensors and Bioelectronics* **2019**, *126*, 664. https://doi.org/10.1016/J.BIOS.2018.11.034.

(163) Mahfouz, N.; Caucci, S.; Achatz, E.; Semmler, T.; Guenther, S.; Berendonk, T. U.; Schroeder, M. High Genomic Diversity of Multi-Drug Resistant Wastewater Escherichia Coli. *Scientific Report* **2018**, *8* (1), 8928. https://doi.org/10.1038/s41598-018-27292-6.

(164) Kappell, A. D.; Kimbell, L. K.; Seib, M. D.; Carey, D. E.; Choi, M. J.; Kalayil, T.; Fujimoto, M.; Zitomer, D. H.; McNamara, P. J. Removal of Antibiotic Resistance Genes in an Anaerobic Membrane Bioreactor Treating Primary Clarifier Effluent at 20 °C. *Environmental Science (Camb)* **2018**, *4* (11), 1783. https://doi.org/10.1039/C8EW00270C.

(165) Hiller, C. X.; Hübner, U.; Fajnorova, S.; Schwartz, T.; Drewes, J. E. Antibiotic Microbial Resistance (AMR) Removal Efficiencies by Conventional and Advanced Wastewater Treatment Processes: A Review. *Science of The Total Environment* **2019**, *685*, 596. https://doi.org/10.1016/j.scitotenv.2019.05.315.

(166) Chaudhary, A. S. A Review of Global Initiatives to Fight Antibiotic Resistance and Recent Antibiotics′ Discovery. *Acta Pharmaceutica Sinica B* **2016**, *6* (6), 552. https://doi.org/10.1016/j.apsb.2016.06.004.

(167) Cars, O.; Hedin, A.; Heddini, A. The Global Need for Effective Antibiotics—Moving towards Concerted Action. *Drug Resistance Updates* **2011**, *14* (2), 68–69. https://doi.org/10.1016/j.drup.2011.02.006.

(168) Yin, J.; Wang, Y.; Xu, X.; Liu, Y.; Yao, L.; Sun, Q. The Progress of Global Antimicrobial Resistance Governance and Its Implication to China: A Review. *Antibiotics* **2021**, *10* (11), 1356. https://doi.org/10.3390/antibiotics10111356.

(169) Klein, E. Y.; Van Boeckel, T. P.; Martinez, E. M.; Pant, S.; Gandra, S.; Levin, S. A.; Goossens, H.; Laxminarayan, R. Global Increase and Geographic Convergence in Antibiotic Consumption between 2000 and 2015. *Proceedings of the National Academy of Sciences* **2018**, *115* (15), e3463. https://doi.org/10.1073/pnas.1717295115.

(170) Roller, R. M.; Lieberman, M. Beyond Wax Printing: The Future of Paper Analytical Device Fabrication. *Sensors and Actuators B Chemical* **2023**, *392,* 134059. https://doi.org/10.1016/j.snb.2023.134059.

(171) Woodward, B.; Istepanian, R. S. H.; Richards, C. I. Design of a Telemedicine System Using a Mobile Telephone. *IEEE Transactions on Information Technology in Biomedicine* **2001**, *5* (1), 13. https://doi.org/10.1109/4233.908361.

(172) Gao, X.; Wu, N. Smartphone-Based Sensors. *Electrochemical Society Interface* **2016**, *25* (4), 79. https://doi.org/10.1149/2.F07164if.

(173) Chowdhury, A. S.; Call, D. R.; Broschat, S. L. PARGT: A Software Tool for Predicting Antimicrobial Resistance in Bacteria. *Scientific Report* **2020**, *10* (1), 11033. https://doi.org/10.1038/s41598-020-67949-9.

(174) Ruppé, E.; Ghozlane, A.; Tap, J.; Pons, N.; Alvarez, A.-S.; Maziers, N.; Cuesta, T.; Hernando-Amado, S.; Clares, I.; Martínez, J. L.; Coque, T. M.; Baquero, F.; Lanza, V. F.; Máiz, L.; Goulenok, T.; de Lastours, V.; Amor, N.; Fantin, B.; Wieder, I.; Andremont, A.; van Schaik, W.; Rogers, M.; Zhang, X.; Willems, R. J. L.; de Brevern, A. G.; Batto, J.-M.; Blottière, H. M.; Léonard, P.; Léjard, V.; Letur, A.; Levenez, F.; Weiszer, K.; Haimet, F.; Doré, J.; Kennedy, S. P.; Ehrlich, S. D. Prediction of the Intestinal

Resistome by a Three-Dimensional Structure-Based Method. *Nature Microbiology* **2018**, *4* (1), 112. https://doi.org/10.1038/s41564-018-0292-6.

(175) Sun, H.; Xiong, L.; Huang, Y.; Chen, X.; Yu, Y.; Ye, S.; Dong, H.; Jia, Y.; Zhang, W. AI-Aided on-Chip Nucleic Acid Assay for Smart Diagnosis of Infectious Disease. *Fundamental Research* **2022**, *2* (3), 476. https://doi.org/10.1016/J.FMRE.2021.12.005.

(176) Duan, S.; Cai, T.; Zhu, J.; Yang, X.; Lim, E. G.; Huang, K.; Hoettges, K.; Zhang, Q.; Fu, H.; Guo, Q.; Liu, X.; Yang, Z.; Song, P. Deep Learning-Assisted Ultra-Accurate Smartphone Testing of Paper-Based Colorimetric ELISA Assays. *Analytica Chimca Acta* **2023**, *1248*, 340868. https://doi.org/10.1016/J.ACA.2023.340868.

(177) Mohsen, M. G.; Kool, E. T. The Discovery of Rolling Circle Amplification and Rolling Circle Transcription. *Accounts of Chemical Research* **2016**, *49* (11), 2540. DOI: 10.1021/acs.accounts.6b00417

(178) Ahn, H.; Batule, B. S.; Seok, Y.; Kim, M.-G. Single-Step Recombinase Polymerase Amplification Assay Based on a Paper Chip for Simultaneous Detection of Multiple Foodborne Pathogens. *Analytical Chemistry* **2018**, *90* (17), 10211. https://doi.org/10.1021/acs.analchem.8b01309.

(179) Li, S. Y.; Cheng, Q. X.; Li, X. Y.; Zhang, Z. L.; Gao, S.; Cao, R. B.; Zhao, G. P.; Wang, J.; Wang, J. M. CRISPR-Cas12a-Assisted Nucleic Acid Detection. *Cell Discovery* **2018**, *4* (1), 1. https://doi.org/10.1038/s41421-018-0028-z.

(180) Teng, F.; Guo, L.; Cui, T.; Wang, X.-G.; Xu, K.; Gao, Q.; Zhou, Q.; Li, W. CDetection: CRISPR-Cas12b-Based DNA Detection with Sub-Attomolar Sensitivity and Single-Base Specificity. *Genome Biology* **2019**, *20* (1), 1. https://doi.org/10.1186/S13059-019-1742-Z.

(181) Wang, B.; Wang, R.; Wang, D.; Wu, J.; Li, J.; Wang, J.; Liu, H.; Wang, Y. Cas12aVDet: A CRISPR/Cas12a-Based Platform for Rapid and Visual Nucleic Acid Detection. *Analytical Chemistry* **2019**, *91* (19), 12156. https://doi.org/10.1021/acs.analchem.9b01526.

(182) Choi, J. H.; Lim, J.; Shin, M.; Paek, S. H.; Choi, J. W. CRISPR-Cas12a-Based Nucleic Acid Amplification-Free DNA Biosensor via Au Nanoparticle-Assisted Metal-Enhanced Fluorescence and Colorimetric Analysis. *Nano Letters* **2021**, *21* (1), 693. https://doi.org/10.1021/acs.nanolett.0c04303.

(183) Rusu, A.; Buta, E. L. The Development of Third-Generation Tetracycline Antibiotics and New Perspectives. *Pharmaceutics* **2021**, *13* (12), 2085. https://doi.org/10.3390/pharmaceutics13122085.

(184) Chopra, I.; Roberts, M. Tetracycline Antibiotics: Mode of Action, Applications, Molecular Biology, and Epidemiology of Bacterial Resistance. *Microbiology and Molecular Biology Reviews* **2001**, *65* (2), 232. https://doi.org/10.1128/MMBR.65.2.232-260.2001.

(185) Grossman, T. H. Tetracycline Antibiotics and Resistance. *Cold Spring Harbor Perspectives in Medicine* **2016**, *6* (4), a025387. https://doi.org/10.1101/cshperspect.a025387.

(186) He, T.; Wang, R.; Liu, D.; Walsh, T. R.; Zhang, R.; Lv, Y.; Ke, Y.; Ji, Q.; Wei, R.; Liu, Z.; Shen, Y.; Wang, G.; Sun, L.; Lei, L.; Lv, Z.; Li, Y.; Pang, M.; Wang, L.; Sun, Q.; Fu, Y.; Song, H.; Hao, Y.; Shen, Z.; Wang, S.; Chen, G.; Wu, C.; Shen, J.; Wang, Y. Emergence of Plasmid-Mediated High-Level Tigecycline Resistance Genes in Animals and Humans. *Nature Microbiology* **2019**, *4* (9), 1450. https://doi.org/10.1038/s41564-019-0445-2.

(187) Ballesté, E.; Pascual-Benito, M.; Martín-Díaz, J.; Blanch, A. R.; Lucena, F.; Muniesa, M.; Jofre, J.; García-Aljaro, C. Dynamics of CrAssphage as a Human Source Tracking Marker in Potentially Faecally Polluted Environments. *Water Research* **2019**, *155*, 233. https://doi.org/10.1016/j.watres.2019.02.042.

(188) Suzuki, S.; Pruden, A.; Virta, M.; Zhang, T. Editorial: Antibiotic Resistance in Aquatic Systems. *Frontiers in Microbiology* **2017**, *8*. 14. https://doi.org/10.3389/fmicb.2017.00014.

(189) Rodriguez-Mozaz, S.; Chamorro, S.; Marti, E.; Huerta, B.; Gros, M.; Sànchez-Melsió, A.; Borrego, C. M.; Barceló, D.; Balcázar, J. L. Occurrence of Antibiotics and Antibiotic Resistance Genes in Hospital and Urban Wastewaters and Their Impact on the Receiving River. *Water Research* **2015**, *69*, 234. https://doi.org/10.1016/j.watres.2014.11.021.

(190) Li, J.; Cheng, W.; Xu, L.; Strong, P. J.; Chen, H. Antibiotic-Resistant Genes and Antibiotic-Resistant Bacteria in the Effluent of Urban Residential Areas, Hospitals, and a Municipal Wastewater Treatment Plant System. *Environmental Science and Pollution Research* **2015**, *22* (6), 4587. https://doi.org/10.1007/s11356-014-3665-2.

(191) Woo, A.; Jung, H. S.; Kim, D. H.; Park, S. G.; Lee, M. Y. Rapid and Sensitive Multiplex Molecular Diagnosis of Respiratory Pathogens Using Plasmonic Isothermal RPA Array Chip. *Biosensors and Bioelectronics* **2021**, *182*. 1. https://doi.org/10.1016/j.bios.2021.113167.

(192) Ge, R.; Dai, H.; Zhang, S.; Wei, J.; Jiao, T.; Chen, Q.; Chen, Q.; Chen, X. A Collection of RPA-Based Photoelectrochemical Assays for the Portable Detection of Multiple Pathogens. *Analytical Chemistry* **2023**, *95* (18), 1. https://doi.org/10.1021/acs.analchem.3c01006.

(193) Geng, Y.; Tan, K.; Liu, L.; Sun, X. X.; Zhao, B.; Wang, J. Development and Evaluation of a Rapid and Sensitive RPA Assay for Specific Detection of Vibrio Parahaemolyticus in Seafood. *BMC Microbiology* **2019**, *19* (1), 1. https://doi.org/10.1186/s12866-019-1562-z.

(194) Wang, P.; Zhang, X.; Shen, H.; Lu, Q.; Li, B.; Liu, X.; Gao, S. A One-Pot RPA-CRISPR Detection Method for Point-of-Care Testing of Enterocytozoon Hepatopenaei Infection in Shrimp. *Sensors and Actuators B Chemicals* **2023**, *374*, 132853. https://doi.org/10.1016/j.snb.2022.132853.

(195) Liu, L.; Duan, J.-J.; Wei, X.-Y.; Hu, H.; Wang, Y.-B.; Jia, P.-P.; Pei, D.-S. Generation and Application of a Novel High-Throughput Detection Based on RPA-CRISPR Technique to Sensitively Monitor Pathogenic

Microorganisms in the Environment. *Science of The Total Environment* **2022**, *838*, 156048. https://doi.org/10.1016/j.scitotenv.2022.156048.

(196) Li, Y.; Shi, Z.; Hu, A.; Cui, J.; Yang, K.; Liu, Y.; Deng, G.; Zhu, C.; Zhu, L. Rapid One-Tube RPA-CRISPR/Cas12 Detection Platform for Methicillin-Resistant Staphylococcus Aureus. *Diagnostics* **2022**, *12* (4), 829. https://doi.org/10.3390/diagnostics12040829.

(197) Wei, H.; Li, J.; Liu, Y.; Cheng, W.; Huang, H.; Liang, X.; Huang, W.; Lin, L.; Zheng, Y.; Chen, W.; Wang, C.; Chen, W.; Xu, G.; Wei, W.; Chen, L.; Zeng, Y.; Lu, Z.; Li, S.; Lin, Z.; Wang, J.; Lin, M. Rapid and Ultrasensitive Detection of *Plasmodium* Spp. Parasites via the RPA-CRISPR/Cas12a Platform. *ACS Infectious Disease* **2023**, *9* (8), 1534. https://doi.org/10.1021/acsinfecdis.3c00087.

(198) Jiang, T.; Hu, X.; Lin, C.; Xia, Z.; Yang, W.; Zhu, Y.; Xu, H.; Tang, H.; Shen, J. Rapid Visualization of Clostridioides Difficile Toxins A and B by Multiplex RPA Combined with CRISPR-Cas12a. *Frontiers in Microbiology* **2023**, *14*. 119395. https://doi.org/10.3389/fmicb.2023.1119395.

(199) Peng, R.; Lu, Z.; Liu, M.; Hu, F. RT-RPA-Assisted CRISPR/Cas12a for Rapid and Multiplex Detection of Respiratory Infectious Viruses Based on Centrifugal Microfluidics. *Sensors and Actuators B Chemicals* **2024**, *399*, 134838. https://doi.org/10.1016/j.snb.2023.134838.

(200) Xu, J.; Ma, J.; Li, Y.; Kang, L.; Yuan, B.; Li, S.; Chao, J.; Wang, L.; Wang, J.; Su, S.; Yuan, Y. A General RPA-CRISPR/Cas12a Sensing Platform for Brucella Spp. Detection in Blood and Milk Samples. *Sensors and Actuators B Chemicals* **2022**, *364*, 131864. https://doi.org/10.1016/j.snb.2022.131864.

(201) Li, Z.; Ding, X.; Yin, K.; Xu, Z.; Cooper, K.; Liu, C. Electric Field-Enhanced Electrochemical CRISPR Biosensor for DNA Detection. *Biosensors and Bioelectronics* **2021**, *192*, 113498. https://doi.org/10.1016/j.bios.2021.113498.

(202) Land, K. J.; Boeras, D. I.; Chen, X.-S.; Ramsay, A. R.; Peeling, R. W. REASSURED Diagnostics to Inform Disease Control Strategies,

Strengthen Health Systems and Improve Patient Outcomes. *Nature Microbiology* **2018**, *4* (1), 46. https://doi.org/10.1038/s41564-018-0295-3.

(203) Bahadır, E. B.; Sezgintürk, M. K. Lateral Flow Assays: Principles, Designs and Labels. *TrAC - Trends in Analytical Chemistry*. 2016, *82*, 286. https://doi.org/10.1016/j.trac.2016.06.006.

(204) Guo, J.; Chen, S.; Guo, J.; Ma, X. Nanomaterial Labels in Lateral Flow Immunoassays for Point-of-Care-Testing. *Journal of Material Scienece and Technology* **2021**, *60*. 90. https://doi.org/10.1016/j.jmst.2020.06.003.

(205) Sena-Torralba, A.; Álvarez-Diduk, R.; Parolo, C.; Piper, A.; Merkoçi, A. Toward Next Generation Lateral Flow Assays: Integration of Nanomaterials. *Chemical Reviews* **2022**, *122* (18), 14881. https://doi.org/10.1021/acs.chemrev.1c01012.

(206) Grant, B. D.; Anderson, C. E.; Williford, J. R.; Alonzo, L. F.; Glukhova, V. A.; Boyle, D. S.; Weigl, B. H.; Nichols, K. P. SARS-CoV-2 Coronavirus Nucleocapsid Antigen-Detecting Half-Strip Lateral Flow Assay Toward the Development of Point of Care Tests Using Commercially Available Reagents. *Analytical Chemistry* **2020**, *92* (16), 11305. https://doi.org/10.1021/acs.analchem.0c01975.

(207) Du, D.; Wang, J.; Wang, L.; Lu, D.; Lin, Y. Integrated Lateral Flow Test Strip with Electrochemical Sensor for Quantification of Phosphorylated Cholinesterase: Biomarker of Exposure to Organophosphorus Agents. *Analytical Chemistry* **2012**, *84* (3), 1380. https://doi.org/10.1021/ac202391w.

(208) Hassan, A. H. A.; Bergua, J. F.; Morales-Narváez, E.; Mekoçi, A. Validity of a Single Antibody-Based Lateral Flow Immunoassay Depending on Graphene Oxide for Highly Sensitive Determination of E. Coli O157:H7 in Minced Beef and River Water. *Food Chemistry* **2019**, *297*, 124965. https://doi.org/10.1016/j.foodchem.2019.124965.

(209) Sivaranjanee, R.; Senthil Kumar, P.; Saravanan, R.; Govarthanan, M. Electrochemical Sensing System for the Analysis of Emerging

Contaminants in Aquatic Environment: A Review. *Chemosphere* **2022**, *294*, 133779. https://doi.org/10.1016/J.CHEMOSPHERE.2022.133779.

(210) Zhang, W.; Wang, L.; Yang, Y.; Gaskin, P.; Teng, K. S. Recent AdVances on Electrochemical Sensors for the Detection of Organic Disinfection Byproducts in Water. *ACS Sensors* **2019**, *4* (5), 1138. https://doi.org/10.1021/acssensors.9b00272.

(211) Zhang, W.; Dixon, M. B.; Saint, C.; Teng, K. S.; Furumai, H. Electrochemical Biosensing of Algal Toxins in Water: The Current State-of-the-Art. *ACS Sensors* **2018**, *3* (7), 1233. https://doi.org/10.1021/acssensors.8b00359.

(212) Bernalte, E.; Arévalo, S.; Pérez-Taborda, J.; Wenk, J.; Estrela, P.; Avila, A.; Di Lorenzo, M. Rapid and On-Site Simultaneous Electrochemical Detection of Copper, Lead and Mercury in the Amazon River. *Sensors and Actuators B Chemicals* **2020**, *307*, 127620. https://doi.org/10.1016/j.snb.2019.127620.

(213) Yang, Z.; Kasprzyk-Hordern, B.; Goggins, S.; Frost, C. G.; Estrela, P. A Novel Immobilization Strategy for Electrochemical Detection of Cancer Biomarkers: DNA-Directed Immobilization of Aptamer Sensors for Sensitive Detection of Prostate Specific Antigens. *Analyst* **2015**, *140* (8), 2628. https://doi.org/10.1039/c4an02277g.

(214) Trasatti, S.; Petrii, O. A. Real Surface Area Measurements in Electrochemistry. *Journal of Electroanalytical Chemistry* **1992**, *327* (1), 353. https://doi.org/10.1016/0022-0728(92)80162-W.

(215) Su, G.; Zhu, M.; Li, D.; Xu, M.; Zhu, Y.; Zhang, Y.; Zhu, H.; Li, F.; Yu, Y. Multiplexed Lateral Flow Assay Integrated with Orthogonal CRISPR-Cas System for SARS-CoV-2 Detection. *Sensors and Actuators B Chemicals* **2022**, *371*. 132537. https://doi.org/10.1016/j.snb.2022.132537.

(216) Li, C.; Lin, N.; Feng, Z.; Lin, M.; Guan, B.; Chen, K.; Liang, W.; Wang, Q.; Li, M.; You, Y.; Chen, Q. CRISPR/Cas12a Based Rapid Molecular Detection of Acute Hepatopancreatic Necrosis Disease in Shrimp.

*Frontiers in Veterinary Science* **2022**, *8*. 819681. https://doi.org/10.3389/fvets.2021.819681.

(217) Lei, R.; Li, L.; Wu, P.; Fei, X.; Zhang, Y.; Wang, J.; Zhang, D.; Zhang, Q.; Yang, N.; Wang, X. RPA/CRISPR/Cas12a-Based On-Site and Rapid Nucleic Acid Detection of Toxoplasma Gondii in the Environment. *ACS Synthetic Biology* **2021**. *11*, 1772. https://doi.org/10.1021/acssynbio.1c00620.

(218) del Río, J. S.; Svobodova, M.; Bustos, P.; Conejeros, P.; O'Sullivan, C. K. Electrochemical Detection of Piscirickettsia Salmonis Genomic DNA from Salmon Samples Using Solid-Phase Recombinase Polymerase Amplification. *Analytical and Bioanalytical Chemistry* **2016**, *408* (30), 8611. https://doi.org/10.1007/s00216-016-9639-0.

(219) Dunn, M. R.; Jimenez, R. M.; Chaput, J. C. Analysis of Aptamer Discovery and Technology. *Nature Reviews Chemistry* **2017**, *1* (10), 1. https://doi.org/10.1038/s41570-017-0076.

(220) DeRosa, M. C.; Lin, A.; Mallikaratchy, P.; McConnell, E. M.; McKeague, M.; Patel, R.; Shigdar, S. In Vitro Selection of Aptamers and Their Applications. *Nature Reviews Methods Primers* **2023**, *3* (1), 54. https://doi.org/10.1038/s43586-023-00238-7.

(221) McConnell, E. M.; Nguyen, J.; Li, Y. Aptamer-Based Biosensors for Environmental Monitoring. *Frontiers in Chemistry* **2020**, *8*. 1. https://doi.org/10.3389/fchem.2020.00434.

(222) Zadeh, J. N.; Steenberg, C. D.; Bois, J. S.; Wolfe, B. R.; Pierce, M. B.; Khan, A. R.; Dirks, R. M.; Pierce, N. A. NUPACK: Analysis and Design of Nucleic Acid Systems. *Journal of Computational Chemistry* **2011**, *32* (1), 170. https://doi.org/10.1002/jcc.21596.

(223) Bi, S.; Yue, S.; Zhang, S. Hybridization Chain Reaction: A Versatile Molecular Tool for Biosensing, Bioimaging, and Biomedicine. *Chemical Society Review* **2017**, *46* (14), 4281. https://doi.org/10.1039/C7CS00055C.

(224) Wu, J.; Lv, J.; Zheng, X.; Wu, Z.-S. Hybridization Chain Reaction and Its Applications in Biosensing. *Talanta* **2021**, *234*, 122637. https://doi.org/10.1016/j.talanta.2021.122637.

(225) Lin, R.; Feng, Q.; Li, P.; Zhou, P.; Wang, R.; Liu, Z.; Wang, Z.; Qi, X.; Tang, N.; Shao, F.; Luo, M. A Hybridization-Chain-Reaction-Based Method for Amplifying Immunosignals. *Nature Methods* **2018**, *15* (4), 275. https://doi.org/10.1038/nmeth.4611.

(226) Zhu, Z.; Wu, C.; Liu, H.; Zou, Y.; Zhang, X.; Kang, H.; Yang, C. J.; Tan, W. An Aptamer Cross-Linked Hydrogel as a Colorimetric Platform for Visual Detection. *Angewandte Chemie - International Edition* **2010**, *49* (6), 1052. https://doi.org/10.1002/anie.200905570.

(227) Yan, L.; Zhu, Z.; Zou, Y.; Huang, Y.; Liu, D.; Jia, S.; Xu, D.; Wu, M.; Zhou, Y.; Zhou, S.; Yang, C. J. Target-Responsive “Sweet” Hydrogel with Glucometer Readout for Portable and Quantitative Detection of Non-Glucose Targets. *Journal of American Chemical Society* **2013**, *135* (10), 3748. https://doi.org/10.1021/ja3114714.

(228) Ma, Y.; Mao, Y.; Huang, D.; He, Z.; Yan, J.; Tian, T.; Shi, Y.; Song, Y.; Li, X.; Zhu, Z.; Zhou, L.; Yang, C. J. Portable Visual Quantitative Detection of Aflatoxin B1 Using a Target-Responsive Hydrogel and a Distance-Readout Microfluidic Chip. *Lab on a Chip* **2016**, *16* (16), 3097. https://doi.org/10.1039/c6lc00474a.

(229) Wei, X.; Tian, T.; Jia, S.; Zhu, Z.; Ma, Y.; Sun, J.; Lin, Z.; Yang, C. J. Target-Responsive DNA Hydrogel Mediated Stop-Flow Microfluidic Paper-Based Analytic Device for Rapid, Portable and Visual Detection of Multiple Targets. *Analytical Chemistry* **2015**, *87* (8), 4275. https://doi.org/10.1021/acs.analchem.5b00532.

(230) Chen, M.; Wang, Y.; Zhao, X.; Zhang, J.; Peng, Y.; Bai, J.; Li, S.; Han, D.; Ren, S.; Qin, K.; Li, S.; Han, T.; Gao, Z. Target-Responsive DNA Hydrogel with Microfluidic Chip Smart Readout for Quantitative Point-of-Care Testing of Creatine Kinase MB. *Talanta* **2022**, *243*. 123338. https://doi.org/10.1016/j.talanta.2022.123338.

(231) Sun, Y.; Li, S.; Chen, R.; Wu, P.; Liang, J. Ultrasensitive and Rapid Detection of T-2 Toxin Using a Target-Responsive DNA Hydrogel. *Sensors and Actuators B Chemical* **2020**, *311*. 127912. https://doi.org/10.1016/j.snb.2020.127912.

(232) Yu, J.; Xiao, S.; Yu, Z.; Hui, Y.; Li, T.; Wu, D.; Bi, W.; Gan, N.; Jia, Z. On-Site and Dual-Mode Detection of Live Vibrio Parahaemolyticus in Waters: A Universal Pathogen Sensing Platform Based on a Smart Hydrogel Aptasensor Imbedded with Gold Nanoclusters. *Sensors and Actuators B Chemical* **2022**, *366*. 131947. https://doi.org/10.1016/j.snb.2022.131947.

(233) Wu, P.; Li, S.; Ye, X.; Ning, B.; Bai, J.; Peng, Y.; Li, L.; Han, T.; Zhou, H.; Gao, Z.; Ding, P. Cu/Au/Pt Trimetallic Nanoparticles Coated with DNA Hydrogel as Target-Responsive and Signal-Amplification Material for Sensitive Detection of Microcystin-LR. *Analytica Chimica Acta* **2020**, *1134*, 96. https://doi.org/10.1016/j.aca.2020.08.004.

(234) Sun, Y.; Qi, S.; Dong, X.; Qin, M.; Zhang, Y.; Wang, Z. Colorimetric Aptasensor Targeting Zearalenone Developed Based on the Hyaluronic Acid-DNA Hydrogel and Bimetallic MOFzyme. *Biosensors and Bioelectronics* **2022**, *212*. 114366. https://doi.org/10.1016/j.bios.2022.114366.

(235) Liu, C.; Gou, S.; Bi, Y.; Gao, Q.; Sun, J.; Hu, S.; Guo, W. Smart DNA-Gold Nanoparticle Hybrid Hydrogel Film Based Portable, Cost-Effective and Storable Biosensing System for the Colorimetric Detection of Lead (II) and Uranyl Ions. *Biosensors and Bioelectronics* **2022**, *210*. 114290. https://doi.org/10.1016/j.bios.2022.114290.

(236) Han, D.; Li, J.; Tan, W. CRISPR Propels a Smart Hydrogel. *Science*. **2019**, *365*, 754. https://doi.org/10.1126/science.aay4198.

(237) Kellner, M. J.; Koob, J. G.; Gootenberg, J. S.; Abudayyeh, O. O.; Zhang, F. SHERLOCK: Nucleic Acid Detection with CRISPR Nucleases. *Nature Protocol* **2019**, *14* (10), 2986. https://doi.org/10.1038/s41596-019-0210-2.

(238) English, M. A.; Soenksen, L. R.; Gayet, R. V; De Puig, H.; Angenent-Mari, N. M.; Mao, A. S.; Nguyen, P. Q.; Collins, J. J. Programmable CRISPR-

Responsive Smart Materials. *Science*, **2019,** *365*, 780. Doi:10.1126/science.aaw5122.

(239) Chen, M.; Zhang, J.; Peng, Y.; Bai, J.; Li, S.; Han, D.; Ren, S.; Qin, K.; Zhou, H.; Han, T.; Wang, Y.; Gao, Z. Design and Synthesis of DNA Hydrogel Based on EXPAR and CRISPR/Cas14a for Ultrasensitive Detection of Creatine Kinase MB. *Biosensors and Bioelectronics,* **2022**, *218*. 114792. https://doi.org/10.1016/j.bios.2022.114792.

(240) Wang, Y.; Peng, Y.; Li, S.; Han, D.; Ren, S.; Qin, K.; Zhou, H.; Han, T.; Gao, Z. The Development of a Fluorescence/Colorimetric Biosensor Based on the Cleavage Activity of CRISPR-Cas12a for the Detection of Non-Nucleic Acid Targets. *Journal of Hazardous Materials* **2023**, *449*. 131044. https://doi.org/10.1016/j.jhazmat.2023.131044.

(241) Qiu, F.; Gan, X.; Yao, J.; Jiang, B.; Yuan, R.; Xiang, Y. CRISPR/Cas12a-Derived Sensitive Electrochemical Biosensing of NF-KB P50 Based on Hybridization Chain Reaction and DNA Hydrogel. *Biosensors and Bioelectronics.* **2022**, *216*, 114665. https://doi.org/10.1016/J.BIOS.2022.114665.

(242) Salimizand, H.; Zomorodi, A. R.; Mansury, D.; Khakshoor, M.; Azizi, O.; Khodaparast, S.; Baseri, Z.; Karami, P.; Zamanlou, S.; Farsiani, H.; Amini, Y.; Moradi, B.; Meshkat, Z.; Salimizand, H.; Hasanzadeh, S.; Sadeghian, H. Diversity of Aminoglycoside Modifying Enzymes and 16S RRNA Methylases in Acinetobacter Baumannii and Acinetobacter Nosocomialis Species in Iran; Wide Distribution of AadA1 and ArmA. *Infection, Genetics and Evolution* **2018**, *66*, 195. https://doi.org/10.1016/J.MEEGID.2018.09.028.

(243) Tang, M.; Li, F.; Yang, M.; Zhang, Y. Degradation of Kanamycin from Production Wastewater with High-Concentration Organic Matrices by Hydrothermal Treatment. *Journal of Environmental Sciences* **2020**, *97*, 11. https://doi.org/10.1016/J.JES.2020.04.032.

(244) Jiang, M.; Karasawa, T.; Steyger, P. S. Aminoglycoside-Induced Cochleotoxicity: A Review. *Frontiers in Cell Neurosciences* **2017**, *11*, 308. https://doi.org/10.3389/FNCEL.2017.00308/BIBTEX.

(245) Song, K. M.; Cho, M.; Jo, H.; Min, K.; Jeon, S. H.; Kim, T.; Han, M. S.; Ku, J. K.; Ban, C. Gold Nanoparticle-Based Colorimetric Detection of Kanamycin Using a DNA Aptamer. *Analytical Biochemistry* **2011**, *415* (2), 175. https://doi.org/10.1016/J.AB.2011.04.007.

(246) Zuker, M. Mfold Web Server for Nucleic Acid Folding and Hybridization Prediction. *Nucleic Acids Research* **2003**, *31* (13), 3406. https://doi.org/10.1093/nar/gkg595.

(247) Popenda, M.; Szachniuk, M.; Antczak, M.; Purzycka, K. J.; Lukasiak, P.; Bartol, N.; Blazewicz, J.; Adamiak, R. W. Automated 3D Structure Composition for Large RNAs. *Nucleic Acids Research* **2012**, *40* (14), e112. https://doi.org/10.1093/nar/gks339.

(248) Sarzynska, J.; Popenda, M.; Antczak, M.; Szachniuk, M. RNA Tertiary Structure Prediction Using RNAComposer in CASP15. *Proteins: Structure, Function, and Bioinformatics* **2023**, *91*, 1790. https://doi.org/10.1002/prot.26578.

(249) Schrödinger LLC. *The PyMOL Molecular Graphics System, 1.8*; **2015.**

(250) Schrödinger LLC. *The AxPyMOL Molecular Graphics Plugin for Microsoft PowerPoint, 1.8*; **2015**.

(251) Schrödinger LLC. *The JyMOL Molecular Graphics Development Component, 1.8*; **2015**.

(252) Hess, B.; Kutzner, C.; van der Spoel, D.; Lindahl, E. GROMACS 4: Algorithms for Highly Efficient, Load-Balanced, and Scalable Molecular Simulation. *Journal of Chemical Theory and Computation* **2008**, *4* (3), 435. https://doi.org/10.1021/ct700301q.

(253) Hart, K.; Foloppe, N.; Baker, C. M.; Denning, E. J.; Nilsson, L.; MacKerell, A. D. Optimization of the CHARMM Additive Force Field for DNA: Improved Treatment of the BI/BII Conformational Equilibrium. *Journal of Chemical*

*Theory and Computation* **2012**, *8* (1), 348. https://doi.org/10.1021/ct200723y.

(254) Trott, O.; Olson, A. J. AutoDock Vina: Improving the Speed and Accuracy of Docking with a New Scoring Function, Efficient Optimization, and Multithreading. *Journal of Computational Chemistry* **2010**, *31* (2), 455. https://doi.org/10.1002/jcc.21334.

(255) Eberhardt, J.; Santos-Martins, D.; Tillack, A. F.; Forli, S. AutoDock Vina 1.2.0: New Docking Methods, Expanded Force Field, and Python Bindings. *Journal of Chemical Information and Modelling* **2021**, *61* (8), 3891. https://doi.org/10.1021/acs.jcim.1c00203.

(256) Vanommeslaeghe, K.; Hatcher, E.; Acharya, C.; Kundu, S.; Zhong, S.; Shim, J.; Darian, E.; Guvench, O.; Lopes, P.; Vorobyov, I.; Mackerell, A. D. CHARMM General Force Field: A Force Field for Drug‐like Molecules Compatible with the CHARMM All‐atom Additive Biological Force Fields. *Journal of Computational Chemistry* **2010**, *31* (4), 671. https://doi.org/10.1002/jcc.21367.

(257) Yu, W.; He, X.; Vanommeslaeghe, K.; MacKerell, A. D. Extension of the CHARMM General Force Field to Sulfonyl‐containing Compounds and Its Utility in Biomolecular Simulations. *Journal of Computational Chemistry* **2012**, *33* (31), 2451. https://doi.org/10.1002/jcc.23067.

(258) Yano-Ozawa, Y.; Lobsiger, N.; Muto, Y.; Mori, T.; Yoshimura, K.; Yano, Y.; Stark, W. J.; Maeda, M.; Asahi, T.; Ogawa, A.; Zako, T. Molecular Detection Using Aptamer-Modified Gold Nanoparticles with an Immobilized DNA Brush for the Prevention of Non-Specific Aggregation. *RSC Advances* **2021**, *11* (20), 11984. https://doi.org/10.1039/D0RA05149G.

(259) Rodríguez Serrano, A. F.; Hsing, I.-M. Prediction of Aptamer–Small-Molecule Interactions Using Metastable States from Multiple Independent Molecular Dynamics Simulations. *Journal of Chemical Information and Modelling* **2022**, *62* (19), 4799. https://doi.org/10.1021/acs.jcim.2c00734.

(260) Han, J.; Ma, P.; Khan, I. M.; Zhang, Y.; Wang, Z. Study of Binding Mechanism of Aptamer to Kanamycin and the Development of Fluorescent

Aptasensor in Milk Detection. *Talanta* **2023**, *260*, 124530. https://doi.org/10.1016/j.talanta.2023.124530.

(261) Subhaswaraj, P.; Siddhardha, B. Molecular Docking and Molecular Dynamic Simulation Approaches for Drug Development and Repurposing of Drugs for Severe Acute Respiratory Syndrome-Coronavirus-2. In *Computational Approaches for Novel Therapeutic and Diagnostic Designing to Mitigate SARS-CoV-2 Infection*; Elsevier, **2022**; 207. https://doi.org/10.1016/B978-0-323-91172-6.00007-8.

(262) Yin, W.; Zhuang, J.; Li, J.; Xia, L.; Hu, K.; Yin, J.; Mu, Y. Digital Recombinase Polymerase Amplification, Digital Loop ‐ Mediated Isothermal Amplification, and Digital CRISPR ‐ Cas Assisted Assay: Current Status, Challenges, and Perspectives. *Small* **2023**, *19* (49). 2303398. https://doi.org/10.1002/smll.202303398.

(263) Yang, H.; Chen, Z.; Cao, X.; Li, Z.; Stavrakis, S.; Choo, J.; deMello, A. J.; Howes, P. D.; He, N. A Sample-in-Digital-Answer-out System for Rapid Detection and Quantitation of Infectious Pathogens in Bodily Fluids. *Analytical and Bioanalytical Chemistry* **2018**, *410* (27), 7019. https://doi.org/10.1007/s00216-018-1335-9.

(264) Park, J. S.; Hsieh, K.; Chen, L.; Kaushik, A.; Trick, A. Y.; Wang, T. Digital CRISPR/Cas ‐ Assisted Assay for Rapid and Sensitive Detection of SARS ‐ CoV ‐ 2. *Advanced Science* **2021**, *8* (5). 2003564. https://doi.org/10.1002/advs.202003564.

(265) Cate, D. M.; Adkins, J. A.; Mettakoonpitak, J.; Henry, C. S. Recent Developments in Paper-Based Microfluidic Devices. *Analytical Chemistry* **2015**, *87* (1), 19. https://doi.org/10.1021/ac503968p.

(266) Yang, Y.; Noviana, E.; Nguyen, M. P.; Geiss, B. J.; Dandy, D. S.; Henry, C. S. Paper-Based Microfluidic Devices: Emerging Themes and Applications. *Analytical Chemistry*. **2017**, *89*, 71. https://doi.org/10.1021/acs.analchem.6b04581.

(267) Akyazi, T.; Basabe-Desmonts, L.; Benito-Lopez, F. Review on Microfluidic Paper-Based Analytical Devices towards Commercialisation. *Analytica Chimica Acta* **2018**, *1001*, 1. https://doi.org/10.1016/j.aca.2017.11.010.

(268) Musile, G.; Agard, Y.; Wang, L.; De Palo, E. F.; McCord, B.; Tagliaro, F. Paper-Based Microfluidic Devices: On-Site Tools for Crime Scene Investigation. *TrAC Trends in Analytical Chemistry* **2021**, *143*, 116406. https://doi.org/10.1016/J.TRAC.2021.116406.

(269) Adedokun, G.; Alipanah, M.; Fan, Z. H. Sample Preparation and Detection Methods in Point-of-Care Devices towards Future at-Home Testing. *Lab on a Chip* **2024**, *24* (15), 3626. https://doi.org/10.1039/D3LC00943B.

(270) Yang, Z.; Xu, G.; Reboud, J.; Ali, S. A.; Kaur, G.; McGiven, J.; Boby, N.; Gupta, P. K.; Chaudhuri, P.; Cooper, J. M. Rapid Veterinary Diagnosis of Bovine Reproductive Infectious Diseases from Semen Using Paper-Origami DNA Microfluidics. *ACS Sensors* **2018**, *3* (2), 403. https://doi.org/10.1021/acssensors.7b00825.

(271) Lee, S. M.; Doeven, E. H.; Yuan, D.; Guijt, R. M. Method for Lysis and Paper-Based Elution-Free DNA Extraction with Colourimetric Isothermal Amplification. *Scientific Report* **2024**, *14* (1), 14479. https://doi.org/10.1038/s41598-024-59763-4.

(272) Seok, Y.; Yin, Q.; Li, R.; Mauk, M. G.; Bai, H.; Bau, H. H. Manually-Operated, Slider Cassette for Multiplexed Molecular Detection at the Point of Care. *Sensors and Actuators B Chemical* **2022**, *369*, 132353. https://doi.org/10.1016/j.snb.2022.132353.

(273) Rodriguez-Mateos, P.; Ngamsom, B.; Ameyo, D.; Wakaba, P.; Shiluli, C.; Iles, A.; Gitaka, J.; Pamme, N. Integrated Microscale Immiscible Phase Extraction and Isothermal Amplification for Colorimetric Detection of Neisseria Gonorrhoeae. *Analytical and Bioanalytical Chemistry* **2023**, *415* (21), 5129. https://doi.org/10.1007/s00216-023-04734-3.

(274) Lopatkin, A. J.; Huang, S.; Smith, R. P.; Srimani, J. K.; Sysoeva, T. A.; Bewick, S.; Karig, D. K.; You, L. Antibiotics as a Selective Driver for

Conjugation Dynamics. *Nature Microbiology* **2016**, *1* (6), 44. https://doi.org/10.1038/nmicrobiol.2016.44.

(275) Rodgers, K.; McLellan, I.; Peshkur, T.; Williams, R.; Tonner, R.; Hursthouse, A. S.; Knapp, C. W.; Henriquez, F. L. Can the Legacy of Industrial Pollution Influence Antimicrobial Resistance in Estuarine Sediments? *Environmental Chemistry Letters*. Springer Verlag June 15, **2019**, 595. https://doi.org/10.1007/s10311-018-0791-y.

(276) Liu, G.; Thomsen, L. E.; Olsen, J. E. Antimicrobial-Induced Horizontal Transfer of Antimicrobial Resistance Genes in Bacteria: A Mini-Review. *Journal of Antimicrobial Chemotherapy* **2022**, *77* (3), 556. https://doi.org/10.1093/jac/dkab450.

(277) Bengtsson-Palme, J.; Kristiansson, E.; Larsson, D. G. J. Environmental Factors Influencing the Development and Spread of Antibiotic Resistance. *FEMS Microbiology Reviews*. Oxford University Press January 1, **2018**, 68. https://doi.org/10.1093/femsre/fux053.

(278) Castañeda-Barba, S.; Top, E. M.; Stalder, T. Plasmids, a Molecular Cornerstone of Antimicrobial Resistance in the One Health Era. *Nature Reviews Microbiology*. **2023**. *22*, 18. https://doi.org/10.1038/s41579-023-00926-x.

(279) Qiu, W.; Sun, J.; Fang, M.; Luo, S.; Tian, Y.; Dong, P.; Xu, B.; Zheng, C. Occurrence of Antibiotics in the Main Rivers of Shenzhen, China: Association with Antibiotic Resistance Genes and Microbial Community. *Science of the Total Environment* **2019**, *653*, 334. https://doi.org/10.1016/j.scitotenv.2018.10.398.

(280) Hutinel, M.; Fick, J.; Larsson, D. G. J.; Flach, C. F. Investigating the Effects of Municipal and Hospital Wastewaters on Horizontal Gene Transfer. *Environmental Pollution* **2021**, *276*. 116733. https://doi.org/10.1016/j.envpol.2021.116733.

(281) Chen, Z.; Duan, Y.; Yin, L.; Chen, Y.; Xue, Y.; Wang, X.; Mao, D.; Luo, Y. Unraveling the Influence of Human Fecal Pollution on Antibiotic Resistance Gene Levels in Different Receiving Water Bodies Using CrAssphage

Indicator Gene. *Journal of Hazardous Material* **2023**, *442*. 13005. https://doi.org/10.1016/j.jhazmat.2022.130005.

(282) Karkman, A.; Pärnänen, K.; Larsson, D. G. J. Fecal Pollution Can Explain Antibiotic Resistance Gene Abundances in Anthropogenically Impacted Environments. *Nature Communications* **2019**, *10* (1). 80. https://doi.org/10.1038/s41467-018-07992-3.

# Appendices

## Appendix A DNAs and RNAs sequences

Generally, the length of the primers is mainly from 16-28 nt, and the two primers should be of comparable length (difference < 3 nt). GC%, i.e., the percentage of guanine and cystine in the sequence, should be in the range of 40-60% to maintain a stable while kinetically active structure. $T_m$, i.e., the melting temperature of the primers should be between 50 ºC and 62 ºC for optimal thermodynamic performance, and the two primers in a pair should have a difference in $T_m$ less than 5 ºC. As for the dual-labelled (fluorophore-quencher) probe, the length should be less than 30 nt, GC% from 40-60%, while its $T_m$ should be 5-10 ºC higher than its paired primers. The amplicon size should be in the range of 70-200 bp with a GC% of 30-80%. Dual-labelled probe is not the only method for PCR result characterisation, fluorescent DNA-binding dye such as EvaGreen (Fisher Scientific, UK) can also be used to monitor PCR process. However, DNA-binding dye shows less specificity in sequence as it emits fluorescence when it intercalates with dsDNA, no matter what the sequence is; while dual-labelled probe only anneals to its complementary sequence and represents fluorescence, leading to improved false-positive issues.

Primer-BLAST NCBI (https://www.ncbi.nlm.nih.gov/tools/primer-blast/) was used to design RT-qPCR primers and probes. The ARG target sequences were retrieved from National Library of Medicine with the NCBI reference number NZ_CP044485.1 (tet(M)), NC_024711.1 (crassphage), and NZ_CP045198.1 (tet(x3)). The 5’ end of the probes were modified with 6-FAM and 3’ end with BHQ-1. The primer sets and probes are selected based on the criteria mentioned above. All RT-qPCR assays are performed in 0.1 mL PCR microtubes in a Quant Studio 3 Real-Time PCR system, and the fluorescence signal of each cycle is recorded. Reaction conditions of each assay were optimised for individual targets and will be specified in Chapter 5 and 6. Synthetic or purified DNA sequences are selected to be the internal positive reference while $ddH_2O$ is used as template in internal negative control, while the rest of the assay composition remains the same for all controls and samples.

Table A.1 Excitation and emission wavelengths of the dye

| Dye | Excitation (nm) | Emission (nm) |
|---|---|---|
| Eva Green | 499 | 526 |
| 6-FAM | 493 | 517 |

## A.1 Primers, probes, crRNAs sequences

R: G or A

Y: C or T

The PCR primer and probes were designed using PrimerBlast with the following principles. Firstly, the resulting amplicon sizes fell into the range of 70 – 200 bp and the target sequences overlapped with the RPA target ones. Then, the length of primers was aimed at 18 – 30 nt, and the melting temperature was designated to be around 60 °C, with a less than 5 °C difference between the two melting temperatures of the primers. The GC % of primers was then determined to be 40 – 60 %. As for the probe. the length was aimed at 20 nt, with a GC % of 30 – 80 % and a melting temperature around 10 °C higher than that of the primers.

Table A.2 qPCR primers and probes sequences

| Target | Primer/Probe | Sequence (5'-3') |
|---|---|---|
| tet(M) | qPCR-M-FP | GGTTTCTCTTGGATACTTAAATCAATCR |
| | qPCR-M-RP | CCAACCATAYAATCCTTGTTCRC |
| | M-probe (6-FAM / BHQ-1) | ATGCAGTTATGGARGGGATACGCTATG GY |
| tet(x3) | qPCR-x3-FP | GCCAATCCCAATAATAATGGTGC |
| | qPCR-x3-RP | GCATTGAAATGTTGATACCGAACG |
| | X-probe (6-FAM / BHQ-1) | TCAGGACAGAAACAGCGTTGCCGA |
| crassphage | qPCR-C-FP | TGTATAGATGCTGCTGCAACTGTACTC |
| | qPCR-C-RP | CGTTGTTTTCATCTTTATCTTGTCCAT |

| | | |
|---|---|---|
| | C-probe (6-FAM / BHQ-1) | CTGAAATTGTTCATAAGCAA |

Table A.3 RPA primers and crRNA sequences

| Target | Primer/Probe | Sequence (5'-3') |
|---|---|---|
| tet(M) | RPA-M-FP | TTTACARTCCGTCACATTCCAACCATAYAATCC |
| | RPA-M-RP | TCGGTTTCTCTTGGATACTTAAATCAATCR |
| | M-crRNA | UAAUUUCUACUAAGUGUAGAUAAAAUGCAGUUAUGGAAGGGAUA |
| tet(x3) | RPA-x3-FP | TGAATGGAAAAATAAAATTCCCTTAGATTTTCA |
| | RPA-x3-RP | CGTATTAATTGTTTGTAAACTTCACTCCATTTG |
| | x3-crRNA | UAAUUUCUACUAAGUGUAGAUUUGAAAAGAUUUUCCAAAUGGAG |
| crassphage | RPA-C-FP | GTTCATAAGCAAATTGATATTTCTATTAAAAGTC |
| | RPA-C-RP | CGTTGTTTTCATCTTTATCTTGTCCATAAA |
| | C-crRNA | UAAUUUCUACUAAGUGUAGAUUGGACAAGAUAAAGAUGAAAACA |

## A.2 Aptamers, initiators and hairpins sequences

Table A.4 aptamer and initiator sequences

| Name | Sequence (5'-3') |
|---|---|
| apori | TGGGGGTTGAGGCTAAGCCGA |
| ap1 | TTTTTGGGGGTTGAGGCTAAGCCGAATTGTAG |
| ap2 | GGGATGATCTGGGGGTTGAGGCTAAGCCGATT |

Table A.5 hairpins sequences

| Name | Sequence (5’-3’) |
|---|---|
| hp1-a | TACGGCTAGCGGCTCGGCATAGACGCCGAGCCGCTAGCCGTAAATGGG |
| hp2-a | GTCTATGCCGAGCCGCTAGCCGTACCCATTTACGGCTAGCGGCTCGGC |
| Init-a | CCCATTTACGGCTAGCGGCTCGGC |
| hp1-b | GAATTGTAGGGTATGATCTGGCGATTTCCAGATCATACCCTAC |
| hp2-b | CCAGATCATACCCTACAATTCGTAGGGTATGATCTGGAAATCG |
| Init-b | CCAGATCATACCCTACAATTC |

## A.3 DNA hydrogel sequences

Table A.6 DNA hydrogel sequences

| Name | Sequence (5’-3’) |
|---|---|
| A-X | acrydite-AAAATACTACAACATG |
| A-Y | acrydite-AAAAACTCGTGACAGA |
| probe-L | TCTGTCACGAGTTTTTTTTTTTTTTTTCATGTTGTAGTA |

## A.4 Measured extracted DNA concentrations from real water samples

Table A.7 Means of measured DNA concentrations of real water samples

| ID | DNA concentration (ng $\mu L^{-1}$) |
|---|---|
| AD1 | 0.0642 |

| | |
|---|---|
| AD2 | 0.0658 |
| 069 | 0.043 |
| 073 | 0.0282 |
| 10/3/22 | 0.266 |
| 17/3/22 | 0.34 |
| 22/3/22 | 0.894 |
| 15/3/22 | 0.552 |
| 7/6/22 | 1.15 |
| 16/6/22 | 0.724 |
| 5/7/22 | 0.752 |
| 7/7/22 | 0.632 |
| 12/7/22 | 0.784 |
| 14/7/22 | 0.328 |
| 19/5/22 | 0.236 |
| 24/5/22 | 3.92 |
| 26/5/22 | 1.94 |

## A.5 qPCR calibration curves and standard plots

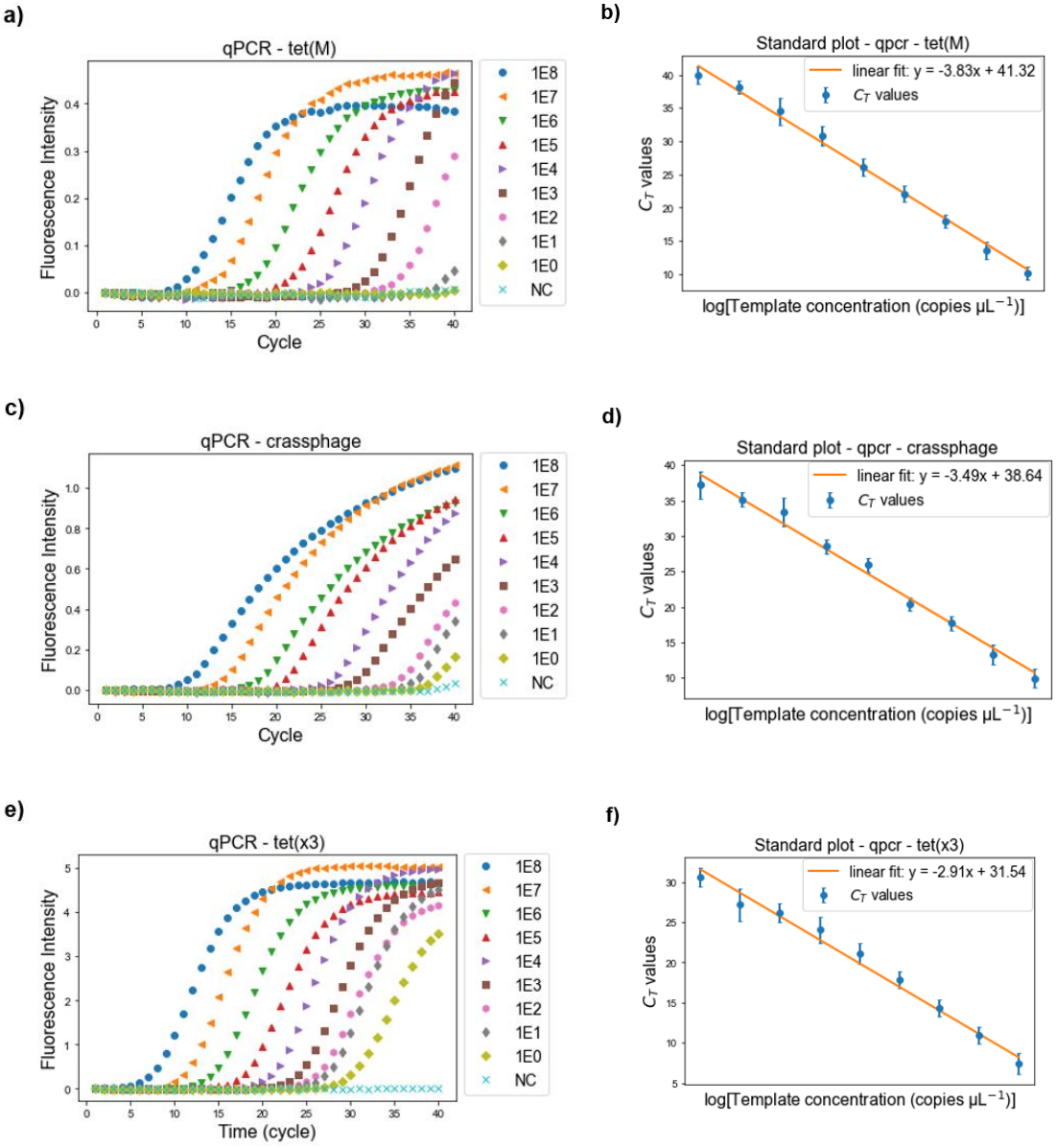


Figure A.1 qPCR results for quantifying three targets. real-time fluorescent amplification curves of 10-fold serial diluted a) tet(M c) crssphage e) tet(x3) ranging from $10^8$ – $10^0$ copies µL$^{-1}$. standard plot of b) tet(M) d) crassphage f) tet(x3) with linear fit. Experiments were done in triplicates. NC: negative control.

## A.6 Optimisation of primer concentration of crassphage and tet(M)

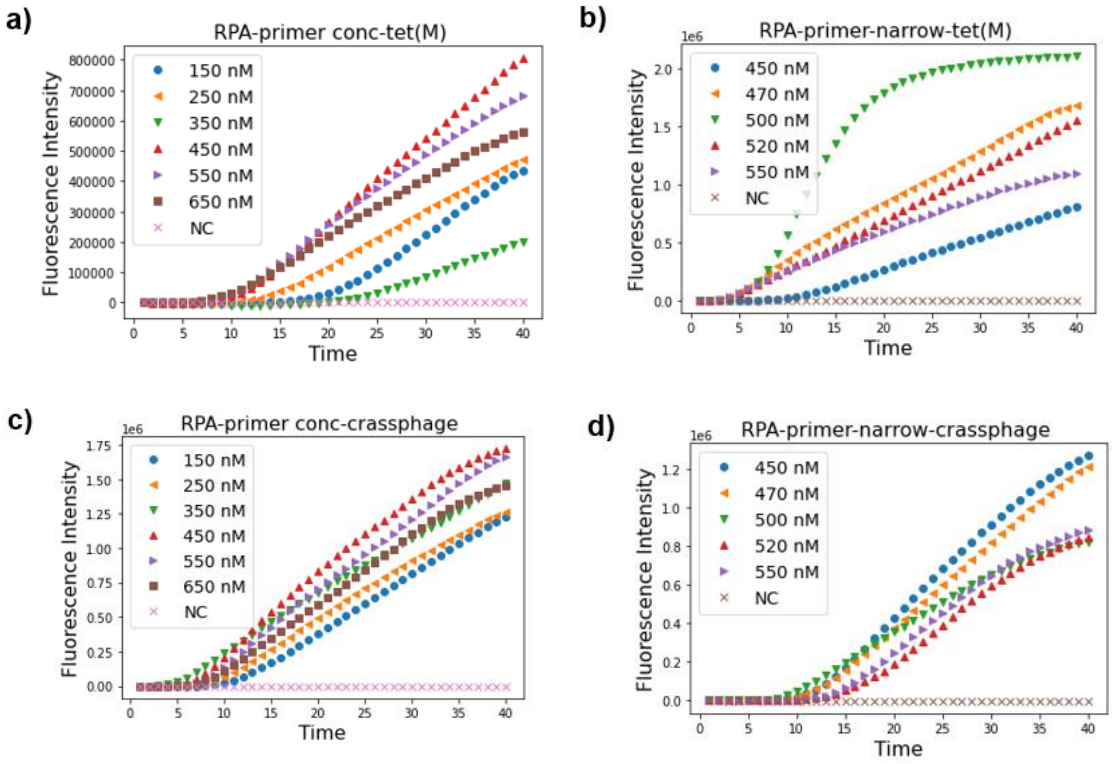


Figure A.2 Primer concentration optimisation of tet(M) and crassphage gene. a) tet(M) primer concentration with a broad range from 150 nM to 650 nM, and b) a narrower concentration range was then evaluated from 450 nM to 550 nM. c) crassphage primer concentration with a broad range from 150 nM to 650 nM, and d) a narrower concentration range was then evaluated from 450 nM to 550 nM. NC: negative control. All assays were repeated three times. The presented curve is a mean of triplicates.

## A.7 HCR-CRISPR/Cas assay condition optimisation

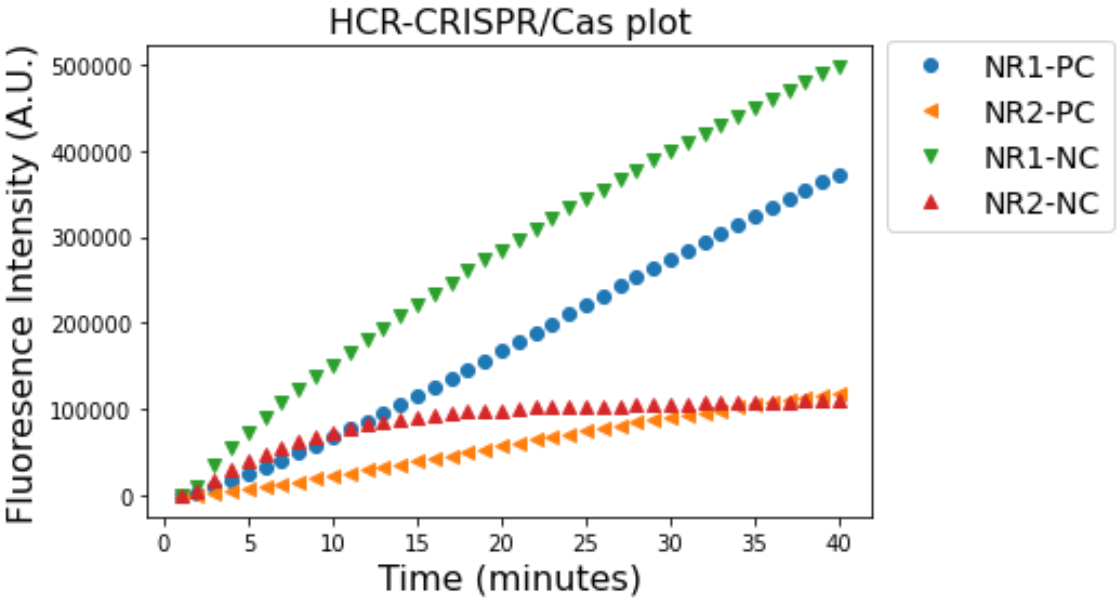


Figure A.3 HCR-CRISPR/Cas reation condition optimisation plots. NR1: new recipe 1. NR2: new recipe 2. PC: initiator added to HCR before CRISPR/Cas. NC: no initiators addec. All experiments were conducted in triplicates and the plot was a mean of them.

NR1: 10 µL CRISPR/Cas solution include 1 µL 1 µM cas12a, 1 µL 1 µM crRNA, 1.5 µL 10 µM ssDNA fluorescent probe, 3 µL 10 x NEB 2.1, 3.5 µL dd$H_2O$.

NR2: 10 µL CRISPR/Cas solution include 4 µL 1 µM cas12a, 2.5 µL 2 µM crRNA, 0.5 µL 10 µM ssDNA fluorescent probe, 1 µL 10 x NEB 2.1, 2 µL dd$H_2O$.

## A.8 CRISPR/Cas probe sequences

Table A.8 Sequences of CRISPR/Cas probes

| Type of CRISPR/Cas probe | Sequences (5’ – 3’) |
|---|---|
| Fluorescent | [6FAM]-TTATTATT –[BHQ1] |
| Lateral flow | [FITC]-TTATTTTATTTTATT-[Biotin] |
| Electrochemical | [ThiC6]-TTATTTTATTTTATT-[Atto-MB2] |